Cooperative Resource Allocation Schemes for Multiple-input Multiple-output Non-orthogonal Multiple Access (MIMO-NOMA) Systems

by

Jiefei Ding

A Thesis submitted to the Faculty of Graduate Studies of

The University of Manitoba

in partial fulfilment of the requirements of the degree of

DOCTOR OF PHILOSOPHY

Department of Electrical and Computer Engineering

University of Manitoba

Winnipeg

Abstract

Currently, multiple-input multiple-output non-orthogonal multiple access (MIMO-NOMA) technology has been considered as a promising multiple access technology for the fifth generation (5G) networks to improve system capacity and spectral efficiency. Integrating NOMA technology with MIMO resource allocation as a mixed-integer programming problem can improve spectrum reuse efficiency through introducing diversity in both power domain and space domain. However, MIMO-NOMA strategy design has a high computational complexity as it has high dimension beamforming vectors and power coefficients and should consider complicated network scenarios. To overcome these issues, this thesis proposes a new MIMO-NOMA strategy, formulates a joint optimization problem, and solve it by a game approach. The closed-form expressions in terms of beamforming vectors and power coefficients are derived, and the main factors that may affect the performance of MIMO-NOMA clustering are analyzed.

Based on this fundamental research, this thesis extends the proposed MIMO-NOMA strategy to many wireless communication scenarios, and combines it with other advanced transmission technologies. More specifically, in chapter 4, a multi-cell MIMO system is studied, which integrates MU clustering problem within a small cell and base station (BS) selection problem among multiple small cells into a joint optimization problem. In chapter 5, the proposed MIMO-NOMA strategy is integrated with cooperative multipoint (CoMP) technology, which is named as CoMP-NOMA. This study investigates a novel cooperation mode, i.e., a single MU may both participate in the intra-cell cooperation (i.e., MU clustering) and inter-cell cooperation (i.e., CoMP) simultaneously. In chapter 6, a UAV

assisted MIMO-NOMA network is investigated, in which UAVs are developed as additional antenna units of the BS and provide services for multiple MUs through cooperating with the BS.

Different from many current works to decouple the whole problem into independent multiple stages, the optimization approach design in this thesis are based on game theory. The employed game approaches (i.e., coalition game and matching game) are improved according to the features of each system model, to drive a distributed solution with low complexity. Moreover, this thesis discusses the optimality and proves the stability for proposed game approaches.

Acknowledgements

Foremost, I would like to express my deepest appreciation to my supervisors, Prof. Jun Cai, who provides valuable technical guidance and constructive suggestions on my research works and directions. I would also like to thank my defense committee, Dr. Pradeepa Yahampth, and Dr. Nan Wu, for taking the time and effort to review my work and provide me with their insightful comments. During the past four years, working with Jun Cai is a valuable experience. His wide knowledge, strong research enthusiasm and hard-working attitude have inspired me during all my PhD period, and will have a profound effect on my future carrier. I also acknowledge University of Manitoba and the Government of Manitoba for providing me with financial support.

I am also thankful to my colleagues in the Network Intelligence and Innovation Lab ($\mathrm{NI}^2\mathrm{L}$): Dr. Changyi Yan, Dr. Shiwei Huang, Dr. Gang Li, I am lucky to be a part of this group where a team spirit truly prevails. Last and the most importantly, I would like to express my deepest gratitude to my family, especially my parents, who always unconditionally support me at any time.

Contents

List of Figures

List of Tables

Chapter 1

Introduction

Currently, multiple-input multiple-output non-orthogonal multiple access (MIMO-NOMA) systems has raised up an explosion of research interest as MIMO has been widely employed in 5G networks. Systematic studies of developing NOMA in 5Gth networks have been started at 2014 [1, 2]. In a primary stage of research, those works were focused on single-input single-output (SISO) system to optimize power allocation or user fairness. The reason for adopting NOMA in SISO owes to its ability of serving multiple users using the same time and frequency resources. However, employing NOMA in MIMO systems is to improve spectrum reuse efficiency through introducing diversity in power domain, which is different from MIMO diversity in the space domain. From this point of view, the design of MIMO-NOMA will be very different from the case of SISO, especially, NOMA power coefficient calculation and successive interference cancellation (CSI) decoding conditions. Besides, the computational complexity is greatly increased. In the following content, we will introduce the definition of MIMO-NOMA, the motivation of our researches, the challenges and the contributions of this thesis in sequence.

1.1 MIMO-NOMA and MIMO-OMA

MIMO is an antenna technology for wireless communications, in which multiple antennas are used at both the source (transmitter) and the destination (receiver) [3]. In a generalized definition, MIMO indicates a multipath propagation technique for sending and receiving more than one data signal simultaneously over the same frequency or time spectrum through the space-time signal processing [4]. MIMO has been employed in many wireless transmission areas due to its advantage of high spectrum efficiency.

MIMO-NOMA is one of employment that explores additional power domain into resource allocation. Similar to NOMA in a single antenna system, signals for different mobile users (MUs) are superposed based on the selected power coefficients and will be transmitted through the same channel. Each MU could detect the desired signals by exploring the successive interference cancellation (SIC) method [5, 6]. However, different from that (NOMA in a single antenna system), MIMO-NOMA involves high dimension beamforming vectors and power coefficients, which brings new properties toward power coefficient calculation and decoding order policy design. Specifically, MIMO-NOMA employs the power coefficient set to distinguish different signals on the power domain.

Different from MIMO-NOMA, MIMO-OMA employs beamforming to spread signal in a specific directions-of-arrival at the transmitter, and separates different signals thorough orthogonal conditions on the space domain at the receivers.

Beamforming is a suboptimal strategy that can transmit data for different MUs simultaneously by using the same time-frequency resource. More specifically, data streams are coded and multiplied by beamforming vectors and then transmitted through multiple antennas [7]. As a result, data for different MUs can be transmitted simultaneously by using the same time-frequency resource without decoding requirements in the receiving end, and also the interference among them can be avoided by Zero-forcing beamforming (ZF). Besides ZF-beamforming in MIMO system, other beamforming approaches, e.g., MMSE beamforming [8], and MRC beamforming [9], were also available for MIMO

transmission. However, through those approaches, different signals would not completely satisfy orthogonal conditions, and interference would be included at received signals. Since they are not available for the MIMO-OMA transmission, this thesis will only consider ZF-beamforming. In summary, MIMO-OMA explores the space-time coding to distinguish different signals on the space domain.

The advantages of MIMO-NOMA can be concluded in three aspects:

- *Higher power and spectrum efficiency:* By exploiting the power domain for user multiplexing, MIMO-NOMA is able to reduce the power consumption due to special diversity. In a MIMO-NOMA cluster, the beamforming vectors of MUs are not necessary to be orthogonal as in MIMO-OMA, due to SIC condition can ensure that the received interference can satisfy SINR (or data rate requirement) after decoding signals. As the power consumption being reduced, more MUs can be served simultaneously, which results in the improvement of spectrum efficiency.

- *Enhanced MU cooperation:* MIMO-NOMA is a kind of MU cooperative transmission approach in MIMO system. Different from device-to-device (D2D), it dose not require a MU as a relay to delivery signals to cooperated MU which has a bad channel condition, but it can remove the signals of the cooperated MUs based on SIC decoding condition. Thus, MIMO-NOMA has a higher transmission efficiency than D2D.

- *Applicable to many wireless transmission scenarios:* MIMO-NOMA can be implemented as a cooperation approach either within a single BS or among multiple BSs, as it can be integrated with many advanced MIMO technologies, such as cloud radio access network (C-RAN) [10] and cooperative multipoint (CoMP) [11]. Moreover, MIMO-NOMA can also be employed in WiFi [12], D2D [13] or mmWave [14] to as a MU cooperative transmission approach.

However, MIMO-NOMA has some disadvantages when it is applied:

- *Channel state information (CSI) should be obtained ahead:* The channel gain information is closely related with the power coefficient calculation, which is the key of SIC condition. Rather than that, the decoding order is also important, which is also based on the channel gain information in many current researches [15].

- *Satisfying SIC condition:* The SIC condition is to ensure that signals from the higher priority MUs can be successfully removed, which requires those signals are higher than some predefined thresholds (it is usually identified by the SINR of the receivers) to become decodable.

- *A high computational complexity:* Forming a MIMO-NOMA cluster should be motivated by improving system performance and also satisfy the SIC condition (i.e., two basic conditions). The computational complexity is incredibly increased with the number of MUs in a cluster, antennas (i.e., dimension of vector), and clustering flexibility (i.e, the number or size of clusters is flexible).

From this point of view, we notice that MIMO-NOMA has to satisfy two basic conditions, which result in MIMO-NOMA not alway be better than MIMO-OMA. Moreover, integrating MIMO-NOMA with many advanced MIMO technologies is challenging but meaningful. This thesis will involve a basic research of a new proposed MIMO-NOMA approach and some applications in C-RAN, CoMP and Unmanned Aerial Vehicle (UAV) association scenarios.

1.1.1 MIMO-NOMA in a single-cell MIMO-NOMA system

In the multi-user and single-cell MIMO system, as shown in Fig. 1.1, we commonly consider MU cooperations in a small cell with a single-BS. In this system, a base station (BS) is equipped with M antennas, and 3 MUs are randomly located, i.e., MU 1, MU 2 and MU 3. The channel gains and beamforming vectors of them are indicated by $\boldsymbol{h}_i$ and $\boldsymbol{w}_i$ for $i \in \{1, 2, 3\}$. If all MUs' signal are transmitted by MIMO-OMA, $\boldsymbol{w}_i$ for $i \in \{1, 2, 3\}$ can be obtained by ZF-beamforming calculation, which satisfies the normalized condition

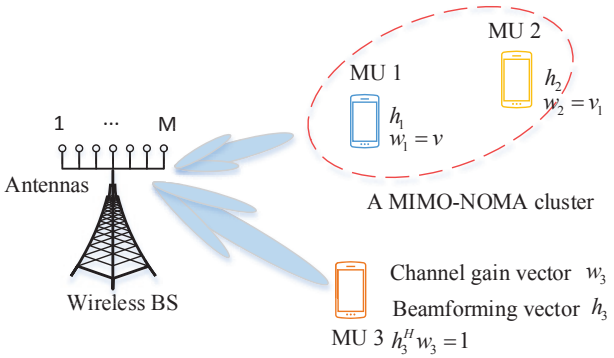

Figure 1.1: MIMO-NOMA

$\boldsymbol{h}_i^H \boldsymbol{w}_i = 1$ and the orthogonal conditions $\boldsymbol{h}_i^H \boldsymbol{w}_j = 0$ $(i \neq j)$. However, if MU1 and MU 2 form a MIMO-NOMA cluster, they will share a same beamforming vector, and their beamforming vectors are changed from $\boldsymbol{w}_i$ to $\boldsymbol{w}_i^{\mathcal{N}} = \boldsymbol{v}$ for $i \in \{1, 2\}$. Then, the non-orthogonal condition within this cluster is indicated by $\boldsymbol{h}_i^H \boldsymbol{w}_j^{\mathcal{N}} \neq 0$ for $i, j = 1, 2, i \neq j$, while the orthogonal condition outside of this cluster is denoted by $\boldsymbol{h}_i^H \boldsymbol{w}_3 = 0$. However, MU 3's signal is transmitted by MIMO-OMA, which will keep the orthogonal condition with all other MUs, i.e., $\boldsymbol{h}_3^H \boldsymbol{w}_i = 0$ for $i, j = 1, 2$. Obviously, in a MIMO-NOMA cluster, the orthogonal condition is invalid.

In this case, the MIMO-NOMA approach design is to integrate beamforming strategies [16–22] and NOMA approach [20,23–28]. Moreover, the cooperation between MUs should be flexible in cluster size and quantity.

1.1.2 MIMO-NOMA in C-RAN networks

C-RAN technology is a novel mobile network architecture which separates the base-band units (BBUs) from the radio access units and migrates them to the cloud, while leaving remote radio heads (RRHs) in the base station (BS) to be responsible for radio frequency signal transmission only [29], as shown in Fig. 1.2 (a). By forming a BBU pool, the baseband processing can be centralized, hence C-RAN is conducive to improve spectrum utilization while maintaining communication quality, and reduce power consumption while offering a better service. In given example of Fig.1.2 (a), RRHs 1, 2 and 3 are close to MU

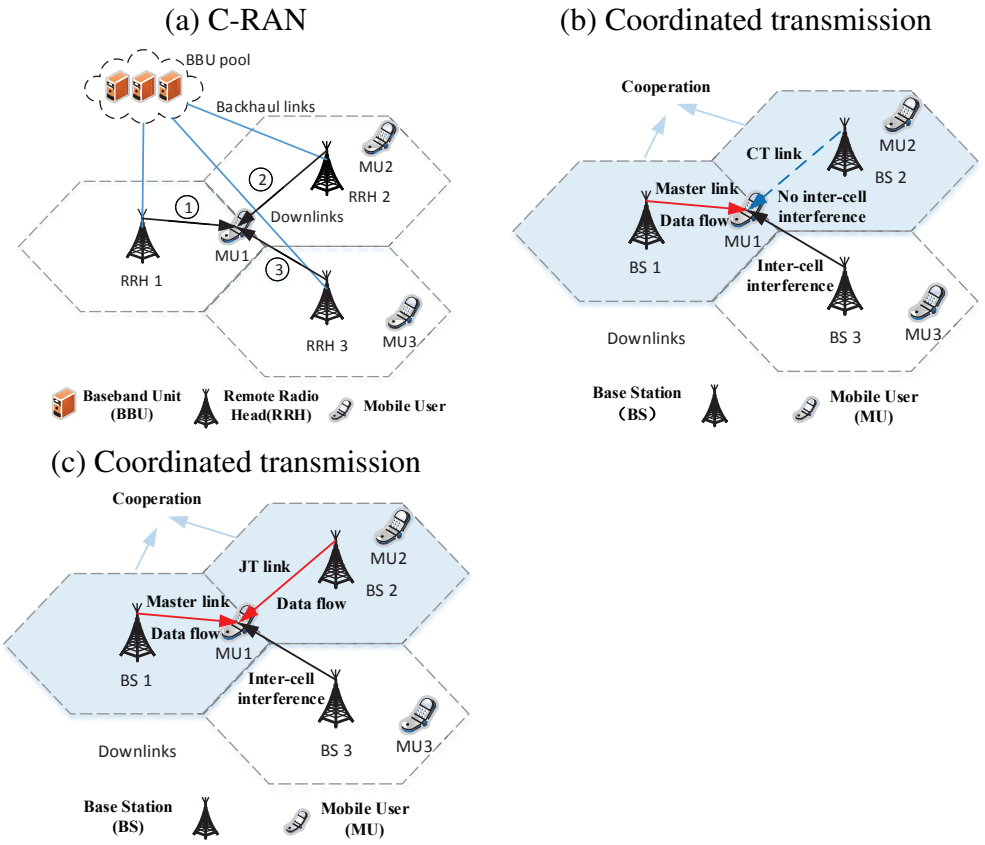

Figure 1.2: Cooperative resource allocation in MIMO system.

1, and can form a cooperation to provide services to it simultaneously. Otherwise, if RRHs 2 and 3 use the same spectrum as RRH 1 for downlink transmission, MU 1 will suffer the interferences from those two RRHs. Except for RRH cooperation, RRH selection (or BS selection) for each MU is another primer issue. In the most of researches, MU will be served by the RRH with the best channel condition, e.g., MU 1 is served by RRH 1. However, as MUs' distribution may be uneven, some RRHs are overloaded, while others are still remaining a lot available resources. Therefore, RRH selection attracts a lot of attention in current researches [30, 31] for a balanced resource allocation.

Due to the centralized management structure, the interference from spectrum reuse can be reduced by RRHs' cooperative resource allocation. A simple case is that BSs would allocate the same spectrum to MUs when their multure interference were lower than a threshold [32]. Currently, CoMP transmission is a main approach to deal with this

problem. In MIMO systems, it can be classified into coordinated transmission (CT) and joint transmission (JT), as shown in Figs. 1.2 (b) and (c) respectively. In the case of CT, the cooperated RRH will not transmit signals to MU, while only allocates beamforming vector to it. In the given example, MU 1 will only receive signal form RRH 1 (the master link), and its received interference is only from RRH 2, because RRH 2 provides a coordinated transmission. More specifically, when RRH 2 calculates its beamforming matrix, the channel gain matrix will include the channel gain of MU 1, so that MU 1 can be orthogonal with other MUs in this RRH. Different from that, JT allows more than one RRH to simultaneously transmit data to a MU in order to improve signal strength. In Fig. 1.2. (c), MU 1 can both receive signals from RRHs 1 and 2. Actually, the JT link and the master link are similar to each other in formulas. However, the master link generally indicates the link from the BS with the best channel condition, which is necessary to each MU, while the JT link is a cooperation link, which exists only for RRH cooperation. Both RRH cooperation approaches can reduce inter-cell interference and optimize system performance. However, JT is more power efficient than CT, while CT will not increase the burden on the backhaul link of RRH, e.g., link between WAN and RRH 2 in Figs, 1.2. (b) and (c).

Employing MIMO-NOMA in C-RAN will bring new features to above mentioned issues. More specifically, MIMO-NOMA is usually conducted within a single RRH between MUs (i.e., intra-cell cooperation), while CoMP is the cooperation among RRHs (i.e., inter-cell cooperation). Integrating MIMO-NOMA with CoMP will create a novel cooperation mode. More specifically, comparing with MIMO-NOMA, the MU clustering and power coefficient should be redesigned since it's transmission may be JT or CT. Comparing with CoMP, when conduct RRH cooperation, each RRH should consider the potential MIMO-NOMA clustering. Therefore, this case is more complicated than any one of them, but benefit from their advantages.

(a) UAV relay (b) Access point (c) UAV BS

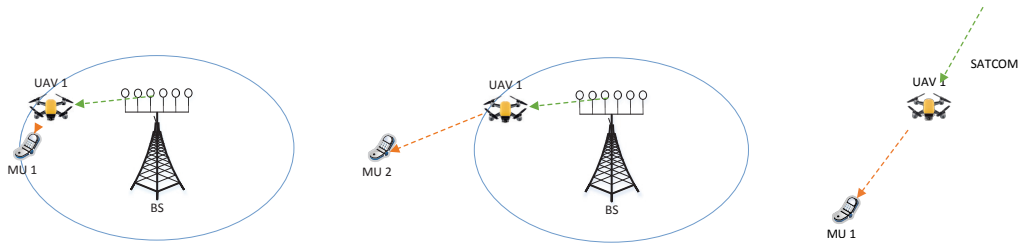

(d) UAV associated MIMO transmission

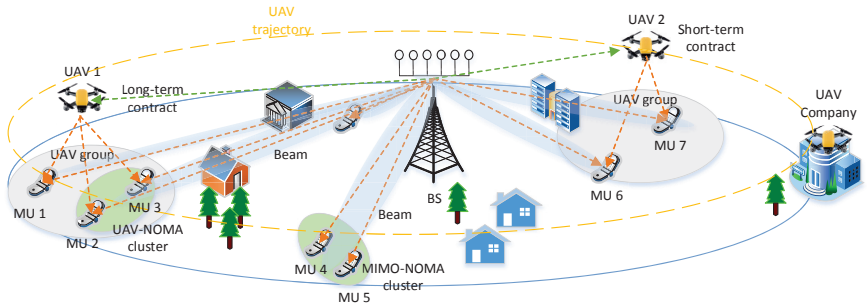

Figure 1.3: UAV applications in wireless communications

1.1.3 MIMO-NOMA with UAV assistance

UAV has been obtained great achievements in aerial photography, drone delivery, aerial inspection and precision agriculture [33], and already been employed into wireless transmissions as it can provide a fast link between the source and a target node. It brings new features to wireless networks, such as, increasing the deployment flexibility of transmitter device whether on location or quantity, or target tracking. In wireless networks, UAV association includes three aspects: relay [34,35], access point [36–38], and small base station (BS) [36, 39]. UAV relay is a popular implementation, which provides a fast link between the source and target nodes in order to increase the data rate or decrease the power consumption [34, 35]. For example, as shown in Fig. 1.3 (a), with the assistance from UAV 1, MU 1 can achieve a higher data rate with a small power consumption, because the distance between the BS and UAV is smaller than that between the BS and MU 1. In 2012, an agreement was reached to dedicate a part of frequency spectrum for exclusive use by UAVs [40]. As a result, in the literature, UAV is assumed to work on an independent

spectrum either between UAV and MU, or the BS and UAVs, hence its transmission only suffered the interference from different UAVs rather than the BS. Besides, UAV also has been employed as an access point to provide network coverage to those MUs in the edge of small cells or the place outside of BS coverage [37, 38], due to its advantages of flexibility and adaptability. For example, MU 2 is outside the coverage of the BS, which cannot access to this BS due to the power limitations of BS and MU device. If UAV 2 is located between them, MU 2 can be accessed to this BS. Moreover, small BS is the most popular usage of UAVs as it can be placed close to the target MU (namely, UAV BS) [36, 39]. For example, if some areas are not under the coverage of any BS, and it requires wireless communication services at some times, the BS can send UAVs to there as temporary small BSs. Another example is that, if some places have temporary high data rate requirements at a specific duration, which is higher than usual and beyond the BS capacity (such as stadium), UAVs can provide a solution for the fast deployment of wireless networks. It is more economic than installing a new BS. However, since the UAV has great limitations on its battery and computational ability, very limited researches are considering to integrate UAV and MIMO transmission. The existing researches include: i) equipping UAV with multiple antennas [41, 42], so that transmission problem becomes 3D dimensional; ii) employing UAV as a relay of uplink transmission [33, 43], in which the transmission from MUs to UAV and from UAV to BS were working on different time slots. Therefore, the study of UAV-MIMO is still in a primary stage, and has great research values.

This thesis considers a new deployment of UAV associated wireless transmission in a MIMO-NOMA system, as shown in Fig. 1.3 (d). Each UAV can provide services to a group of MUs, and in each group, MUs can work on either UAV-OMA or UAV-NOMA transmission modes. In our considered scenario, UAVs cloud be regarded as an extra antenna of the BS, which can augment the signal strength with less power consumption. Especially, it reuse the same spectrum of the BS for downlink transmission. For this case, we design a new beamforming strategy for UAV-NOMA which is an integration of UAV-MIMO and NOMA technologies. Moreover, we notice that UAV placement and the BS

resource allocation are the prerequisite of each other. More specifically, the UAV location selection should depend on the BS resource allocation results, which means that the UAV should be placed close to a MU or a group of MUs to reduce the power consumption. However, without UAV placement, the BS cannot get the optimal resource allocation result if CSI is not available. Thus, integrating UAVs in MIMO-NOMA systems is very challenging.

1.2 Contribution of the Thesis

This thesis addresses on a fundamental research, i.e., MIMO-NOMA clustering, and three extensions, i.e., joint resource allocation in multi-cell MIMO-NOMA systems, combining CoMP with MIMO-NOMA (i.e., CoMP-NOMA) in C-RAN networks, and UAV assisted MIMO-NOMA transmission.

1.2.1 MIMO-NOMA clustering

There has many researches on NOMA wireless transmission in SISO network, while its extensions on MIMO networks are very limited and still in a primary stage. Due to high complexity, existing works on MIMO-NOMA were usually consider a simplified model, such as, an identity beamforming matrix [28, 44], a fixed NOMA cluster [45], or a 2-MU system [27]. By the fact that, as the number of antennas increased, the number of MUs served simultaneously is also increased. However, in our observations, the size of a MIMO-NOMA cluster may not be the larger the better, and some MUs may not be able to be grouped together as they violating the SIC condition. Motivated by this, we address on a flexible MIMO-NOMA clustering approach for system resource optimization, in which both MIMO-OMA and MIMO-NOMA are available for data transmission.

In section III, we propose a new cluster beamforming strategy for MU clustering to minimize the total power consumption. Our main focus includes two aspects: to construct a joint optimization problem and to resolve a multi-user clustering problem. In the first

aspect, we design a novel cluster beamforming strategy to let MIMO beamforming and NOMA power allocation to be jointly optimized. More specifically, this strategy can derive a closed-form resource allocation solution for a specific cluster, and which can be employed on MU clustering process so as to make the resource management and MU clustering to be jointly optimized. For the second aspect, an improved coalition game is proposed to manage MU clustering for power minimization. Moreover, we consider two alternative scenarios, i.e., a power coefficient set (MIMO-NOMA1) or a single power coefficient (MIMO-NOMA2) for power allocation to demonstrate the advantages of our proposed MIMO-NOMA strategy. By further comparing with two existing clustering approaches in literature (i.e., the channel gain-correlation based and the channel gain-difference based approaches), we show that the proposed scheme is more effective in reducing the total number of formed coalitions and the total power consumption. The main contributions of this work are summarized as follows.

- We propose a novel cluster beamforming strategy for MIMO-NOMA and employ it under two scenarios, i.e., MIMO-NOMA1 and MIMO-NOMA2. We employ a general beamforming approach (zero-forcing beamforming) to simplify the computation of our proposed cluster beamforming strategy, so that the peer effect during MU clustering is canceled. Through equivalent transformation, the NOMA power coefficient allocation can be integrated with the beamforming calculation. Moreover, we derive an optimal decoding order which can perform better than the existing works in terms of power reduction.

- We formulate MU clustering as a coalition game due to its advantages of a distributed optimization, so that it has a fast convergence speed and the flexible cluster size. To find the optimal result for the total power consumption minimization, we further make some improvements on the traditional coalition game by following the particle swarm optimization (POS) method which adjusts the utility function for each MU towards a global optimal solution.

- We analyze three major factors that may affect the performance of a MIMO-NOMA cluster: the radius of MUs, the radius difference between two MUs, and the channel correlation coefficient. In simulations, we observe that the radius of the cell-edge MU and the real part of channel correlation coefficient are the key factors influencing power consumption. Based on this fact, we find the radius thresholds under the considered simulation environment.

Based on this research, we employ our proposed MIMO-NOMA clustering approach (i.e., MIMO-NOMA1) into different MIMO systems and integrate it with advanced transmission technologies.

1.2.2 Multi-cell MIMO-NOMA systems

As the MIMO system has been widely deployed and becomes a very important part of our daily life. Employing MIMO-NOMA in a multi-cell system will be an inexorable trend. The fundamental issue of it is that the interference from the spectrum reusing of small cells, especially providing service to the cell edge user will consume much more power than cell central user. Moreover, as the distribution of MUs may be unbalanced, some BS may have a lot of requests from MUs, while others have a lot of reserving resources, such as power. This will result in MUs in different locations may not be able to get a fair and satisfied services. There are two fundamental approaches to address on this issue: CoMP and Heterogeneous networks. Different from them, we provide a new solution to deal with this issue, i.e., MIMO-NOMA. MIMO-NOMA clustering is usually used to manage MU cooperation within a small cell, while it can also to be regarded as a MU migration approach between small cells, i.e., let neighbor BS to provide service to some MUs. Therefore, from this point of view, this problem will involve BS selection, MU clustering and resource allocation.

In section V, we reconsider the complicated MIMO-NOMA resource allocation problem in a multi-cell MIMO-NOMA system with two objectives: sum data rate maximization (O1) and relative fairness (O2), and propose a two-side coalitional matching approach in

order to achieve win-win solutions. The necessary requirements for obtaining a core stable coalitional matching under different objective functions are also derived. Extensive comparisons have been provided in simulations by considering different objective functions, different optimization approaches, and different cluster sizes. The main contributions of this work are summarized as follows.

- We propose a novel cluster beamforming strategy for MIMO-NOMA and derive a closed-form solution for resource allocation based on zero-forcing beamforming. Based on this strategy, NOMA power coefficient allocation can be integrated into beamforming calculation, and the correlation among MUs within a same BS can be eliminated.

- We propose a two-side coalitional matching approach under the consideration of preferences on both MU side and BS side to derive a win-win strategy. We further prove the stability of this proposed approach to ensure system convergence.

- We introduce a new objective function, which reflects the relative fairness among MUs. We identify the weight of each BS to be the number of accessed MUs in this BS based on the fact that the number of accessed MUs is related with the required spatial division of antenna beams. Therefore, MU fairness is associated with the sum data rate.

- We employ the Pauta Criterion as a way of system performance evaluation for the win-win strategy. By eliminating the outliers (i.e., MUs with extreme high data rates), the Pauta Criterion guarantees the obtained results satisfy the conditions that: i) the sum data rate is high; and ii) the difference between the maximum and minimum data rates of MUs is small.

1.2.3 CoMP-NOMA C-RAN networks

As we mentioned before, CoMP targets on interference reducing or cancellation when spectrum is reused by nearby BSs or RRHs. Combining CoMP with MIMO-NOMA

will bring more variety to the RRH cooperation. Three basic CoMP-NOMA approaches are considered in this thesis: JT-NOMA, CT-NOMA and Hybrid-NOMA. The first two approaches which are corresponding to CT and JT in CoMP, the last one is due to our considered NOMA clustering is flexible on size, and the grouped MUs may served by different kind of links (i.e., CT link, JT link or master link).

We start formulating a joint resource allocation problem to minimize the system total power consumption while maximizing the number of accessed MUs. This problem involves the inter-cell cooperation (i.e., CoMP) and the intra-cell cooperation (i.e., MIMO-NOMA), so that modeling CoMP-NOMA approach should base on the properties of CoMP and MIMO-NOMA, and this integration is a new type of cooperation (relates to both the inter-cell cooperation and intra-cell cooperation). To further reduce the computational complexity, we decouple RRH cooperation and MU cooperation, which is solved by our proposed two-stage approaches. In the simulation, we show the advantages of our proposed CoMP-NOMA approach with respect to power and spectral efficiencies. The main contributions of this work are summarized as follows.

- A novel CoMP-NOMA approach (including JT- NOMA, CT-NOMA and Hybrid-NOMA) is proposed based on our work in Chapter 3, and its closed-form solutions can be derived. The SIC and decoding order are discussed.

- A two stage approach is proposed to derive a efficient solution, which design is based on the fact that RRH cooperation has a higher priority than NOMA clustering due to RRH cooperation is more efficient on power reduction than MU cooperation.

- We compares CT and JT links in RRH cooperation and analysis the pro. and con. of them, and observe that JT is more power efficient than CT, while CT will not increase the burden on backhaul link. Thus, we can conclude that the hybrid one can obtain the highest performance due to its can better adapt to different situations.

1.2.4 UAV assisted MIMO-NOMA systems

This work is base on a big assumption that in the near future, UAV are widely used in our daily life for different purpose, such as drone delivery, aerial inspection, precision agriculture [33] and so on. Thus, UAV renting services will be very popular, due to the fact that UAV can provide a fast link between source and target nodes. Due to the data traffic is time varied, the benefit from renting the nearby UAVs for working includes: i) it is a timely response measure to deal with any suddenly requirements from MUs, and the BS can save the investment on the occasional requirement; ii) it is more fast than sending an owned UAV to a specific place; iii) it can save money for UAV maintenance and operation. Currently, we are the first to propose this application, and believe that it is meaningful for future UAV deployment.

In section VI, we propose new algorithms on BS resource management and UAV renting to facilitate the integration of UAVs in MIMO-NOMA wireless networks. Since UAV participation may change channel gain vectors, we redesign beamforming strategies for UAV associated MIMO transmission, and propose a new UAV-NOMA approaches based on a joint MIMO-NOMA strategy. Since UAV's CSI may not be available for the BS before renting a UAV, we propose a profit estimation approach, based on which we can obtain a closed-form function of power reduction. Moreover, we design a contract theoretic framework for UAV renting service, which allows UAV with a single antenna to serve for MIMO transmission. The main contributions of this work are summarized as follows.

- We propose a novel BS beamforming strategy for a UAV associated MIMO transmission and derive a closed-form solution for deriving power allocation and UAV-MIMO beamforming under the consideration of multiple UAVs with a flexible MU grouping.

- We propose a UAV-NOMA strategy to manage resource allocation for UAV renting MIMO-NOMA system, which integrates both UAV-MIMO beamforming and MIMO-NOMA beamforming (i.e., UAV-NOMA beamforming).

- We design a novel framework for UAV renting services based on contract theory. The BS can choose the short-term contract or the long-term contract with respect to different scenarios, which is triggered by the estimated benefits of BS. We also propose a profit estimation approach for the BS when UAV's CSI is unavailable.

- We employ a many-to-many matching game to solve the joint optimization of MU grouping and resource allocation based on the information of UAV channels. If this information is not available, we propose a 2-layer matching game approach to group MU and optimize resource allocation. Both stability and optimality of the proposed methods are proved analytically.

1.3 Game Theory for Cooperative Resource Allocation

Game theory is a mathematical tool to model and analyze situations of interactive decision making [46]. For more than half a century, game theory has been received significant achievements at economics, politics, sociology, psychology, communication, control, computing, and transportation [47]. During the past years, combining game theory with the design of efficient distributed algorithms for wireless networks has been widely adopted. Device-to-device communication [48, 49], fog computing [50, 51] were the most popular applications, due to the competition or cooperation relationships between players were straightforward, and also the physic models were easy to be transformed into player's utility functions. Currently, game theory has been used to investigate the distributed solution for a complex problem, due to its advantages of fast convergence and low complexity. For example, the potential game was used to develop reinforcement learning for an equilibrium solution, i.e., if the formulated function is proved to be a potential game, it will have a convergent solution [52].

In this thesis we use game theory to solve cooperation problems, which include MU clustering, RRH cooperation, UAV association. Comparing with a centralized manner, the advantages of employing game theory for system optimization include:

- *It can reduce the computational complexity.* As the development of large-scale, multi-MU, and heterogeneous communication systems, the control flexibility, the potential expandability and the computation efficiency became fundamental issues to evaluate the performance of system optimization. As a result, game approaches are adopted by many researchers for the Nash or Pareto equilibrium solution, which have the lower computational complexity than centralized algorithms. In this thesis, we transform a centralized problem to be a distributed one and solve it by a distributed algorithm. More specifically, we can split the whole problem into many parts, and each part is responsible by a player. Thus, each player only needs to make a local information-based decision, so that the computational complexity can be reduced.

- *It can improve the computational capacity.* As a distributed design, it allows the variety of network entities to be involved into the control strategy and conducted by cloud computing technology. More specifically, they could act as independent and selfish decision makers, and follow a certain principle to make decision until converge to a common agreement. As a result, the distributed control mode is preferable than the centralized one, as it has a higher robustness and a lower computational cost. Nash equilibrium and Pareto optimality are two frequently-used principles. After proving the existence of an equilibrium solution, they can finally converged.

- *It can fulfill the requirement of user satisfaction or the quality of service (QoS).* As the strategy of each player is triggered by improving it's own utility, user satisfaction or the quality of service (QoS) can be greatly ensured in the final solution. Moreover, game theory was superior on the study of cooperation behaviors than the convex optimization approaches.

- *It has high flexibility and is easy to be extended for a large scale system.* Due to the distributed utility design, it is very convenient to be employed for a large scale system with many players considered. Moreover, if a game is proved to be stable (i.e., core

stable or existing equilibrium solution), due to the computational complexity of each player is unchanged, increasing the number of players only increases the iteration that reaching the final convergent solution.

The basic classification of game theory includes non-cooperative game and cooperative game. The difference of them could be distinguished by its' name, i.e., players in the non-cooperative game would try to maximize its' own utility and act to be selfish, while players in the cooperative game would maximize the group utility and share the benefits with cooperators. With the development of game theory, many advanced game approaches were designed to be more specialized for different scenarios or applications. In this thesis, coalition game and matching game are main considered approaches, and all approaches are improved according to considered network scenarios.

For the MU clustering problem, the coalition game was a powerful tool for all kinds of clustering problems. It could be a ground coalition game, in which each player has only two choices: join the coalition cluster or leave it to be independent. For example, in [53], a coalition formation game was proposed to group multiple BSs in small cells. As a result, they could perform cluster-wise joint beamforming. Another kind of coalition game was named as the distributed coalition game. It means that there were probably existing more than one clusters, and all players were allowed to form a cluster with any other player if the condition was satisfied. The condition for a stable coalition game was based on the merge-and-split rule, which would lead to the Pareto-optimal solution. In [54], a standard distributed coalition game was employed to solve the MU clustering problem in order to form a virtual multiple antenna system. Moreover, the cluster size could be fixed or flexible according to the requirements of networks.

For antenna selection (or BS selection) problem, the matching game was an efficient approach. The basic ideal of a matching game was to form a two-sided matching market, and in each side the object (utility function) could be same or different [55]. According to the size of choice, it could be further classified as, one-to-one (i.e., the players in each side can only form a cluster with only one player in the other side), many-to-one/one-to-many

(i.e., the players in the side B can form a cluster with more than one players in the side A, while the players in the side A can only choose one player in the side B as the cooperator), and many-to-many (i.e., players in both sides can have more than one cooperators). In [56], the proposed joint uplink/downlink subcarrier allocation problem was modeled as a two-sided stable matching game, in which the joint uplink/downlink QoS requirements of the users were satisfied. In [57], through the many-to-one stable matching game framework, the multiple network operators were allowed to share some of their spectrums to maximize the social welfare of the network. Based on the advantage of the matching game, we can employ it on the following problems: MIMO antenna selection, MU clustering with fixed number of clusters, or BS selection.

1.3.1 Coalition game

Coalition game is widely used as an efficient cooperation strategy for the players with cooperation relationships. Take MIMO-NOMA for example, if MUs are regard as players of a cooperation progress, cooperation behaviors among them can be modeled as coalition formation game. However, if players include MU and BS, since there may exist three different cooperations: among BSs, among MUs, and between BS and MU, the traditional coalition game cannot deal with this problem without improvements. In this section, we only introduce the traditional coalition game. The improvements on coalition game for our addressed problems will be introduced in the corresponding chapters.

The coalition game has two types of classifications: i) the grand coalition game and the coalition formation game; and ii) with transferable payoff and with non-transferable payoff. The difference between the grand coalition game and the coalition formation game is that the formed cluster is one or many. In the grand coalition, all players has two strategies: join or not join the predefined cluster. However, for the coalition formation game, each player has to decide to join which cluster, hence the strategy space is larger than the former. The coalition game with transferable payoff means that a player in a cluster can transfer part of its utility to the players in the same cluster, so that the group utility can be distributed by

many ways, such as equal division, divisions by the Shapley value, and so on. However, in the coalition game with non-transferable payoff, each player in a cluster can only have its share of utility, which is not shareable. In this thesis, we only consider about the coalition formation game.

Coalition game has four basic components:

- *The set of player:* It usually denoted by N, such as, MUs in a wireless networks.
- *A coalition S:* The players in N will decide either join or not join a coalition. Here, S is an uniformed notation, it could be S_1, S_2... and so on.
- *Mapping: v:* It is defined as a function that maps each group of players to a real-valued payoff, i.e., utility function of a singer player or a coalition cluster.
- *Group utility division policy:* transferable payoff or non-transferable payoff.

Thus, a coalitional game can be defined by the pair (N, v). In a coalition game, each player's behavior is motivated by its utility, which means that if a player found joining (or leaving) S can improve its utility, it will perform corresponding behavior.

The fundamental issue of formulating a coalition game is that the final solution is stable and optimal. The stable solutions include core stable solution and Pareto equilibrium solution. The basic idea and principles of each kind of solution will be introduced separately as follows.

Core stable solution

Definition 1.3.1. *The core of a coalition game is no empty iff no player has an incentive to leave or join any group to improve its utility. Otherwise, the core is empty.*

For example, consider a five-player game with $N = \{1, 2, 3, 4, 5\}$, and let $S_1 = \{1, 2, 3\}$, $S_2 = \{4\}$, $S_3 = \{5\}$, and $S_4 = \{4, 5\}$. Then, two partitions are existing: $B_1 = \{S_1, S_2, S_3\}$ and $B_2 = \{S_1, S_4\}$. If B_2 is a core solution in the case of transferable payoff, the utility of players should satisfy $v(S_1) + v(S_4) > \sum_{i \in N} v(i)$, while in the case of

non-transferable payoff, it should satisfy $v(i, S_4) > v(4)$ for $i \in S_4$. However, a coalition game may exist many core solutions. If $v(S_1) + v(S_2) + v(S_3) = v(S_1) + v(S_4)$, both B_1 and B_2 are core solution. The reasons of empty core include: i) no cooperation can improve the players' utility, i.e., $v(S_1) + v(S_2) + v(S_3) = v(S_1) + v(S_4) = \sum_{i \in N} v(i)$; and ii) a cycle exists [58]. The reasons of existing a cycle in a coalition game for different problems are varied. We use given example to explain a possible case. In a coalition game, if the utilities of all players are mutual effect, we may have $v(S_1) > v(1) + v(2) + v(3)$ and $v(S_4) < v(4) + v(5)$, and B_1 is formed. After that, we find $v(S_4) > v(4) + v(5)$, and S_4 is formed. However, this cluster will bring a negative effect to a formed coalition S_1, and make $v'(S_1) < v'(1) + v'(2) + v'(3)$.Then, this coalition, i.e., S_1 will split, which makes $v(S_4) < v(4) + v(5)$. Then, the cycle is formed.

There are some principles to determine whether a coalition game has core stable solutions [47]:

- The formulated game is a convex coalition game, i.e., $v(S_1) + v(S_1) \leq v(S_1 \cap S_2) + v(S_1 \cup S_2), \forall S_1, S_2 \in N$.
- The group utility must be comprehensive. It means that in a coalition cluster, the utility of any players will be higher than that of subsets, i.e., $v(i, S_1) \geq v(i)$ or $v(S'), \forall S' \subseteq S_1 \subseteq N$.
- The utilities of all players in a cluster should be larger than that when they leave this cluster.

In summary, if we follow this instruction, we can claim that the proposed coalition game has core stable solutions. Since a coalition game may have many core stable solutions, the nucleolus is defined as the best allocation strategy for system performance improvement. For example, if the objective of proposed problem is to minimize the BS power consumption, the nucleolus is the solution which has the minimum total power consumption.

Pareto equilibrium solution

The Pareto equilibrium solution is another way to search for solution in coalition game, which is claimed to be Pareto-optimal.

Definition 1.3.2. *Consider a coalition game with N players. If $B_2 = \{S_1, S_4\}$ is Pareto optimal, there is no other feasible partitions B_1 with the utility for each player i satisfying $v(i, B_2) \leq v(i, B_1)$ ($i \in N$).*

The Pareto equilibrium solution belongs to the core stable solution with higher requirements. In the case of a core stable solution, the condition for a player joining (or splitting) a coalition is that the utility of it is increased. However, the Pareto optimal solution is more strict than that. It requires that the behavior of any player will not bring the negative effect to the corresponding coalition cluster. For example, i) the utility of all players in a cluster will not be decreased and lower than any MUs leaving from this cluster; and ii) If a player joins a coalition cluster S, it will not decrease the utilities of any players in this cluster.

The Pareto equilibrium solution is more complicated than the core stable solution. To find the Pareto equilibrium solution, designing a coalition game should follow three basic principles: a well-defined order of player's preference (i.e., Pareto order), the merge-and-split rule and the stability discussion.

Definition 1.3.3. *To compare two possible coalition clusters, such as $S_5 = \{1, 2\}$ and $S_6 = \{1, 3\}$, if $v(1, S_5) > v(1, S_2)$, the player 1 prefers S_5 than S_6. We denote this primitive binary relation by $\succ$, i.e., $S_5 \succ_1 S_6$.*

Thus, for each player, it will have a preference order for all possible coalition clusters based on its utility function.

The merge-and-split rule is defined as follows.

- Merge: For any player $i \in N$, it may be merged into a coalition cluster S, if it prefers this cluster than others, and all players in this cluster (i.e., $j \in S$) are also prefer this

combined cluster $S' = \{i \cup S\}$, i.e., when $v(i, S) > v(i)$ and $S' \succ S$ for $j \in S$, player i will be merged into it $\{i, S\} \rightarrow S'$.

- Split: For any coalition cluster S, if any player $j \in S$ can obtain a larger utility in a smaller coalition cluster, it will split from this cluster.

The ideal behind the merge-and-split rule is that, for either merge or split behavior, all related players should reach the agreement that this coalition solution is their preferred. Thus, the merge-and-split rules with Pareto order can be regard as a dynamic coalition formation algorithm. The stability of Pareto equilibrium solution is defined by a defection function $\mathbb{D}$.

Definition 1.3.4. *A partition $B_2 = \{S_1, S_4\}$ is $\mathbb{D}$-stable if no groups of players can benefit from changing its strategy.*

The $\mathbb{D}$ stability includes $\mathbb{D}_{hp}$ and $\mathbb{D}_c$. $\mathbb{D}_{hp}$ is a weak equilibrium-like stability, which implies that no players have an interest in performing a merge or a split operation. In $\mathbb{D}_c$, the outcome of the arbitrary merge-and-split approach from any given initial state is unique. There are two necessary and sufficient conditions to justify that a coalition exists $\mathbb{D}_c$ solution.

- For each disjoint subset of a coalition cluster, i.e., S_1 and S_2, $\{S_1 \cup S_2\} \subseteq i$, and $S = \{S_1 \cup S_2\}$, the condition for S formed is that $\{S_1 \cup S_2\}^i \rhd \{S_1, S_2\}^i$.

- For each player $i \in N$, its possible coalition cluster is incompatible. It means that i) its utilities on different possible coalition clusters are different, so that the preference of it is strict; and ii) no cycle exists.

The notation $\subseteq$ indicates domination, which means that the combined set $\{S_1 \cup S_2\}$ is better than any subsets, i.e., S_1 and S_2, in the benefit of player i. If the final solution satisfies these two conditions, we can claim that the Pareto equilibrium solution exists and can be derived by periodically taking distributed merge-and-split decisions.

According to those descriptions, in this thesis, MIMO-NOMA clustering and UAV-NOMA clustering can be modeled by coalition game strategies, in which MUs can be regarded as game players, and its utility function can be defined by the benefits from the cooperative transmission.

1.3.2 Matching game

Matching game is initial from a two-sided-market design (e.g., workers and employers, interns and hospitals, students and universities) [59]. A matching problem is given by: i) players in two different sides; ii) each player in each side has its preference toward players in the other side [55]. For example, in the multi-cell MIMO-NOMA systems, the problem of BS selection can be modeled as an one-to-many matching game. It include two sides: the MU side and the BS side, and the objectives of players in different sides can be different.

From the past development, matching problems can be summarized into three main classifications from easy to complicated: one-to-one, one-to-many and many-to-many, which are defined by the size of the cluster that a player can form. For example, if a MU can only select one BS as the service provider, while each BS can serve for many MUs simultaneously, it can be regarded as an one-to-many matching game. Therefore, in the case of many-to-many matching game, players in both sides can select many players in the other side. For example, in UAV assisted MIMO-NOMA systems, each UAV can provide services to many MUs, while MUs can also select many UAVs for data transmission assistance.

The stability of a matching game is judged by a condition: there are no blocking pairs existed. More specifically, let $\Gamma \subseteq A \times B$ denote the set of acceptable pairs, μ indicate a stable matching solution. It should satisfy the condition that for any pair (A,B) (in an one-by-one matching game) from μ, i) player $a \in A$ prefers $b \in B$ than other players in its preference list, i.e., $\mu(a) = b$, and ii) player b prefers to accept a than any other available choices, i.e., $\mu(b) = a$. A blocking pair exists, such as (a, b'), if player a prefer b' more than $\mu(a)$, and player b' prefers to accept a than any available choices. This description can

extend to the case of one-to-many and many-to-may. The only different is that a player will have a preference toward a set of players in the other side.

By the classical result of Gale-Shapley algorithm [60], a stable solution can always be obtained. For a better description, we assume the players in the side A are a_1,..., a_n, while the players in the side B are b_1,..., b_m. The steps are:

- Step 1: Each player in the side A sends a request to its most preferred player in the side B.
- Step 2: Each player in the side B holds the most preferred player from the receiving requests, and rejects the rest of them.
- Step 3: If a player in the side A is rejected, it will delete the corresponding option in its preference list, and re-send a request to its most preferred player in the side B.
- Stop : When no further requests are send, the holding request in the side of B will be accepted.

If a stable solution exists, it is identified as A-optimal. It means that the final solution is the optimal choices of the A side, while not for the B side, which also is the drawback of this algorithm.

There are many studies on manipulating this approach to be a more advisable solution. Especially, in the case of one-to-many and many-to-many approach, pairwise-stable matchings and core-stable matchings are two basic solutions of improvement, and the setwise-stable is a combination of them. However, the key point of them is that no blocking pairs are existed in the final solution, so that no system cycle will exist. The basic concepts of one-to-many and many-to-many matching are similar, which are listed as following.

Definition 1.3.5. *A matching μ is blocked by an individual $i \in A \cup B$, if there exists any player $j \in \mu(i)$ and $\emptyset \succeq_i j$.*

Therefore, if a matching is not blocked by any individual, we name it as an individual rational matching.

Definition 1.3.6. *A matching μ is blocked by a pair $(a', b') \in A \times B$. It means that, in matching μ, a' and b' are not matched together, i.e., $\mu(a') \neq b$ and $\mu(b') \neq a$. However, it has i) $a' \succeq'_b i$ for player $i \in \mu(a')$ and $b' \succeq'_a j$ for player $j \in \mu(b')$.*

Definition 1.3.7. *A matching μ is pairwise-stable if it is not blocked by any individual or a pair.*

For one-to-one matching problem, if every player has strict preference, an A-optimal solution is pairwise-stable.

Definition 1.3.8. *A matching μ is corewise-stable if it is not dominated by any other matching.*

For example, μ is weakly dominated by an individually rational matching μ' via a pair (a', b'). It means that all players in this thesis will satisfy: i) if $i \in a'$, it has $\mu'(i) \succeq_i \mu(i)$; and ii) if $j \in b'$, it has $\mu'(j) \succeq_j \mu(j)$.

If all players have strict preference or max-min preference, the deferred acceptance algorithm can yield a pairwise-stable solution. The max-min preference [61] is proposed for one-to-many and many-to-many matching games. Since a player in the B side may hold a group of players in the side A, in the max-min preference, we identify S_1 and S_2 as the sets of holding players in the side B, and the number of them are denoted as $|S_1|$ and $|S_2|$,

- (i) If S_2 is a subset of S_1, we have $S_1 \succ_B S_2$.
- (ii) If $|S_1| > |S_2|$ and B strictly prefers the least preferred player in S_1 to that in S_2, we have $S_1 \succ_B S_2$.

Besides the max-min preference, other approach is also available if it can make the players in the side B rank the group of players of the side A. In this thesis, our formulated utility function could satisfy this condition.

We assume the maximum number of players can be selected or accepted in two sides are α_A and α_B. If $\alpha_A = 1$, it means that the player in the A side can only select one player

in the other side, and it is a many-to-one matching game if $\alpha_B > 1$. The steps of deferred acceptance algorithm are:

- Step 1: Each player in the side A sends requests to its most preferred player in the side B, and the total number of requests should be less than α_A.
- Step 2: Each player in the side B holds the most preferred selections from the receiving requests, and rejects the rest of them. The total number of holding requests should be less than α_B.
- Step 3: If a player in the side A is rejected by some players in the side B, it will delete the corresponding option in its preference list, and re-send a request to its most preferred player in the side B. Total number of requests should be less than α_A.
- Stop : When no further requests are send, the holding requests in the side of B will be accepted.

Since no player in the side of A will select a same player twice, it always come out a stable solution, i.e., pairwise-stable solution. However, a pairwise-stable solution may not be the corewise-stable solution. For a better understanding of these two concepts, we use an example to explain the difference between the pairwise-stable solution and the corewise-stable solution. The preferences of both sides are listed as

$$\succ_{a_1}: b_3, b_2, b_1; \succ_{a_2}: b_2, b_3, b_1; \succ_{a_3}: b_3, b_1, b_2;$$
$$\succ_{b_1}: a_1, a_2, a_3; \succ_{b_2}: a_2, a_1, a_3; \succ_{b_3}: a_3, a_1, a_2.$$

After employing the deferred acceptance algorithm, the pairwise-stable solution is μ, in which $\mu(b_1) = \{a_2, a_3\}$, $\mu(b_2) = \{a_1, a_3\}$ and $\mu(b_3) = \{a_1\}$. It is also a corewise-stable solution. However, this matching game exists another corewise-stable solution μ', in which $\mu'(b_1) = \{a_1, a_2\}$, $\mu'(b_2) = \{a_2, a_3\}$ and $\mu'(b_3) = \{a_3\}$. This solution is not a pairwise-stable solution, as $\{b_3, b_2\} \succ_{a_1} \{b_2, b_1\}$ and $\{a_3, a_1\} \succ_{b_3} \{a_3, a_2\}$, (a_1, b_3) will block μ'.

For the problems of BS selection and UAV association, the matching game was an efficient approach, in which the cooperation between two sides can be modeled as matching

process. However, due to a joint consideration of MIMO-NOMA, the MU preference will be affected by MU clustering. Therefore, the traditional approach should be improved for a pairwise-stable solution.

1.4 Challenges

The challenges of those researches can be summarized into three aspects:

- System optimization is extremely complicated. Since many variables and limitations should be considered (such as the vectorial channel gain, the different kinds of cooperation between MUs or BSs, the traffic capacity, and the CSI estimations), the system optimization becomes a multi-variable (or even with multi-objective) optimization problem. Besides, in the most of cases, we need to consider more than one kind of cooperations to make it feasible for different scenarios. The most effective way is to explore the inner relationship hidden behind the multi-variable for a joint design.

- The optimization approach should be flexible and fast convergent. As the computation complexity is greatly increased with the number of MUs, BSs and antennas, the distributed optimization approach will be more superior than a centralized one. Therefore, in this thesis we will discuss about how to employ game theory to solve a centralized optimization problem in cooperative resource allocation of MIMO systems.

- New requirements of smartness and robustness are raised for the future MIMO systems. It requires system not only to have an intelligent response for different requirements from MUs but also be durable for possible system failure. The potential solution is to involve MUs' willing into resource management or let them participate in system resource allocation to form a half-distributed control system.

The rest of this thesis is organized as follows. In Chapter II, we review the existing

researches on cooperative resource allocation in MIMO system. In Chapter III, we introduce our proposed MIMO-NOMA approach, and formulate a joint resource allocation for power reduction. In Chapter IV, we formulate a multi-cell MIMO-NOMA resource allocation problem, which joint considers BS cooperation and MU clustering. In Chapter V, we combine MIMO-NOMA with CoMP in a C-RAN network. In Chapter VI, we employ MIMO-NOMA into a UAV associated MIMO network, and propose a UAV-NOMA transmission approach.

Chapter 2

Literature Review

MIMO systems have been studied for a long time. However, as the continuous development of wireless networks (from the 1G to current B5G networks), MIMO-NOMA has been considered as an important technology to improve system performance. Moreover, game theory on system optimization is popular due to its fast convergent speed and low calculation complexity.

2.1 MIMO-NOMA approach

The fundamental ideal of MIMO-NOMA was a combination of NOMA and MIMO, which was an extension of NOMA technology in a single antennal BS scenario in [62]. In [26], the MIMO-NOMA was proved to be strictly better than MIMO-OMA in terms of sum channel capacity. Unfortunately, it only used the SIC condition to remove the inter-cluster interference, while not considering the successfully decoding condition. If considered a multiple-MU scenario with random distribution around BS, MIMO-NOMA might not be better than MIMO-OMA, which is analyzed in Chapter 3. Thus, we think that MIMO-NOMA and MIMO-OMA strategies should both exist in the system. Research in [63] investigated the relationship between the size of cluster and the sum data rate. It claimed that when power limitation is not considered, MIMO-NOMA would be always

better than MIMO-NOMA. Unfortunately, this research only considered to remove inter-cluster interference based on the benefit from NOMA, while not discussing the availability of SIC condition. In Follows, first, we give a brief introduction of all studies of MIMO-NOMA technology, and then focus on the area of resource allocation of MIMO-NOMA.

Currently, MIMO-NOMA technology has been widely employed in 5G networks, which includes the area of mmWave [14, 64–66], D2D, V2V [67], relay [68, 69], pilot assignment in massive MIMO [70–73], HetNet system [74, 75], and visible light communication [76]. Besides those employments, some researches are focused on advanced MIMO-NOMA technology, which includes novel precoding algorithm [27, 77–79], decoding strategy design [80], outage probability evaluation under imperfect CSI [81], uplink transmission [82], and resource allocation [20, 24, 25, 25, 68, 81, 81, 83, 83, 83–85, 85, 86, 86, 87, 87–89, 89–91]. Almost all of them focued on the resource allocation problem. Clustering strategy design can be related with an advanced decoding strategy, which includes MU ordering management, power coefficient calculation and MU selection. MU ordering management means to decode MU messages by a certain order. Both MU ordering management and power coefficient calculation should satisfy CSI condition. It means that, for any MU, the detected signals of MUs in the front of its decoding order should be larger than its received signal (we will give more details in the later chapter). However, in the most of researches, which concerned decoding strategy design, MU selection was not generally put into considerations. In [77], a linear precoding approach was proposed for signal superposition for a randomly paired MIMO-NOMA cluster. In [78], interference alignment (IA) technology was applied into MIMO-NOMA, which is a decoding strategy to align the unwanted received signals into an interference-subspace. In [27], MED (minimum Euclidean distance) precoding algorithm was proposed, and user pairing was based on the condition number or orthogonality defect for a 2-MU cluster owing to this special precoding strategy.

In those researches, the designed clustering strategies were simply based on the feature of channel gains (such as correlation coefficients), and each of them has a prominent

purpose of optimization, such as QoS guaranteed [77] or combined with other decoding strategy [78]. After that, resource management can be formulated as an optimization problem to further optimize the power allocation. Moreover, in [80], a linear minimum mean-square error (LMMSE) multi-user detector was designed for a low-complexity computations of the receiving ends.

More researches were concentrated on a joint problem of clustering and resource allocation. Note that in the earlier work, due to the high complexity of computation, most of works adopt a simple clustering strategy (e.g., correlation coefficients [83] and channel gain differences [20] are two fundamental strategies for MU clustering [25]). The correlation coefficient is calculated by

$$v_{i,j} = \begin{cases} 0 & \text{if } \left|10\log|\boldsymbol{h}_i|^2 - 10\log|\boldsymbol{h}_j|^2\right| \leq 3dB, \\ \left|\tilde{\boldsymbol{h}}_i \cdot \tilde{\boldsymbol{h}}_j\right|, & \text{Otherwise,} \end{cases} \tag{2.1}$$

where $\boldsymbol{h}_i$ and $\tilde{\boldsymbol{h}}_i$ are channel gains of MU i with and without path-loss coefficient, respectively. The correlation coefficient is leveraged by the orientations of MUs. For example, if they are located in the same direction of transmission, e.g., MUs 1 and 2 in Fig. 1.1, their transmit beam will be overlapped, and $\left|\tilde{\boldsymbol{h}}_i \cdot \tilde{\boldsymbol{h}}_j\right| = r_i r_j$. Otherwise, this value will be reduced as their included angle is increased. This strategy employs the condition $\left|10\log|\boldsymbol{h}_i|^2 - 10\log|\boldsymbol{h}_j|^2\right| \leq 3dB$ to ensure that the distance between two MUs is larger than a predefined value based on the SIC condition.

The channel gain difference is based on the fact that the distance between two MUs should be large enough. It can be denoted by

$$\pi_{i,j} = \begin{cases} ||\boldsymbol{h}_i| - |\boldsymbol{h}_j||, & \text{if } \frac{|\boldsymbol{h}_i \cdot \boldsymbol{h}_j|}{|\boldsymbol{h}_i||\boldsymbol{h}_j|} > 0.4, \\ 0, & \text{Otherwise.} \end{cases} \tag{2.2}$$

Both strategies are only available for a 2-MU cluster. In [25], the dynamic power allocation was modeled by maximizing the total data rate while satisfied CSI condition for each single cluster, which is a separated process of MU clustering. In the early work, MIMO-NOMA clustering was assumed to be simple, e.g., 2-MU cluster, fixed power

allocation strategy. In [24], a MU pairing was conducted between two MUs within two radius ranges according to the effective small scale fading gain (i.e., the MU will pair with the other MU in different radius ranges with a larger channel gain-correlation value), in which the MU closed to cell-edge should be first decoded. The cognitive radio inspired power allocation strategy was compared with the fixed power strategy, which is derived by the SIC condition. In [68, 84], MU clustering was combined with the antenna selection problem in a MIMO system, in which MUs in different clusters were working with different antenna sets to satisfy orthogonal condition, while in the same cluster, MUs have the same set of antenna with different power coefficients. MU clustering and antenna selection were solved by a matching approach, and the utility of each player (i.e., MU) was defined by the channel gain-correlation value. However, this work considered a simple case of 2-MU cluster and fixed power coefficient. Rather than that, a further research about the orientation related MU clustering approach was raised up in [85], which proposed a beam division-NOMA (BD-NOMA) to demonstrate that MUs in a cluster should be located in the same beam. In this research, MUs which have the same statistical channel characteristic (i.e., large-scale channel gain) would be regarded in the same beam, and MU clustering was to find the best 2-MU group which has the maximum total SINR value in each beam. The power allocation was jointly optimized with MU clustering process based on the CSI condition.

MU clustering in a multiple-MU MIMO system was studied by [81, 86, 87]. The basic steps of them can be summarized by: i) divide all MUs into several groups based on the order of their channel gains (e.g., mean value or 2-norm square value); ii) select one MU in each group to form a cluster. The first step is based on the fact that a cluster should include a cell-central MU and a cell-edge MU. More specifically, in [86], all MUs were divided into two groups by their order of the 2-norm square of channel gains. Then, MUs in two different groups with the maximum difference in channel gains were paired first. Until all MUs were paired with the other MU, the step of MU clustering was finished. After that, authors formulated a max-min sum data rate problem to calculate the power allocation.

In [87], a low complexity beamforming and user selection scheme were investigated, in which all MUs were divided into G groups by their mean value of channel gains. More specifically, in each time slot, only one user will be selected from each group and served by the shared spectrum resource. In this paper, MUs in the same group are regarded as the same choice to a MIMO-NOMA cluster, which is based on the fact that users in the same group will have similar mean value of channel gains (i.e., with similar distance from the BS). Therefore, MU clustering is to randomly select MU from each group However, according to researches [83, 85], we already learn that the orientation of MU plays an important role in MU clustering. Thus, the proposed MU clustering approach is not an efficient strategy. The similar model was also studied in [81], which aimed to derive a closed-form outage probability under imperfect CSI. Furthermore, in [88], authors explored the complex-valued power allocation coefficients to stagger the user signals in phase. This design can remove the inter-cluster interference without using ZF beamforming. However, this research didn't involve MU clustering into system optimization.

MU clustering should be considered into resource allocation to formulate a joint problem. However, existing works do not really combine the MU clustering with the resource allocation, because MU clustering and resource allocation (i.e., power allocation) are usually separated considered, i.e., with different objectives, and proceeding in different steps. Researches [89] focused on the resource allocation problem under the condition of a fixed cluster, and most of them are based on correlation coefficients [83] strategy due to the good performance. The research in [89] focused on power allocation for ultra-reliable low-latency communications, which included the inter-cluster and intra-cluster power allocations. In the proposed framework, the MU clusters were considered to be predefined and fixed. Then, the whole problem can be decoupled into two sub problems: i) optimize the inter-cluster power coefficient to minimize the maximum of the delay target violation probability; and ii) minimize the intra-cluster power allocation under the condition that delay target violation probability should be less than a predefined bound. In [90], a dynamic user clustering algorithm was proposed to divide users into a number

of clusters. Then, a joint optimization of channel allocation and power allocation was formulated to maximize the sum effective capacity of all users. However, the clustering approach is simply based on the channel gain correlation coefficient and solved by an iteration approach. Other dynamic power allocation approach such as in [91] was designed to maximize the sum data rate of a 2-MU cluster. Without of generality, the most difficult part in those researches is how to integrate the MIMO-NOMA clustering with resource allocation, which is a mixed integer programming, and all of them are adopted a two-stage approach due to the huge complexity. However, if we consider the case of real applications, MU clustering shouldn't be restricted to the case of 2-MU cluster with different radium ranges or within a limited orientation conditions, while it should be a flexible size of cluster with any radium ranges. It is because the three conditions (the size of cluster, the radium range, and the orientation limitations) will jointly decide the performance of MU clustering. If we only consider some of them as the judgement of MU clustering, and then proceeded it by a linear calculation approach, the performance of MU clustering wouldn't be good enough. That is the biggest motivation of our proposed MU clustering strategy, which makes the MU clustering and resource allocation become a real joint optimization problem.

After introduce the current work of literature, we can classify the work of MU clustering which employ multi-stage optimization approaches into two categories:

i) MUs were grouped in the first stage based on their locations, e.g., the channel gain-correlation based clustering approach [83], and the channel gain-difference based approach [20]. After MU clustering, the MU group set was fixed based on an assumption that NOMA was always better than OMA. Then, system optimization could be formulated to be a problem by adjusting power allocation coefficients or calculating beamforming vectors to minimize the power consumption or maximize the sum-rate. However, this design is not applicable for a large scale MIMO system, as NOMA may not be always better than OMA. Moreover, as we demonstrated in Chapter 3, the performance of MIMO clustering will be influenced by the distance between MUs, the channel correlation coefficient and the

beamforming strategy. In addition, decoupling MU clustering and the system optimization might result in solution deviated from the optimum.

ii) In the first stage, an optimization was conducted on a specific NOMA cluster to get a closed-form solution for power allocation and beamforming strategy [17]. Then, it could be applied to search for an optimal cluster set among a large quantity of MUs to maximize system performance. However, this approach could only be implemented for a 2-MU system. In [92], matching game approach was employed in a MU clustering optimization in the networks with a single antenna BS, where users and sub-channels were considered as two sets of players. This heuristic algorithm grouped MUs into limited sub-channels and maximized the total sum-rate without limitations on MU cluster size.

Therefore, to maximize the benefits from MU clustering, the joint optimization and cluster flexibility are important in the future research.

2.2 MIMO-CoMP and MIMO C-RAN

CoMP has been widely employed in MIMO BS cooperation as it could effectively deal with the inter-cell interference. In previous research, some limitations were setup on the number of cooperated BS or MU clusters for the case of the multi-objective optimization [93, 94]. In resent research, MU dynamic clustering was excavated to make CoMP become adaptive in multi-cell MIMO systems. As a result, the cooperations became flexible and adaptive to most of MIMO scenarios [95]. The other tendency was that the advanced algorithms were employed for MU clustering and multi-objective optimization, such as the evolutionary algorithms in [96], and the particle swarm optimization in [97].

C-RAN was a key technology for 5G networks and has been implemented in the most of radio access networks from macro cells to femtocells [32]. Due to ultra-dense deployment of small cells, interference avoidance and power efficiency became two fundamental issues for a network design. To reduce the inter-cell interference, small cell cooperation was adopted by many existing works. In [32, 98], authors presented a centralized control

strategy in the BBU pool to improve spectral efficiency by baseband reusing and effectively eliminate the inter-cell interference. Besides, the RRH cooperation could also improve the down-link throughput of C-RAN in [99,100]. Since they focus on the case of single antenna BS with independent spectrums, the power efficiency was not regarded as an optimization objective for a large-scale C-RAN system. To improve network power efficiency, the cooperation approach for a single mobile user (MU) in MIMO systems was demonstrated in [101, 102].

In resent researches, combining CoMP and C-RAN is a preferred research scenario to study RRHs' cooperation management in a larger area. In [103], authors employed a semi-dynamic clustering approach to maximize the average network throughput. This approach lined up all possible BS cooperations before new cooperation was formed, then selected the best one for each time. This result in some limitations of the proposed approach: i) the computation time would be largely increased with the number of MUs, and ii) in each iteration, the beamforming vectors were changed, which would disrupt the previous order, and might result in the final result away from optimum. RRH cooperation was also addressed in [104], where authors investigated the JT coordinated approach for multi-point transmission in a C-RAN implementation of LTE-A HetNet. In this work, MUs were assumed to be greedy and tried to maximize their own throughput, so that the network overall throughput might not be maximized. Power efficiency optimization was studied in [105], in which authors proposed a dynamic clustering approach based on user locations and channel propagation features in order to eliminate inter-cell interference and improve the quality of communications in a highly dense BS deployment. In order to simplify the calculation, beamforming calculation and power allocation were independently managed, and the simulation only considered a case of small quantity of MUs. As a result, the optimization problem can be formulated as an optimization of a vector. In [106], authors employed BS cooperation through JT to minimize power consumption. The beamforming vectors of cooperated RRHs set were derived by the weighted ℓ_1/ℓ_2-norm minimization approach. However, this approach was too specific to be extended to CT or other

beamforming methods.

Chapter 3

MIMO-NOMA clustering

3.1 Introduction

This section is to introduce a new cluster beamforming strategy and our proposed MIMO-NOMA clustering approach. We formulate a joint optimization problem which integrating MU clustering and power allocation to minimize the total power consumption. In simulations, we compared our proposed approach with two existing clustering approaches in literature (i.e., the channel gain-correlation based and the channel gain-difference based approaches), and analyze its properties and performance. The main contributions of this work are summarized as follows.

- We propose a novel cluster beamforming strategy for MIMO-NOMA and employ it under two scenarios, i.e., MIMO-NOMA1 and MIMO-NOMA2. We employ a general beamforming approach (zero-forcing beamforming) to simplify the computation of our proposed cluster beamforming strategy, so that the peer effect during MU clustering is canceled. Through equivalent transformation, the NOMA power coefficient allocation can be integrated with the beamforming calculation. Moreover, we derive an optimal decoding order which can perform better than the existing works in terms of power reduction.

- We formulate MU clustering as a coalition game due to its advantages of a distributed

optimization, so that it has a fast convergence speed and the flexible cluster size. To find the optimal result for the total power consumption minimization, we further make some improvements on the traditional coalition game by following the particle swarm optimization (POS) method which adjusts the utility function for each MU towards a global optimal solution.

- We analyze three major factors that may affect the performance of a MIMO-NOMA cluster: the radius of MUs, the radius difference between two MUs, and the channel correlation coefficient. In simulations, we observe that the radius of the cell-edge MU and the real part of channel correlation coefficient are the key factors influencing power consumption. Based on this fact, we find the radius thresholds under the considered simulation environment.

Notations: $\|.\|$ and $|.|$ denote the 2-norm and the absolute value, respectively. $(.)^*$, $(.)^\dagger$ and $(.)^H$ stand for the conjugate transpose, the pseudo-inverse, and the Hermitian, respectively. $\Re(.)$ and $\Im(.)$ denote the real part and the imaginary part of a complex value, respectively. $NC(,)$ represents the complex normal distribution.

3.2 System Model

In this chapter, we first present the considered system model, which includes beamforming model, signal model and power model in both MIMO-OMA and MIMO-NOMA scenarios. Since the MIMO-NOMA signal models for the different cluster sizes are only different in the dimension of vectors, we present a case of 2 MUs (mobile users) for the explanation purpose. Then, we formulate an optimization problem which includes resource management and NOMA clustering.

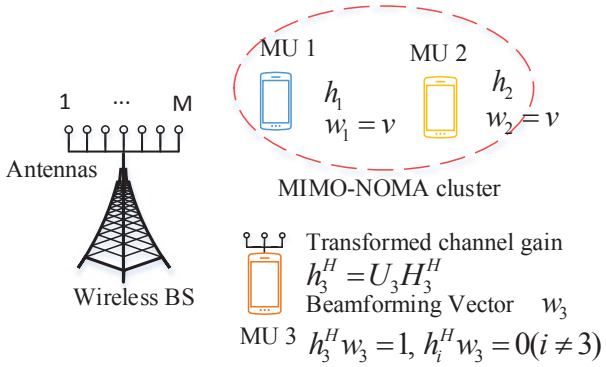

Figure 3.1: MIMO-NOMA

3.2.1 Cluster beamforming model

Considering a single cell downlink MIMO system, it has one base station (BS) (equipped with M antennas) and N MUs (each of them are equipped with n_t antennas), in which $M \geq N$. Without loss of generality, we assume that BS is equipped with the well-separated ideal antenna elements in a sufficiently complex propagation environment, so that there are no directivity and mutual coupling among antennas, and CSI information is perfect. Let$\boldsymbol{h}_u \in R^{M\times 1}and\boldsymbol{w}_u \in R^{M\times 1}$denote the channel gain vector and beamforming vector from the BS to MU u, respectively. $\boldsymbol{W} = [\boldsymbol{w}_1, ..., \boldsymbol{w}_N]$ and $\boldsymbol{H} = [\boldsymbol{h}_1^T, ..., \boldsymbol{h}_N^T]^T$ denote the beamforming matrix and the channel gain matrix for all MUs, respectively. The difference between MIMO-OMA and MIMO-NOMA is that the orthogonal condition does not exist among MUs in the same cluster. As the example in Fig. 3.1, for a MU, it may have two states: served by MIMO-OMA (MO); or served MIMO-NOMA in a cluster (MN) as a cell-center user or a cell-edge user. Towards a MU in the MO state, e.g., MU_3, its beamforming vector should satisfy the orthogonal conditions (i.e., $\boldsymbol{h}_i^H \boldsymbol{w}_3 = 0, i \in N, i \neq 3$), and the normalized condition ($\boldsymbol{h}_3^H \boldsymbol{w}_3 = 1$). However, for MUs in a MIMO-NOMA cluster (e.g., MU_1 and MU_2), they share a same beamforming vector $\boldsymbol{v}$ which satisfies $\boldsymbol{h}_1^H \boldsymbol{v} \neq 0$, $\boldsymbol{h}_2^H \boldsymbol{v} \neq 0$ and $\boldsymbol{h}_3^H \boldsymbol{v} = 0$.

If all MUs are served by MIMO-OMA, and the beamforming matrix is calculated by the ZF-beamforming (zero-forcing beamforming) strategy [22, 107]. Because of the zero-

interference condition ($\boldsymbol{h}_j^H \boldsymbol{w}_k = 0$ for $j \neq k$), the interference among MUs access to the same BS can be cancelled. Thus, we have

$$\boldsymbol{W} = \boldsymbol{H}^{\dagger} = \boldsymbol{H}^{*}(\boldsymbol{H}\boldsymbol{H}^{*})^{-1}. \tag{3.1}$$

Note that beamforming vectors for all MUs are determined at the same time. Thus, a change to one MU's beamforming vector (e.g., it is grouped in a different cluster), all MUs' beamforming vectors need to be recalculated. This effect is named as the peer effect and has been ignored in most existing works. In the next section, we will show that our proposed approach can effectively avoid such peer effects.

3.2.2 Signal model

Let $G = \{g_1, g_2, ..., g_\alpha\}$ denote a set of clusters, and there are a total of α MIMO-NOMA clusters. In this set, a cluster is denoted as $g_k = \{g_{k,1}, g_{k,2}, ..., g_{k,n_k}\}$, where there are n_k MUs sharing the same beamforming vector and being aligned from the cell-center to the cell-edge, i.e., $g_{k,1}$ and g_{k,n_k} denote a cell-center user and a cell-edge user, respectively.

For a specific MU i in the MO state, the received signal y_i can be expressed as

$$y_i = \boldsymbol{h}_i^H \boldsymbol{w}_i^{'} \sqrt{p_i} x_i + n_i, \tag{3.2}$$

where $\boldsymbol{w}_i^{'} \in R^{M \times 1}$is the beamforming vector allocated to MU i, p_i is the transmit power (Since$\|\boldsymbol{w}_i\|^2$is unnormalized, the actual BS's power consumption is calculated as in (3.4)), x_i is the data symbol transmitting to MU i, and n_i denotes the additive white Gaussian noise with zero mean and variance σ_i^2. We assume $n_i/x_i^2 = \sigma^2$ for all MUs. For a guaranteed quality of service, it is required that the signal-to-interference-plus-noise ratio (SINR) at MU i is larger than a pre-determined threshold δ as

$$\gamma_i = \frac{\left|\boldsymbol{h}_i^H \boldsymbol{w}_i^{'} \sqrt{p_i}\right|^2}{\sigma^2} \geq \delta. \tag{3.3}$$

To meet the minimal SINR requirement, the BS' power consumption can be expressed as

$$P_i = \left\|\boldsymbol{w}_i'\right\|^2 p_i = \frac{\left\|\boldsymbol{w}_i'\right\|^2}{\left|\boldsymbol{h}_i^H \boldsymbol{w}_i'\right|^2}\sigma^2\delta = \left\|\boldsymbol{w}_i'\right\|^2\sigma^2\delta. \tag{3.4}$$

If MU i and MU j are grouped as a MIMO-NOMA cluster k, i.e., $g_k = \{g_{k,1} = i, g_{k,2} = j\}$, the signal vector to be transmitted by the BS is given by

$$\boldsymbol{s_k} = \sqrt{p_k}\begin{bmatrix} v_{k,1}(\sqrt{\mu_{i,1}}x_i + \sqrt{\mu_{j,1}}x_j) \\ \vdots \\ v_{k,M}(\sqrt{\mu_{i,M}}x_i + \sqrt{\mu_{j,M}}x_j) \end{bmatrix}, \tag{3.5}$$

where $\boldsymbol{\mu_\varepsilon} = \{\sqrt{\mu_{\varepsilon,1}}, ..., \sqrt{\mu_{\varepsilon,M}}\}$ is the NOMA power coefficient set for signal x_ε, $\varepsilon = i, j$. On each antenna, let $\mu_{i,n} + \mu_{j,n} = 1$. Besides, the beamforming vector of the cluster k is denoted by $\boldsymbol{v_k} = \{v_{k,1}, ..., v_{k,M}\}$, and the transmit power is indicated by p_k. Note that in [24], MIMO-NOMA is ordinarily considered as an extension of single-antenna NOMA, so that a single power coefficient was employed to each MU on all antennas, i.e., $\mu_{i,1} = \mu_{i,2} = ... = \mu_{i,M}$. However, in this thesis, we consider a more general case by relaxing the power coefficients on different antennas to be different [17, 108]. We term these two cases as MIMO-NOMA1 (with a power coefficient set) and MIMO-NOMA2 (with a single power coefficient).

For MIMO-NOMA1, note that NOMA employs the power coefficient set to distinguish different signals on the power domain while MIMO beamforming working the space domain. To simplify calculations, we combine the beamforming vector $\boldsymbol{v}_k$ and the power coefficient $\sqrt{\mu_{j,m}}$ to transform the original superposed transmit signal formation into a new form as shown in (3.6). Note that the beamforming vectors for cluster members are different and non-orthogonal. Let

$$\boldsymbol{v_k} = \begin{bmatrix} \sqrt{p_i w_{i,1}^2 + p_j w_{j,1}^2} \\ \vdots \\ \sqrt{p_i w_{i,M}^2 + p_j w_{j,M}^2} \end{bmatrix},$$

$$\sqrt{p_k}\sqrt{\mu_{\varepsilon,m}} = \frac{\sqrt{p_\varepsilon} w_{\varepsilon,m}}{v_{k,m}} \text{ for } m \in M, \text{ and } \varepsilon = i, j.$$

The transmit signal vector can be transformed into

$$\boldsymbol{s_k} = \boldsymbol{w_i}\sqrt{p_i}x_i + \boldsymbol{w_j}\sqrt{p_j}x_j, \tag{3.6}$$

where the transformed beamforming vectors for MU i and MU j are denoted by $\boldsymbol{w_i}$ and $\boldsymbol{w_j}$, respectively, and the corresponding allocated power parameters are indicated by p_i and p_j. Note that $\boldsymbol{w_i}$ and $\boldsymbol{w_j}$ are different and non-orthogonal.

For MIMO-NOMA2, the transmit signal vector can be reformulated as

$$\boldsymbol{s_k} = \boldsymbol{v_k}\sqrt{p_k}(\sqrt{\mu_{i,1}}x_i + \sqrt{\mu_{j,1}}x_j). \tag{3.7}$$

For both cases in MIMO-NOMA, the received signal at MU ε is $y_\varepsilon = \boldsymbol{h}_\varepsilon^H \boldsymbol{s_k} + n_\varepsilon$ ($\varepsilon = i, j$), and the SINR condition (3.3) is applied.

3.2.3 Problem formulation

Our objective is to minimize the total power consumption, and the system optimization problem can be formulated as

$$\min_{\boldsymbol{W},\boldsymbol{\mu},\boldsymbol{p}} \sum_{i=1}^{N} P_i(\boldsymbol{w}_i, \mu_i, p_i), \tag{3.8a}$$

$$\text{s.t.} \quad (3.3) \quad \text{and} \tag{3.8b}$$

$$\boldsymbol{h}_i\boldsymbol{w}_j \begin{cases} \neq 0 \ \text{If MUs} \ i \ \text{and} \ j \ \text{are in the same cluster}, \\ = 0 \qquad\qquad \text{Otherwise}. \end{cases} \tag{3.8c}$$

$$\gamma_i^j \geq \zeta\delta, \tag{3.8d}$$

where P_i is the power consumption for MU i (as calculated in (3.10) and (3.20)). Note that P_i is determined by the beamforming vector $\boldsymbol{w}_i$, the transmit power p_i and the power allocation coefficient μ_i (in the MN state $0 < \mu_i < 1$, and in the MO state $\mu_i = 1$). Constraint (3.8d) indicates that the achievable rate (or SINR) of decoding signal should be larger than a predefined threshold $\zeta\delta$ (ζ is a predefined parameter within (0,1]) in order to ensure successful SIC decoding (refer to appendix A.4) [109]. Moreover, for the simplicity

of expression, we denotes beamforming matrix, power matrix and the power allocation coefficient matrix as $\boldsymbol{W}, \boldsymbol{p}, \boldsymbol{\mu}$, respectively.

3.3 Beamforming Strategy for a MIMO-NOMA Cluster

In this chapter, we formulate a partial ZF-beamforming problem for MIMO-NOMA clusters and introduce our cluster beamforming strategy for both MIMO-NOMA1 and MIMO-NOMA2 scenarios. In this strategy, we try to minimize the group power consumption and get the closed-form solutions. For explanation purpose, we start our discussion from the case of the 2-MU cluster, and then discuss its extension to the general multi-MU case.

3.3.1 MIMO-NOMA1 for a 2-MU cluster

We consider MUs i and j (located from the cell-center to the cell-edge), and the pre-determined decoding order for them is in the reverse order. After decoding the superposed message, the received signals for MU i and MU j can be respectively represented as

$$\begin{aligned} y_i &= \boldsymbol{h}_i^H \boldsymbol{s}_{\boldsymbol{k}} + n_i = \boldsymbol{h}_i^H \boldsymbol{w}_i \sqrt{p_i} x_i + n_i, \\ y_j &= \boldsymbol{h}_j^H \boldsymbol{s}_{\boldsymbol{k}} + n_j = \boldsymbol{h}_j^H \boldsymbol{w}_j \sqrt{p_j} x_j + \boldsymbol{h}_j^H \boldsymbol{w}_i \sqrt{p_i} x_i + n_j. \end{aligned} \tag{3.9}$$

To meet the minimal SINR requirement, the power consumption for MU i and MU j can be respectively expressed as

$$\begin{aligned} P_i &= \|\boldsymbol{w}_i\|^2 p_i = \frac{\|\boldsymbol{w}_i\|^2}{\left|\boldsymbol{h}_i^H \boldsymbol{w}_i\right|^2} \sigma^2 \delta = \|\boldsymbol{w}_i\|^2 \sigma^2 \delta, \\ P_j &= \|\boldsymbol{w}_j\|^2 p_j = \frac{\|\boldsymbol{w}_j\|^2}{\left|\boldsymbol{h}_j^H w_j\right|^2} (\left|\boldsymbol{h}_j^H \boldsymbol{w}_i\right|^2 p_i + \sigma^2) \delta = \|\boldsymbol{w}_j\|^2 (\left|\boldsymbol{h}_j^H \boldsymbol{w}_i\right|^2 p_i + \sigma^2) \delta. \end{aligned} \tag{3.10}$$

A basic condition for forming a MIMO-NOMA cluster is that its total power consumption is lower than that before clustering. According to (3.4), if MU i and MU j are both in the MO state, the total power consumption is

$$P_i' + P_j' = \left\|\boldsymbol{w}_i'\right\|^2 \sigma^2 \delta + \left\|\boldsymbol{w}_j'\right\|^2 \sigma^2 \delta, \tag{3.11}$$

where $\boldsymbol{w}_i^{'}$ and $\boldsymbol{w}_j^{'}$ are the beamforming vectors in the MO state and can be directly obtained by (3.1). The power reduction by adopting MIMO-NOMA can be calculated by

$$\begin{aligned}\Delta P_k &= P_i^{'} + P_j^{'} - (P_i + P_j) \\ &= \left\|\boldsymbol{w}_i^{'}\right\|^2 \sigma^2\delta + \left\|\boldsymbol{w}_j^{'}\right\|^2 \sigma^2\delta - (\|\boldsymbol{w}_i\|^2\sigma^2\delta + \|\boldsymbol{w}_j\|^2(\left|\boldsymbol{h}_j^H\boldsymbol{w}_i\right|^2 p_i + \sigma^2)\delta).\end{aligned} \tag{3.12}$$

By considering the possible computing cost for NOMA as Ω, we set $\Delta P_k > \Omega$ (e.g., $\Omega = 0.01w$) as the condition for a beneficial MIMO-NOMA cluster. Obviously, if $\Delta P_k < \Omega$, a NOMA cluster k will not be formed. To maximize ΔP_k, the optimal beamforming vectors can be derived based on the following optimization problem

$$\min f(\boldsymbol{w}_i, \boldsymbol{w}_j) = \|\boldsymbol{w}_i\|^2 + \|\boldsymbol{w}_j\|^2(\left|\boldsymbol{h}_j^H\boldsymbol{w}_i\right|^2\delta + 1). \tag{3.13}$$

According to ZF-beamforming strategy, the beamforming vectors of MUs in a cluster should be orthogonal with all out-of-cluster MUs' channel gains, but non-orthogonal with those of MUs inside this cluster. Let $\boldsymbol{H} = [\boldsymbol{h}_i^T, \boldsymbol{h}_j^T, \boldsymbol{h}_1^T, ...\boldsymbol{h}_N^T]^T \in R^{N\times M}$ be a reorganized channel gain matrix and $\boldsymbol{W} = [\boldsymbol{w}_i, \boldsymbol{w}_j, \boldsymbol{w}_1, ...\boldsymbol{w}_N] \in R^{M\times N}$ be the beamforming matrix. Then, we have

$$\begin{aligned}\boldsymbol{HW} &= \begin{bmatrix} \boldsymbol{h}_i^T & \boldsymbol{h}_j^T & \boldsymbol{h}_1^T \dots \boldsymbol{h}_N^T \end{bmatrix}^T \begin{bmatrix} \boldsymbol{w}_i & \boldsymbol{w}_j & \boldsymbol{w}_1 \dots \boldsymbol{w}_N \end{bmatrix} \\ &= \begin{bmatrix} 1 & \lambda & \boldsymbol{0}_{2\times(N-2)} \\ \beta & 1 & \\ \boldsymbol{0}_{(N-2)\times 2} & & \boldsymbol{I}_{(N-2)\times(N-2)} \end{bmatrix}_{N\times N} = \boldsymbol{T},\end{aligned} \tag{3.14}$$

where β and λ are two non-zero parameters denoting the non-orthogonal relationship within a cluster [108]. From the definition of beamforming matrix in the MO state $\boldsymbol{W}^{'}$ as determined in (3.1), we have

$$\boldsymbol{W} = \boldsymbol{H}^*(\boldsymbol{HH}^*)^{-1}\boldsymbol{HW} = \boldsymbol{W}^{'}\boldsymbol{T}. \tag{3.15}$$

From (3.15), we notice that beamforming vectors for a NOMA cluster is actually in a linear space expanded by the related beamforming vectors in the MO state ($\boldsymbol{w}_i^{'}$ and $\boldsymbol{w}_j^{'}$), i.e., $\boldsymbol{w}_i = \boldsymbol{w}_i^{'} + \beta\boldsymbol{w}_j^{'}$ and $\boldsymbol{w}_j = \boldsymbol{w}_j^{'} + \lambda\boldsymbol{w}_i^{'}$. Thus, one of our most important observations is

that the cluster beamforming vectors in the MN state are only determined by coefficients β and λ and have no effects on other MUs' beamforming vectors. Therefore, we can avoid the peer effect.

From (3.15), the beamforming vector $\boldsymbol{w}_j$ of MU j in the MN state can be derived by

$$\|\boldsymbol{w}_j\|^2 = \left\|\boldsymbol{w}_j^{'}\right\|^2 \beta^2 + 2\beta \boldsymbol{w}_i^{'} \boldsymbol{w}_j^{'} + \left\|\boldsymbol{w}_i^{'}\right\|^2. \tag{3.16}$$

For simplifying notations, in the following, we define notation $\boldsymbol{w}_i^{'}\boldsymbol{w}_j^{'}$ which equals to $\boldsymbol{w}_i^{'T}\boldsymbol{w}_j^{'}$ in the real-valued case or $\Re(\boldsymbol{w}_i^{'})\Re(\boldsymbol{w}_j^{'}) + \Im(\boldsymbol{w}_i^{'})\Im(\boldsymbol{w}_j^{'})$ in the complex-valued case. Thus, problem (3.13) can be transformed into an expression with only two variables (i.e., β and λ) as

$$\begin{aligned} &\min f(\boldsymbol{w}_i, \boldsymbol{w}_j) = g(\lambda, \beta) = (\left\|\boldsymbol{w}_j^{'}\right\|^2 \beta^2 + 2\beta \boldsymbol{w}_i^{'} \boldsymbol{w}_j^{'} + \left\|\boldsymbol{w}_i^{'}\right\|^2) \\ &+ (\left\|\boldsymbol{w}_i^{'}\right\|^2 \lambda^2 + 2\lambda \boldsymbol{w}_j^{'} \boldsymbol{w}_i^{'} + \left\|\boldsymbol{w}_j^{'}\right\|^2)(\delta(\left|\boldsymbol{h}_j^H \boldsymbol{w}_j^{'}\right|^2 \beta^2 + 2\beta \left|\boldsymbol{h}_j^H \boldsymbol{w}_i^{'}\right| \left|\boldsymbol{h}_j^H \boldsymbol{w}_j^{'}\right| + \left|\boldsymbol{h}_j^H \boldsymbol{w}_i^{'}\right|^2) + 1). \end{aligned} \tag{3.17}$$

We notice that, after NOMA decoding, the impact of MU j on MU i is eliminated. Thus, the power consumption of MU j only depends on β, and λ only appears in the second term of (3.17). Moreover, $\|\boldsymbol{w}_i\|^2$ and $(\left|\boldsymbol{h}_j^H \boldsymbol{w}_i\right|^2 \delta + 1)$ are always larger than zero in any value of β. Therefore, $\min \|\boldsymbol{w}_j\|^2$ is the necessary condition of $\min f(\boldsymbol{w}_i, \boldsymbol{w}_j)$, and $\|\boldsymbol{w}_j\|^2$ can be regarded as an independent sub-optimization problem. We calculate the 1st and the 2nd derivatives of (3.17) with respect to λ. Since $\frac{\partial^2 g(\lambda,\beta)}{\partial \lambda^2} = 2\left\|\boldsymbol{w}_i^{'}\right\|^2 > 0$, $g(\lambda, \beta)$ will reach the minimal point when $\frac{\partial g(\lambda,\beta)}{\partial \lambda} = 0$, which results in $\lambda = -\frac{\boldsymbol{w}_j^{'}\boldsymbol{w}_i^{'}}{\left\|\boldsymbol{w}_i^{'}\right\|^2}$. Then, $g(\lambda, \beta)$ can be simplified as

$$g(\lambda, \beta) = g(\beta) = (\left\|\boldsymbol{w}_j^{'}\right\|^2 \beta^2 + 2\beta \boldsymbol{w}_i^{'} \boldsymbol{w}_j^{'} + \left\|\boldsymbol{w}_i^{'}\right\|^2) + \|\boldsymbol{w}_j\|^2 (\delta \beta^2 + 1). \tag{3.18}$$

Similarly, since $\frac{\partial^2 g(\beta)}{\partial \beta^2} = 2(\left\|\boldsymbol{w}_j^{'}\right\|^2 + \delta \|\boldsymbol{w}_j\|^2) > 0$, by letting $\frac{\partial g(\beta)}{\partial \beta} = 0$, we have

$$\beta = \frac{-B}{2A} = \frac{-\boldsymbol{w}_i^{'}\boldsymbol{w}_j^{'}}{\left\|\boldsymbol{w}_j^{'}\right\|^2 + \delta\|\boldsymbol{w}_j\|^2} = \frac{-\left\|\boldsymbol{w}_i^{'}\right\|^2 \boldsymbol{w}_i^{'}\boldsymbol{w}_j^{'}}{\left\|\boldsymbol{w}_i^{'}\right\|^2 \left\|\boldsymbol{w}_j^{'}\right\|^2 (1+\delta) - \delta\left|\boldsymbol{w}_i^{'}\boldsymbol{w}_j^{'}\right|^2}. \tag{3.19}$$

Note that, for a beneficial NOMA cluster, the decoding order is the descending order of the Euclidian 2-norm of beamforming vectors in the MO state (as shown in appendix

A.1). For example, if $\left\|\boldsymbol{w}_j^{'}\right\|^2 < \left\|\boldsymbol{w}_i^{'}\right\|^2$, MU_i is decoded firstly. Otherwise, we should first decode MU_j. Note that this decoding order has not been shown in any existing works and can ensure that the power reduction is maximized.

3.3.2 MIMO-NOMA1 for a cluster with the size larger than 2

We now extend our analysis to a general case, where there are more than 2 MUs in a MIMO-NOMA cluster. For analysis purpose, we consider that there are n MUs in a cluster locating from the cell-center to the cell-edge, indexed from 1 to n. In addition, the pre-determined decoding order is in the reverse order. According to (3.14), the beamforming vector of MU i can be calculated by $\boldsymbol{w}_i = \lambda_{i1}\boldsymbol{w}_1^{'} + \lambda_{i2}\boldsymbol{w}_2^{'} + ... + \lambda_{in}\boldsymbol{w}_n^{'}, i = 1, 2, ...n$ and $\lambda_{ii} = 1$. After decoding the superposed message, the received signals and corresponding power consumptions for MU i can be derived by

$$\begin{aligned} y_i &= \boldsymbol{h}_i^H \boldsymbol{w}_i \sqrt{p_i} x_i + \textstyle\sum_{\epsilon=1}^{i-1} (\boldsymbol{h}_i^H \boldsymbol{w}_\epsilon \sqrt{p_\epsilon} x_\epsilon) + n_i, \\ P_i &= \|\boldsymbol{w}_i\|^2 (\textstyle\sum_{\epsilon=1}^{i-1} \left|\boldsymbol{h}_i^H \boldsymbol{w}_\epsilon\right|^2 p_\epsilon + \sigma^2)\delta. \end{aligned} \tag{3.20}$$

Specifically, the power consumptions for MUs n and $n-1$ are respectively equal to

$$\begin{aligned} P_{n-1} &= \|\boldsymbol{w}_{n-1}\|^2 p_{n-1} = \|\boldsymbol{w}_{n-1}\|^2 (\lambda_{1n-1}^2 p_1 + ... + \lambda_{n-2n-1}^2 p_{n-2} + \sigma^2)\delta, \\ P_n &= \|\boldsymbol{w}_n\|^2 p_n = \|\boldsymbol{w}_n\|^2 (\lambda_{1n}^2 p_1 + ... + \lambda_{n-1n}^2 p_{n-1} + \sigma^2)\delta. \end{aligned} \tag{3.21}$$

To determine λ_{ij}, $i, j = 1, 2, ...n$, the objective function is to minimize the overall power consumption, i.e., The objective function is denoted by

$$\min P_1 + ... + P_n.$$

Based on the similar observations in (3.17), we propose a recursive process to determine the beamforming vectors following the order from MU n to MU 1. Specifically, since the parameters from λ_{n1} to λ_{nn-1} are only related with $\|\boldsymbol{w}_n\|^2$ as power allocation p_n is positive, the first subproblem for determining MU n's beamforming vector is denoted as

$$\min g(\lambda_{n1}, ..., \lambda_{nn-1}) = \|\boldsymbol{w}_n\|^2 = \lambda_{n1}^2 \boldsymbol{w}_1^{'2} + ... + \boldsymbol{w}_n^{'2} + 2\lambda_{n1}^2 \lambda_{n2}^2 \boldsymbol{w}_1^{'2} \boldsymbol{w}_2^{'2} + ... + 2\lambda_{n1}^2 \boldsymbol{w}_1^{'2} \boldsymbol{w}_n^{'2}.$$

The solution can be derived by letting the 1st derivatives of the objective function be zero, i.e.,

$$
\begin{aligned}
&[\lambda_{n1}, \lambda_{n2}, ..., \lambda_{nn-1}] = BA^{-1}, \\
&A = \begin{bmatrix} \left\|\boldsymbol{w}_1^{'}\right\|^2 & \boldsymbol{w}_1^{'}\boldsymbol{w}_2^{'} & ... & \boldsymbol{w}_1^{'}\boldsymbol{w}_{n-1}^{'} \\ \boldsymbol{w}_2^{'}\boldsymbol{w}_1^{'} & \left\|\boldsymbol{w}_2^{'}\right\|^2 & ... & \boldsymbol{w}_2^{'}\boldsymbol{w}_{n-1}^{'} \\ \vdots & \vdots & & \vdots \\ \boldsymbol{w}_{n-1}^{'}\boldsymbol{w}_1^{'} & \boldsymbol{w}_{n-1}^{'}\boldsymbol{w}_2^{'} & ... & \left\|\boldsymbol{w}_{n-1}^{'}\right\|^2 \end{bmatrix}, B = -[\boldsymbol{w}_1^{'}\boldsymbol{w}_n^{'}, \boldsymbol{w}_2^{'}\boldsymbol{w}_n^{'}, ..., \boldsymbol{w}_{n-1}^{'}\boldsymbol{w}_n^{'}].
\end{aligned} \tag{3.22}
$$

After that, we substitute this solution back to the objective function, and formulate the second subproblem to determine the beamforming vector of MU $n-1$ as (based on the fact that $p_{n-1} > 0$)

$$\min g(\lambda_{n-11}, ..., \lambda_{n-1n}) = \|\boldsymbol{w}_{n-1}\|^2 + \|\boldsymbol{w}_n\|^2 \lambda_{n-1n}^2.$$

Following the similar procedure as in (3.22), we can derive $\lambda_n - 1j$, $j = 1, 2, ..., n$. By substituting the solution back to the objective function, we can derive the subproblem for MU $n-2$. This process will be continued till all MUs have been considered.

To better illustrate this recursive solution process, we use a 3-MU cluster $g_k = \{i, j, l\}$ as an example to explain the analysis details as follows. To meet the minimal SINR requirement, the received signal and the power consumption for MU l (which for MUs i and j are the same as in (3.9) and (3.10)) can be expressed as

$$
\begin{aligned}
y_l &= \boldsymbol{h}_l^H \boldsymbol{w}_l \sqrt{p_l} x_l + \sum_{\epsilon=i,j} (\boldsymbol{h}_l^H \boldsymbol{w}_\epsilon \sqrt{p_\epsilon} x_\epsilon) + n_l, \\
P_l &= \|\boldsymbol{w}_l\|^2 (\left|\boldsymbol{h}_l^H \boldsymbol{w}_i\right|^2 p_i + \left|\boldsymbol{h}_l^H \boldsymbol{w}_j\right|^2 p_j + \sigma^2)\delta.
\end{aligned} \tag{3.23}
$$

where $p_i = \sigma^2\delta, p_j = (\left|\boldsymbol{h}_j^H \boldsymbol{w}_i\right|^2 p_i + \sigma^2)\delta$.

Similar to (3.14), beamforming vectors for a 3-MU NOMA cluster are determined by

$$[\boldsymbol{w}_i, \boldsymbol{w}_j, \boldsymbol{w}_l] = [\boldsymbol{w}_i^{'}, \boldsymbol{w}_j^{'}, \boldsymbol{w}_l^{'}] \begin{bmatrix} 1 & \lambda_1 & \lambda_2 \\ \lambda_3 & 1 & \lambda_4 \\ \lambda_5 & \lambda_6 & 1 \end{bmatrix}, \tag{3.24}$$

and the coefficients λ_ϵ ($\epsilon = 1, 2, ..., 6$) can be derived based on the following optimization problem to minimize the total power consumption as

$$\min g(\lambda_1, ..., \lambda_6) = P_i + P_j + P_l. \tag{3.25}$$

Starting from MU_k beamforming vector $\|\boldsymbol{w}_l\|^2$, we have

$$\min \|\boldsymbol{w}_l\|^2 = \left\|\boldsymbol{w}_i^{'}\right\|^2 \lambda_2^2 + \left\|\boldsymbol{w}_j^{'}\right\|^2 \lambda_4^2 + 2\boldsymbol{w}_i^{'}\boldsymbol{w}_j^{'}\lambda_2\lambda_4 + 2\boldsymbol{w}_i^{'}\boldsymbol{w}_l^{'}\lambda_2 + 2\boldsymbol{w}_j^{'}\boldsymbol{w}_l^{'}\lambda_4 + \left\|\boldsymbol{w}_l^{'}\right\|^2 \tag{3.26}$$

The solution is

$$\lambda_2 = \frac{\boldsymbol{w}_j^{'}\boldsymbol{w}_l^{'}\boldsymbol{w}_i^{'}\boldsymbol{w}_j^{'} - \boldsymbol{w}_i^{'}\boldsymbol{w}_l^{'}\left\|\boldsymbol{w}_j^{'}\right\|^2}{\left\|\boldsymbol{w}_j^{'}\right\|^2\left\|\boldsymbol{w}_i^{'}\right\|^2 - |\boldsymbol{w}_i^{'}\boldsymbol{w}_j^{'}|^2}, \lambda_4 = \frac{\boldsymbol{w}_i^{'}\boldsymbol{w}_l^{'}\boldsymbol{w}_i^{'}\boldsymbol{w}_j^{'} - \boldsymbol{w}_j^{'}\boldsymbol{w}_l^{'}\left\|\boldsymbol{w}_i^{'}\right\|^2}{\left\|\boldsymbol{w}_j^{'}\right\|^2\left\|\boldsymbol{w}_i^{'}\right\|^2 - |\boldsymbol{w}_i^{'}\boldsymbol{w}_j^{'}|^2}.$$

Thus, we have $\boldsymbol{w}_l = \boldsymbol{w}_i^{'}\lambda_2 + \boldsymbol{w}_j^{'}\lambda_4 + \boldsymbol{w}_l^{'}$, and (25) can be transformed into

$$\begin{aligned} &\min g(\lambda_1, ..., \lambda_6) = (\|\boldsymbol{w}_j\|^2(\left|\boldsymbol{h}_j^H\boldsymbol{w}_i\right|^2\delta + 1) + \\ &\theta\delta\left|\boldsymbol{h}_l^H\boldsymbol{w}_j\right|^2(\left|\boldsymbol{h}_j^H\boldsymbol{w}_i\right|^2\delta + 1)) + (\|\boldsymbol{w}_i\|^2 + \theta(\delta\left|\boldsymbol{h}_l^H\boldsymbol{w}_i\right|^2 + 1)), \end{aligned} \tag{3.27}$$

where $\theta = \|\boldsymbol{w}_l\|^2$. Next, we focus on $\boldsymbol{w}_j$. Since $(\left|\boldsymbol{h}_j^H\boldsymbol{w}_i\right|^2\delta + 1) > 0$, a second sub-optimization is formulated as

$$\begin{aligned} &\min \|\boldsymbol{w}_j\|^2\alpha + \left|\boldsymbol{h}_l^H\boldsymbol{w}_j\right|^2\beta = \alpha\left\|\boldsymbol{w}_i^{'}\right\|^2\lambda_1^2 + (\alpha\left\|\boldsymbol{w}_l^{'}\right\|^2 + \beta)\lambda_6^2 \\ &+2\alpha\boldsymbol{w}_i^{'}\boldsymbol{w}_l^{'}\lambda_1\lambda_6 + 2\alpha\boldsymbol{w}_i^{'}\boldsymbol{w}_j^{'}\lambda_1 + 2\alpha\boldsymbol{w}_j^{'}\boldsymbol{w}_l^{'}\lambda_6 + \alpha\left\|\boldsymbol{w}_j^{'}\right\|^2, \end{aligned} \tag{3.28}$$

where $\alpha = (\left|\boldsymbol{h}_j^H\boldsymbol{w}_i\right|^2\delta + 1)$ and $\beta = \alpha\theta\delta$. We obtain

$$\lambda_1 = \frac{\boldsymbol{w}_i^{'}\boldsymbol{w}_j^{'}(\left\|\boldsymbol{w}_l^{'}\right\|^2 + \theta\delta) - \boldsymbol{w}_i^{'}\boldsymbol{w}_l^{'}\boldsymbol{w}_j^{'}\boldsymbol{w}_l^{'}}{|\boldsymbol{w}_i^{'}\boldsymbol{w}_l^{'}|^2 - \left\|\boldsymbol{w}_i^{'}\right\|^2(\left\|\boldsymbol{w}_l^{'}\right\|^2 + \theta\delta)}, \lambda_6 = \frac{\left\|\boldsymbol{w}_i^{'}\right\|^2\boldsymbol{w}_j^{'}\boldsymbol{w}_l^{'} - \boldsymbol{w}_i^{'}\boldsymbol{w}_j^{'}\boldsymbol{w}_i^{'}\boldsymbol{w}_l^{'}}{|\boldsymbol{w}_i^{'}\boldsymbol{w}_l^{'}|^2 - \left\|\boldsymbol{w}_i^{'}\right\|^2(\left\|\boldsymbol{w}_l^{'}\right\|^2 + \theta\delta)},$$

and $\boldsymbol{w}_j = \boldsymbol{w}_i^{'}\lambda_1 + \boldsymbol{w}_j^{'} + \boldsymbol{w}_l^{'}\lambda_6$. With these results, problem (3.25) can be further simplified as

$$\begin{aligned} \min g(\lambda_1, ..., \lambda_6) &= \|\boldsymbol{w}_i\|^2 + \left|\boldsymbol{h}_j^H\boldsymbol{w}_i\right|^2(\|\boldsymbol{w}_j\|^2\delta + \theta\delta^2\left|\boldsymbol{h}_l^H\boldsymbol{w}_j\right|^2) + \theta\delta\left|\boldsymbol{h}_l^H\boldsymbol{w}_i\right|^2 \\ &= (\left\|\boldsymbol{w}_j^{'}\right\|^2 + \alpha^{'})\lambda_3^2 + (\left\|\boldsymbol{w}_l^{'}\right\|^2 + \beta^{'})\lambda_5^2 + 2\boldsymbol{w}_j^{'}\boldsymbol{w}_l^{'}\lambda_3\lambda_5 + 2\boldsymbol{w}_i^{'}\boldsymbol{w}_j^{'}\lambda_3 + 2\boldsymbol{w}_i^{'}\boldsymbol{w}_l^{'}\lambda_5 + \left\|\boldsymbol{w}_i^{'}\right\|^2, \end{aligned} \tag{3.29}$$

where $\alpha^{'} = (\left\|\boldsymbol{w}_j^{'}\right\|^2\delta + \left|\boldsymbol{h}_l^H\boldsymbol{w}_j\right|^2\delta^2\theta)$, $\beta^{'} = \theta\delta$. We have

$$\lambda_3 = \frac{\boldsymbol{w}_i^{'}\boldsymbol{w}_j^{'}(\left\|\boldsymbol{w}_l{}^{'}\right\|^2+\beta^{'})-\boldsymbol{w}_i^{'}\boldsymbol{w}_l^{'}\boldsymbol{w}_j^{'}\boldsymbol{w}_l^{'}}{|\boldsymbol{w}_j^{'}\boldsymbol{w}_l^{'}|^2-(\left\|\boldsymbol{w}_j^{'}\right\|^2+\alpha^{'})(\left\|\boldsymbol{w}_l{}^{'}\right\|^2+\beta^{'})}, \lambda_5 = \frac{\boldsymbol{w}_i^{'}\boldsymbol{w}_l^{'}(\left\|\boldsymbol{w}_j^{'}\right\|^2+\alpha^{'})-\boldsymbol{w}_i^{'}\boldsymbol{w}_j^{'}\boldsymbol{w}_j^{'}\boldsymbol{w}_l^{'}}{|\boldsymbol{w}_j^{'}\boldsymbol{w}_l^{'}|^2-(\left\|\boldsymbol{w}_j^{'}\right\|^2+\alpha^{'})(\left\|\boldsymbol{w}_l{}^{'}\right\|^2+\beta^{'})},$$

and $\boldsymbol{w}_i{=}\boldsymbol{w}_i^{'}{+}\boldsymbol{w}_j^{'}\lambda_3{+}\boldsymbol{w}_l^{'}\lambda_5$. In summary, the closed-form solution of beamforming strategy for a 3-MU cluster is obtained by three steps, and in each step, the optimization is linear.

3.3.3 MIMO-NOMA2 for a cluster with a size of 2

In MIMO-NOMA2, a same power allocation coefficient is employed for different antennas. Thus, the received signals for MU i and MU j can be represented as

$$\begin{aligned} y_i &= \boldsymbol{h}_i^H\boldsymbol{s}_{\boldsymbol{k}}+n_i = \boldsymbol{h}_i^H\boldsymbol{v}_k\sqrt{p_k}\sqrt{\mu_{i,1}}x_i+n_i, \\ y_j &= \boldsymbol{h}_j^H\boldsymbol{s}_{\boldsymbol{k}}+n_j = \boldsymbol{h}_j^H\boldsymbol{v}_k\sqrt{p_k}\sqrt{\mu_{j,1}}x_j+\boldsymbol{h}_j^H\boldsymbol{v}_k\sqrt{p_k}\sqrt{\mu_{i,1}}x_i+n_j. \end{aligned} \tag{3.30}$$

With the minimal SINR requirement satisfied, the power consumption for them can be respectively expressed as

$$\begin{aligned} P_i &= \|\boldsymbol{v}_k\|^2 p_k\mu_{i,1} = \frac{\|\boldsymbol{v}_k\|^2}{\left|\boldsymbol{h}_i^H\boldsymbol{v}_k\right|^2}\sigma^2\delta, \\ P_j &= \|\boldsymbol{v}_k\|^2 p_k\mu_{j,1} = \frac{\|\boldsymbol{v}_k\|^2}{\left|\boldsymbol{h}_j^H\boldsymbol{v}_{\boldsymbol{k}}\right|^2}(\left|\boldsymbol{h}_j^H\boldsymbol{v}_k\right|^2 p_k\mu_{i,1}+\sigma^2)\delta \\ &= \|\boldsymbol{v}_k\|^2(\frac{\delta}{\left|\boldsymbol{h}_i^H\boldsymbol{v}_{\boldsymbol{k}}\right|^2}+\frac{1}{\left|\boldsymbol{h}_j^H\boldsymbol{v}_{\boldsymbol{k}}\right|^2})\sigma^2\delta. \end{aligned} \tag{3.31}$$

To minimize the total power consumption, we formulate an optimization problem as

$$\min f(\boldsymbol{v}_k) = \|\boldsymbol{v}_k\|^2(\frac{\delta+1}{\left|\boldsymbol{h}_i^H\boldsymbol{v}_{\boldsymbol{k}}\right|^2}+\frac{1}{\left|\boldsymbol{h}_j^H\boldsymbol{v}_{\boldsymbol{k}}\right|^2})\sigma^2\delta. \tag{3.32}$$

Since the cluster beamforming vector $\boldsymbol{v}_k$ should be orthogonal to channel gain vectors of MU l (i.e., $\boldsymbol{h}_l{}^H\boldsymbol{v}_k = 0, l \in M, l \neq \{i,j\}$), according to (3.14), $\boldsymbol{v}_k$ should be in the linear space determined by $\boldsymbol{w}_i^{'}$ and $\boldsymbol{w}_j^{'}$. We rewrite $\boldsymbol{v}_k$ as $\boldsymbol{v}_k = \beta\boldsymbol{w}_i^{'}+\lambda\boldsymbol{w}_j^{'}$. Then, problem (3.32) can also be transformed with respect to β and λ as

$$\min g(\beta,\lambda) = (\left\|\boldsymbol{w}_i^{'}\right\|^2\beta^2+2\beta\lambda\boldsymbol{w}_i^{'}\boldsymbol{w}_j^{'}+\left\|\boldsymbol{w}_j^{'}\right\|^2\lambda^2)(\tfrac{\delta+1}{\beta^2}+\tfrac{1}{\lambda^2}). \tag{3.33}$$

From (33), we notice that $g(\beta,\lambda)$ is only determined by the ratio of $\frac{\beta}{\lambda}$. Thus, without

loss of generality, we assume that $\beta = \chi\lambda$, and let $\lambda = 1$, so that $\beta = \chi$. Then, the optimization problem can be reformulated as

$$f(\boldsymbol{v}_k) = g(\chi) = (\left\|\boldsymbol{w}_i^{'}\right\|^2 \chi^2 + 2\chi \boldsymbol{w}_i^{'}\boldsymbol{w}_j^{'} + \left\|\boldsymbol{w}_j^{'}\right\|^2)(\tfrac{\delta+1}{\chi^2}+1). \tag{3.34}$$

Although the optimal result of χ can be obtained by letting $\frac{\partial g(\chi)}{\partial \chi} = 0$, the closed-form solution cannot be derived directly. If the distance between two MUs in a cluster is large, the cell-edge MU will consume much more energy than the cell-center MU, i.e., $\left\|\boldsymbol{w}_i^{'}\right\|^2 \ll \left\|\boldsymbol{w}_j^{'}\right\|^2$ and $\beta \gg \lambda$, and we have $\frac{\delta+1}{\chi^2} \ll 1$. By letting $\frac{\delta+1}{\chi^2} = 0$, problem (3.32) can be approximated as

$$\min g(\chi) = (\left\|\boldsymbol{w}_i^{'}\right\|^2 \chi^2 + 2\chi \boldsymbol{w}_i^{'}\boldsymbol{w}_j^{'} + \left\|\boldsymbol{w}_j^{'}\right\|^2). \tag{3.35}$$

Since $\frac{\partial^2 g(\chi)}{\partial \chi^2} = 2\left\|\boldsymbol{w}_i^{'}\right\|^2 > 0$, by letting $\frac{\partial g(\chi)}{\partial \chi} = 0$, we have the closed-form solution as $\chi = -\frac{\boldsymbol{w}_i^{'}\boldsymbol{w}_j^{'}}{\left\|\boldsymbol{w}_i^{'}\right\|^2}$. The accuracy of the approximation will be decreased as two MUs get closer. However, if two MUs are too close, condition $\Delta P_k > \theta$ may not be satisfied. In the simulation part, we will show that this approximate solution is in high-accuracy. Moreover, the result of χ for $\frac{\delta+1}{\chi^2} \geq 1$ does not exist as shown in appendix A.2. In summary, for MIMO-NOMA2 scenario, we can simplify the objective function based on the fact that $\left\|\boldsymbol{w}_i^{'}\right\|^2 \ll \left\|\boldsymbol{w}_j^{'}\right\|^2$. Moreover, from (3.31), we have $\frac{\mu_{i,1}}{\mu_{j,1}} = \frac{\left|\boldsymbol{h}_j^H \boldsymbol{v_k}\right|^2}{\delta\left|\boldsymbol{h}_j^H \boldsymbol{v_k}\right|^2 + \left|\boldsymbol{h}_i^H \boldsymbol{v_k}\right|^2}$, then we can get the allocated power coefficients ($\mu_{i,1}$ and $\mu_{j,1}$).

3.3.4 MIMO-NOMA2 for a cluster with the size large than 2

For the cluster with n ($n > 2$) MUs, the beamforming vector of MU i can be calculated by $\boldsymbol{v}_k = \lambda_1 \boldsymbol{w}_1^{'} + \lambda_2 \boldsymbol{w}_2^{'} + ... + \lambda_n \boldsymbol{w}_n^{'}$. After decoding the superposed message and approximation, the received signals and corresponding power consumptions for MU i can be derived by

$$y_i = \boldsymbol{h}_i^H \boldsymbol{v}_k \sqrt{p_k}(\sqrt{\mu_{i,1}} x_i + \sum_{j=1}^{i-1} \sqrt{\mu_{j,1}} x_j) + n_i.$$

$$P_i = \|\boldsymbol{v}_k\|^2 (\frac{1}{\left|\boldsymbol{h}_i^H \boldsymbol{v_k}\right|^2} + \sum_{j=1}^{i-1} \frac{\delta(1+\delta)^{(i-1-j)}}{\left|\boldsymbol{h}_j^H \boldsymbol{v_k}\right|^2}) \sigma^2 \delta.$$

The objective function can be denoted as

$$\min g(\lambda_1, ..., \lambda_n) = \|\boldsymbol{v}_k\|^2 (\sum_{j=1}^{i-1} \frac{(\delta+1)^{(n-j)}}{\lambda_j^2} + \frac{1}{\lambda_n^2})\sigma^2\delta. \tag{3.36}$$

If $\frac{(\delta+1)^{(n-j)}}{\lambda_j^2}$ is the largest one, after approximation, the objective function can be transformed as

$$\min g(\lambda_1, ..., \lambda_n) = \|\boldsymbol{v}_k\|^2 (\frac{(\delta+1)^{(n-j)}}{\lambda_j^2})\sigma^2\delta.$$

Following the same way as in (22), we can obtain the closed form solution by

$$[\frac{\lambda_1}{\lambda_j}, ..., \frac{\lambda_{j-1}}{\lambda_j}, \frac{\lambda_{j+1}}{\lambda_j}, ..., \frac{\lambda_n}{\lambda_j}] = -[\boldsymbol{w}_1'\boldsymbol{w}_j', ..., \boldsymbol{w}_n'\boldsymbol{w}_j'] \begin{bmatrix} \|\boldsymbol{w}_1'\|^2 & \boldsymbol{w}_1'\boldsymbol{w}_2' & ... & \boldsymbol{w}_1'\boldsymbol{w}_n' \\ \boldsymbol{w}_1'\boldsymbol{w}_2' & \|\boldsymbol{w}_2'\|^2 & ... & \boldsymbol{w}_2'\boldsymbol{w}_n' \\ \vdots & \vdots & & \vdots \\ \boldsymbol{w}_1'\boldsymbol{w}_n' & \boldsymbol{w}_2'\boldsymbol{w}_n' & ... & \|\boldsymbol{w}_n'\|^2 \end{bmatrix}^{-1}.$$

For example, in a 3-MU cluster $g_k = \{i, j, l\}$, the received signal and the power consumption for MU l (which for MUs i and j are shown in (3.30) and (3.31)) can be written as

$$\begin{aligned} &y_l = \boldsymbol{h}_l^H \boldsymbol{v}_k \sqrt{p_k}\sqrt{\mu_{l,1}} x_l + \boldsymbol{h}_l^H \boldsymbol{v}_k \sqrt{p_k}\sqrt{\mu_{i,1}} x_i + \boldsymbol{h}_l^H \boldsymbol{v}_k \sqrt{p_k}\sqrt{\mu_{j,1}} x_j + n_l, \\ &P_l = \|\boldsymbol{v}_k\|^2 p_k \mu_{l,1} = \|\boldsymbol{v}_k\|^2 (\frac{\delta(\delta+1)}{|\boldsymbol{h}_i^H \boldsymbol{v_k}|^2} + \frac{\delta}{|\boldsymbol{h}_j^H \boldsymbol{v_k}|^2} + \frac{1}{|\boldsymbol{h}_l^H \boldsymbol{v_k}|^2})\sigma^2\delta. \end{aligned} \tag{3.37}$$

Similarly, we assume that $\boldsymbol{v_k} = \lambda_1 \boldsymbol{w}_i + \lambda_2 \boldsymbol{w}_j + \lambda_3 \boldsymbol{w}_l$ and $\lambda_2 = \alpha\lambda_1$, $\lambda_3 = \beta\lambda_1$. In order to minimize the total power consumption, the optimization function is given by

$$\begin{aligned} \min g(\alpha, \beta) = &(\|\boldsymbol{w}_i'\|^2 + \alpha^2 \|\boldsymbol{w}_j'\|^2 + \beta^2 \|\boldsymbol{w}_l'\|^2 + \\ &2(\alpha \boldsymbol{w}_i'\boldsymbol{w}_j' + \beta \boldsymbol{w}_i'\boldsymbol{w}_l' + \alpha\beta \boldsymbol{w}_j'\boldsymbol{w}_l'))((\delta+1)^2 + \frac{\delta+1}{\alpha^2} + \frac{1}{\beta^2}). \end{aligned} \tag{3.38}$$

In this case, problem (38) is determined by the value of α and β. Since i is the cell-center MU and l is the cell-edge MU, we have $\|\boldsymbol{w}_i'\|^2 \ll \|\boldsymbol{w}_l'\|^2$, $\lambda_1 \gg \lambda_3$ and $(\delta+1)^2 \ll \frac{1}{\beta^2}$. If MU j is close to MU i, we have $\frac{(\delta+1)}{\alpha^2} \ll \frac{1}{\beta^2}$. Thus, the objective function can be

approximated as

$$\min g(\alpha,\beta)=(\left\|\boldsymbol{w}_i^{'}\right\|^2+\alpha^2\left\|\boldsymbol{w}_j^{'}\right\|^2+\beta^2\left\|\boldsymbol{w}_l^{'}\right\|^2+2\alpha\boldsymbol{w}_i^{'}\boldsymbol{w}_j^{'}+2\beta\boldsymbol{w}_i^{'}\boldsymbol{w}_l^{'}+2\alpha\beta\boldsymbol{w}_j^{'}\boldsymbol{w}_l^{'})\frac{1}{\beta^2} \quad (3.39)$$

We first consider β as a constant, and let $\frac{\partial(g(\alpha,\beta))}{\partial\alpha}=0$ because $\frac{\left\|\boldsymbol{w}_j^{'}\right\|^2}{\beta^2}>0$. As $\frac{\partial^2(g(\alpha,\beta))}{\partial\alpha^2}=\frac{\left\|\boldsymbol{w}_j^{'}\right\|^2}{\beta^2}>0$, the objective function will reach the minimum point when $\alpha=-\frac{\boldsymbol{w}_i^{'}\boldsymbol{w}_j^{'}+\boldsymbol{w}_j^{'}\boldsymbol{w}_l^{'}\beta}{\left\|\boldsymbol{w}_j^{'}\right\|^2}$. Then, substituting α to (38), it can be further simplified as

$$\begin{aligned}\min g(\beta)=&\frac{1}{\left\|\boldsymbol{w}_j^{'}\right\|^2}((\left\|\boldsymbol{w}_j^{'}\right\|^2\left\|\boldsymbol{w}_l^{'}\right\|^2-\left|\boldsymbol{w}_j^{'}\boldsymbol{w}_l^{'}\right|^2)\\&+\frac{2(\left|\boldsymbol{w}_i^{'}\boldsymbol{w}_l^{'}\right|^2\left\|\boldsymbol{w}_j^{'}\right\|^2-\left|\boldsymbol{w}_j^{'}\boldsymbol{w}_l^{'}\right|\left|\boldsymbol{w}_i^{'}\boldsymbol{w}_j^{'}\right|)}{\beta}+\frac{\left\|\boldsymbol{w}_i^{'}\right\|^2\left\|\boldsymbol{w}_j^{'}\right\|^2-\left|\boldsymbol{w}_i^{'}\boldsymbol{w}_j^{'}\right|^2}{\beta^2}).\end{aligned} \quad (3.40)$$

Since the second derivative is $\frac{\partial^2(g(\beta))}{\partial\beta^2}=\frac{\left\|\boldsymbol{w}_i^{'}\right\|^2\left\|\boldsymbol{w}_j^{'}\right\|^2-\left|\boldsymbol{w}_i^{'}\boldsymbol{w}_j^{'}\right|^2}{\left\|\boldsymbol{w}_j^{'}\right\|^2\beta^4}>0$, $g(\beta)$ reaches the minimum point when

$$\beta=\frac{\left|\boldsymbol{w}_i^{'}\boldsymbol{w}_j^{'}\right|^2-\left\|\boldsymbol{w}_i^{'}\right\|^2\left\|\boldsymbol{w}_j^{'}\right\|^2}{\left|\boldsymbol{w}_i^{'}\boldsymbol{w}_l^{'}\right|^2\left\|\boldsymbol{w}_j^{'}\right\|^2-\left|\boldsymbol{w}_j^{'}\boldsymbol{w}_l^{'}\right|\left|\boldsymbol{w}_i^{'}\boldsymbol{w}_j^{'}\right|},\alpha=-\frac{\left|\boldsymbol{w}_i^{'}\boldsymbol{w}_j^{'}\right|\left|\boldsymbol{w}_i^{'}\boldsymbol{w}_l^{'}\right|-\left|\boldsymbol{w}_j^{'}\boldsymbol{w}_l^{'}\right|\left\|\boldsymbol{w}_i^{'}\right\|^2}{\left|\boldsymbol{w}_i^{'}\boldsymbol{w}_l^{'}\right|^2\left\|\boldsymbol{w}_j^{'}\right\|^2-\left|\boldsymbol{w}_j^{'}\boldsymbol{w}_l^{'}\right|\left|\boldsymbol{w}_i^{'}\boldsymbol{w}_j^{'}\right|}.$$

Otherwise, if MU j is close to MU l, we may have $\frac{(\delta+1)}{\alpha^2}>\frac{1}{\beta^2}$. The objective function can be approximated as

$$\min g(\alpha,\beta)=(\delta+1)(\frac{\left\|\boldsymbol{w}_i^{'}\right\|^2}{\alpha^2}+\left\|\boldsymbol{w}_j^{'}\right\|^2+\frac{\beta^2\left\|\boldsymbol{w}_l^{'}\right\|^2}{\alpha^2}+\frac{2\boldsymbol{w}_i^{'}\boldsymbol{w}_j^{'}}{\alpha}+\frac{2\beta\boldsymbol{w}_i^{'}\boldsymbol{w}_l^{'}}{\alpha^2}+\frac{2\beta\boldsymbol{w}_j^{'}\boldsymbol{w}_l^{'}}{\alpha}). \quad (3.41)$$

Following the same way, we can get

$$\alpha=\frac{\left|\boldsymbol{w}_i^{'}\boldsymbol{w}_l^{'}\right|^2-\left\|\boldsymbol{w}_i^{'}\right\|^2\left\|\boldsymbol{w}_l^{'}\right\|^2}{\left|\boldsymbol{w}_i^{'}\boldsymbol{w}_j^{'}\right|^2\left\|\boldsymbol{w}_l^{'}\right\|^2-\left|\boldsymbol{w}_j^{'}\boldsymbol{w}_l^{'}\right|\left|\boldsymbol{w}_i^{'}\boldsymbol{w}_l^{'}\right|},\beta=-\frac{\left|\boldsymbol{w}_i^{'}\boldsymbol{w}_j^{'}\right|\left|\boldsymbol{w}_i^{'}\boldsymbol{w}_l^{'}\right|-\left|\boldsymbol{w}_j^{'}\boldsymbol{w}_l^{'}\right|\left\|\boldsymbol{w}_i^{'}\right\|^2}{\left|\boldsymbol{w}_i^{'}\boldsymbol{w}_j^{'}\right|^2\left\|\boldsymbol{w}_l^{'}\right\|^2-\left|\boldsymbol{w}_j^{'}\boldsymbol{w}_l^{'}\right|\left|\boldsymbol{w}_i^{'}\boldsymbol{w}_l^{'}\right|}.$$

According to [110], the SIC approach is based on the evaluation of received signal strength which is used to determine the weight (or precoders) on each decoding layer. Such received signal strength depends on channel gains, beamforming vectors, and power distribution. In MIMO-NOMA1, the received signal strengths for different signals are distinguished by the product of the channel gain vector, the transformed beamforming vector and the power coefficient. While in MIMO-NOMA2, since the channel gains, the beamforming vectors and the power allocations are same for different users, the received

signal strength for different signals can be distinguished by the power coefficients. Take a 2-MU cluster for example. In the case of MIMO-NOMA1, for MU j in (3.9), the precoders of x_j and x_i are determined by $\sqrt{p_j}$ and $\lambda\sqrt{p_i}$. However, in the case of MIMO-NOMA2, for MU j in (3.30), the precoders of x_j and x_i are determined by$\sqrt{\mu_{j,1}}$ and $\sqrt{\mu_{i,1}}$. Therefore, although different precoders are used in MIMO-NOMA1, there is no extra overhead introduced. This observation can be easily extended to a cluster with any size.

3.4 MIMO-NOMA Clustering Approach

Based on the aforementioned NOMA cluster beamforming design, we have two observations: i) power reduction can be achieved through MU clustering; ii) the maximum power reduction for a cluster is only related to MUs in this cluster but independent with other out-of-cluster MUs. Based on these two observations, MU clustering problem becomes a grouping problem for exploring an optimal cluster set. In this chapter, a new coalition game approach is proposed to solve such grouping problem by exploring players' cooperative behaviors.

The conditions for grouping MUs together include: the potential cluster is beneficial, and MUs can be successfully decoded (refer to appendix A.4) [109]. We assume that all MUs are willing to join this clustering process and try to maximize their utilities which are assigned by the BS. The utility function of MU i is evaluated by the average value of cluster power reduction ΔP_k ,i.e.,

$$U_i = \begin{cases} \Delta P_k/n_k, & i \in g_k, \\ 0, & Otherwise. \end{cases} \tag{3.42}$$

In a traditional coalition game, the cluster with a higher power reduction will be more potentially formed. Thus, the final clustering result may be the best choice for each player (leading to Pareto optimality) but may not be the global optimal solution in terms of minimizing the total power consumption. For example, considering four MUs (A, B, C and

D) in a coalition game, the potential clusters are g_1=$\{MU_A, MU_B\}$, g_2=$\{MU_B, MU_C\}$ and g_3=$\{MU_C, MU_D\}$, and the achievable power reductions for them are $\Delta P_1 = \Delta P_3 = 2$, $\Delta P_2 = 3$, respectively. The Pareto optimal solution is $G = \{g_2\}$ because MU_B and MU_C will obtain the maximum utility 1.5. However, the global optimal solution is $G = \{g_1, g_3\}$ as the total power reduction is 4. Therefore, some improvement on the traditional coalition game should be proposed. By considering the fact that a global optimal solution may be obtained when both the utility of each MU and the number of formed clusters are considered. We introduce a random variable into the design of utility function as in particle swarm optimization (PSO) approach [111] to achieve a balance between the number of formed clusters and the power reduction. The newly designed utility function $U_i^*(t)$ is defined as

$$U_i^*(t) = U_i - \kappa(t) \sum_{j=1}^{n_k} U_{g_j}, \tag{3.43}$$

where U_i is the average group utility in (42), U_{g_j} is the average group utility of cluster member MU j before a new cluster is formed, and $\kappa(t)$ denotes an update rate. This update rate is worked for MU i only when other cluster members (such as $j \in g_k$ and $j \neq i$) are already in different clusters and with non-zero utilities. Therefore, to make MU j split from its former cluster and join a newly cluster with MU i, utility of the newly cluster should be large enough to overcome the penalty of splitting. Note that $\kappa(t)$ is critical to the optimal solution, and the traditional coalition game is a special case when $\kappa(t) = 0$. For the stability of a coalition game, $\kappa(t)$ is only updated after all MUs converge to a Pareto optimal solution. We define t as the time to update $\kappa(t)$, which follows

$$\begin{aligned} \kappa(t) &= \begin{cases} \kappa(t-1) + \theta_1 rand(1) \Delta U(t), & \Delta U(t) > 0, \\ \kappa(t-1) + \theta_2 rand(1), & Otherwise. \end{cases} \\ \Delta U(t) &= \sum_{j=1}^{N} P_j(t) - \sum_{j=1}^{N} P_j^*, \end{aligned} \tag{3.44}$$

where $rand(1)$ is a random variable within 0 to 1, $P_j(t)$ is the current result of power consumption, P_j^* is the minimum power consumption resulted from the history, and θ_1 and

θ_2 are two parameters related to speed. Note that the update rate depends on the difference between the optimal result and the current result, and it can adjust the utility function to escape from the local optimal result and toward the global optimal solution.

After defining the utility functions of all MUs, the merge-and-split rule is applied, which is defined as follows.

Definition 3.4.1. *Consider two sets of coalitions* $\mathcal{G}_A = \{MU_i^A \cup MU_{j_1}^A ... \cup MU_{j_n}^A\}$ *and* $\mathcal{G}_B = \{MU_i^B \cup MU_{k_1}^B ... \cup MU_{k_l}^B\}$*, which are two potential coalition groups for* MU_i*. Here,* MU_i^A *means that MU* i *is in the coalition group* A*. For MU* i*, if and only if its utility in group* A *(denoted by* $U(\mathcal{G}_A)$*) is larger than its utility in group* B *(*$U(\mathcal{G}_A) > U(\mathcal{G}_B)$*), the coalition* $\mathcal{G}_A$ *is preferred over* $\mathcal{G}_B$ *by* Pareto order*, denoted by* $\mathcal{G}_A^{MU_i} \rhd \mathcal{G}_B^{MU_i}$.

- *Merge:* For any individual MU from i to j_n, if $\mathcal{G}_A \rhd \{MU_i, MU_{j_1}, ..., MU_{j_n}\}$ and $\mathcal{G}_A = \{MU_i \cup MU_{j_1}, ... \cup MU_{j_n}\}$, then merge $\{MU_i, MU_{j_1}, ..., MU_{j_n}\}$ to $\mathcal{G}_A$, denoted by $\{MU_i, MU_{j_1}, ..., MU_{j_n}\} \rightarrow \mathcal{G}_A$.

- *Split:* For any coalitions $\mathcal{G}_A$ and $\mathcal{G}_B$, if $\mathcal{G}_B^{MU_i} \rhd \mathcal{G}_A^{MU_i}$, then split $\mathcal{G}_A$ into $\{MU_i, MU_{j_1}, ..., MU_{j_n}\}$ and merge it into a new coalition $\mathcal{G}_B$, denoted by $\{\mathcal{G}_A, MU_{k_1} ..., MU_{k_l}^B\} \rightarrow \{\mathcal{G}_B, MU_{j_1} ..., MU_{j_n}\}$.

By the merge-and-split rule, a stable coalition formation result can be found as a Pareto optimal solution [112]. We notice that if a cluster can achieve the maximal power reduction, it will be a choice with the maximum utility to each cluster member, and thus it has a higher chance of being formed. The update rate $\kappa(t)$ will be changed after each iteration. Therefore, within a single iteration, if there is no cluster with the same utility, the Pareto optimal solution is unique. Moreover, we define the $\mathbb{D}_c$ stable as in [47], where the existence and convergence proof are also available in our cases. For the different iterations, the adjustment of $\kappa(t)$ may lead to the convergence on different Pareto optimal solutions. Then, we can find one solution with the minimal power consumption as the optimal solution by the following approach.

1) Initialization

Let the best result of power consumption and the update rate be initialized as $P^* = 0$ and $k(t) = 0$, respectively, when the current update time is $t = 1$.

2) Iteration

- **Step 1:** Randomly group all MUs into different clusters and employ the split-and-merge rule on each MU to form coalitions. Then, find the potential cluster and repeat coalition formation process until none of MU changes its strategy to improve the utility.

- **Step 2:** If the current total power consumption $\sum_{j=1}^{N} P_j$ is lower than P^*, record the solution and update $P^* = \sum_{j=1}^{N} P_j^*$. Then, update $\kappa(t+1)$ by (40) and let $t = t + 1$ until $t > T$.

Here T is a predefined maximum iteration depending on the number of MUs, so that $t = T$ means the end of the iteration.

3.4.1 Single-cluster performance analysis

In this section, we evaluate the performance of a given MIMO-NOMA cluster and the proposed clustering approach. In the simulation, we first demonstrate the impact of three main factors on the NOMA clustering and ultimately the system performance in terms of power reduction. After that, we will focus on illustrating the superiority of our proposed clustering approach by comparing with two existing ones in the literature. Since MU are randomly distributed under our settings, the probability of forming a competitively large size cluster is very low (the reason will be given in Fig. 3.6).

Consider a single cell network with a radius of 400m and a centrally located BS. The number of antennas at the BS is $M = 20$ or $M = 40$. The variance of Gaussian noise is $\sigma_u^2 = -135dBm$. The SINR requirement is $\delta = 4dB$. Similar to the existing works [113, 114], the channel model settings include: the 3GPP long term evolution (LTE) pathloss parameters ($\alpha = 3.76$ and $\beta = 10^{-14.81}$), the Rayleigh fading with zero mean and unit variance ($\Gamma_i^{(n)} \sim CN(0,1)$), a log-normal shadowing $\gamma_i \sim N(0,8)dB$, and the transmit

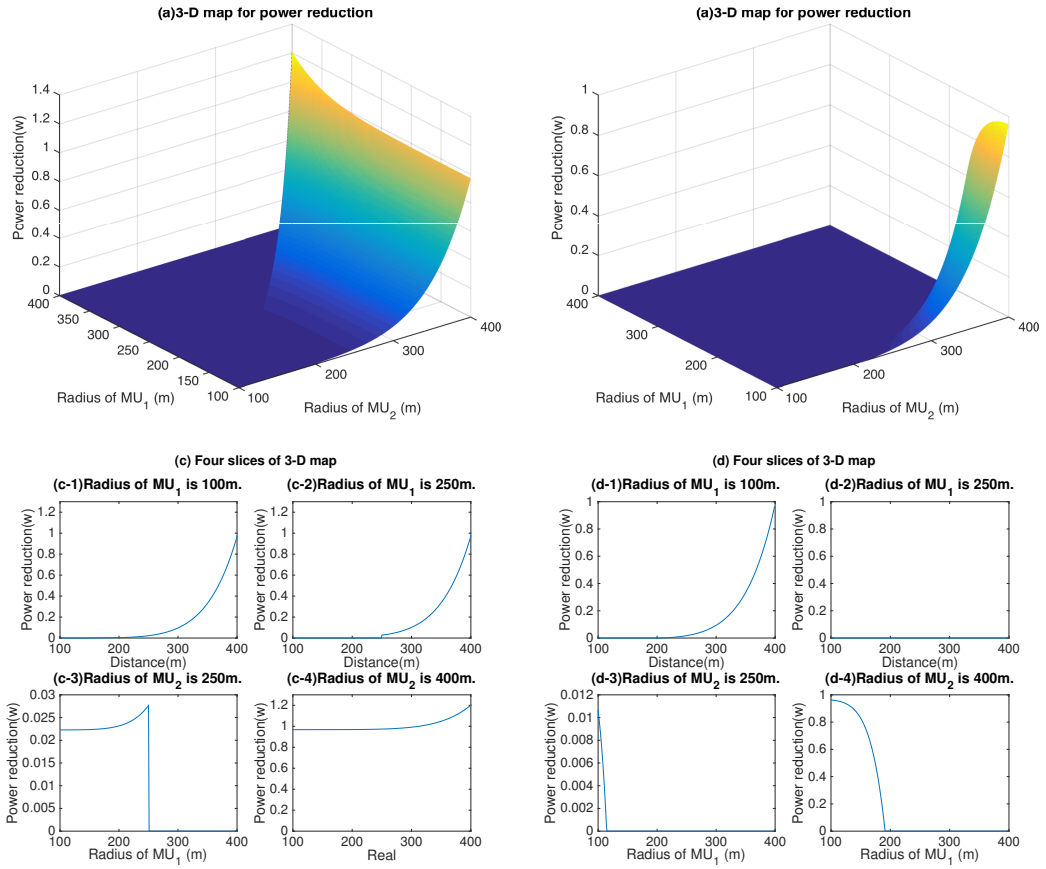

Figure 3.2: 3-D map for power reduction in MIMO-NOMA1 and MIMO-NOMA2.

antenna power gain $G = 9dB$. The channel coefficient between MU i and the BS's mth antenna is modeled as

$$h_i^{(m)} = \Gamma_i^{(m)} \sqrt{G\beta d_i^{-\alpha} \gamma_i}, \tag{3.45}$$

where d_i is the radius of MU i (i.e., the distance between MU i and the BS).

For explanation purpose, we focus on a 2-MU cluster. The impacts of three factors on the performance of power reduction are analyzed: the radius of MUs, the radius difference between two MUs, and the channel correlation coefficient. We randomly generate the locations and channel gain vectors of 10 MUs, with 5 cell-center MUs locating within radius [100, 150]m, and 5 cell-edge MUs locating within radius [346, 400]m. Then, we select one cell-center MU, namely MU_1, and one cell-edge MU, namely MU_2, to form a MIMO-NOMA cluster. The correlation between these two MUs and the shadowing

coefficient are fixed by $-0.2402 - 0.1579i$ and $1.4dB$, respectively. The only thing to be changed is the radius of MU_1 or MU_2 from $110m$ to $350m$. The radius of them should satisfy a condition that MU_1 is always smaller than MU_2 to keep MU_1 always to be a cell-center MU compared with the location of MU_2. Simulation results for MIMO-NOMA1 and MIMO-NOMA2 are shown in Fig. 3.2.

Fig. 3.2(a) shows the variance of power reduction resulted from clustering with respect to the radius $R_1(R_2)$ of the cluster member $MU_1(MU_2)$, under the MIMO-NOMA1 scenario. To observe the variance, we select four cross section views as shown in Fig. 3.2(c) by fixing one MU's radius while changing the other. As shown in Figs. 3.2(c-1) and (c-2), power reduction increases with R_2 if the radius of MU_1 is given. However, given the radius of MU_2 as shown in Figs. 3.2(c-3) and (c-4), the variance of power reduction with respect to R_1 is not that obvious unless MU_2 locates at the cell edge. By comparing Figs. 3.2(c-2) with (c-4), we can see that a larger power reduction is obtained when MUs are both close to the cell edge. Therefore, for MIMO-NOMA1, we can conclude that the power reduction is mainly determined by the radius of the cell-edge MU, so that a cell-edge MU is the necessary condition to form a beneficial cluster.

These observations imply the existence of radius thresholds in separating the area of the cell-center and the cell-edge, which can be used to narrow down the searching space of beneficial NOMA clusters. To evaluate the minimal radius for a cell-edge MU, we generate a pair of MUs which include MU_1 (radius is fixed to $100m$) and MU_2 (radius changes from $100m$ to $400m$). The Rayleigh fading coefficients are generated randomly with a sample quantity of 2000, while the shadowing coefficient is fixed by 1.4dB. Simulation shows that when the radius of MU_2 is smaller than $233m$, the power reduction is less than $0.01w$ for most of channel gain correlation coefficients. Therefore, the radius threshold for a cell-edge MU can be selected by $233m$.

The simulation results in MIMO-NOMA2 is shown in Fig. 3.2 (b) and (d). As shown in Fig. 3.2(d-1), power reduction increases with R_2 if MU_1 is located at the cell center. However, different from MIMO-NOMA1, if a MIMO-NOMA2 cluster only has cell-center

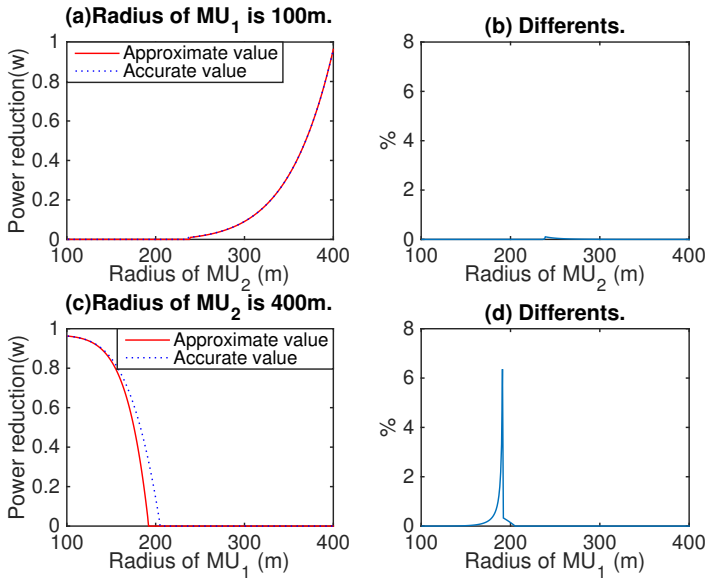

Figure 3.3: Comparison, MU_1 radius is fixed in (a) and (b), MU_2 radius is fixed in (c) and (d).

MUs (as the case in Fig. 3.2(d-3)) or cell-edge MUs (as shown in Fig. 3.2(d-2)), the power reduction is close to zero. In Fig. 3.2(d-4), power reduction decreases with R_1 if MU_2 is located at the cell edge. Thus, a beneficial cluster needs a cell-center MU and a cell-edge MU. In addition, by comparing Figs. 3.2(a) and (b), for a same pair of MUs, it is shown that MIMO-NOMA1 can achieve a better power efficiency than MIMO-NOMA2.

Since the result of MIMO-NOMA2 is an approximate solution, we have to discuss its accuracy, and show the comparison between the accurate results and the approximate ones in Fig. 3.3. The percentage of error is equal to the accurate result minus the approximate result and divide by the approximate result. From Figs. 3.3(b) and (d), we can observe that the approximate results are nearly the same as the accurate ones when the distance between MU_1 and MU_2 is sufficiently large. The percentage of error is less than 7% in this case. Besides, we notice that the area of the percentage of error larger than 0.1% in 3(b) (or 3(d)) is [237, 240]m (or [169, 202]m), which is a small area when compared with that lower than 0.1% [241, 400]m (or [100, 168]m). Therefore, to improve the accuracy of results, we can suitably set up radius thresholds for both cell-center MUs and cell-edge MUs and the minimum distance between them.

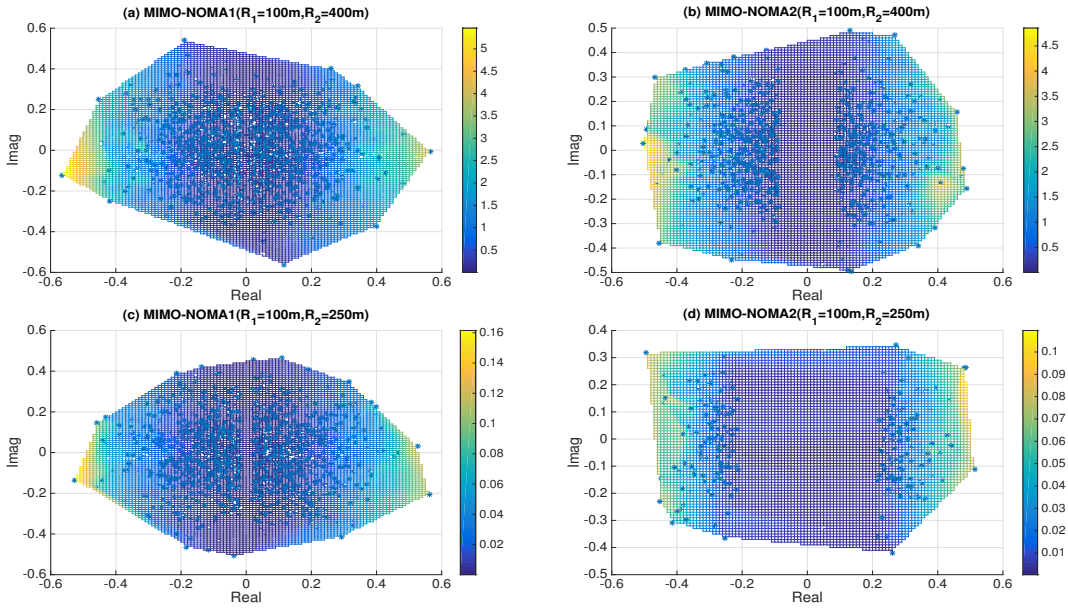

Figure 3.4: Vertical view of correlation coefficient results

For obtaining the radius threshold of a cell-edge MU, the simulation process is the same as that of MIMO-NOMA1 and the radius threshold is $236m$ for power reduction larger than $0.01w$. For deriving the radius threshold of a cell-center MU, we fix the radius of MU_2 as $400m$ and change the radius of MU_1 from $100m$ to $400m$. The results show that the radius threshold is $285m$ for power reduction larger than $0.01w$. To ensure the percentage of error less than 0.1%, the minimum distance between them is $185m$. Note that since the log-normal shadowing is fixed as 1.4 under our settings, we need to consider the real log-normal shadowing value before we employing these radius threshold.

Fig. 3.4 shows the effects of channel gain correlation coefficient on power reduction in the vertical view, where the color in color bar from dark to light means the amount of power reduction from low to high. The channel gain correlation coefficient between MU_1 and MU_2 is a randomly generated complex value and other settings are fixed. The radius of MU_1 and MU_2 are fixed as $100m$ and $400m$ as shown in Figs. 3.4(a) and (b), and $100m$ and $270m$ as shown in Figs. 3.4(c) and (d), respectively. From these figures, we can observe that the power reduction is positively associated with the absolute value of the real part of correlation coefficient while weakly associated with the imaginary part. There is a

gap around zero of x-axis which indicates that if two MUs' correlation coefficient is within this gap, they can not form a beneficial NOMA cluster. We compare MIMO-NOMA1 with MIMO-NOMA2 in the same radius condition by noticing Figs. 3.4(a) and 4(b) or Figs. 3.4(c) and (d), and find that the gap in MIMO-NOMA1 is smaller than that in MIMO-NOMA2. It further illustrates that the solution space of MIMO-NOMA1 is larger than that of MIMO-NOMA2. Besides, by comparing Figs. 3.4(a) with (c) or Figs. 3.4(b) with (d), the gap becomes broadened, and the value of color bar is reduced, when MU_2 is getting close to the cell center. This is because R_2 has the larger influence on power reduction. The detailed explanation is in appendix A.3.

3.4.2 MU clustering result

To evaluate the performance of our proposed MU clustering approach (power-reduction based approach), two existing approaches in literature are also simulated as benchmarks: the channel gain-correlation based approach [83] and the channel gain-difference based approach [20]. Both of them are the two-stage optimization, where MU clustering and system optimization apply independently handled. The main procedures of these two approaches are listed as follows.

1) The channel gain-correlation based approach

Step 1: Generate a metric vector $v_{i,j}$ for all MUs as

$$v_{i,j} = \begin{cases} 0 & \text{if } \left|10\log|\boldsymbol{h}_i|^2 - 10\log|\boldsymbol{h}_j|^2\right| \leq 3dB, \\ \left|\tilde{\boldsymbol{h}}_i \cdot \tilde{\boldsymbol{h}}_j\right|, & \text{Otherwise,} \end{cases} \tag{3.46}$$

where $\boldsymbol{h}_i$ and $\tilde{\boldsymbol{h}}_i$ are channel gains of MU i with and without path-loss coefficient, respectively.

Step 2: Group MUs into MIMO-NOMA clusters according to the descending order of $v_{i,j}$.

Step 3: Calculate the beamforming matrix and the power reduction. Note that the stronger user in a cluster is the MU with a larger $|\boldsymbol{h}_i|$.

2) The channel gain-difference based approach

Step 1: Generate a metric vector $\pi_{i,j}$ representing the channel gain-difference as

$$\pi_{i,j} = \begin{cases} ||\boldsymbol{h}_i| - |\boldsymbol{h}_j||, & \text{if} \frac{|\boldsymbol{h}_i \cdot \boldsymbol{h}_j|}{|\boldsymbol{h}_i||\boldsymbol{h}_j|} > 0.4, \\ 0, & \text{Otherwise.} \end{cases} \tag{3.47}$$

Step 2: Group MUs into MIMO-NOMA clusters according to the descending order of $\pi_{i,j}$.

Step 3: In this approach, the channel gain matrix is composed by the channel gains of MIMO-OMA MUs and the stronger MUs (i.e., with a larger $|\boldsymbol{h}_i|$) in clusters. Then, calculate the beamforming matrix and the total power reduction.

The channel gain-correlation based approach is used for MIMO-NOMA1 (denoted by MIMO-NOMA1-CO), and the channel gain-difference based approach is used for MIMO-NOMA2 (denoted by MIMO-NOMA2-GD).We further denote the proposed power-reduction based approach for MIMO-NOMA1 as MIMO-NOMA1-PO and for MIMO-NOMA2 as MIMO-NOMA2-PO, and both of them are managed by the traditional coalition game approach. In the following simulations, the BS is equipped with $M = 40$ antennas, and all MUs are distributed within a radius range of [100,500]m. Since the different MUs' distribution and channel gains may result in a large difference on total power consumption, we compare and evaluate the system performance by a normalized average power consumption (denoted by NPC), i.e., for the result of 50 sets of randomly generated data, normalize them by the results of MIMO-OMA, and then calculate the average value.

From Fig. 3.5, we notice that the normalized power consumption is decreased with the number of MUs for all approaches. It means that NOMA-MIMO can reduce more power consumption in the large-scale system. Besides, MIMO-NOMA1 is better than MIMO-NOMA2 in improving the energy efficiency as it is more flexible on power coefficient settings. In addition, compared with the approach in literature, MIMO-NOMA1-PO (MIMO-NOMA2-PO) is better than MIMO-NOMA1-CO (MIMO-NOMA2-GD) in the scenario of MIMO-NOMA1 (MIMO-NOMA2). Thus, we can conclude that the power-reduction based approach obviously outperforms both the channel gain-correlation

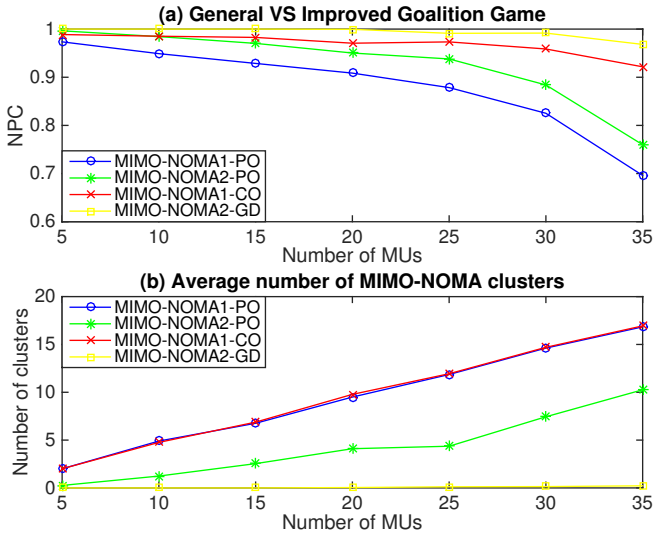

Figure 3.5: Power reduction results comparison for different clustering approaches.

based and the channel gain-difference based approaches. Moreover, the performance improvement becomes more obvious with the number of MUs even in the case of the same number of MIMO-NOMA clusters as shown in Fig. 3.5(b). It results from the fact that the power-reduction based approach is a joint optimization approach, so that it can be more efficient in finding an optimum MIMO-NOMA cluster set than the counterparts.

The results of fixed (denoted as PO2) and flexible (denoted as PO3) cluster size conditions are compared in Fig. 3.6(a) and (b). For the case of fixed (or flexible) cluster size, a MIMO-NOMA cluster can only include 2 MUs (2 or 3 MUs). In this figure, MIMO-NOMA1-PO2-M1 (MIMO-NOMA2-PO3-M1) denotes the result of power-reduction based approach with fixed (flexible) cluster size condition by the traditional coalition game approach in MIMO-NOMA1 (MIMO-NOMA2) scenario. Simulation results show that the result with the flexible cluster size condition is better than without that in both MIMO-NOMA1 and MIMI-NOMA2. Besides, the difference between fixed and flexible cluster sizes are gradually increased with the number of MUs as shown in Fig. 3.6(b), and the difference is more obvious in MIMO-NOMA1 than MIMO-NOMA2. However, we notice that in Fig. 3.6(b), the difference in MIMO-NOMA1 decreases when the number of MUs is larger than 30. It means that a larger size cluster may not always be better than a smaller

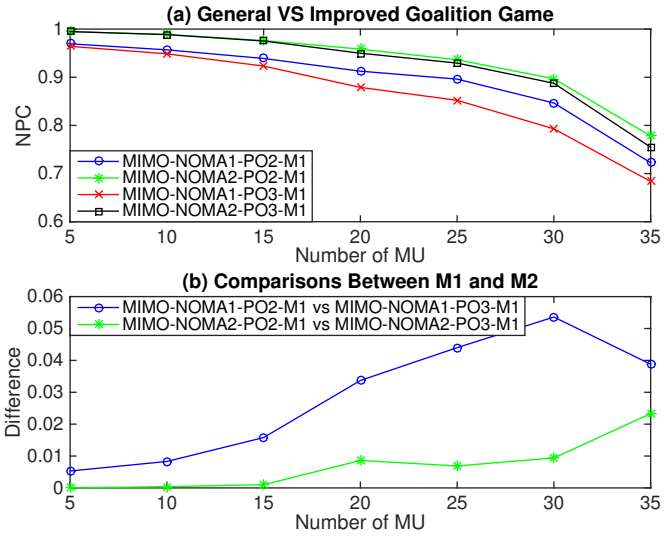

Figure 3.6: Results with different cluster size limitations.

one in terms of average power reduction, because i) the power reduction hinges on the channel gain correlation coefficient and ii) the MU density increases with the number of MUs. In summary, MIMO-NOMA1 with the flexible cluster size condition performs better than the other cases, and the cluster size is affected by the MU density and distribution.

The results based on the improved coalition game (denoted as M2) and the traditional coalition game (denoted as M1) are compared in Fig. 3.7(a) and (b). In Fig. 3.7(a), we only compare two results between MIMO-NOMA1-PO3-M1 and MIMO-NOMA1-PO3-M2. The result of MIMO-NOMA1-PO3-M1 (MIMO-NOMA1-PO3-M2) is obtained by employing MIMO-NOMA1 with a flexible cluster size condition and operating by the traditional (improved) coalition game. We notice that the improved coalition game achieves a lower power consumption than the traditional coalition game, and such improvement has an increasing trend as the number of MUs increases. Moreover, for the case of MIMO-NOMA2 or in the fixed cluster size condition, results are in the same tendency as shown in Fig. 3.7(b). Furthermore, Fig. 3.7(b) compares M1 and M2 for 4 different cases, and the curves show the difference between them, e.g., the result of MIMO-NOMA1-PO2-M1 minus that of MIMO-NOMA1-PO2-M2. Thus, the difference means that M1 has much more power consumption than M2. In this figure, the difference value of MIMO-NOMA1 is

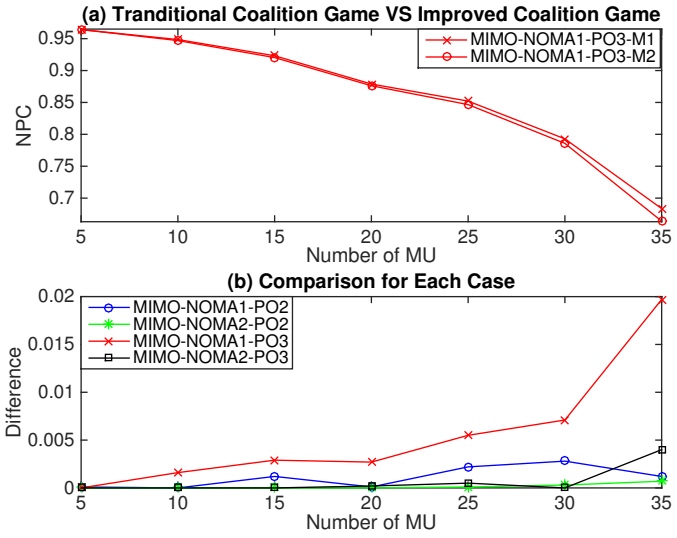

Figure 3.7: Results for MIMO-NOMA 1 with different game approaches.

larger than that of MIMO-NOMA2. Moreover, we observe that a small difference appears as the solution space is small (i.g., with a small quantity of MUs, or in MIMO-NOMA2 cases). Besides, we notice a significant increase in Fig. 3.7(b) on both MIMO-NOMA1-PO3 and MIMO-NOMA2-PO3 curves when the number of MUs is larger than 30 and both of them have the flexible cluster size condition. Therefore, we can conclude that the improved coalition game can find a better result than the traditional coalition game approach, especially when a large quantity of MUs and the flexible cluster size condition are considered.

Chapter 4

Multi-cell MIMO-NOMA

4.1 Introduction

Resource management in multi-cell multiple-input multiple-output non-orthogonal multiple access (MIMO-NOMA) is challenged by computational complexity, flexible clustering, and potential channel correlation. In this chapter, we focus on a combined resource allocation problem: NOMA mobile user (MU) clustering and the base station (BS) selection, to improve system data rate. We consider two objectives: sum data rate maximization ($\boldsymbol{O}_1$) and relative fairness ($\boldsymbol{O}_2$), and propose a two-side coalitional matching approach in order to achieve win-win solutions. The necessary requirements for obtaining a core stable coalitional matching under different objective functions are also derived. Extensive comparisons have been provided in simulations by considering different objective functions, different optimization approaches, and different cluster sizes. The main contributions of this chapter are summarized as follows.

- We propose a novel cluster beamforming strategy for MIMO-NOMA and derive a closed-form solution for resource allocation based on zero-forcing beamforming.

Following this strategy, NOMA power coefficient allocation can be integrated into beamforming calculation, and the correlation among MUs within a same BS can be eliminated.

- We propose a two-side coalitional matching approach under the consideration of preferences on both the MU side and the BS side to derive a win-win strategy. We further prove the stability of this proposed approach to ensure system convergence.

- We introduce a new objective function, which reflects the relative fairness among MUs. We identify the weight of each BS to be the number of accessed MUs in this BS based on the fact that the number of accessed MUs is related with the required spatial division of antenna beams, so that MU fairness is associated with the sum data rate.

- We employ the Pauta Criterion as a way of system performance evaluation for the win-win strategy. By eliminating the outliers (i.e., MUs with extreme high data rates), the Pauta Criterion guarantees the obtained results satisfy the conditions that: i) the sum data rate is high; and ii) the difference between the maximum and minimum data rates of MUs is small.

4.2 System Model

4.2.1 Beamforming model

Consider a L-cell downlink MIMO-NOMA system with a BS in the center of each cell. Each BS is equipped with M antennas, and there are N single-antenna MUs randomly distributed in the system. Let $\boldsymbol{h}_{li} = [h_{1li}, ..., h_{Mli}] \in C^{1\times M}$ denote the channel gain vector from BS l to MU i. Then, we can define $\boldsymbol{W}_l = [\boldsymbol{w}_{l1}^H, ..., \boldsymbol{w}_{ln_l}^H]^H$ and $\boldsymbol{H}_l = [\boldsymbol{h}_{l1}^H, ..., \boldsymbol{h}_{ln_l}^H]^H$ to denote the beamforming matrix and the channel gain matrix of BS l (n_l is the number of

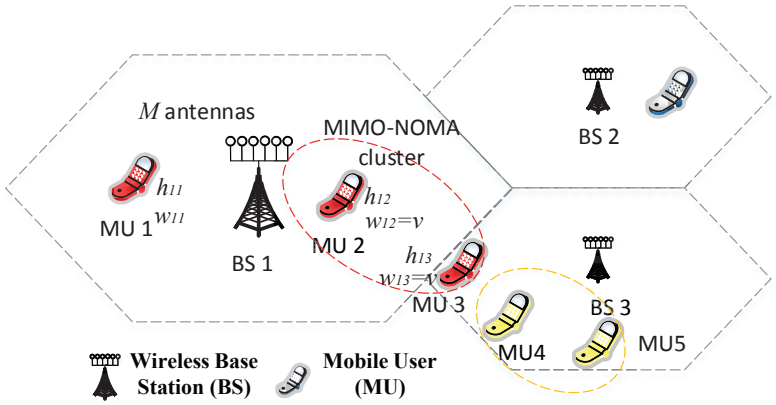

Figure 4.1: A multi-cell MIMO-NOMA system

MUs served by this BS), respectively. In the OMA state, the beamforming matrix can be calculated as [22]

$$\boldsymbol{W}_l^{'} = \boldsymbol{H}_l^{\dagger} = \boldsymbol{H}_l^{*}(\boldsymbol{H}_l\boldsymbol{H}_l^{*})^{-1}. \tag{4.1}$$

4.2.2 Signal model

Let $G_l = \{\mathcal{G}_{l_1}, \mathcal{G}_{l_2}, ..., \mathcal{G}_{l_K}\}$ denote a set of K MIMO-NOMA clusters in BS l. In each cluster, such as $\mathcal{G}_{l_d} = \{\ g_{l_d,1}, g_{l_d,2}, ..., g_{l_d,k_d}\}$, we assume that there are k_d MUs lined up in the reverse order of successive interference cancellation (SIC) decoding. In this work, we consider a more general case that the power coefficients on different antennas are different [108].

For MU i in the OMA state, the received signal y_{li} from BS l can be calculated as

$$y_{li} = \boldsymbol{h}_{li}^{H}\boldsymbol{w}_{li}^{'}\sqrt{p_{li}}x_i + \sum_{u\neq i}\sum_{j\in B, j\neq l}\boldsymbol{h}_{ij}^{H}\boldsymbol{w}_{uj}^{'}\sqrt{p_{uj}}x_u + \mathcal{N}_i, \tag{4.2}$$

where $\boldsymbol{w}_{li}^{'} \in R^{M\times 1}$ is the beamforming vector allocated to this MU i, p_{li} is the transmit power (since $\left\|\boldsymbol{w}_{li}^{'}\right\|^2$ is unnormalized, the actual BS's power consumption is calculated as in (4.6)), x_i is the data symbol transmitting to MU i, and $\mathcal{N}_i$ denotes the additive white Gaussian noise with zero mean and variance σ_i^2. $B = \{1, 2, ..., L\}$ denotes the set of BSs.

If MU i belongs to a MIMO-NOMA cluster l_d, i.e., $i \in \{g_{l_d,1}, ..., g_{l_d,k_d}\}$(to simplify the notation of subscripts, we assume $g_{l_d,1} = 1$,...,$g_{l_d,k_d} = k_d$), signals of MUs in this cluster will be superposed based on NOMA power coefficients. Based on [108], the superposed transmit signal can be written as

$$\boldsymbol{s}_{ld} = \boldsymbol{w}_{l1}\sqrt{p_{l1}}x_1 + ... + \boldsymbol{w}_{lk_d}\sqrt{p_{lk_d}}x_{k_d}, \tag{4.3}$$

where $\boldsymbol{w}_{li}$ and p_{li} denote the redefined beamforming vectors and the redefined transmit power for this MU i, respectively to [108]. $\boldsymbol{w}_{li} = \{w_{i1}, ...w_{iM}\}$ can be obtained by the weighted sum of $\boldsymbol{w}_{l1}^{'}, ..., \boldsymbol{w}_{lk_d}^{'}$.

Then, after SIC decoding, the received signal y_{li} can be written as

$$\begin{aligned} y_{li} = \boldsymbol{h}_{li}^H \boldsymbol{s}_{l_d} + \mathcal{N}_i = \boldsymbol{h}_{li}^H \boldsymbol{w}_{li}\sqrt{p_{li}}x_i + \\ \sum_{u=1}^{i-1} \boldsymbol{h}_{li}^H \boldsymbol{w}_{lu}\sqrt{p_{lu}}x_u + \sum_{u\neq i}\sum_{j\in B-l} \boldsymbol{h}_{ji}^H \boldsymbol{w}_{ju}\sqrt{p_{ju}}x_u + \mathcal{N}_i. \end{aligned} \tag{4.4}$$

Through SIC decoding (refer to appendix B.7), signals of MUs from $i+1$ to k_d can be decoded and cancelled, while those of
MUs from 1 to i–1 will be regarded as the intra-cell interference. Comparing (4.2)and (4.4), the only difference of the received signals between the NOMA state and the OMA state is the un-cancelled intra-cell interference (denoted as $I_{li}^{[2]}$). Denote the inter-cell interference as $I_{li}^{[1]}$. By assuming $\mathcal{N}_i/x_i^2 = \mathcal{N}_j/x_j^2 = \sigma^2$ and $x_i^2 = x_j^2$, the signal-to-interference-plus-noise ratio (SINR) for this MU i in both states can be obtained as

$$\gamma_{li} = \frac{\left|\boldsymbol{h}_{li}^H \boldsymbol{w}_{li}^{'}\sqrt{p_{li}}\right|^2}{I_{li}+\sigma^2}, \text{and } I_{li} = \begin{cases} I_{li}^{[1]}, & \text{if MIMO-OMA}, \\ I_{li}^{[1]} + I_{li}^{[2]}, & \text{if MIMO-NOMA}, \end{cases} \tag{4.5}$$

where $I_{li}^{[1]} = \sum_{u\neq i} |\sum_{j\in B-l} \boldsymbol{h}_{ji}^H \boldsymbol{w}_{ju}\sqrt{p_{ju}}x_u|^2$, $I_{li}^{[2]} = \sum_{u=1}^{i-1} |\boldsymbol{h}_{li}^H \boldsymbol{w}_{lu}\sqrt{p_{lu}}x_u|^2$. Therefore, the achievable rate of MU i can be calculated as $R_{li} = log_2(1+\gamma_{li})$, and the power consumption of it in both states at SINR γ_{li} can be derived as

$$P_{li} = \left\|\boldsymbol{w}_{li}^{'}\right\|^2 p_{li} = \left\|\boldsymbol{w}_{li}^{'}\right\|^2 (I_{li} + \sigma^2)\gamma_{li}. \tag{4.6}$$

4.2.3 Problem formulation

In this work, we consider the following two objectives.

Sum data rate maximization ($\boldsymbol{O}_1$)

The problem can be formulated as

$$\boldsymbol{O}_1 : \max_{\boldsymbol{W},\boldsymbol{p}} \sum_{l=1}^{L} \sum_{i=1}^{n_l} R_{li}(\boldsymbol{w}_{li}, p_{li}), \tag{4.7a}$$

$$\text{s.t.} \quad R_{li} = R_{lj} \quad \text{for all} \quad i, j \in n_l, \tag{4.7b}$$

$$\sum_{i=1}^{N} P_{li} = P \quad \text{and}, \tag{4.7c}$$

$$\boldsymbol{h}_{li}\boldsymbol{w}_{lj} \begin{cases} \neq 0 \text{ If MUs } i \text{ and } j \text{ are in the same cluster}, \\ = 0 \qquad\qquad\qquad \text{Otherwise}, \end{cases} \tag{4.7d}$$

$$\gamma_{li}^{j} > \gamma_{li}^{j-1}, \text{ with the decoding order } j > i, \tag{4.7e}$$

where P_{li} is the power consumption of BS l for MU i (as calculated in (4.6) and the closed form results for different scenarios are given in (4.10)) which is determined by the beamforming vector $\boldsymbol{w}_{li}$ and the transmit power p_{li}. ζ is a predefined parameter. We use a general notation $\boldsymbol{W}$ to denote the beamforming of all BSs. The similar definition is employed on $\boldsymbol{p}$. Constraint (4.7b) indicates the transmission fairness requirements that all MUs obtain a same transmit date rate if served by a same BS. Constraint (4.7c) means that the total power consumption of each BS should be lower than P. Constraint (4.7d) indicates the orthogonal condition for MUs in a MIMO-NOMA cluster. Constraint (4.7e) indicates the successful SIC decoding conditions (refer to Appendix B.7) [109].

Relative fairness ($\boldsymbol{O}_2$)

We consider a weighted fairness optimization, which is inspired by the Harmonic fairness [115, 116]. The weight of each BS is determined by the number of MUs it served, which is based on the fact that the total power consumption is limited by P, and it's data rate variation is related with the number of accessed MUs. Therefore, our defined weights can associate the fairness with the sum data rate. The newly designed objective function is

$$\boldsymbol{O}_2 : \min \sum_{l=1}^{L} \frac{n_l}{R_l}. \tag{4.8}$$

Compared with maximizing overall date rates $\boldsymbol{O}_1$, the domination effect is removed as R_l appears in the denominator. If a MU selects a BS with a large weight, it may result in a great reduction on the sum data rate. Comparing with max-min fairness (in Appendix B.3), each MU will prefer the BS which provides higher data rate while having fewer MUs. After some manipulations, the optimization problem with the newly proposed objective function can be written as

$$\boldsymbol{O}_2 : \min_{\boldsymbol{W},\boldsymbol{p}} \sum_{l=1}^{L} \sum_{i=1}^{n_l} \frac{n_l P_{li}}{P\gamma_{li}(\boldsymbol{w}_{li}, p_{li})}, \tag{4.9a}$$

$$\text{s.t} \ \ \text{(4.7b)-(4.7e)}, \tag{4.9b}$$

where P_{li} is the corresponding power consumption of MU i as calculated in (6).

4.3 MIMO-NOMA Cluster Scheduling

In this section, we derive the resource allocation strategy (which includes the NOMA beamforming strategy and power allocations) for a MIMO-NOMA cluster in a single BS to maximize the total data rate. We show the derivation of a n-MU MIMO-NOMA cluster first, and then give the closed form solution for 2-MU and 3-MU NOMA clusters as examples.

4.3.1 MIMO-NOMA resource allocation for a n-MU cluster

Consider a cluster with n MUs (i.e., $\mathcal{G}_{l_d} = \{1, 2, ..., n\}$). The pre-determined decoding order is from n to 1. According to (4.4) and (4.6), after decoding messages, the received signal and corresponding power consumption for MU $i \in \{1, 2, .., n\}$ can be calculated as

$$\begin{aligned} y_{li} &= \boldsymbol{h}_{li}^H \boldsymbol{w}_{li}\sqrt{p_{li}}x_i + \sum_{k=1}^{i-1}(\boldsymbol{h}_{li}^H \boldsymbol{w}_{lk}\sqrt{p_{lk}}x_k) + \sum_{u\neq ij\in B-l}\sum \boldsymbol{h}_{ij}^H \boldsymbol{w}_{uj}\sqrt{p_{uj}}x_u + \mathcal{N}_i, \\ P_{li} &= \|\boldsymbol{w}_{li}\|^2 (I_{li} + \sum_{k=1}^{i-1} \left|\boldsymbol{h}_{li}^H \boldsymbol{w}_{lk}\right|^2 p_{lk} + \sigma^2)\delta. \end{aligned} \tag{4.10}$$

The NOMA beamforming vector of this MU i is calculated as $\boldsymbol{w}_{li} = \lambda_{i1}\boldsymbol{w}_{l1}^{'} + \lambda_{i2}\boldsymbol{w}_{l2}^{'} + ... + \lambda_{in}\boldsymbol{w}_{ln}^{'}$, and $\lambda_{ii} = 1$ [108]. We can calculate the power consumptions of MUs n and $n-1$ as

$$\begin{aligned} P_{ln-1} &= \|\boldsymbol{w}_{ln-1}\|^2 p_{ln-1} = \|\boldsymbol{w}_{ln-1}\|^2 (I_{ln-1} + \lambda_{1n-1}^2 p_{l1} + ... + \lambda_{n-2n-1}^2 p_{ln-2} + \sigma^2)\delta, \\ P_{ln} &= \|\boldsymbol{w}_{ln}\|^2 p_{ln} = \|\boldsymbol{w}_{ln}\|^2 (I_{ln} + \lambda_{1n}^2 p_{l1} + ... + \lambda_{n-1n}^2 p_{ln-1} + \sigma^2)\delta. \end{aligned} \tag{4.11}$$

Minimizing the group power consumption can be derived by beamforming coefficients $\lambda_{ij}, i, j \in \{1, 2, ...n\}$

$$\min_{\{\lambda_{11},...,\lambda_{n,n}\}} P_{l1} + ... + P_{ln} = f(\lambda_{11}, ..., \lambda_{n,n}), \tag{4.12a}$$

$$\text{s.t.} \quad \lambda_{ii+1}^2 > (1+\delta), \text{and } \lambda_{ij}^2 > (1+\gamma_{li}^{j-1})\lambda_{ij-1}^2, \text{if } j > i, \tag{4.12b}$$

where (4.12b) is the SIC condition, which is the transformation of (4.7e) as shown in Appendix B.7. Such problem can be recursively solved by the order from MU n to MU 1. The first subproblem for determining MU n's beamforming vector is

$$\begin{aligned} &\min f(\lambda_{n1}, ..., \lambda_{nn-1}) = \|\boldsymbol{w}_{ln}\|^2 \\ &= \lambda_{n1}^2 \boldsymbol{w}_{l1}^{'2} + ... + \boldsymbol{w}_{ln}^{'2} + 2\lambda_{n1}\lambda_{n2}\boldsymbol{w}_{l1}^{'}\boldsymbol{w}_{2}^{'} + ... + 2\lambda_{n1}\boldsymbol{w}_{l1}^{'}\boldsymbol{w}_{ln}^{'}. \end{aligned} \tag{4.13}$$

Table 4.1: Algorithm of data rate calculation

1. Calculate NOMA beamforming as δ;
2. Update $\delta' = \frac{P}{\sum_{i=1}^{n_l} \left\|\boldsymbol{w}_{li}'\right\|^2 p_{li} + \sum_{d=1}^{K} \sum_{i=1}^{k_d} P_{li}(\delta)} \delta$;
3. If $\delta' = \delta$, end the iteration. Otherwise, let $\delta = \delta'$ and go to 1.

The solution can be derived by letting the 1st-order derivative of $f(.)$ be zero, i.e.,

$$\begin{aligned} &[\lambda_{n1}, \lambda_{n2}, ..., \lambda_{nn-1}] = BA^{-1}, \\ &\text{where } B = -[\boldsymbol{w}_{l1}'\boldsymbol{w}_{ln}', \boldsymbol{w}_{l2}'\boldsymbol{w}_{ln}', ..., \boldsymbol{w}_{ln-1}'\boldsymbol{w}_{ln}'], \\ &A = \begin{bmatrix} \left\|\boldsymbol{w}_{l1}'\right\|^2 & \boldsymbol{w}_{l1}'\boldsymbol{w}_{l2}' & ... & \boldsymbol{w}_{l1}'\boldsymbol{w}_{ln-1}' \\ \vdots & \vdots & & \vdots \\ \boldsymbol{w}_{ln-1}'\boldsymbol{w}_{l1}' & \boldsymbol{w}_{ln-1}'\boldsymbol{w}_{l2}' & ... & \left\|\boldsymbol{w}_{ln-1}'\right\|^2 \end{bmatrix}. \end{aligned} \tag{4.14}$$

After that, we substitute (4.14) into (4.12) and formulate the second subproblem for $\lambda_{n-11}, ..., \lambda_{n-1n}$, which is based on the fact that $p_{ln-1} > 0$, i.e.,

$$\min f(\lambda_{n-11}, ..., \lambda_{n-1n}) = \left\|\boldsymbol{w}_{ln-1}\right\|^2 + \left\|\boldsymbol{w}_{ln}\right\|^2 \lambda_{n-1n}^2.$$

Similarly, λ_{n-1j} (for $j = 1, 2, ..., n$) can be derived accordingly. By substituting obtained solutions back to the objective function, we can formulate the subproblem for $\lambda_{n-21}, ..., \lambda_{n-2n}$. This process continues till all MUs have been considered. After that, we calculate SINR and data rate for each MU following the approach in table 4.1. To better illustrate this recursive method, we show the derivation progress for 2-MU and 3-MU clusters as examples.

4.3.2 MIMO-NOMA solutions for 2-MU and 3-MU clusters

Beamforming vectors for a 2-MU MIMO-NOMA cluster (e.g., $\mathcal{G}_{l_d}=\{1,2\}$) is obtained by

$$[\boldsymbol{w}_{l1}, \boldsymbol{w}_{l2}] = [\boldsymbol{w}_{l1}^{'}, \boldsymbol{w}_{l2}^{'}] \begin{bmatrix} 1 & \lambda_{12} \\ \lambda_{21} & 1 \end{bmatrix}. \tag{4.15}$$

According to (4.10), power consumption can be represented as

$$\begin{aligned} P_{l1} &= \|\boldsymbol{w}_{l1}\|^2 p_{l1} = \|\boldsymbol{w}_{l1}\|^2 (I_{l1}^{[1]} + \sigma^2)\delta, \\ P_{l2} &= \|\boldsymbol{w}_{l2}\|^2 p_{l2} = \|\boldsymbol{w}_{l2}\|^2 (I_{l2}^{[1]} + \left|\boldsymbol{h}_{l2}^H \boldsymbol{w}_{l1}\right|^2 p_{l1} + \sigma^2)\delta. \end{aligned} \tag{4.16}$$

According to (4.14), we have

$$\begin{aligned} &A = \left\|\boldsymbol{w}_{l1}^{'}\right\|^2, B = -\boldsymbol{w}_{l2}^{'T}\boldsymbol{w}_{l1}^{'}, \\ &\lambda_{12}^* = -\frac{\boldsymbol{w}_{l2}^{'T}\boldsymbol{w}_{l1}^{'}}{\left\|\boldsymbol{w}_{l1}^{'}\right\|^2} \text{ and } \lambda_{12} = sign(\lambda_{12}^*)\max\{|\lambda_{12}^*|, \sqrt{(1+\delta)}\}. \end{aligned} \tag{4.17}$$

Then, we take λ_{12} back to $P_{l1} + P_{l2}$ and update A and B as

$$A = \left\|\boldsymbol{w}_{l2}^{'}\right\|^2 + \|\boldsymbol{w}_{l2}\|^2\delta, B = -\boldsymbol{w}_{l2}^{'T}\boldsymbol{w}_{l1}^{'}, \text{so that } \lambda_{21} = \frac{B}{A}. \tag{4.18}$$

Similarly, for a 3-MU MIMO-NOMA cluster (e.g., $\mathcal{G}_{l_d} = \{1, 2, 3\}$), NOMA beamforming vectors are calculated by

$$[\boldsymbol{w}_{l1}, \boldsymbol{w}_{l2}, \boldsymbol{w}_{l3}] = [\boldsymbol{w}_{l1}^{'}, \boldsymbol{w}_{l2}^{'}, \boldsymbol{w}_{l3}^{'}] \begin{bmatrix} 1 & \lambda_1 & \lambda_2 \\ \lambda_3 & 1 & \lambda_4 \\ \lambda_5 & \lambda_6 & 1 \end{bmatrix}, \tag{4.19}$$

and the coefficients λ_ϵ ($\epsilon = 1, 2, ..., 6$) can be derived based on the following optimization problem

$$\min f(\lambda_1, ..., \lambda_6) = P_{l1} + P_{l2} + P_{l3}. \tag{4.20}$$

To meet the minimal SINR requirement, the received signal and the power consumption for MU3can be expressed as

$$\begin{aligned} y_{l3} &= \boldsymbol{h}_{l3}^H \boldsymbol{w}_{l3}\sqrt{p_{l3}}x_3 + \sum_{u=1,2}(\boldsymbol{h}_{l3}^H \boldsymbol{w}_{lu}\sqrt{p_{lu}}x_u) + \sum_{u\neq 3}\sum_{j\in B-l}\boldsymbol{h}_{l3}^H \boldsymbol{w}_{ju}\sqrt{p_{ju}}x_u + \mathcal{N}_3, \\ P_{l3}(\delta) &= \|\boldsymbol{w}_{l3}\|^2 (I_{l3}^{[1]} + \left|\boldsymbol{h}_{l3}^H \boldsymbol{w}_{l1}\right|^2 p_{l1} + \left|\boldsymbol{h}_{l3}^H \boldsymbol{w}_{l2}\right|^2 p_{l2} + \sigma^2)\delta, \end{aligned} \tag{4.21}$$

where $p_{l1} = (I_{l1}^{[1]} + \sigma^2)\delta, p_{l2} = (I_{l2}^{[1]} + \left|\boldsymbol{h}_{l2}^H \boldsymbol{w}_{l1}\right|^2 p_{l1} + \sigma^2)\delta$.

Starting from MU 3's beamforming vector $\|\boldsymbol{w}_{l3}\|^2$, we have

$$\begin{aligned} A &= \begin{bmatrix} \left\|\boldsymbol{w}_{l1}^{'}\right\|^2 & \boldsymbol{w}_{l2}^{'T}\boldsymbol{w}_{l1}^{'} \\ \boldsymbol{w}_{l2}^{'T}\boldsymbol{w}_{l1}^{'} & \left\|\boldsymbol{w}_{l2}^{'}\right\|^2 \end{bmatrix}, B = -\begin{bmatrix} \boldsymbol{w}_{l1}^{'T}\boldsymbol{w}_{l3}^{'} & \boldsymbol{w}_{l2}^{'T}\boldsymbol{w}_{l3}^{'} \end{bmatrix}, \\ \lambda_2 &= \frac{\boldsymbol{w}_{l2}^{'}\boldsymbol{w}_{l3}^{'}\boldsymbol{w}_{l1}^{'}\boldsymbol{w}_{l2}^{'} - \boldsymbol{w}_{l1}^{'}\boldsymbol{w}_{l3}^{'}\left\|\boldsymbol{w}_{l2}^{'}\right\|^2}{\left\|\boldsymbol{w}_{l2}^{'}\right\|^2\left\|\boldsymbol{w}_{l1}^{'}\right\|^2 - |\boldsymbol{w}_{l1}^{'}\boldsymbol{w}_{l2}^{'}|^2}, \lambda_4^* = \frac{\boldsymbol{w}_{l1}^{'}\boldsymbol{w}_{l3}^{'}\boldsymbol{w}_{l1}^{'}\boldsymbol{w}_{l2}^{'} - \boldsymbol{w}_{l2}^{'}\boldsymbol{w}_{l3}^{'}\left\|\boldsymbol{w}_{l1}^{'}\right\|^2}{\left\|\boldsymbol{w}_{l2}^{'}\right\|^2\left\|\boldsymbol{w}_{l1}^{'}\right\|^2 - |\boldsymbol{w}_{l1}^{'}\boldsymbol{w}_{l2}^{'}|^2} \end{aligned} \tag{4.22}$$

and $\lambda_4 = sign(\lambda_4^*)\max\{|\lambda_4^*|, \sqrt{1+\delta}\}$.

Then, taking them back to (4.20), we will get

$$\begin{aligned} A &= \begin{bmatrix} \left\|\boldsymbol{w}_{l1}^{'}\right\|^2 & \boldsymbol{w}_{l1}^{'T}\boldsymbol{w}_{l3}^{'} \\ \boldsymbol{w}_{l1}^{'T}\boldsymbol{w}_{l3}^{'} & \left\|\boldsymbol{w}_{l3}^{'}\right\|^2 + \|\boldsymbol{w}_{l3}\|^2\delta \end{bmatrix}, B = -\begin{bmatrix} \boldsymbol{w}_{l1}^{'T}\boldsymbol{w}_{l2}^{'} & \boldsymbol{w}_{l3}^{'T}\boldsymbol{w}_{l2}^{'} \end{bmatrix}, \\ \lambda_1^* &= \frac{\boldsymbol{w}_{l1}^{'}\boldsymbol{w}_{l2}^{'}\left(\left\|\boldsymbol{w}_{l3}^{'}\right\|^2 + \|\boldsymbol{w}_{l3}\|^2\delta\right) - \boldsymbol{w}_{l1}^{'}\boldsymbol{w}_{l3}^{'}\boldsymbol{w}_{l2}^{'}\boldsymbol{w}_{l3}^{'}}{|\boldsymbol{w}_{l1}^{'}\boldsymbol{w}_{l3}^{'}|^2 - \left\|\boldsymbol{w}_{l1}^{'}\right\|^2\left(\left\|\boldsymbol{w}_{l3}^{'}\right\|^2 + \|\boldsymbol{w}_{l3}\|^2\delta\right)}, \lambda_6 = \frac{\left\|\boldsymbol{w}_{l1}^{'}\right\|^2\boldsymbol{w}_{l2}^{'}\boldsymbol{w}_{l3}^{'} - \boldsymbol{w}_{l1}^{'}\boldsymbol{w}_{l2}^{'}\boldsymbol{w}_{l1}^{'}\boldsymbol{w}_{l3}^{'}}{|\boldsymbol{w}_{l1}^{'}\boldsymbol{w}_{l3}^{'}|^2 - \left\|\boldsymbol{w}_{l1}^{'}\right\|^2\left(\left\|\boldsymbol{w}_{l3}^{'}\right\|^2 + \|\boldsymbol{w}_{l3}\|^2\delta\right)}, \end{aligned} \tag{4.23}$$

and $\lambda_1 = sign(\lambda_1^*)\max\{|\lambda_1^*|, \sqrt{1+\delta}\}$. If $\lambda_1^2 < \frac{\lambda_2^2}{1+\gamma_{l1}^2}$ is not satisfied, we adjust λ_1 to be a smaller value but still satisfy $\lambda_1 > \sqrt{1+\delta}$. If this condition can not be satisfied, this cluster will not be formed. By taking them back to (4.20) again, we have

$$\begin{aligned} A &= \begin{bmatrix} \left\|\boldsymbol{w}_{l2}^{'}\right\|^2 + \|\boldsymbol{w}_{l2}\|^2\delta + \lambda_6^2\|\boldsymbol{w}_{l3}\|^2\delta^2 & \boldsymbol{w}_{l2}^{'T}\boldsymbol{w}_{l3}^{'} \\ \boldsymbol{w}_{l2}^{'T}\boldsymbol{w}_{l3}^{'} & \left\|\boldsymbol{w}_{l3}^{'}\right\|^2 + \|\boldsymbol{w}_{l3}\|^2\delta \end{bmatrix}, \\ B &= -\begin{bmatrix} \boldsymbol{w}_{l2}^{'T}\boldsymbol{w}_{l1}^{'} & \boldsymbol{w}_{l3}^{'T}\boldsymbol{w}_{l1}^{'} \end{bmatrix}, \\ \lambda_3 &= \frac{\boldsymbol{w}_{l1}^{'}\boldsymbol{w}_{l2}^{'}\left(\left\|\boldsymbol{w}_{l3}{}^{'}\right\|^2 + \beta^{'}\right) - \boldsymbol{w}_{l1}^{'}\boldsymbol{w}_{l3}^{'}\boldsymbol{w}_{l2}^{'}\boldsymbol{w}_{l3}^{'}}{|\boldsymbol{w}_{l2}^{'}\boldsymbol{w}_{l3}^{'}|^2 - \left(\left\|\boldsymbol{w}_{l2}^{'}\right\|^2 + \alpha^{'}\right)\left(\left\|\boldsymbol{w}_{l3}{}^{'}\right\|^2 + \beta^{'}\right)}, \lambda_5 = \frac{\boldsymbol{w}_{l1}^{'}\boldsymbol{w}_{l3}^{'}\left(\left\|\boldsymbol{w}_{l2}^{'}\right\|^2 + \alpha^{'}\right) - \boldsymbol{w}_{l1}^{'}\boldsymbol{w}_{l2}^{'}\boldsymbol{w}_{l2}^{'}\boldsymbol{w}_{l3}^{'}}{|\boldsymbol{w}_{l2}^{'}\boldsymbol{w}_{l3}^{'}|^2 - \left(\left\|\boldsymbol{w}_{l2}^{'}\right\|^2 + \alpha^{'}\right)\left(\left\|\boldsymbol{w}_{l3}{}^{'}\right\|^2 + \beta^{'}\right)}, \end{aligned} \tag{4.24}$$

where $\alpha^{'} = \|\boldsymbol{w}_{l2}\|^2\delta + \lambda_6^2\|\boldsymbol{w}_{l3}\|^2\delta^2, \beta^{'} = \|\boldsymbol{w}_{l3}\|^2\delta$.

4.4 Two-side Coalitional Matching

Based on the aforementioned MIMO-NOMA cluster beamforming design, in this section, we propose a two-side coalitional matching approach for achieving data rate improvement at both BSs and MUs.

4.4.1 MIMO-NOMA clustering approach

Since we can obtain the closed form solution for a MIMO-NOMA cluster based on δ, the power reduction before and after clustering can be calculated as

$$\begin{aligned}\Delta P_{g_{ld}}(\delta) &= \sum_{i=1}^{k_d} \left\|\boldsymbol{w}_{li}^{'}\right\|^2 p_{li} - \sum_{i=1}^{k_d} P_{li}(\delta) \\ &= \delta \sum_{i=1}^{k_d} (I_{li} + \sigma^2) \sum_{j=1, j\neq i}^{k_d} |\lambda_{ji}| \left|\boldsymbol{w}_{li}^{'} \boldsymbol{w}_{lj}^{'}\right|.\end{aligned} \tag{4.25}$$

If $\Delta P_{g_{ld}}(\delta) > 0$ and successful decoding conditions [109] can be satisfied, forming MUs into a cluster becomes feasible, called a beneficial NOMA cluster. Since the power budget of a BS is fixed to be P, which is shared by all MUs under it's service, the power reduction of MIMO-NOMA clustering implies the data rate improvement on this BS. Moreover, in appendix B.1, we show that for a beneficial NOMA cluster, the decoding order is determined by the descending order of the Euclidian 2-norm of beamforming vectors in the OMA state. For example, if $\left\|\boldsymbol{w}_{lj}^{'}\right\|^2 < \left\|\boldsymbol{w}_{li}^{'}\right\|^2$, MU i is decoded firstly. Otherwise, we should first decode MU j.

In each BS, all MUs share the same data rate, but their total power consumption is limited by the power budget. By forming a new cluster, the power reduction will benefit for all MUs served by this BS, and their data rates will be improved. Therefore, we can transform this maximum data rate problem into a minimum power consumption problem for MIMO-NOMA clustering. According to the solution we obtained in (4.25), the power reduction is only related with MUs in this cluster, and has no interaction effect to other MUs. Therefore, according to [108], the approach is shown in Table 4.1. We first fix SINR,

and calculate the utility (i.e., power reduction) of all beneficial clusters. Then, we employ coalition game to obtain a clustering. After that, we calculate and update the data rate, and re-calculate the power reduction of the clustering result, until the algorithm converges. This approach can ensure system convergence as the power reduction of each MU is linear related to its achievable data rate as in (4.25).

The proposed coalition game is conducted in three steps: i) each MU selects the clustering strategy which will improve it's utility; ii) each MU employs the split-and-merge rule to judge whether a coalition should be formed; iii) Each MU repeats the coalition formation process until no MU changes it's strategy.

Definition 4.4.1. *Consider two sets of coalitions* $\mathcal{G}_{l_1} = \{g_{l_1,1}, g_{l_1,2}, ..., g_{l_1,k_1}\}$ *and* $\mathcal{G}_{l_2} = \{g_{l_2,1}, g_{l_2,2}, ..., g_{l_2,k_2}\}$*, which are two potential coalition groups for MU* i*, i.e.,* $i \in \mathcal{G}_{l_1} \cup \mathcal{G}_{l_2}$*. If and only if it's utility in group* l_1 *(denoted by* $U(\mathcal{G}_{l_1})$*) is larger than that in group* l_2*, i.e.,* $U(\mathcal{G}_{l_1}) > U(\mathcal{G}_{l_2})$*, the coalition* $\mathcal{G}_{l_1}$ *is preferred over* $\mathcal{G}_{l_2}$ *by* Pareto order*, denoted by* $\mathcal{G}^i_{l_1} \rhd \mathcal{G}^i_{l_2}$.

- *Merge:* For any MU $i \in \mathcal{G}_{l_1}$, if $U(\mathcal{G}_{l_1})$ is larger than the sum utility of any subset of $\mathcal{G}_{l_1}$, then merge MU i to $\mathcal{G}_{l_1}$.
- *Split:* For any coalition $\mathcal{G}_{l_1}$, if $\mathcal{G}^i_{l_2} \rhd \mathcal{G}^i_{l_1}$, then split $\mathcal{G}_{l_1}$ and merge this MU i into a new coalition $\mathcal{G}_{l_2}$.

4.4.2 Two-side coalitional matching approach

In our system, there are two sides: the MU side (each MU tries to maximize it's utility through selecting a suitable BS and forming a suitable cluster) and the BS side (each BS will accept MUs who can improve it's utility).

On the BS side, since BSs are cooperative, we focus on an average utility of all involved

BSs. For example, consider the situation that MU i leaves from BS l_1 and joins BS l_2. In $\boldsymbol{O}_1$, the utilities of BS l_2 are calculated by

$$U_{l_1 i}^{[2]} = U_{l_2 i}^{[2]} = 0.5(U_{l_1 i} + U_{l_2 i}), \tag{4.26}$$

where $U_{l_1 i} = (\gamma_{l_1 i}^{*}+1)^{(n_{l_1}-1)} - (\gamma_{l_1 i}+1)^{n_{l_1}}$ and $U_{l_2 i} = (\gamma_{l_2 i}^{*}+1)^{(n_{l_2}+1)} - (\gamma_{l_2 i}+1)^{n_{l_2}}$. $\gamma_{l_1 i}$ and $\gamma_{l_1 i}^{*}$ ($\gamma_{l_2 i}$ and ${\gamma_{l_2 i}}^{*}$) denote the SINR values before and after this MU i leaves BS l_1 (joins BS l_2), respectively. n_{l_1} and n_{l_2} are the numbers of MUs accessed to BSs l_1 and l_2, respectively. The utility $U_{l_1 i}^{[2]}$ of BS l_1 is only used to compare and decide which MU in it's cell should be served by a nearby BS (i.e., a MU selects a different BS) first.

In $\boldsymbol{O}_2$, the BSs' utilities are derived as

$$\begin{aligned} &\hat{U}_{l_1 i}^{[2]} = \hat{U}_{l_2 i}^{[2]} = 0.5(\tfrac{n_{l_1} P_{l_1 i}}{P\gamma_{l_1 i}} - \tfrac{n_{l_2} P_{l_2 i}}{P\gamma_{l_2 i}}), \\ &P_{l_1 i} = \begin{cases} P_{l_1 i}^{'}, & \text{if in MIMO-OMA,} \\ P_{l_1 i}^{'} - \frac{P_{l_1 i}^{'}}{P_{l_1 i}^{'} + \sum_{j \in g_{l_1}} P_{l_1 j}^{'}} \Delta P_{g_{l_1}}, & \text{if in MIMO-NOMA,} \end{cases} \end{aligned} \tag{4.27}$$

where $P_{l_1 i}^{'}$ is the power consumption of MU i in BS l_1 when it is in the OMA state. In the NOMA state, the corresponding power consumption is equal to $P_{l_1 i}^{'}$ minus it's share of power reduction $\Delta P_{g_{l_1}}$.

The utility on the MU side is defined as the achievable SINR value, i.e.,

$$\begin{aligned} &U_{l_1 i}^{[1]}(or \quad \hat{U}_{l_1 i}^{[1]}) = \gamma_{l_1 i}, \\ &U_{l_2 i}^{[1]}(or \quad \hat{U}_{l_2 i}^{[1]}) = \begin{cases} \gamma_{l_2 i}^{*}, & \text{if } U_{l_2 i}^{[2]} > 0 (or \quad \hat{U}_{l_2 i}^{[2]} > 0), \\ 0, & \text{otherwise.} \end{cases} \end{aligned} \tag{4.28}$$

Note that MU preference relies on the achievable SINR value, and the evaluation of it is based on a certain combination of MU cluster and BS selection, rather than $\gamma_{l_2 i}$ only. If $U_{l_2 i}^{[2]} < 0$ (or $\hat{U}_{l_2 i}^{[2]} < 0$), BS will reject the requests from MUs who may decrease it's utility.

The steps of the proposed two-side coalitional matching approach are shown as follows.

1) Initialization

Each MU selects the nearest BS as it's initial access BS. Then, BSs calculate the beamfoming matrix in the OMA state. Let $\pi_{MU} = \{A_1, A_2, ...A_K\} \in Core(N^{MU}, (\succeq_i^{MU})_{i \in N^{MU}})$ denote the core of MUs. In the initial state, $\pi_{MU} = \{1, 2, ..., N\}$ as no MU cluster is formed.

2) Iteration

- **Step 1:** Calculate MIMO-NOMA clustering in each BS by the merge-and-split rule, until the core is found. If the new core π'_{MU} is equal to π_{MU}, stop the iterations. Otherwise, go to step 2.
- **Step 2:** Calculate the utilities of both sides. On the MU side, each MU will select the BS with the maximum utility. If the selected BS is different from it's accessed BS, a request will be sent to this new BS. If two selections have a same utility, it will select the BS with the larger data rate.
- **Step 3:** On the BS side, each BS (such as BS 3 in Fig. 4.1) may have requests in two directions: receiving (as MU 6 selects BS 3) and sending (as MU 3 selects BS 2). It will rank all requests by the descending order of their utilities. If the request of the maximum utility is in the receiving direction, it will be accepted. Otherwise, requests in the receiving direction will be rejected. Update the beamfoming matrixes at all BSs, and go to step 1.

4.4.3 Stability of coalitional matching

We define $\succeq_i^{MU}(\succeq_l^{BS})$ to denote the primitive binary relation (which is strict preference and indifference) of MU i (or BS l). We employ A and A' to denote different MUs or different groups of MU, and $B \in L$ to denote the BS set. Note that there are no coalitions

on the BS side. For all $i \in S$, $S \subseteq N \cup L$, if we have $A \succeq_i^{MU} A'$, we say that $(\succeq_i^{MU})_{i \in S}$ satisfies the common ranking property. Then, the core is not empty [117].

Obviously, this common property cannot be satisfied without coordination between two sides as the utilities of MU and BS are different. However, our designed approach is a combination of coalitional matching and hedonic games because the BS can only accept or refuse the requests from MUs, while each MU sends it's request according to it's utility. Therefore, BS gives the priority to groups from the MU side. With this design, the condition of existing no-empty cores is relaxed by dropping the common ranking property in the MU side. In such a case, for all $i \in N$, if we have $A \succeq_i^{MU} A'$, we say that $(\succeq_i^{MU})_{i \in S}$ satisfies the common ranking property. Then, the core is not empty.

Theorem 4.4.1. *In our proposed coalitional matching game approach, each MU has the preference towards a group of MU clusters with respect to a specific BS. Those groups satisfy the common ranking property [117].*

Proof. *Proof:* In a single small cell, the utilities of all beneficial MU clusters are usually different. It means that MU's preferences on different clusters satisfy the common ranking property. Therefore, the BS has a convergent solution to MIMO-NOMA clustering. In the case of multiple BSs, if A and A' do not satisfy the common ranking property, it must satisfy the condition that they have the same achievable data rate. If they are selected by the same BS, such as (A, l_1) and (A', l_1), the utilities of them are commonly different which ensure they have different achievable data rates. If they are selected by different BSs and have the same achievable data rate, for any $i \in A \cap A'$, the order of A and A' follows this MU's preferences on BSs, i.e., the BS with a higher data rate. Therefore, all MUs satisfy the common ranking property. □

The special feature of the coalitional matching is that the own-side coalitions are dominant over interaction effect (effect between different sides). For all $i \in N$ and matching pairings (A, B), $(A', B') \in N_i^{MU} \times L$, $(A, B) \succeq_i (A', B')$, iff (i) $A \succeq_i^{MU} A'$; (ii)

or $A \sim_i^{MU} A'$ ($\sim$ means equal) and $B \succeq_i^{BS} B'$. For all $l \in L$ and (A, B), $(A', B) \in 2^N \times L$, $(A, B) \succeq_l (A', B)$, iff $A \succeq_l^{BS} A'$. If $(\succeq_i^{MU})_{i \in S}$ and $(\succeq_l^{BS})_{l \in S}$ are strict and the core is nonempty, the core stable coalitional matching exists [117].

Definition 4.4.2. *If a matching pair $C = (A, l_1)$ can be blocked by $C'' = (A'', l_1)$, it means that any entity $i \in C''$ will prefer C more than C''. A coalitional matching is core stable if it cannot be blocked. Otherwise, there are several possible coalitional matchings that respect to these core partitions.*

To prove that our proposed approach is core stable, we first give an example to explain the key issue which makes the coalitional matching is not core stable. Then, we extend it to the general case. Consider a set of MUs $\{i_1, i_2, i_3, i_4\}$ and a set of BSs $\{l_1, l_2\}$. Let the preference profiles be specified below:

$$
\begin{aligned}
&A = \{i_1, i_4\}; A' = \{i_1, i_2\}; A'' = \{i_3, i_4\}; A''' = \{i_1, i_3, i_4\};\\
&A \succ_{i_1}^{MU} A' \succ_{i_1}^{MU} A''' \succ_{i_1}^{MU} ...; A' \succ_{i_2}^{MU} ...;\\
&A''' \succ_{i_3}^{MU} \{i_3\} \succ_{i_3}^{MU} A'' \succ_{i_3}^{MU} ...; A \succ_{i_4}^{MU} A''' \succ_{i_4}^{MU} A'' \succ_{i_4}^{MU} ...;\\
&l_1 \succ_{i_1}^{BS} l_2 \succ_{i_1}^{BS} ....; l_2 \succ_{i_2}^{BS} ....; l_1 \succ_{i_3}^{BS} ....; l_1 \succ_{i_4}^{BS} ....;\\
&A''' \succ_{l_1}^{BS} A \succ_{l_1}^{BS} A'' \succ_{l_1}^{BS} ...; A' \succ_{l_2}^{BS} .....
\end{aligned}
$$

The combinations include: $C = (A, l_1)$, $C' = (A', l_2)$, $C'' = (A'', l_1)$ and $C''' = (A''', l_1)$, and the common ranking is $A \succ_i^{MU} A''' \succ_i^{MU} A''$. There are two possible coalitional matchings: C, (i_2, l_2) and $\{i_3, \varnothing\}$ (called coalition matching I); and $C'''$and (i_2, l_2) (called coalition matching II). We notice that Cwill be blocked by C'''as $A''' \succ_{l_1}^{BS} A$ and $A''' \succ_{i_3}^{MU} \{i_3\}$, and C'''will be blocked by C because $A \succ_{i_1}^{MU} A' \succ_{i_1}^{MU} A'''$ and $\{i_3\} \succ_{i_3}^{MU} A''$. Thus, the core stable coalitional matching does not exist.

More specifically, if system exist a loop, the obtained solution is unstable. We make a further statement on the forming process of this loop. The initial states of MUs and BSs are $\{i_1, i_2, l_2\}$, $\{i_3\}$ and (i_4, l_1). We denote the utilities of BS l_1 in $C$and C''as $U_{l_1 i_1}^{[2]}$ and $U_{l_1 i_3}^{[2]}$, and those of MUs as $U_{l_1 i_1}^{[1]}$ and $U_{l_1 i_3}^{[1]}$, respectively. Since $A \succ_{l_1}^{BS} A''$, we have $U_{l_1 i_1}^{[2]} > U_{l_1 i_3}^{[2]}$.

As $A \succ_{i_1}^{MU} A'$, we obtain $U_{l_1 i_1}^{[1]} > U_{l_2 i_1}^{[1]} > 0$. Since $\{i_3\} \succ_{i_3}^{MU} A''$, if $U_{l_1 i_1}^{[2]} > 0$, MU i_1 will send request to BS l_1, and C is formed. Thus, we obtain coalition matching I. After that, we re-evaluate the utilities of both sides and denote them as $U_{l_1 i_3}^{*[2]}$ and $U_{l_1 i_3}^{*[1]}$. As $A''' \succ_{i_3}^{MU} \{i_3\}$, MU i_3 finds that it's SINR can be improved by joining BS l_1, so that it will send the request to this BS. If $U_{l_1 i_3}^{*[2]} > 0$, BS l_1 accepts this request and C'''' will be formed. Thus, C is blocked by C''''. We have coalition matching II. However, MU i_1 finds that $U_{l_1 i_1}^{*[1]} < U_{l_2 i_1}^{[1]}$ as $A' \succ_{i_1}^{MU} A'''$. If $U_{l_1 i_1}^{*[2]} < 0$, MU i_1 will select C' rather than C''''. Thus, C'''' is blocked by C', and coalition matching II is unstable and splits into C' and C'' after i_1 leaves. However, as $\{i_3\} \succ_{i_3}^{MU} A''$ and $U_{l_1 i_3}^{[2]} < 0$, C'' is unstable and further decomposed into $\{i_3\}$ and (i_4, l_1). The system state comes to the initial state.

In summary, according to the special feature of our proposed approach, the key factor of existing a system loop is that in any state of system, there always exists one MU whose accessed BS is not the one with a maximum utility. After several iterations, if the system state will circulate among several specific states, it means that algorithm exists a loop, and those states will be related to a common BS. For such an observation, the possible cases are listed in the next subsection, and we prove that such loop dose not existed in the proposed approach.

In our case, in the initial state, the nearest BS will be regarded as the original BS of a MU to calculate the utility and reduce the computational complexity (due to only small part of MUs in the cell-edge will select other BSs provide services). Therefore, if a MU select a different BS, it includes two BSs' strategies in different directions: the original BS sending a request to the selected BS; and the selected BS receiving a request from the original BS. Based on the example we give before, forming a loop must involve 2 pairings related with a same BS, and the forming process of a system loop includes four steps: i) MU i joins a BS; ii) MU j joins this BS; iii) MU i leaves this BS; and iv) MU j leaves this BS. Considering 2 pairings may have different directions and relate with 2 or 3 BSs, all possible cases can be concluded into 3 possible pairings (**P1**-**P3**) as shown in Fig. 4.2. In Fig. 4.2, BS 2 has

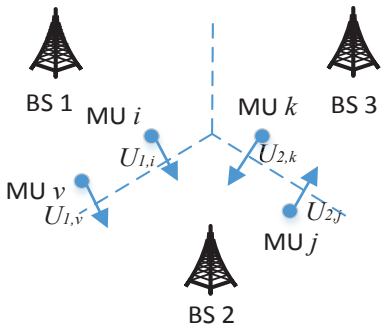

Figure 4.2: Examples of possible system loops

MUs in the receiving direction (e.g., MUs i, k and v) and in the sending direction (e.g., MU j), and 2 pairings may relate with 2 BSs (e.g., **P3**) or 3 BSs (e.g, **P1** and **P2**).

- **P1**: 3 related BSs and different directions (i.e., $i = i_1$ and $j = i_3$ or $i = i_3$ and $j = i_1$).
- **P2**: 3 related BSs but a same direction (i.e., $i = i_1$ and $k = i_3$).
- **P3**: 2 related BSs and a same direction (i.e., $i = i_1$ and $v = i_3$).

The system is stable if coalitional matchings in those cases (i.e., from **P1** to **P3**) are unblocked. We first consider the objective of sum data rate $\boldsymbol{O}_1$.

In the case of **P1**, if MU i selects BS 2 (i.e., leaves from BS 1 and joins BS 2), the data rate of BS 1 is changed from γ_{1i} to $\gamma_{1i}^{'}$, while that of BS 2 is changed from γ_{2i} to $\gamma_{2i}^{'}$. The utilities of BSs 1 and 2 are equal to $U_{1i}^{[2]}$ and $U_{2i}^{[2]}$, respectively. Similarly, if MU j leaves from BS 2 and joins BS 3, the data rate of BS 2 is changed from γ_{2j} to $\gamma_{2j}^{''}$, while that of BS 3 is changed from γ_{3j} to $\gamma_{3j}^{'}$. These utilities are equal to,

$$\begin{aligned} U_{1i}^{[2]} = U_{2i}^{[2]} &= (\gamma_{1i}^{'} + 1)^{(n_1-1)} - (\gamma_{1i} + 1)^{n_1} + (\gamma_{2i}^{'} + 1)^{(n_2+1)} - (\gamma_{2i} + 1)^{n_2}, \\ U_{2j}^{[2]} = U_{3j}^{[2]} &= (\gamma_{2j}^{''} + 1)^{(n_2-1)} - (\gamma_{2j} + 1)^{n_2} + (\gamma_{3j}^{'} + 1)^{(n_3+1)} - (\gamma_{3j} + 1)^{n_3}, \end{aligned} \tag{4.29}$$

where n_2 and n_3 are the numbers of MUs in BSs 2 and 3, respectively. If $U_{1i}^{[2]} > 0 > U_{2j}^{[2]}$,

MU i will first join BS 2. After that, $U_{2j}^{[2]}$ will change to $U_{2j}^{*[2]}$ as

$$U_{2j}^{*[2]} = (\gamma_{2j}^{'''}+1)^{n_2} - (\gamma_{2j}^{'}+1)^{n_2+1} + (\gamma_{3j}^{'}+1)^{(n_3+1)} - (\gamma_{3j}+1)^{n_3}. \tag{4.30}$$

If $U_{2j}^{*[2]} > 0$ and $\gamma_{3j}^{'} > \gamma_{2j}^{'}$, MU j will also leave BS 2, and the utility of $U_{1i}^{[2]}$ will become $U_{1i}^{*[2]}$ as

$$U_{1i}^{*[2]} = (\gamma_{1i}^{'}+1)^{(n_1-1)} - (\gamma_{1i}+1)^{n_1} + (\gamma_{2i}^{'''}+1)^{n_2} - (\gamma_{2i}^{''}+1)^{(n_2-1)}. \tag{4.31}$$

We notice that ii) will be a core stable coalition matching if $\gamma_{2i}^{'''} > \gamma_{1i}$. Since $U_{1i}^{[2]} > U_{2j}^{[2]}$ and $\gamma_{2i}^{'} = \gamma_{2j}^{'}$, we have

$$(\gamma_{1i}^{'}+1)^{(n_1-1)} - (\gamma_{1i}+1)^{n_1} + (\gamma_{2i}^{'}+1)^{(n_2+1)} > (\gamma_{2j}^{''}+1)^{(n_2-1)} + (\gamma_{3j}^{'}+1)^{(n_3+1)} - (\gamma_{3j}+1)^{n_3}.$$

Similarly, as $U_{1i}^{*[2]} > U_{2j}^{*[2]}$, we have $\gamma_{2i}^{'''} = \gamma_{2j}^{'''}$ and

$$(\gamma_{1i}^{'}+1)^{(n_1-1)} - (\gamma_{1i}+1)^{n_1} - (\gamma_{2j}^{''}+1)^{(n_2-1)} > -(\gamma_{2i}^{'}+1)^{(n_2+1)}(\gamma_{3j}^{'}+1)^{(n_3+1)} - (\gamma_{3j}+1)^{n_3}.$$

Therefore, $U_{1i}^{*[2]} > U_{2j}^{*[2]} > 0$. Since $\gamma_{2i}^{'''} > \gamma_{2i}^{'} = \gamma_{2j}^{'} > \gamma_{1i}$, the process will stop at step ii). If we let $U_{1i}^{[2]} < U_{2j}^{[2]}$ and $U_{1i}^{*[2]} > 0$, we will also obtain the same conclusion that $U_{2j}^{*[2]} > U_{1i}^{*[2]} > 0$, and the process will stop at step ii). Thus, the system loop can not be formed.

In the case of **P2**, we suppose that $U_{1i}^{[2]} = U_{2i}^{[2]} > U_{3k}^{[2]} = U_{2k}^{[2]}$ as $C \succeq_l^{BS} C'$, where

$$U_{3k}^{[2]} = (\gamma_{3k}^{'}+1)^{(n_3-1)} - (\gamma_{3k}+1)^{n_3} + (\gamma_{2k}^{''}+1)^{(n_2+1)} - (\gamma_{2k}+1)^{n_2}. \tag{4.32}$$

Following the same way, MU i joins MU 2 first, and makes $U_{3k}^{[2]}$ change to $U_{3k}^{*[2]}$ as

$$U_{3k}^{*[2]} = (\gamma_{3k}^{'}+1)^{(n_3-1)} - (\gamma_{3k}+1)^{n_3} + (\gamma_{2k}^{'''}+1)^{(n_2+2)} - (\gamma_{2k}^{'}+1)^{(n_2+1)}. \tag{4.33}$$

If $U_{3k}^{*[2]} > 0$, MU k will also join MU 2, and $U_{1i}^{[2]}$ becomes $U_{1i}^{*[2]}$ as

$$U_{1i}^{*[2]} = (\gamma_{1i}^{'}+1)^{(n_1-1)} - (\gamma_{1i}+1)^{n_1} + (\gamma_{2i}^{'''}+1)^{(n_2+2)} - (\gamma_{2i}^{''}+1)^{(n_2+1)}. \tag{4.34}$$

Obviously, we will have $U_{1i}^{*[2]} > U_{3k}^{*[2]} > 0$. Since $\gamma_{2k}^{''} < \gamma_{3k}$ and $\gamma_{2k}^{'''} > \gamma_{3k}$ conflict to each

other, **P2** will not satisfy the basic condition of a loop. If $\gamma_{2k}^{''} > \gamma_{3k}$ and $\gamma_{2i}^{'''} > \gamma_{1i}$, the process will stop at step ii). If $\gamma_{2k}^{''} > \gamma_{3k}$ and $\gamma_{2i}^{'''} < \gamma_{1i}$, due to $U_{1i}^{*[2]} > 0$, the utility of MU i when it gets back to BS 1 will be $-U_{1i}^{*[2]}$. Thus, MU i will not send the request, and the process will stop at step ii). Thus, the system loop dose not exist.

In the case of **P3**, we assume that $U_{1i}^{[2]} = U_{2i}^{[2]} > U_{1v}^{[2]} = U_{2v}^{[2]}$, which leads to MU i joining BS 2 first with $U_{1v}^{[2]}$ changed to $U_{1v}^{*[2]} > 0$. After that, MU v will also join BS 2, and we get $U_{1i}^{*[2]}$. The related equations are listed as follows.

$$
\begin{aligned}
U_{1v}^{[2]} &= (\gamma_{1v}^{''}+1)^{(n_1-1)} - (\gamma_{1v}+1)^{n_1} + (\gamma_{2v}^{''}+1)^{(n_2+1)} - (\gamma_{2v}+1)^{n_2}, \\
U_{1v}^{*[2]} &= (\gamma_{1v}^{'''}+1)^{(n_1-2)} - (\gamma_{1v}^{'}+1)^{(n_1-1)} + (\gamma_{2v}^{'''}+1)^{(n_2+2)} - (\gamma_{2v}^{'}+1)^{(n_2+1)}, \\
U_{1i}^{*[2]} &= (\gamma_{1i}^{'''}+1)^{(n_1-2)} - (\gamma_{1i}^{''}+1)^{(n_1-1)} + (\gamma_{2i}^{'''}+1)^{(n_2+2)} - (\gamma_{2i}^{''}+1)^{(n_2+1)}.
\end{aligned}
$$

Therefore, we still have $U_{1i}^{*[2]} > U_{1v}^{*[2]} > 0$ and $\gamma_{2i}^{'''} = \gamma_{2v}^{'''} > \gamma_{iv}^{'} = \gamma_{2i}^{'} > \gamma_{1i}$, which makes the process stop in step ii). Thus, the system loop dose not exist as well.

For the objective function $\boldsymbol{O}_2$, we use the same way to analyze three cases.

In the case of **P1**, the related utility functions can be written as

$$
\begin{aligned}
&U_{1i}^{[2]} = 0.5\left(\frac{n_1 P_{1i}}{P\gamma_{1i}} - \frac{(n_2+1)P_{2i}}{P\gamma_{2i}^{'}}\right) = 0.5\left(\frac{n_1 P_{1i}}{P\gamma_{1i}} - \frac{(n_2+1)\left\|\boldsymbol{w}_{2i}^{'}\right\|^2 (I_{2i}+\sigma^2)}{P}\right), \\
&U_{2j}^{[2]} = 0.5\left(\frac{n_2 \|\boldsymbol{w}_{2j}\|^2 (I_{2j}+\sigma^2)}{P} - \frac{(n_3+1)P_{3j}}{P\gamma_{3j}^{'}}\right), \\
&U_{2j}^{*[2]} = 0.5\left(\frac{(n_2+1)\left\|\boldsymbol{w}_{2j}^{'}\right\|^2 (I_{2j}+\sigma^2)}{P} - \frac{(n_3+1)P_{3j}}{P\gamma_{3j}^{'}}\right), U_{1i}^{*[2]} = 0.5\left(\frac{n_1 P_{1i}}{P\gamma_{1i}} - \frac{n_2\left\|\boldsymbol{w}_{2i}^{''}\right\|^2 (I_{2i}+\sigma^2)}{P}\right),
\end{aligned}
$$

where $\left\|\boldsymbol{w}_{2i}^{'}\right\|^2 > \left\|\boldsymbol{w}_{2i}^{''}\right\|^2$ and $\|\boldsymbol{w}_{2j}\|^2 < \left\|\boldsymbol{w}_{2j}^{'}\right\|^2$ (according to Appendix B.2). Therefore, $U_{1i}^{*[2]} > 0$. Since $\gamma_{2i}^{'''} > \gamma_{1i}$, the process will stop at ii). Thus, the system loop can not be formed.

In the case of **P2**, the related utility functions are

$$
\begin{aligned}
&\hat{U}_{1i}^{[2]} = 0.5\left(\frac{n_1 P_{1i}}{P\gamma_{1i}} - \frac{(n_2+1)\left\|\boldsymbol{w}_{2i}^{'}\right\|^2 (I_{2i}+\sigma^2)}{P}\right), \hat{U}_{3k}^{[2]} = 0.5\left(\frac{n_3 P_{3k}}{P\gamma_{3k}} - \frac{(n_2+1)\left\|\boldsymbol{w}_{2k}^{''}\right\|^2 (I_{2k}+\sigma^2)}{P}\right), \\
&\hat{U}_{3k}^{*[2]} = 0.5\left(\frac{n_3 P_{3k}}{P\gamma_{3k}} - \frac{(n_2+2)\left\|\boldsymbol{w}_{2k}^{'''}\right\|^2 (I_{2k}+\sigma^2)}{P}\right), \hat{U}_{1i}^{*[2]} = 0.5\left(\frac{n_1 P_{1i}}{P\gamma_{1i}} - \frac{(n_2+2)\left\|\boldsymbol{w}_{2i}^{'''}\right\|^2 (I_{2i}+\sigma^2)}{P}\right).
\end{aligned} \tag{4.35}
$$

Obviously, when MU i joins BS 2, the utility of $\hat{U}_{3k}^{[2]}$ will be reduced to $\hat{U}_{3k}^{*[2]}$. If $\hat{U}_{3k}^{*[2]} > 0$, MU k will also join BS 2, and the utility of $\hat{U}_{1,i}^{[2]}$ will be decreased to $\hat{U}_{1i}^{*[2]}$. Since $\gamma_{2k}^{''} < \gamma_{3k}$ and $\gamma_{2k}^{'''} > \gamma_{3k}$ conflict with each other, **P2** will not satisfy the basic condition of a loop. If $\gamma_{2k}^{''} > \gamma_{3k}$ and $\gamma_{2i}^{'''} > \gamma_{1i}$, the process will stop at step ii). If $\gamma_{2k}^{''} > \gamma_{3k}$ and $\gamma_{2i}^{'''} < \gamma_{1i}$, the core stable solution depends on $\hat{U}_{1i}^{*[2]}$. According to Appendix B.3, we can obtain $\frac{\left\|\boldsymbol{w}_{2i}^{'}\right\|^2}{\left\|\boldsymbol{w}_{2k}^{''}\right\|^2} = \frac{\left\|\boldsymbol{w}_{2i}^{'''}\right\|^2}{\left\|\boldsymbol{w}_{2k}^{'''}\right\|^2}$. Therefore, if $\left\|\boldsymbol{w}_{2i}^{'''}\right\|^2 > \left\|\boldsymbol{w}_{2k}^{'''}\right\|^2$, $\hat{U}_{1i}^{*[2]} < 0$, the process will stop at step iii) Otherwise, the process will stop at step ii) Thus, the system loop dose not exist.

In the case of **P3**, we list the related utility functions as

$$\begin{aligned}
\hat{U}_{1i}^{[2]} &= 0.5\left(\frac{n_1\left\|\boldsymbol{w}_{1i}^{'}\right\|^2(I_{1i}+\sigma^2)}{P} - \frac{(n_2+1)\left\|\boldsymbol{w}_{2i}^{'}\right\|^2(I_{2i}+\sigma^2)}{P}\right),\\
\hat{U}_{1v}^{[2]} &= 0.5\left(\frac{n_1\left\|\boldsymbol{w}_{1v}^{'}\right\|^2(I_{1v}+\sigma^2)}{P} - \frac{(n_2+1)\left\|\boldsymbol{w}_{2v}^{''}\right\|^2(I_{2v}+\sigma^2)}{P}\right),\\
\hat{U}_{1v}^{*[2]} &= 0.5\left(\frac{(n_1-1)\left\|\boldsymbol{w}_{1v}^{'}\right\|^2(I_{1v}+\sigma^2)}{P} - \frac{(n_2+2)\left\|\boldsymbol{w}_{2v}^{'''}\right\|^2(I_{2v}+\sigma^2)}{P}\right),\\
\hat{U}_{1i}^{*[2]} &= 0.5\left(\frac{(n_1-1)\left\|\boldsymbol{w}_{1i}^{''}\right\|^2(I_{1i}+\sigma^2)}{P} - \frac{(n_2+2)\left\|\boldsymbol{w}_{2i}^{'''}\right\|^2(I_{2i}+\sigma^2)}{P}\right).
\end{aligned} \tag{4.36}$$

According to Appendix B.2, it is easy to observe that if $\hat{U}_{1i}^{[2]} > \hat{U}_{1v}^{[2]}$, we will have $\hat{U}_{1i}^{*[2]} > \hat{U}_{1v}^{*[2]} > 0$. Since $\gamma_{2i}^{'''} > \gamma_{1i}$, the process will stop at step ii). Thus, the system loop can not be formed.

In summary, no loop will exist in the process of coalitional matching, and thus our proposed coalitional matching approach is core stable. For $\boldsymbol{O}_1$, the process will stop at ii), while for $\boldsymbol{O}_2$, the final solution depends on the beamforming vectors of related MUs.

4.4.4 Complexity analysis

The computational complexity analysis is inspired by [118] which counted the computation loop and entities. We first analyze the computational complexity for three basic components: data rate calculation, MIMO-NOMA clustering, and BS selection. The two-stage approach, the max-min fairness approach and the greedy approach are given

Table 4.2: Computational complexity

Approach \ Objective	Sum data rate	Relative fairness
Two-stage	$O(N*(L-1)*Nt*n_1+$ $L*\sum_{i=2}^{c}\binom{ave(N)}{i}+Nt)$	
Greedy	$O((4*N*(L-1)*\sum_{i=2}^{c}\binom{ave(N)}{i}$ $*Nt+L*\sum_{i=2}^{c}\binom{ave(N)}{i}+Nt)*n_2)$	
Coalitional matching	$O((4*N*(L-1)*\sum_{i=2}^{c}\binom{ave(N)}{i}*$ $Nt+L*\sum_{i=2}^{c}\binom{ave(N)}{i}+Nt)*n_2)$	$O((4*N*(L-1)*\sum_{i=2}^{c}\binom{ave(N)}{i}$ $*ave(N)+L*\sum_{i=2}^{c}\binom{ave(N)}{i}+Nt)$ $*n_2)$

in Appendix B.4, B.5 and B.6, respectively.

- The data rate calculation includes system level and BS level for sum data rate evaluation and local utilities evaluation, separately. At the system level, each BS will adjust the power allocation for MUs based on current environments (i.e., interferences) until reaching the convergence. Therefore, we assume that the system converges to a stable state requiring t predefined iterations (note that t will be increased with the number of MUs N), and the complexity can be denoted by$O(Nt)$. At the BS level, if relative fairness is considered, a BS needs to update it's data rate when it's accessed MUs are changed. If a MU moves from one BS to the other, only 2 BSs will need to update the data rate. Thus, for each MU's selection, it has complexity $O(2ave(N))$ (here we assume that each BS has $ave(N)=\frac{N}{L}$ MUs).

- MIMO-NOMA clustering within each BS is determined by the number of MUs (e.g., $ave(N)$ from the average meaning) and the cluster size c. Since the closed form solution for any size cluster is attainable, the computational complexity of MIMO-NOMA clustering can be determined as $O(\sum_{i=2}^{c}\binom{ave(N)}{i})$.

- The computational complexities of BS selection for joint and disjoint approaches are different. In the case of two-side coalitional matching approach, BS selection is combined with MIMO-NOMA clustering. Therefore, for each MU, the computational complexity is $O(2*(L-1)*\sum_{i=2}^{c}\binom{ave(N)}{i}*ave(N))$ for the relative fairness

or $O(2*(L-1)*\sum_{i=2}^{c}\binom{ave(N)}{i}*Nt)$ for the sum data rate maximization. In the case of disjoint approaches, such as the two-stage approach and the greedy approach, the computational complexity of BS selection for each MU is $O((L-1)*Nt)$.

In the two-stage approach, in each iteration, only one MU strategy of BS selection with the maximum utility will be accepted by the corresponding BS, and BS selection utilities will be updated after that. We assume that n_1 is the maximum number of iterations for system convergence. In the two-side approach and greedy approach, each BS will make decision independently, which will result in more MU strategies being accepted in each iteration. We assume that n_2 is the maximum number of iterations in this case, so that it may be less than n_1. We list the computational complexity for different approaches in Table 4.2.

4.5 Numerical Results

In this section, we make comparisons in respect to: i) MIMO-NOMA clustering strategy; ii) different objective functions; iii) two-stage approach and two-side coalitional matching approach; and iv) 2-MU cluster and multi-MU cluster. Moreover, in order to illustrate the advantages of our proposed approaches, we implement the numerical simulation in different MU distribution scenarios: uniform and nonuniform distributions, and different radium limitations.

4.5.1 Parameter settings

A 7-cell cellular network ($L=7$) is considered. In each cell, the radius is $400m$, and a BS is located in the center. Other parameter settings include: $M=40$ antennas at each BS, the variance of Gaussian noise $\sigma_u^2=-50dBm$ and the power limitation $P=35W$. MUs are

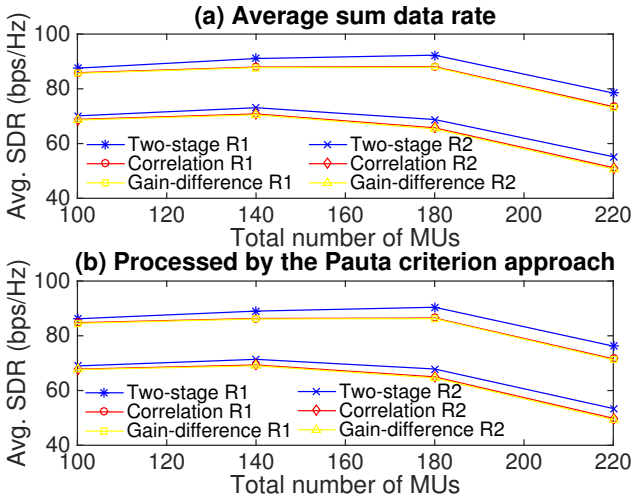

Figure 4.3: Comparisons: the correlation based approach and the gain-difference based approach.

randomly distributed within a $2\times1.697km^2$ area, which is generated by uniform distribution (i.e., the probabilities of MU located at all BSs are the same) or nonuniform distributions (i.e., the probabilities of MU located at different BSs are different). Spectrum resources are shared by all BSs. We consider two radium limitations of MU distribution: [100,400]m and [250,400]m (corresponding to R1 and R2 in following figures), to restrict the minimum distance from the nearest BS. Each set of data including locations and channel gain vectors is randomly generated. To reduce the effects from different environmental settings, each result is the average solution of 10 sets of data.

Similar to the existing work [113, 114], the channel model settings include: the 3GPP long term evolution (LTE) pathloss parameters ($\alpha = 3.76$ and $\beta = 10^{-14.81}$), the Rayleigh fading with zero mean and unit variance ($\Gamma_i^{(n)} \sim CN(0,1)$), a log-normal shadowing $\gamma_i \sim N(0dB, 8dB)$, and the transmit antenna power gain $G = 9dB$. The channel coefficient between MU i and the BS's nth antenna is modeled as

$$h_i^{(n)} = \Gamma_i^{(n)} \sqrt{G\beta d_i^{-\alpha}\gamma_i}, \tag{4.37}$$

where d_i is the distance between MU i and the BS.

The Pauta Criterion is adopted as it is proposed for outlier detection of sample data

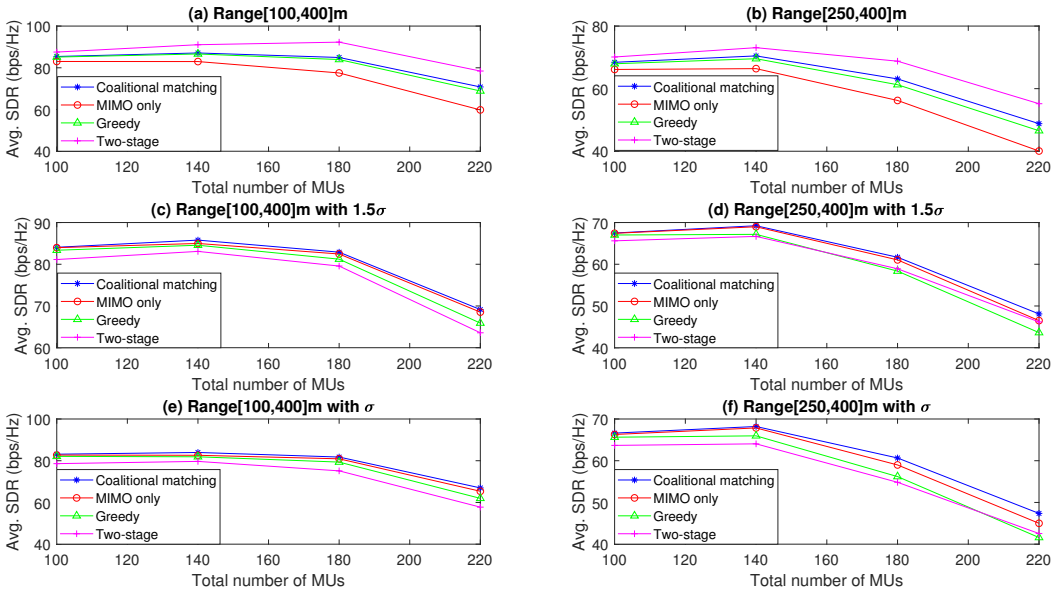

Figure 4.4: Approach comparisons: the two-side coalitional matching approach, the two-stage approach and the greedy approach.

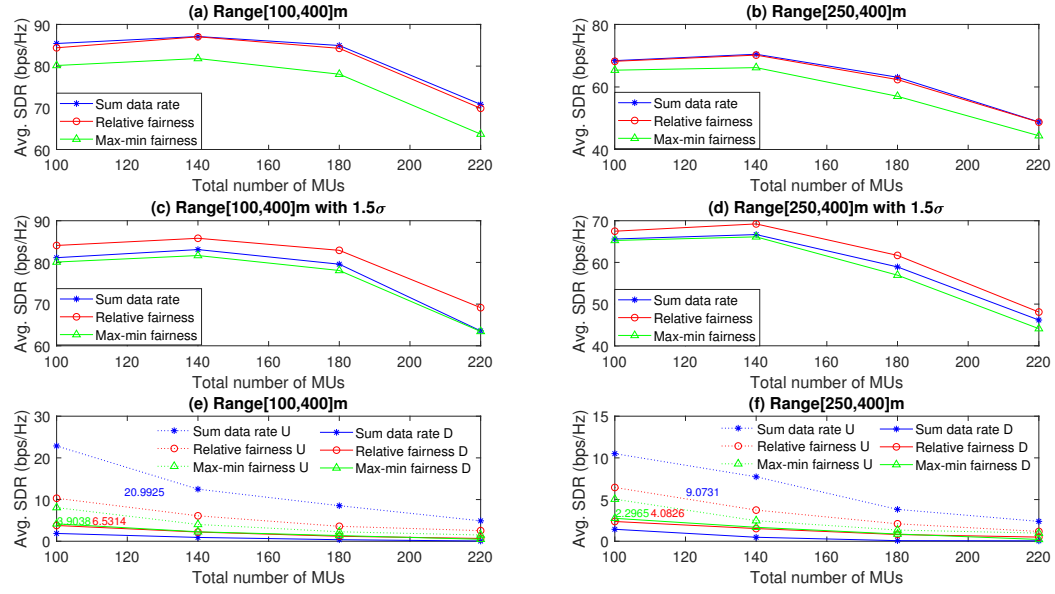

Figure 4.5: Different objectives: the sum data rate, the max-min fairness and the relative fairness.

with gross error or random error. The sum data rate and fairness are two different ways to evaluate the system performance. However, the Pauta Criterion is an approach to give a comprehensive evaluation rather than using a weighted summation of them. By this way,

if fairness is high, system performance is mainly based on the sum data rate. If a few MUs have extremely high data rate, system performance is mainly based on MU fairness. For example, there are two BSs (i.e., BS_1 and BS_2) serving for 2 MUs and 6 MUs, respectively. Case I is that the transmission data rates of them are 10bps/Hz and 2bps/Hz. Case II is that the transmission data rates of them are 5bps/Hz and 4bps/Hz. Obviously, the sum data rate of case I is larger than case II. However, case II is better than case I if the Pauta Criterion approach is employed to re-evaluate the sum data rate as 10bps/Hz will be replaced by $\overline{X} + \sigma = 7.46$bps/Hz. Thus, the contribution of MUs with extremely high data rate on system performance is reduced. Pauta criterion approach provides us a flexible way of evaluation which is available for any environment settings. To be applied in our case, we make three modifications: i) we adopt σ and 1.5σ as the judging standard; ii) the outliers only indicate MUs whose data rates are extremely higher than other MUs; iii) the data rate of outliers will be reduced to $\overline{X}+\sigma$ (or1.5σ). Then, the steps of Pauta criterion approach are listed in Table 4.3, in which $X_i = R_{li}$ denotes the data rate of a single MU i. To have large enough samples and exclude the negative effect from environment settings, we classify the results from different approaches into a same set of samples if they have same environment settings.

4.5.2 MIMO-NOMA clustering strategy

Two other approaches in the literature are also simulated for comparison: the correlation based approach [83] and the gain-difference based approach [20]. For both approaches, a two-stage optimization is employed, and the 2-MU MIMO-NOMA clustering is considered in each BS. In the correlation based approach, we first group MUs based on the correlation metric vector and then calculate the precoding matrix for all MUs to minimize the system power consumption. In the gain-difference based approach, we first group MUs based on gain-differences and then calculate the beamforming matrix to minimize the system power consumption. Differently, in this approach, the channel gain matrix is determined by the

Table 4.3: Algorithm of Pauta criterion

1. Calculate mean $\overline{X}$ of X_i $(i = 1, 2, ..., n)$;
2. Calculate standard deviation σ;
3. If $X_i - \overline{X} > \sigma(\text{or} 1.5\sigma)$, X_i is the outliner, and $X_i = \overline{X} + \sigma(\text{or} 1.5\sigma)$.

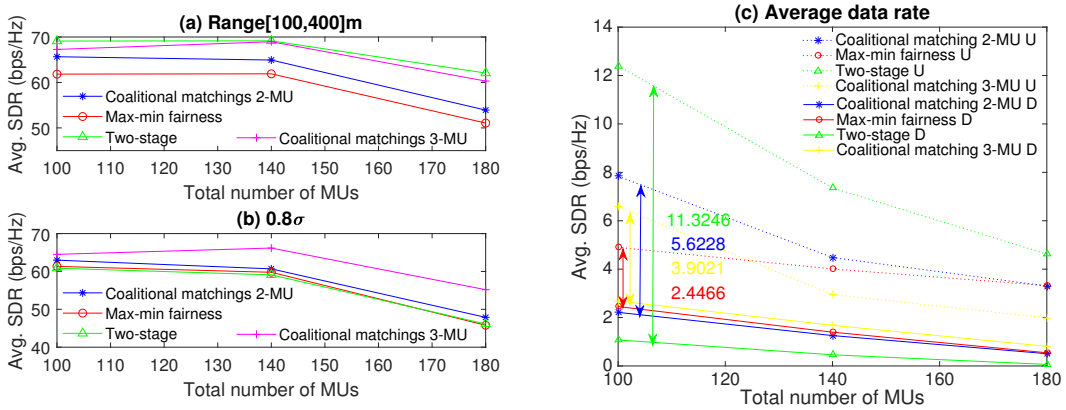

Figure 4.6: Comparisons in nonuniform distributions.

channel gain of MU with a larger $|\boldsymbol{h}_{li}|$ in a cluster.

For comparison purpose, we employ the proposed two-stage approach (in Appendix B.4) to maximize the sum data rate. Fig. 4.3 shows the average sum data rate (Avg. SDR), which indicates that our MIMO-NOMA clustering strategy performs better than other two approaches even employing the Pauta criterion approach to re-evaluate those results (with 1.5σ). It is because our proposed MIMO-NOMA clustering approach is motivated by the improvement of transmit data rate, rather than based on the features of MU channel states as in the counterparts.

4.5.3 Approach comparisons

We compare the proposed approach with other approaches, i.e., two-stage approach and greedy approach in Fig. 4.4. Since existing work in this area is very limited, those approaches are redesigned by us as shown in Appendices B.4 and B.6, respectively. To compare MIMO-NOMA with MIMO-OMA, we set MIMO only approach as a benchmark

which only considers BS selection without MIMO-NOMA clustering. The objective is to maximize the sum data rate. From Figs. 4.3 (a) and (b), we notice that the two-stage approach can obtain the solution with the highest value of the average data rate. However, if we re-evaluate those results by the Pauta Criterion approach, the two-side coalitional matching approach has the highest performance than others as shown in Figs. 4.3 (c) and (d). It indicates that our proposed win-win strategy prevents the BS improving its data rate at the cost of lowing related MU's benefit. For example, the sum data rate can be improved if MU i moves from BS l_1 to l_2. However, if MU i finds that this move will decrease it's data rate, it will refuse to do it for the benefit of itself. In other approaches, MU benefits are disregarded by the BS if the sum data rate can be improved, so that the number of outliers may be increased. After re-evaluated by the Pauta criterion approach, the data rate of outliers will be reduced to the upper bound ($\overline{X}$+σ or $\overline{X}$+1.5σ). Therefore, the system performance on sum data rate will be decreased. Moreover, if we reduce the judging standard to be 1σ as shown in (e) and (f), the upper bound is decreased, and the reduction on the sum data rate will be increased, which increases the difference among different approaches. Moreover, the complexity for the two-side coalitional matching approach and the two-stage approach are $O(1.79 \times 10^8 t n_2)$ and $O(1.18 \times 10^5 t n_1)$ if $N = 140$. The complexity for an exhaust algorithm is $O(1.90{\times}10^{47} t)$. In summary, the two-side coalitional matching approach can achieve a win-win purpose, while it's computational complexity is just a little bit higher than the two-stage approach.

4.5.4 Different objective functions

In Fig. 4.5, three different objectives are compared. Except the max-min fairness (i.e., $\boldsymbol{O}_3$) is conducted by the max-min approach, others are running by the two-side coalitional matching approach. Comparing the results in Figs. 3.5 (a) and (c) ((b) and (d)), we notice that the result of relative fairness (i.e., $\boldsymbol{O}_2$) is close to that of the sum data rate (i.e., $\boldsymbol{O}_1$) before re-evaluated by the Pauta Criterion approach, while it becomes obviously larger

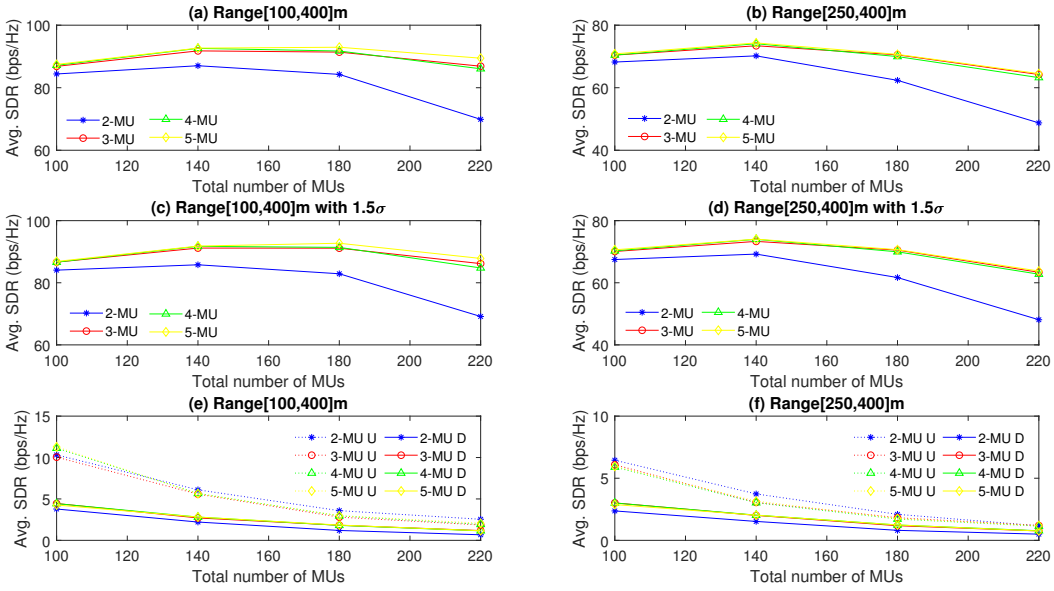

Figure 4.7: Different cluster sizes.

after that. Briefly, $\boldsymbol{O}_2$ can further improve MUs' benefits without decreasing the system sum data rate. It reveals that two-side coalitional matching approach can achieve a better win-win solution under the condition of $\boldsymbol{O}_2$. Moreover, after employing the Pauta Criterion approach, the results of $\boldsymbol{O}_1$ is close to that of $\boldsymbol{O}_3$, which verifies that the high sum date rate of $\boldsymbol{O}_1$ is due to outliers' domination effect. Furthermore, by comparing the difference between the maximum data rate (U) and the minimum data rate (D) of three approaches, $\boldsymbol{O}_2$ provides a better fairness to MUs.

If MUs are nonuniform distributed, the number of outliers in the system is increased, and the load of system will become unbalanced. In such a case, we randomly select 4 BSs, which have the number of MUs two times more than other 3 BSs, while the other settings are same as before. System performances of three different objectives are compared in Fig. 4.6. Different from Fig. 4.5, the results of $\boldsymbol{O}_2$ is in the middle between $\boldsymbol{O}_1$ and $\boldsymbol{O}_3$, while it is slightly larger than that of $\boldsymbol{O}_1$ and $\boldsymbol{O}_3$ after re-evaluated by 0.8σ. Moreover, the difference between $\boldsymbol{O}_1$ and $\boldsymbol{O}_3$ is increased. It reveals that, if the negative effect from the outliers is increased, $\boldsymbol{O}_3$ will sacrifice more BS benefits to improve MU fairness, while $\boldsymbol{O}_2$

achieves a tradeoff between $\boldsymbol{O}_3$ and $\boldsymbol{O}_1$. Furthermore, we notice that when the cluster size is increased from 2 to 3, system performance is obviously improved, while the complexity is increased from $O(1.27 \times 10^7 n_2)$ to $O(8.93 \times 10^7 n_2)$.

4.5.5 Multi-MU cluster

The size of cluster will bring positive effects to system performance, as shown in Fig. 4.7. We notice that when the cluster size is increased, system performance is first increased, and then tends to be stable when cluster size is larger than 4. It indicates that a larger cluster size will increase the flexibility of grouping and let more MUs join NOMA clusters to increase their data rates. However, the positive effect from the cluster size quickly reaches the upper bound. This phenomenon can be explained by our previous observations in Chapter 3, which claimed that a beneficial cluster should satisfy the conditions in terms of channel correlation coefficient and radius. Thus, the probability of forming a small size beneficial cluster is much higher than that with a large size, so that the system performance will not be further increased greatly with the cluster size when it is larger than 4. Moreover, the computational complexity is incredible increased with the cluster size. For example, if cluster size is increased from 4 to 5, the computational complexity will be increased from $O(4.15 \times 10^8 n_2)$ to $O(1.45 \times 10^9 n_2)$ when $N = 140$. Thus, under our simulation environment settings, the best cluster size is 3.

Chapter 5

Hybrid CoMP-NOMA

5.1 Introduction

In this chapter, we extend our MIMO-NOMA strategy for a C-RAN network, and integrate it with CoMP technology (including joint transmission and coordinated transmission, i.e., JT and CT), which is named as hybrid CoMP-NOMA. We formulate a joint resource allocation problem to minimize the system total power consumption while maximizing the number of accessed MUs. To further reduce the computational complexity, we decouple RRH cooperation and MU cooperation, and give RRH cooperation a higher priority based on the fact that RRH cooperation is more efficient on power reduction than MU cooperation. In the simulation, we show the advantages of our proposed CoMP-NOMA approach with respect to power and spectral efficiencies. Note that our work is different from references [119,120] in terms of CoMP-NOMA approach design and flexible cluster conditions. The main contributions of this work are summarized as follows.

- We propose a novel CoMP-NOMA approach, which is also a hybrid of inter RRH cooperation and intra RRH cooperation. Different from MIMO-NOMA, which MU

can only join a single cluster, CoMP-NOMA allowed a MU join multiple clusters served by nearby RRHs. The closed form of solution is derived to decide whether adopting CoMP-NOMA or CoMP-MIMO.

- We formulate a joint resource allocation problem to minimize the system total power consumption while maximizing the total number of accessed MUs. By this way, the system capacity can be evaluated by the total number of served MUs times the data rate of them, and when power consumption is minimized, system capacity is maximum.

- We decouple this problem by the fact that RRH cooperation is more efficient on power reduction than MU cooperation, and propose a two-stage approach with an acceptable computational complexity.

5.2 CoMO-NOMA System

Different from the chapter before, we consider L RRHs, each of which locates at the centre of one cell, and is equipped with M antennas, as shown in Fig. 5.1. RRHs communicate with the BBU pool through wired communications (i.e., backhaul links) for baseband processing. The total number of MUs is N, and each of them can receive signals from all RRHs as the spectrum reuse rate is 1. In this system, we consider both RRH cooperation and MU cooperation.

The motivation of RRH cooperation is to coordinately allocate resources for cell-edge MUs which may cause large interference to other MUs. We classify three different links into two categories: the master link and the cooperation link (e.g., JT link or CT link). Thus, a RRH cooperation can be described as adding a cooperation link into the system. For example, MU 1 has a master link from RRH i in Fig. 5.1. If RRH i and RRH k form a cooperation, we add a cooperation link to MU 1 from RRH k. Since the channel

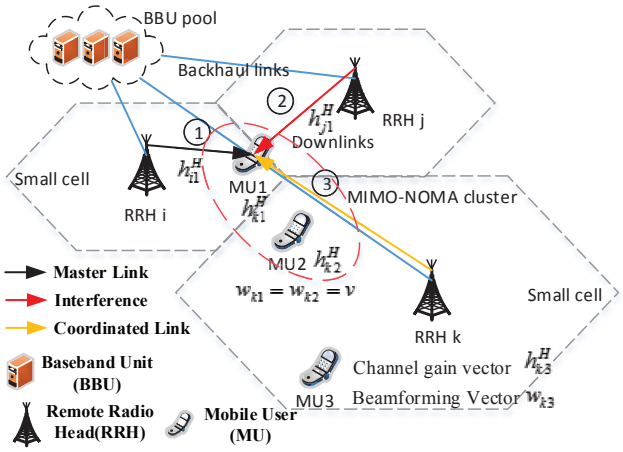

Figure 5.1: CoMP-NOMA MIMO system

condition degrades rapidly with the distance between RRH and MU, the cooperation links for a specific MU should come from its nearby RRHs. Moreover, MU cooperation is conducted through NOMA clustering. Each MU has two downlink transmission states: MIMO-OMA or MIMO-NOMA. If a MU both in a MIMO-NOMA cluster and served by CoMP, it is the case of CoMP-NOMA. Thus, the only difference between MIMO-NOMA and CoMP-NOMA is that the RRH cooperation should consider CSI condition, which makes JT-NOMA and CT-NOMA has multiple cases. Thus, the closed form solution of power coefficient and decoding order are different from before. However, the deviation progress of power coefficient is similar to MIMO-NOMA.

5.2.1 Signal model

Let $\boldsymbol{h}_{ni}^H = [h_{ni,1}^H, ..., h_{ni,M}^H]^H \in C^{1\times M}$ and $\boldsymbol{H}_i = [\boldsymbol{h}_{1i}^H, ..., \boldsymbol{h}_{li}^H]^H$ denote the channel gain vector from RRH i to MU n and the channel gain matrix of RRH i, respectively. Here, we assume that $\boldsymbol{H}_i$ is available before scheduling. If all MUs are served by MIMO-OMA, the beamforming matrix $\boldsymbol{W}_i = [\boldsymbol{w}_{1i}^H, ..., \boldsymbol{w}_{li}^H]^H$ can be calculated by the ZF-beamforming (zero-forcing beamforming) strategy. Let $G_i = \{g_{i_1}, g_{i_2}, ..., g_{i_K}\}$ denote the set of K MIMO-NOMA clusters in RRH i. In each cluster (such as $g_{i_k} = \{g_{1i_k}, g_{2i_k}, ..., g_{di_k}\}$,

$k \in \{1, .., K\}$), there are d MUs sharing a same beamforming vector and aligning from the cell-center to the cell-edge.

For MU n, without CoMP, if it is transmited by MIMO-OMA in RRH i, the received signals y_{ni} can be calculated as

$$y_{ni}=a_{ni}\boldsymbol{h}_{ni}^{H}\boldsymbol{w}_{ni}^{'}\sqrt{p_{ni}}x_n+\sum_{u\neq n}^{N}\sum_{j\in L-i}a_{nj}\boldsymbol{h}_{nj}^{H}\boldsymbol{w}_{uj}^{*}\sqrt{p_{uj}}x_u+\nu_n, \tag{5.1}$$

where $\boldsymbol{w}_{ni}^{'} \in R^{M\times 1}$ is the beamforming vector allocated to MU n and can be obtained from (5.1). p_{ni} indicates the transmit power, which can be used to calculate the actual power consumption P_{ni} by multiplying $\|\boldsymbol{w}_{ni}{}'\|^2$ as in (5.6). x_n is the data (bit) transmitting to MU n. ν_n denotes the additive white Gaussian noise with zero mean and variance σ^2. a_{ni} denotes the large-scale channel gain to indicate the share of power consumption on RRH i. Thus, if MU n has only one master link, a_{ni}=1 [103]. Otherwise, $0 < a_{ni} < 1$. To simplify the notation of beamforming vector, we employ an uniform notation $\boldsymbol{w}_{ni}^{*}$ to replace $\boldsymbol{w}_{ni}^{'}$ and $\boldsymbol{w}_{ni}$ to denote the beamforming vector in either the MIMO-OMA or the MIMO-NOMA state.

If MU n in MIMO-NOMA cluster k (we assume $g_{i_k} = \{g_{1i_k} = 1, ..., g_{ni_k} = n, ..., g_{di_k} = d\}$ to simplify the notation of subscripts), the superposed signal can be denoted as

$$\begin{aligned} &\boldsymbol{s}_{i_k} = p_{i_k}\boldsymbol{v}_{i_k}(\boldsymbol{\rho}_{1i}x_1 + ... + \boldsymbol{\rho}_{di}x_d), \\ &\boldsymbol{\rho}_{1i} = \left[\sqrt{\rho_{ni,1}}, ..., \sqrt{\rho_{ni,M}} \right]^T \text{for} \quad n \in \{1, ..., d\}, \end{aligned} \tag{5.2}$$

where $\boldsymbol{v}_{i_k}$, $\boldsymbol{\rho}_{1i}$ and p_{i_k} are NOMA beamforming vector, power coefficient set and the cluster transmit power, respectively. According to [108], (5.3) can be rewritten as

$$\boldsymbol{s}_{i_k} = a_{1i}\boldsymbol{w}_{1i}\sqrt{p_{1i}}x_1 + ... + a_{di}\boldsymbol{w}_{di}\sqrt{p_{di}}x_d. \tag{5.3}$$

Here, $\boldsymbol{w}_{1i}$ is a redefined NOMA beamforming vector for MU 1, which is obtained from our proposed NOMA beamforming strategy. p_{1i} denotes the transmit power. Based on it, the

corresponding $\boldsymbol{v}_{i_k}$, $\rho_{ni,m}$ and p_{i_k} can be derived as

$$\begin{aligned}
&\boldsymbol{v}_{i_k}=\Big[v_{i_k,1},...,v_{i_k,M}\Big]=\begin{bmatrix}\sqrt{\frac{p_{1i}}{p_{ni}}w_{1i,1}^2a_{1i}^2+...+\frac{p_{di}}{p_{ni}}w_{di,1}^2a_{di}^2}\\ \vdots \\ \sqrt{\frac{p_{1i}}{p_{ni}}w_{1i,M}^2a_{1i}^2+...+\frac{p_{di}}{p_{ni}}w_{di,M}^2a_{di}^2}\end{bmatrix}^T,\\
&\sqrt{\rho_{ni,m}}=\frac{\sqrt{p_{ni}}w_{ni,m}a_{di}}{\sqrt{p_{i_k}}v_{i_k,m}},\text{for}\, m\in M\,\text{and}\, n\in\{1,...,d\},\\
&p_{i_k}=p_{1i}a_{1i}^2+...+p_{di}a_{di}^2.
\end{aligned}$$

For a guaranteed quality of service, it is required that the signal-to-interference-plus-noise ratio (SINR) at MU n is larger than a pre-determined threshold δ. Without considering CoMP, the SINR of a MU n both in the MIMO-OMA and the MIMO-NOMA states can be simply denoted as

$$\gamma_{ni}=\frac{a_{ni}^2\left|\boldsymbol{h}_{ni}^H\boldsymbol{w}_{ni}^*\sqrt{p_{ni}}\right|^2}{I_n+\sigma^2}\geq\delta, \tag{5.4}$$

where I_n denotes the interference term which may include the inter-cell interferences $I_n^{[2]}$ and intra-cell interferences $I_n^{[1]}$. $I_n^{[1]}$ is due to the un-cancelled signals from MU 1 to MU $n-1$ in the MIMO-NOMA state. Thus,

$$\begin{aligned}
&I_n=\begin{cases}I_n^{[2]}, & \text{MIMO-OMA state},\\ I_n^{[1]}+I_n^{[2]}, & \text{MIMO-NOMA state}.\end{cases}\\
&I_n^{[1]}=\textstyle\sum_{u=1}^{n-1}\left|a_{ui}\boldsymbol{h}_{ni}^H\boldsymbol{w}_{ui}\sqrt{p_{ui}}x_u\right|^2,\\
&I_n^{[2]}=\textstyle\sum_{u\neq n}^{N}\left|\sum_{j\in B-i}a_{uj}\boldsymbol{h}_{nj}^H\boldsymbol{w}_{uj}^*\sqrt{p_{uj}}x_u\right|^2.
\end{aligned} \tag{5.5}$$

The power consumption of MU n in both states can be obtained by [103]

$$P_{ni}=\|\boldsymbol{w}_{ni}^*\|^2p_{ni}a_{ni}^2=\|\boldsymbol{w}_{ni}^*\|^2(I_n+\sigma^2)\gamma_{ni}a_{ni}^2. \tag{5.6}$$

5.2.2 Problem formulation

Our objective is to minimize the total power consumption under the condition of maximizing the accessed MUs, so that the system optimization problem can be formulated as

$$\min_{\boldsymbol{W},\boldsymbol{p}} \sum\nolimits_{i=1}^{L} \sum\nolimits_{n=1}^{l_i} P_{ni}(\boldsymbol{w}_{ni}, p_{ni}), \tag{5.7a}$$

$$\text{s.t.} \sum\nolimits_{n=1}^{l_j} P_{ni} \leq P_{\max}, \tag{5.7b}$$

$$\sum\nolimits_{n=1}^{l_i} x_n \leq \mu, \quad \text{for all} \quad i \in L, \tag{5.7c}$$

$$\boldsymbol{h}_{ni}\boldsymbol{w}_{li} \begin{cases} \neq 0 & \text{If MUs } n \text{ and } l \text{ are in the same cluster,} \\ = 0 & \text{Otherwise,} \end{cases} \tag{5.7d}$$

$$\sum\nolimits_{i=1}^{L} \sum\nolimits_{n=1}^{l_i} (P_{ni} > 0) > \kappa. \tag{5.7e}$$

Here, P_{ni} is the power consumption of RRH i for MU n, which is determined by the beamforming vector $\boldsymbol{w}_{ni}^{*}$ and the transmit power p_{ni}. Constrain (5.7b) means that the total power consumption of each RRH should be lower than a threshold P_{max}. Constrain (5.7c) is to ensure that the amount of downlink data transmission should be less than the capacity of backhaul link μ. Constrain (5.7d) denotes the orthogonal and non-orthogonal conditions. Constrain (5.7e) is to require the total number of accessed MUs should larger than κ to achieve the purpose that system can access MUs as many as possible. κ will be adjusted in the progress of optimization.

5.3 CoMP-NOMA

In this section, we first introduce RRH cooperation. Then, we combine it with MIMO-NOMA to obtain our proposed CoMP-NOMA approach, i.e., JT-NOMA and CT-NOMA. We consider three different links, and all of them are available for NOMA clustering.

However, we notice that the master link and JT link are used for signal transmission. The only difference between them is the large-scale channel gain, i.e., $a_{ui} = 1$ or $0 < a_{ui} < 1$. Therefore, their closed-form solutions for NOMA clustering are same, which will be discussed at JT-NOMA without specific distinctions.

5.3.1 RRH cooperation

For any MU n, if it has one master link from RRH i and one cooperation link from RRH j, its SINR can be denoted as

$$\gamma_{ni} = \frac{a_{ni}^2 \left| \boldsymbol{h}_{ni}^H \boldsymbol{w}_{ni}^* \sqrt{p_{ni}} \right|^2 + a_{nj}^2 \left| \boldsymbol{h}_{nj}^H \boldsymbol{w}_{nj}^* \sqrt{p_{nj}} \right|^2}{I_n + \sigma^2} = \frac{p_{ni}}{I_n + \sigma^2} \geq \delta,$$

where a_{ni} and a_{nj} denote the large-scale channel gains and satisfy $a_{ni}^2 + a_{nj}^2 = 1$[103]. If this cooperation link is CT, we have $a_{nj} = 0$. Otherwise, $a_{nj} = \frac{\|\boldsymbol{h}_{nj}\|^2}{\|\boldsymbol{h}_{ui}\|^2 + \|\boldsymbol{h}_{uj}\|^2} > 0$ to determine the share of the transmit power for MU n on different RRHs (i.e., $p_{ni} = p_{nj} = p_n$ obtained from (5.8)). After multiply this index, the actual power consumption on RRH j can be calculated as ${a_{uj}}^2 \|\boldsymbol{w}_{uj}\|^2 p_{uj}$. Note that adding a new cooperation link will result in the change of the power consumption of MUs in RRH j, which further changes the interferences toward other RRHs. However, since such influence reduces very quickly with the distance. We include only the closet RRHs, such as RRHs i, j and k, in power calculation.

$$p_n = \begin{cases} \delta(\sum_{u \neq n} \left| \sum\limits_{j=B-\{i,j\}} a_{uj} \boldsymbol{h}_{nj}^H \boldsymbol{w}_{uj}^* \sqrt{p_{uj}} \right|^2 + \sigma^2), & \text{if MIMO-OMA,} \\ \delta(\sum_{u=1}^{n-1} \left| \boldsymbol{h}_{ni}^H \boldsymbol{w}_{ui} \sqrt{p_{ui}} x_u \right|^2 + \sum_{u \neq n} \left| \sum\limits_{j=B-\{i,j\}} a_{uj} \boldsymbol{h}_{nj}^H \boldsymbol{w}_{uj}^* \sqrt{p_{uj}} \right|^2 + \sigma^2) & \text{if MIMO-NOMA.} \end{cases} \tag{5.8}$$

CT link

Before RRH cooperation, the interference to MU n served by RRH i is from RRHs j and k. By adding a CT link from RRH j, the interference is only from RRH k. The power

reduction on RRH i before and after adding a CT link can be calculated as

$$\begin{aligned}&\Delta P_i = \Delta p_{ni}\|\boldsymbol{w}_{ni}^*\|^2,\\&\Delta p_{ni} = p_{ni} - p_{ni}^{'} = \delta(\textstyle\sum_{u\in l_j} a_{uj}^2\left|\boldsymbol{h}_{nj}^H\boldsymbol{w}_{uj}^*\right|^2 p_{uj} - T_{nj}),\end{aligned} \tag{5.9}$$

where p_{ni} and $p_{ni}^{'}$ are the transmit powers before and after RRH cooperation. T_{nj} is used to denote the decoding interference when MU n joins a MIMO-NOMA cluster in RRH j. By letting T_{nj} be the maximum intra-cell interference of all potential clusters, we can effectively decoupled RRH cooperation and MU cooperation, which greatly reduce the complexity in searching the solution.

Let ΔP_j denote the power reduction on RRH j, and $\boldsymbol{w}_{nj}^{''}$ is the recalculated beamforming vector in the MIMO-OMA state. Then, we have

$$\Delta P_j = \sum_{u\in l_j} p_{uj}\left(\left\|\boldsymbol{w}_{uj}^{''}\right\|^2 - \left\|\boldsymbol{w}_{uj}^*\right\|^2\right) - \Delta p_{ni}\sum_{u\in l_j} a_{ni}^2\left|\boldsymbol{h}_{ui}^H\boldsymbol{w}_{ni}\right|^2\left\|\boldsymbol{w}_{uj}^{''}\right\|^2,$$

where $\boldsymbol{w}_{uj}^*$ and $\boldsymbol{w}_{uj}^{''}$ are the beamforming vectors before and after RRH cooperation, respectively.

JT link

Since the JT link implements data transmission, it will bring new interference to all other MUs. In this case, ΔP_i and Δp_{ui} can be derived as

$$\begin{aligned}&\Delta P_i = \Delta p_{ni}\|\boldsymbol{w}_{ni}^*\|^2 - \textstyle\sum_{u\in l_i, u\neq n} a_{nj}^2\left|\boldsymbol{h}_{uj}^H\boldsymbol{w}_{nj}\right|^2 p_{nj}\|\boldsymbol{w}_{ui}^*\|^2,\\&\Delta p_{ni} = \delta(\textstyle\sum_{u\neq n}\left|\sum_{l\in\{j,k\}} a_{ul}\boldsymbol{h}_{nl}^H\boldsymbol{w}_{ul}^*\sqrt{p_{ul}}\right|^2 + \sigma^2)\\&-\delta(\textstyle\sum_{u\neq n, u\in l_k}\left|a_{uk}\boldsymbol{h}_{nk}^H\boldsymbol{w}_{uk}^*\sqrt{p_{uk}}\right|^2 + \sigma^2 + T_{nj})a_{ni}^2.\end{aligned} \tag{5.10}$$

The approximation of power reduction at RRH j can be presented as

$$\Delta P_j \approx \sum_{u\in l_j} p_{uj}\left(\left\|\boldsymbol{w}_{uj}^{''}\right\|^2 - \left\|\boldsymbol{w}_{uj}^*\right\|^2\right) - \Delta p_{ni}\sum_{u\in l_j} a_{ni}^2\left|\boldsymbol{h}_{ui}^H\boldsymbol{w}_{ni}^*\right|^2\left\|\boldsymbol{w}_{uj}^{''}\right\|^2 + p_{nj}a_{nj}^2\left\|\boldsymbol{w}_{uj}^{''}\right\|^2,$$

where $p_{nj} = \delta(\sum_{u\neq n, u\in l_k}\left|a_{uk}\boldsymbol{h}_{nk}^H\boldsymbol{w}_{uk}^*\sqrt{p_{uk}}\right|^2 + \sigma^2)$.

In summary, the overall power consumption reduction due to RRH cooperation equals

$$\Delta P_{ij} = \Delta P_i - \Delta P_j. \tag{5.11}$$

Note that $\Delta P_{ij} > 0$ is the condition of a beneficial RRH cooperation.

5.3.2 JT-NOMA

If MU n is in MIMO-NOMA cluster k of RRH i (e.g., g_{i_k}=$\{g_{1i_k}$=$1, ..., g_{ni_k}$=$n, ..., g_{di_k}$=$d\}$), after decoding the superposed message, the received signal at MU n can be represented in (5.12). To satisfy the SINR requirement, the power consumption for MU n can be calculated by (5.13).

$$\begin{aligned} &y_{ni} = \boldsymbol{h}_{ni}^H \boldsymbol{s}_k + I_n^{[2]} + \nu_n = \\ &\begin{cases} a_{ni}\boldsymbol{h}_{ni}^H \boldsymbol{w}_{ni}\sqrt{p_{ni}}x_i + I_n^{[2]} + \nu_n, & \text{if } n = 1, \\ a_{ni}\boldsymbol{h}_{ni}^H \boldsymbol{w}_{ni}\sqrt{p_{ni}}x_i + \sum_{u=1}^{n-1} a_{ui}\boldsymbol{h}_{ni}^H \boldsymbol{w}_{ui}\sqrt{p_{ui}}x_u + I_n^{[2]} + \nu_n, & \text{otherwise.} \end{cases} \end{aligned} \tag{5.12}$$

$$\begin{aligned} &P_{ni} = \|\boldsymbol{w}_{ni}\|^2 p_{ni} = \\ &\begin{cases} \|\boldsymbol{w}_{ni}\|^2 a_{ni}^2 (I_n^{[2]} + \sigma^2)\delta, & \text{if } n = 1, \\ \|\boldsymbol{w}_{ni}\|^2 a_{ni}^2 (\sum_{u=1}^{n-1} \left|\boldsymbol{h}_{ni}^H \boldsymbol{w}_{ui}\right|^2 a_{ui}^2 p_{ui} + I_n^{[2]} + \sigma^2)\delta, & \text{otherwise.} \end{cases} \end{aligned} \tag{5.13}$$

Obviously, T_{nj} in (5.9) is determined by $I_n^{[1]} = \sum_{u=1}^{n-1} a_{ui}^2 \left|\boldsymbol{h}_{ni}^H \boldsymbol{w}_{ui}\right|^2 p_{ui}$. We now design beamforming vectors to reduce the power consumption, i.e.,

$$\min P_{1i} + ... + P_{di}. \tag{5.14}$$

Notice that $\boldsymbol{w}_{ni}$ will affect the power consumption of MUs from n to d. Thus, we can derive $\boldsymbol{w}_{nd}$ first and then substitute the solution back to (5.14) to derive $\boldsymbol{w}_{nd-1}$ till $\boldsymbol{w}_{n1}$. The detailed procedure can be found in [11] and we only use a 2-MU case as an example to describe the solution procedure. Given a 2-MU cluster $g_{i_k} = \{1, 2\}$, $\boldsymbol{w}_{2i}$ can be determined

from

$$\min \|\boldsymbol{w}_{2i}\|^2.$$

After that, the problem for $\boldsymbol{w}_{1i}$ can be formulated as

$$\min \|\boldsymbol{w}_{1i}\|^2 + \|\boldsymbol{w}_{2i}\|^2 a_{2i}^2 \left|\boldsymbol{h}_{2i}^H \boldsymbol{w}_{1i}\right|^2 \delta.$$

We can derive the closed-form solution for a 2-MU cluster as

$$\begin{aligned} &\boldsymbol{w}_{1i} = \boldsymbol{w}_{1i}^{'} + \beta \boldsymbol{w}_{2i}^{'}, \boldsymbol{w}_{2i} = \boldsymbol{w}_{2i}^{'} + \lambda \boldsymbol{w}_{1i}^{'}, \\ &\beta = \frac{-\left\|\boldsymbol{w}_{1i}^{'}\right\|^2 \boldsymbol{w}_{1i}^{'} \boldsymbol{w}_{2i}^{'}}{\left\|\boldsymbol{w}_{1i}^{'}\right\|^2 \left\|\boldsymbol{w}_{2i}^{'}\right\|^2 (1+\delta a_{2i}^2) - \delta a_{2i}^2 \left|\boldsymbol{w}_{1i}^{'} \boldsymbol{w}_{2i}^{'}\right|^2}, \lambda = -\frac{\boldsymbol{w}_{2i}^{'} \boldsymbol{w}_{1i}^{'}}{\left\|\boldsymbol{w}_{1i}^{'}\right\|^2}. \end{aligned} \tag{5.15}$$

By forming a MIMO-NOMA cluster, the power saving can be calculated as

$$\begin{aligned} &\Delta P_{g_{i_k}} = P_{1i}^{'} + P_{2i}^{'} - (P_{1i} + P_{2i}) \\ &= \delta a_{1i}^2 (I_1^{[2]} + \sigma^2) |\boldsymbol{w}_{1i} \boldsymbol{w}_{2i}| |\beta| + \delta a_{2i}^2 (I_2^{[2]} + \sigma^2) |\boldsymbol{w}_{1i} \boldsymbol{w}_{2i}| |\lambda|. \end{aligned}$$

If $\Delta P_{g_{i_k}} > \theta$ ($\theta = 0.01w$), g_{i_k} is defined as a beneficial MIMO-NOMA cluster. The condition of successful SIC decoding and the decoding order are discussed in [121].

5.3.3 CT-NOMA

In CT-NOMA, no data will be transmitted on CT links. Thus, given a MIMO-NOMA cluster k ($g_{i_k} = \{1, ..., d\}$), at least one MU in this cluster has a JT link or a master link connected with RRH i. Otherwise, this NOMA cluster will not exist. As usual, we use 2-MU cluster $g_{i_k} = \{1, 2\}$ as an example. The similar procedure can be applied to any size clusters. If only MU 1 has a CT link, after decoding the superposed message, the received signal of MU 2 on MU 1 has been cancelled. The interference from MU 1 to MU 2 is zero as no signals will be transmitted at CT link, i.e., $I_2^{[1]} = 0$. Obviously, the power consumption

of this cluster can be calculated as

$$P_{1i} + P_{2i} = \|\boldsymbol{w}_{2i}\|^2 p_{2i} = \|\boldsymbol{w}_{2i}\|^2 a_{2i}^2 (I_2^{[2]} + \sigma^2)\delta. \tag{5.16}$$

Thus, the power consumption is minimum when $\lambda = -\frac{\boldsymbol{w}_{2i}^{'}\boldsymbol{w}_{1i}^{'}}{\|\boldsymbol{w}_{1i}^{'}\|^2}$. Then, the total power reduction becomes

$$\Delta P_{g_{ik}} = \delta a_{2i}^2 (I_2^{[2]} + \sigma^2)\left|\boldsymbol{w}_{1i}^{'}\boldsymbol{w}_{2i}^{'}\right||\lambda|. \tag{5.17}$$

The condition of successful SIC decoding is $\lambda^2 > (1+\delta)$.

If only MU 2 has a CT link, the power consumption of this cluster can be denoted as

$$P_{1i} + P_{2i} = \|\boldsymbol{w}_{1i}\|^2 p_{1i} = \|\boldsymbol{w}_{1i}\|^2 a_{1i}^2 (I_1^{[2]} + \sigma^2)\delta. \tag{5.18}$$

Similarly, we obtain the closed-form solution $\beta = -\frac{\boldsymbol{w}_{2i}^{'}\boldsymbol{w}_{1i}^{'}}{\|\boldsymbol{w}_{2i}^{'}\|^2}$ for power minimization and the power reduction

$$\Delta P_{g_{ik}} = \delta a_{1i}^2 (I_1^{[2]} + \sigma^2)\left|\boldsymbol{w}_{1i}^{'}\boldsymbol{w}_{2i}^{'}\right||\beta|. \tag{5.19}$$

Note that the transmission of MU 1 will bring interference to MU 2, so that

$$I_2^{[1]} = \beta^2 a_{1i}^2 (I_1^{[2]} + \sigma^2)\delta.$$

5.3.4 Cooperation scheduling

MU cooperation only involves a small group of MUs, while RRH cooperation will affect much more MUs and thus becomes more efficient on power reduction. Through T_{ni}, we can decouple RRH cooperation and MU cooperation, and give RRH cooperation a high priority. Therefore, the MU cooperation will be adjusted based on the result from RRH cooperation. Moreover, in a single RRH, the power reduction for a cluster only relates to MUs in this cluster but independent with other out-of-cluster MUs, and interference

$I_{ni}^{[2]}$ only relates to the power reduction rather than MIMO-NOMA beamforming strategy. Therefore, in MU cooperation, for each iteration, we only need to update the power reduction of each cluster. We summarized the solution process as follows.

1) Initialization

We determine the master link for each MU and use (5.1) to initiate the beamforming vectors for all MUs, i.e., $\boldsymbol{W}^{'}$ and $\boldsymbol{W}^{*} = \boldsymbol{W}^{'}$.

2) RRH cooperation

- **Step 1:** We calculate the power reduction for all possible RRH cooperation and group all beneficial RRH cooperation which satisfy both power and backhaul limitations, and sort them into a set $C = \{c_1, ...\}$ in a descending order.
- **Step 2:** If C is empty and beamforming matrix $\boldsymbol{W}^{'}$ (or $\boldsymbol{W}^{*}$) is unchanged, stop iteration. Otherwise, we select the first RRH cooperation and add its cooperation link into the system. Update beamforming vectors and go back to step 1, until there is no change on beamforming vectors.

3) MU cooperation

- **Step 3:** Initiate MIMO-NOMA cluster set $G_i = G_i^* = \{\}$ for RRH $i \in L$, calculate interference $I_{ni}^{[2]}$ of each MUs and go to step 4.
- **Step 4:** For each RRH (e.g., RRH i), we find all feasible MIMO-NOMA clusters and arrange them into a set $R_i = \{r_1, r_2, ..., r_L\}$ with the decreasing order of their average power reductions. If R_i is empty for all RRHs, go to step 1.
- **Step 5:** We select the first cluster in R_i, i.e., r_1, to join G_i. Then, we delete all clusters in R_i which contain MUs in r_1, and repeat this step till R_i is empty.

- **Step 6:** If $G_i^* = G_i$ for all $i \in L$, we update beamforming vectors $\boldsymbol{W}^*$, decoding interference T_{ni} and go to step 1. Otherwise, $G_i^* = G_i$.

- **Step 7:** Update interference $I_{ni}^{[2]}$ of each MUs, and recalculate the power reduction of all clusters in order to renew R_i. Here, we let $G_i = \{\}$ and go to step 4.

Since we can obtain the closed form solutions of all RRH cooperation and MIMO-NOMA clusters, it is very easy to compare all possible combination of MUs through exhausted searching. Moreover, we assume the size of MIMO-NOMA cluster is less than 3. Thus, the complexity of the proposed algorithm is approximated to be $O(N^{n_1} + \mu(\mu-1)^2 n_2 n_3 L)$, where n_1 denotes the number of formed cooperation links, n_2 indicates iterations of two stages, and n_3 is the average number of iterations of MU cooperation.

5.4 Numerical Results

Consider a 7-cell MIMO network, in which the radius of each cell is 400m. MUs are randomly located in this area. The number of antennas at each RRH is $M = 20$. The variance of Gaussian noise is $\sigma_u^2 = -50dBm$. The SINR requirement is $\delta = 4dB$. Similar to [113], the parameters of channel model include: the 3GPP long term evolution (LTE) pathloss parameters ($\alpha = 3.76$ and $\beta = 10^{-14.81}$), the Rayleigh fading with zero mean and unit variance ($\Gamma_i^{(n)} \sim NC(0,1)$), a log-normal shadowing $\gamma_i \sim N(0dB, 8dB)$, and the transmit antenna power gain $G = 9dB$. For comparison, we consider the following four approaches.

- **No-cooperation transmission (No-co):** Each MU only has one master link for data transmission.

- **Hybrid CoMP transmission (Hybrid):** Only RRH cooperation (joint CT and JT) is considered.

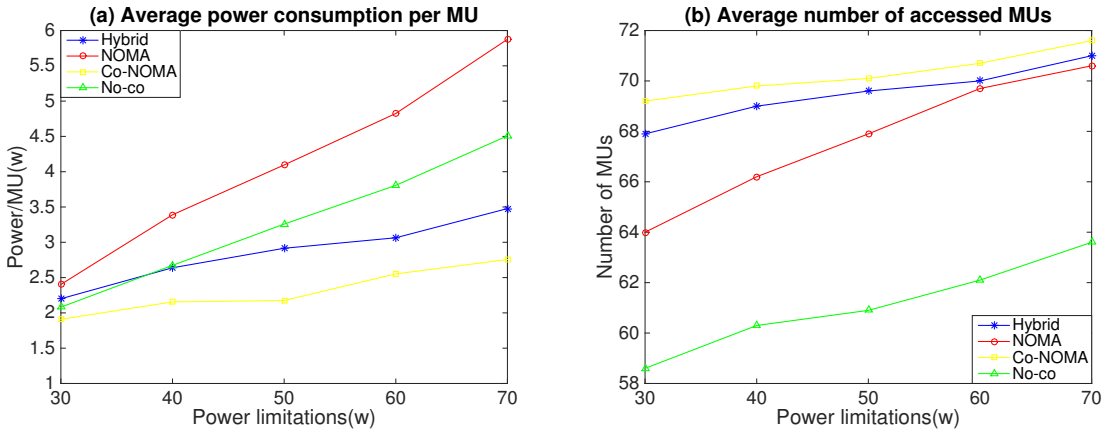

Figure 5.2: System performance on different limitations of power.

- **MIMO-NOMA transmission (NOMA):** In each RRH, MUs may form MIMO-NOMA clusters to optimize power consumption without consideration of RRH cooperation.

- **CoMP-NOMA transmission (Co-NOMA):** It combines hybrid CoMP and MIMO-NOMA approaches.

Note that due to restriction on power and the backhaul link capacity, some MUs may not be able to access any RRH for downlink signal transmission. In this case, those MUs will be served at different time slots or in different sub-channels. To better analyze different cooperation, in this situation, our consideration only focus on one sub-channel, and the system performance in terms of: i) the number of accessed MUs; and ii) the total power consumption. In following simulations, each outcome is the average from 10 randomly generated data within the radius range of [280,400]m. The outcomes of different approaches are obtained from the same set of data.

The results of system performance with respect to different transmit power limitations are shown in Fig. 5.2. The capacity of backhaul link is fixed to be μ=14. As the increase of accessed MUs, the required spatial division on beamforming calculation is also increased, so that the power consumption will grow up fast. In Fig. 5.2, NOMA has the highest power consumption than the other approaches, and the power consumption of the Hybrid

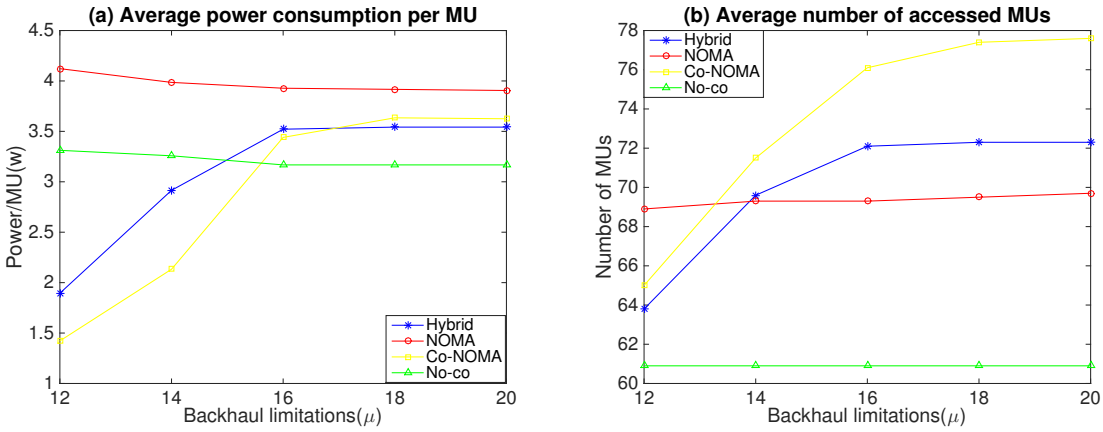

Figure 5.3: System performance on different backhaul capacities.

approach is close to No-co. However, the number of accessed MUs by No-co is smallest. From the point of view of power reduction only, RRH cooperation (i.e., CoMP) is more efficient than MU cooperation (i.e., NOMA). However, Co-NOMA can allow more MUs to be accessed by RRHs, which indicates that the performance of Co-NOMA is best, i.e., the power consumption is lowest while the number of accessed MUs is highest. Similarly, to allow more MUs to be accessed by RRHs, NOMA will consume more power than No-Co. If the maximum transmit power continues to increase, the differences on power consumptions of 3 cooperation approaches are increased, while the number of accessed MUs becomes similar. It means that with the relaxation of power limitation, the backhaul limitation becomes the main factor to restrict the number of accessed MUs. Moreover, the complexity in this case is approximated to be $O(6.9485E + 37)$.

Fig. 5.3 shows results of system performance with respect to different backhaul limitations, in which the transmit power limitation on each RRH is fixed to be P_{max}=50w. We notice that the performances of Hybrid and Co-NOMA are firstly increased and then become stable with the increase of backhaul limitations. It reveals that the backhaul limitation is the main factor to determine RRH cooperation (JT or CT) when the transmit power limitation is fixed. Since NOMA and No-co do not have cooperation links, their performance is mostly unchanged (affected by P_{max}). We also observe an interesting result that at μ=12, Co-NOMA allows less MUs than NOMA. It is because when the backhaul

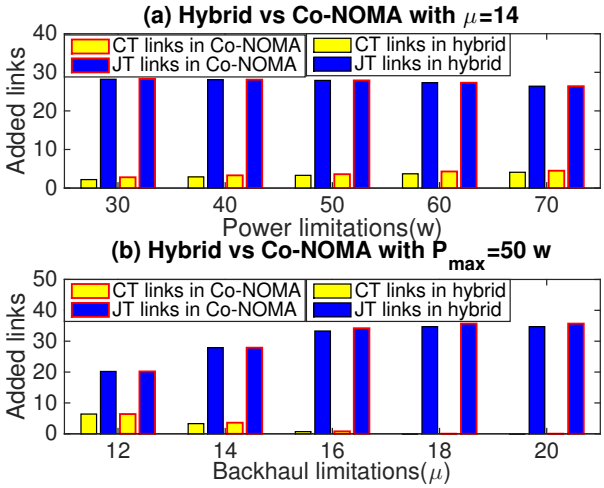

Figure 5.4: Quantities of cooperation links.

limitation becomes the main factor to decide the number of accessed MUs, CoMP will decrease the power consumption by forming more JT links. As a result, it will increase the traffic on backhaul links and prevent more MUs to be accessed. In this case NOMA can access more MUs while also having a higher power consumption. From this point of view, Co-NOMA focus more on improving power efficiency than spectrum efficiency. Moreover, with the increase of backhaul limitation, the power consumptions of CoMP and Co-NOMA tend to be close, while their number of accessed MUs are very different. It is due to the fact that the power limitation becomes the main factor to affect the total power consumption, which leverages more RRH cooperation to increase the number of accessed MUs. Under this circumstances, NOMA clustering offers further supports to RRH cooperation which allow more MUs to be accessed.

Fig. 5.4 shows the number of added cooperation links in Hybrid and Co-NOMA. In Fig. 5.4 (a), we notice that the number of JT links will be decreased with the increase of transmit power limitation, while that of CT links is increased. It is because JT links will increase the traffic on backhaul links. As P_{max} increases, more MUs will be allowed, and the number of JT links will be restricted by backhaul capacity. However, since JT is more power efficient than CT, more JT links are established. In Fig. 5.4 (b), when the backhaul limitation is

$\mu = 12$, since the number of JT links is restricted, while CT links are responsible for load balance, the number of accessed MUs of the Hybrid approach is slightly higher than the No-co approach, while the total power consumption of it becomes less. If we increase the backhaul limitation, JT will be the major of RRH cooperation which allows more MUs to be accessed. Moreover, the cooperation links of Co-NOMA are slightly more than Hybrid as NOMA can further reduce power consumption of RRHs. If a RRH has more connected MUs, it can obtain a larger power reduction through MIMO-NOMA clustering, which in turn stimulates more RRH cooperation formed on this RRH. In summary, hybrid CoMP increases the flexibility towards different environment settings.

Chapter 6

UAV-NOMA

6.1 Introduction

In this chapter, we propose new algorithms on BS resource management and UAV renting to facilitate the integration of UAVs in MIMO-NOMA wireless networks. Due to UAV participant will change the channel gain vectors, we redesign beamforming strategies for UAV assisted MIMO transmission, and propose two different UAV-NOMA approaches based on a joint MIMO-NOMA strategy. Since UAV's CSI may not available for BS before renting a UAV, we propose an profit estimation approach based on we obtained closed-form function of power reduction. Through our designed contract theoretic framework, the contract of BS will base on the estimated benefits of itself, and UAV companies deploy their unoccupied UAV to serve for BS. The main contributions of this thesis are summarized as follows.

- We propose a novel BS beamforming strategy for UAV assisted MIMO-NOMA system and derive a closed-form solution for deriving power allocation, beamforming vector and the UAV-MIMO beamforming coefficient under the situation of multiple

UAVs with a flexible NOMA cluster size.

- We propose an UAV-NOMA strategy to manage resource allocation for UAV assisted MIMO-NOMA system, which integrates the UAV-MIMO beamforming and the MIMO-NOMA beamforming (i.e., UAV-NOMA beamforming) jointly.

- We design a novel framework for UAV renting services based on contract theory. The BS can choose either a short-term contract or a long-term contract, with respect to different scenarios, which is triggered by the estimated benefits of BS. We also propose a profit estimation approach for BS under the situation without UAV's CSI.

- We employ a many-to-many matching game to solve the joint optimization of MU grouping and resource allocation based on the information of UAV channels. If this information is not available as in case of long-term contract, we propose a 2-layer matching game approach to group MU and optimize resource allocation. Both stability and optimality are proved.

For convenience, following table lists some important notations used in this work.

Notation	Meaning
N, M, L	the number of MUs, antennas and UAVs
$\boldsymbol{H}$	the channel gain matrix
$\boldsymbol{W}$	the MIMO-OMA beamforming matrix
$\boldsymbol{h}_i, h'_{li}$	the channel gains of MU i from the BS, and UAV l; $\hat{\boldsymbol{h}}_i = [\boldsymbol{h}_i, h'_{li}]^T$
$\boldsymbol{w}_i$	the MIMO-OMA beamforming for MU i
$\boldsymbol{w}_i^*, w'_{li}$	the UAV-MIMO beamforming coefficients at the BS, and UAV l; $\hat{\boldsymbol{w}}_i = [\boldsymbol{w}_i^*, w'_{li}]$
$\boldsymbol{w}_i^{\aleph}$	the MIMO-NOMA (or UAV-NOMA) beamforming for MU i
g_l	a UAV group l
$\mathcal{G}_{c_1}$	a MIMO-NOMA (or UAV-NOMA) cluster c_1
$\triangle P_{g_l}, \triangle P_{\mathcal{G}_{c_1}}$	the total power reductions of UAV group l and cluster $\mathcal{G}_{c_1}$
U_{li}^I, U_{li}^{III}	the utilities of MU player i to select l in case of the short-term contract (I) and the long-term contract (III) when a single UAV is available for renting
U_l^I	the utility of UAV player l when a single UAV is available for renting
$U_{\boldsymbol{K}_i i}^{II}$	the utility of MU player i served by UAVs $l \in \boldsymbol{K}_i$ if multiple UAVs are available for renting
U_l^{II}	the utility of UAV player l when multiple UAVs are available for renting

6.2 UAV-renting MIMO-NOMA System

Fig. 6.1 shows a downlink UAV renting MIMO-NOMA system, which has one BS (equipped with M antennas), N MUs ($M \geq N$) and L UAVs. Each MU or UAV is equipped with a single antenna. Besides the traditional transmission mode of MIMO-OMA or MIMO-NOMA, the assistance from UAVs generates two new transmission modes, called UAV-MIMO and UAV-NOMA, distinguished by whether MUs are involved in NOMA clusters. We consider rotary-wing UAVs, which could be i) hovering when they provide

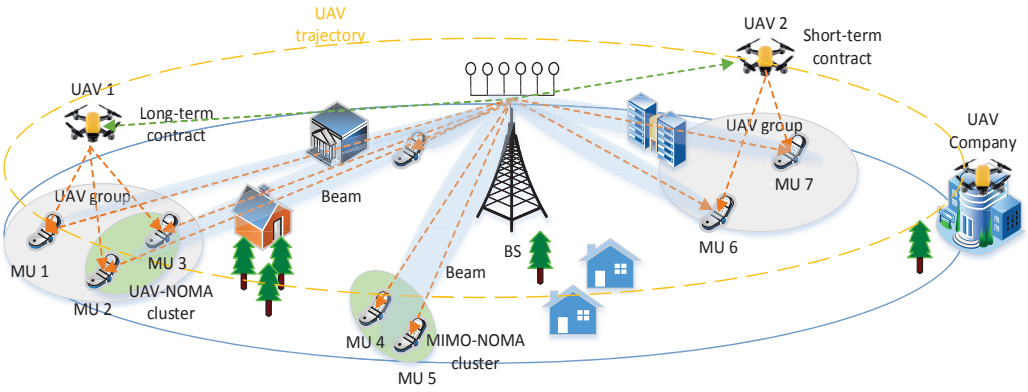

Figure 6.1: UAV renting MIMO-NOMA wireless networks

transmission services; or ii) move around the cell edge (i.e., UAV trajectory) when they are available for renting. In MIMO-NOMA and MIMO-OMA, MUs are served by the BS, e.g., MUs 4 and 5. However, in UAV-MIMO and UAV-NOMA, MUs are served by UAVs and the BS, e.g., MUs 1-3. Note that, MUs can form a UAV-NOMA cluster only if they are served by the same UAVs. Obviously, UAV association and NOMA clustering interact with each other. In UAV associated transmission, the BS should transmit required signals and corresponding beamforming coefficients to the UAV first through a dedicated channel [40]. [1] After that the UAV and the BS will transmit signals to MUs simultaniously. Note that all downlink transmissions occupy the same spectrum, and the multiple access is achieved through beamforming. [2]

We consider two types of contracts. The short-term contract (signing for S minutes) is a pro-active selling approach and designed for the situation that the UAV is flying at a predefined trajectory [3] with a certain speed and forwarding the estimated channel state information (CSI) to the BS at each time slot (defined as the BS scheduling duration). Different from it, the long-term contract (last for T minutes) can appoint the UAV location

[1] In 2012, an agreement was reached to dedicate a part of frequency spectrum for exclusive use by UAVs [40].

[2] To achieve this purpose, we may consider full duplex at UAVs or two-time-slot structure as in relay systems.

[3] The UAV trajectory is determined by UAV companies for different purposes. In this work, we assume the UAV trajectory is around the BS's cell-edge.

and have a lower unit cost, while CSI is not available before signing a contract. Thus, the BS may have a risk of gaining low benefit if some MUs move out of the UAV covered area before the contract is expired. The renting price of a short-term (or long-term contract) is denoted by $P^{[s]} = P * S$ (or $P^{[l]} = P * T + P^{[t]}$), where P is the price per minute, and $P^{[t]}$ is the travel fee. For both contracts, the BS needs to estimate its potential profit before signing a contract, and it can sign different types of contracts with different UAVs. After signing a contract with the BS, the UAV will turn to hovering mode to provide transmission service. After the contract is expired, the BS will renew the contract (i.e., continue or stop) based on its current situation. If the contract is ended, the UAV will turn to the travel mode and continue traveling at its trajectory until it is not available for renting service. For an easy understanding, we will formulate an optimization problem after introducing power and beamforming models.

6.3 MIMO-NOMA and UAV-MIMO Beamforming Models

In this section, the power model, the UAV-MIMO beamforming model, and MIMO-NOMA beamforming model are introduced.

6.3.1 Power model

For notation simplicity, we focus on a single time slot and remove the time variable t. Let $\boldsymbol{h}_i \in R^{M\times 1}$ and $\boldsymbol{w}_i \in R^{M\times 1}$ denote the channel gain vector and beamforming vector from the BS to MU i, respectively. $\boldsymbol{W} = [\boldsymbol{w}_1, ..., \boldsymbol{w}_N]$ and $\boldsymbol{H} = [\boldsymbol{h}_1, ..., \boldsymbol{h}_N]^T$ denote the beamforming matrix and the channel gain matrix for all MUs, respectively. We consider the ZF-beamforming (zero forcing) strategy [22, 107], and $\boldsymbol{W}$ in case of MIMO-OMA

transmission can be calculated as

$$\boldsymbol{W} = \boldsymbol{H}^{\dagger} = \boldsymbol{H}^{*}(\boldsymbol{H}\boldsymbol{H}^{*})^{-1}. \tag{6.1}$$

For a specific MU i, the received signal y_i can be obtained by

$$y_i = \boldsymbol{h}_i^H \boldsymbol{w}_i \sqrt{p_i} x_i + n_i,$$

where p_i is the transmit power, x_i is the data for MU i, and n_i denotes the additive white Gaussian noise with zero mean and variance σ_i^2. We assume $n_i/x_i^2 = \sigma^2$ for all MUs. For a guaranteed quality of service, it requires that the signal-to-interference-plus-noise ratio (SINR) at MU i should be larger than its pre-determined threshold δ_i as

$$\gamma_i = \frac{\left|\boldsymbol{h}_i^H \boldsymbol{w}_i \sqrt{p_i}\right|^2}{\sigma^2} \geq \delta_i.$$

Thus, the BS' minimum power consumption can be expressed as

$$P_i = \left\|\boldsymbol{w}_i^{'}\right\|^2 p_i = \frac{\left\|\boldsymbol{w}_i^{'}\right\|^2}{\left|\boldsymbol{h}_i^H \boldsymbol{w}_i^{'}\right|^2} \sigma^2 \delta_i = \left\|\boldsymbol{w}_i^{'}\right\|^2 \sigma^2 \delta_i. \tag{6.2}$$

In case of UAV associated MIMO transmission, the UAV will cause interference to all MUs outside of this UAV group. Besides, the beamforming vectors of MUs need to be recalculated when they join this group to overcome the inter-group interference. If UAV $l \in L$ provides service for a group of MUs $g_l = \{1, 2, 3\}$, and MU i ($i \neq g_l$) is in the outside of this group, the received signals of MU 1 and i can be respectively expressed as,

$$\begin{aligned} y_1 &= \hat{\boldsymbol{h}}_{l1}^H \hat{\boldsymbol{w}}_{l1} \sqrt{p_{l1}} x_1 + \sum_{k=1, k\neq l}^{L} \sum_{j \in g_k} h_{k1}^{'} w_{kj}^{'} \sqrt{p_{kj}} x_j + n_1, \\ y_i &= \boldsymbol{h}_i^H \boldsymbol{w}_i \sqrt{p_i} x_i + \sum_{k=1}^{L} \sum_{j \in g_k} h_{ki}^{'} w_{kj}^{'} \sqrt{p_{kj}} x_j + n_i, \end{aligned} \tag{6.3}$$

where $h_{l1}^{'}$ is the channel gain of UAV l for MU 1, and $w_{l1}^{'}$ is the UAV-MIMO beamforming coefficient. Therefore, the channel gain vector and beamforming vector for UAV-MIMO are indicated by $\hat{\boldsymbol{h}}_1 = [\boldsymbol{h}_1^T, h_{l1}^{'}]^T$ and $\hat{\boldsymbol{w}}_1 = [\boldsymbol{w}_1^{*T}, w_{l1}^{'}]^T$.

Note that, the power consumptions for MU 1 are from the BS (i.e., P_1) and the UAV l_1

(i.e., P_{l1}). However, the power consumption for MU i is only from the BS (i.e., P_i). We have

$$\begin{aligned} p_{l1} &= (\sum_{k=1,k\neq l}^{L} \sum_{j\in g_k} \left|h_{k1}^{'} w_{kj}^{'}\right|^2 p_{kj} + \sigma^2)\delta_1, \\ P_1 &= \|\boldsymbol{w}_1^*\|^2 p_{l1}, P_{l1} = w_{l1}^{'2} p_{l1}, P_i = \|\boldsymbol{w}_i\|^2 (\sum_{k=1}^{L} \sum_{j\in g_k} \left|h_{ki}^{'} w_{kj}^{'}\right|^2 p_{kj} + \sigma^2)\delta_i. \end{aligned} \tag{6.4}$$

6.3.2 UAV-MIMO beamforming model

If m MUs are served by a single UAV l, i.e., $g_l = \{l_1, ..., l_m\}$ (we assume that $l_1 = 1$,...,$l_m = m$ for simplifying notations). The formed beams of such m MUs should be orthogonal to each other, i.e., $\hat{\boldsymbol{h}}_j^H \hat{\boldsymbol{w}}_i = 0$, where $i, j \in g_l, i \neq j$. Moreover, to ensure that MU k ($k \notin g_l$) keeps orthogonal to MUs $i \in g_l$, i.e., $\boldsymbol{h}_i^H \boldsymbol{w}_k = 0$ and $\boldsymbol{h}_k^H \boldsymbol{w}_i = 0$, the MIMO-OMA beamforming $\boldsymbol{W}$ (calculated by (6.1)) is used to derive UAV-MIMO beamforming. The channel gain of MU i changes to be $\hat{\boldsymbol{h}}_{li} = [\boldsymbol{h}_i^T, h_{li}^{'}]^T$ when $i \in g_l$. Then, we can assume $\boldsymbol{w}_i^* = \lambda_{11}\boldsymbol{w}_1 + ... + \lambda_{1m}\boldsymbol{w}_m$ to maintain $\boldsymbol{h}_k^H \boldsymbol{w}_1^* = 0$. Let $\hat{\boldsymbol{h}}_j^H \hat{\boldsymbol{w}}_i = 0$. We can calculate the coefficients $\lambda_{i1}...\lambda_{im}$ as

$$\begin{aligned} \left[\boldsymbol{h}_i^T, h_{li}^{'}\right] \begin{bmatrix} \lambda_{i1}\boldsymbol{w}_i + ... + \lambda_{im}\boldsymbol{w}_m \\ w_{li}^{'} \end{bmatrix} &= 1, \\ \left[\boldsymbol{h}_j^T, h_{lj}^{'}\right] \begin{bmatrix} \lambda_{i1}\boldsymbol{w}_1 + ... + \lambda_{im}\boldsymbol{w}_m \\ w_{li}^{'} \end{bmatrix} &= 0, \text{for } j \neq i, i, j \in g_l. \end{aligned} \tag{6.5}$$

Then,

$$\lambda_{i1} = -h_{l1}^{'} w_{li}^{'}, ..., \lambda_{ii} = 1 - h_{li}^{'} w_{li}^{'}, ... \tag{6.6}$$

From (6.6), we notice that minimizing the total BS power consumption is equivalent to

$$\min \delta_1 In_1 \|\boldsymbol{w}_1^*\|^2 + \delta_2 In_2 \|\boldsymbol{w}_2^*\|^2 + ... + \delta_m In_m \|\boldsymbol{w}_m^*\|^2, \tag{6.7}$$

where In_i indicates MU i's interference. Let $w_{l1}^{'} = a_{l1} + b_{l1}i, ..., w_{lm}^{'} = a_{lm} + b_{lm}i$ and $\boldsymbol{B}_l = h_{l1}^{'}\boldsymbol{w}_1 + ... + h_{lm}^{'}\boldsymbol{w}_m$. After some manipulations (refer to Appendix C.4), (6.7) can

be rewritten as

$$\begin{aligned}&\min \delta_1 In_1((a_{l1}^2+b_{l1}^2)\|\boldsymbol{B}_l\|^2-2(a_{l1}\boldsymbol{w}_1\boldsymbol{B}_l-b_{l1}\boldsymbol{w}_1\check{\boldsymbol{B}}_l))+...\\&+\delta_m In_m((a_{lm}^2+b_{lm}^2)\|\boldsymbol{B}_l\|^2-2(a_{lm}\boldsymbol{w}_m\boldsymbol{B}_l-b_{lm}\boldsymbol{w}_m\check{\boldsymbol{B}}_l)).\end{aligned} \tag{6.8}$$

We give two definitions for simple expression: i) notation $\boldsymbol{w}_i\boldsymbol{B}_l$ equals $\boldsymbol{w}_i^T\boldsymbol{B}_l$ in the real-valued case or $\Re(\boldsymbol{w}_i)\Re(\boldsymbol{B}_l)+\Im(\boldsymbol{w}_i)\Im(\boldsymbol{B}_l)$ in the complex-valued case; ii) we define a notation $\check{\boldsymbol{B}}_l=[b_2-b_1i,...,b_{2M}-b_{2M-1}i]$, if $\boldsymbol{B}_l=[b_1+b_2i,...,b_{2M-1}+b_{2M}i]$. From (6.8), we can derive

$$w_{li}^{'}=\frac{\boldsymbol{w}_i\boldsymbol{B}_l-\boldsymbol{w}_i\check{\boldsymbol{B}}_li}{\|\boldsymbol{B}_l\|^2}, \text{for } i\in g_l. \tag{6.9}$$

Therefore, we have the following closed-form solution (refer to Appendix C.1)

$$\begin{aligned}&\|\boldsymbol{w}_i^*\|^2=\|\boldsymbol{w}_i\|^2-\tfrac{(\boldsymbol{w}_i\boldsymbol{B}_l)^2+(\boldsymbol{w}_i\check{\boldsymbol{B}}_l)^2}{\|\boldsymbol{B}_l\|^2},\\&\|\hat{\boldsymbol{w}}_i\|^2=\|\boldsymbol{w}_i\|^2-\tfrac{(\boldsymbol{w}_i\boldsymbol{B}_l)^2+(\boldsymbol{w}_i\check{\boldsymbol{B}}_l)^2}{\|\boldsymbol{B}_l\|^2}+\tfrac{(\boldsymbol{w}_i\boldsymbol{B}_l)^2+(\boldsymbol{w}_i\check{\boldsymbol{B}}_l)^2}{\|\boldsymbol{B}_l\|^4},\\&\hat{\boldsymbol{w}}_i=\begin{bmatrix}\lambda_{i1}\boldsymbol{w}_1+...+\lambda_{im}\boldsymbol{w}_m\\w_{li}^{'}\end{bmatrix}, \text{for } i,j\in g_l.\end{aligned} \tag{6.10}$$

Then, we can derive the total power reduction of this UAV group

$$\triangle P_{g_l}=\sum^{i\in g_l}\frac{(\boldsymbol{w}_i\boldsymbol{B}_l)^2+(\boldsymbol{w}_i\check{\boldsymbol{B}}_l)^2}{\|\boldsymbol{B}_l\|^2}p_i, \tag{6.11}$$

which will be used to formulate the utility function of each MU later. Note that without NOMA clustering, the transmission power can be reduced by increasing the number of antennas, so that the best UAV group should include all MUs. However, according to our conclusion in Fig. 6.2, UAV-MIMO may not always be better than MIMO-NOMA, so that grouping all MUs into UAV groups may not reduce the total power consumption.

If a single MU served by two UAVs (e.g., UAVs l and n) simultaneously, and their group of MUs are $g_l=\{1,2,...,i\}$ and $g_n=\{i,i+1,...,m\}$ respectively, similar to (6.5),

we have

$$\begin{aligned}
&\left[\boldsymbol{h}_i^T, h_{li}^{'}, h_{ni}^{'}\right]\begin{bmatrix} \boldsymbol{w}_i - w_{li}^{'}\boldsymbol{B}_l - w_{ni}^{'}\boldsymbol{B}_n \\ w_{li}^{'} \\ w_{ni}^{'} \end{bmatrix} = 1, \\
&\left[\boldsymbol{h}_j^T, h_{lj}^{'}\right]\begin{bmatrix} \boldsymbol{w}_i - w_{li}^{'}\boldsymbol{B}_l - w_{ni}^{'}\boldsymbol{B}_n \\ w_{li}^{'}(\text{ or } w_{ni}^{'}) \end{bmatrix} = 0, \text{for } j \neq i, j \in g_l(\text{ or } g_n),
\end{aligned}$$

where $\boldsymbol{B}_l = \sum_{k=1}^{i} h_{lk}^{'}\boldsymbol{w}_k$ and $\boldsymbol{B}_n = \sum_{k'=i}^{m} h_{lk'}^{'}\boldsymbol{w}_{k'}$. Following the similar procedure, we can derive

$$\boldsymbol{w}_i^* = \boldsymbol{w}_i - w_{li}^{'}\boldsymbol{B}_l - w_{ni}^{'}\boldsymbol{B}_n, \tag{6.12}$$

and the power reduction of MU i is changed to be

$$\triangle P_i = (\|\boldsymbol{w}_i\|^2 - \left\|\boldsymbol{w}_i - w_{li}^{'}\boldsymbol{B}_l - w_{ni}^{'}\boldsymbol{B}_n\right\|^2)p_i. \tag{6.13}$$

This calculation can be extended to general cases when MUs are served by more UAVs.

6.3.3 MIMO-NOMA beamforming

MIMO-NOMA clustering aims to minimize power consumption, which derivation process is similar to our previous work in in Chapter 3. Differently, we consider each MU has different data rate requirement. For a 2-MU NOMA cluster (e.g., $\mathcal{G}_{c_1} = \{1, 2\}$), the closed-form solutions to the MIMO-NOMA beamforming can be calculated as

$$\begin{aligned}
&\xi_{21} = -\frac{\boldsymbol{w}_2\boldsymbol{w}_1}{\|\boldsymbol{w}_1\|^2}, \xi_{12} = \frac{-\boldsymbol{w}_1\boldsymbol{w}_2}{\|\boldsymbol{w}_1\|^2 + \left\|\boldsymbol{w}_2^{\aleph}\right\|^2\delta_2} = \frac{-\|\boldsymbol{w}_1\|^2\boldsymbol{w}_1\boldsymbol{w}_2}{\|\boldsymbol{w}_1\|^2\|\boldsymbol{w}_2\|^2(1+\delta_2) - \delta_2|\boldsymbol{w}_1\boldsymbol{w}_2|^2}, \\
&\boldsymbol{w}_1^{\aleph} = \boldsymbol{w}_1 + \xi_{12}\boldsymbol{w}_2, \boldsymbol{w}_2^{\aleph} = \xi_{21}\boldsymbol{w}_1 + \boldsymbol{w}_2,
\end{aligned} \tag{6.14}$$

and the power reduction of this cluster after clustering can be computed as

$$\triangle P_{\mathcal{G}_{c_1}} = (\delta_1 In_1|\xi_{12}| + \delta_2 In_2|\xi_{21}|)|\boldsymbol{w}_1\boldsymbol{w}_2|.$$

For a 3-MU NOMA cluster (e.g., $\mathcal{G}_{c_2}=\{1,2,3\}$), the closed-form solutions are

$$\begin{aligned}
&\xi_{31}=\tfrac{\boldsymbol{w}_2\boldsymbol{w}_3\boldsymbol{w}_1\boldsymbol{w}_2-\boldsymbol{w}_1\boldsymbol{w}_3\|\boldsymbol{w}_2\|^2}{\|\boldsymbol{w}_2\|^2\|\boldsymbol{w}_1\|^2-|\boldsymbol{w}_1\boldsymbol{w}_2|^2}, \xi_{32}=\tfrac{\boldsymbol{w}_1\boldsymbol{w}_3\boldsymbol{w}_1\boldsymbol{w}_2-\boldsymbol{w}_2\boldsymbol{w}_3\|\boldsymbol{w}_1\|^2}{\|\boldsymbol{w}_2\|^2\|\boldsymbol{w}_1\|^2-|\boldsymbol{w}_1\boldsymbol{w}_2|^2},\\
&\xi_{21}=\tfrac{\boldsymbol{w}_1\boldsymbol{w}_2(\|\boldsymbol{w}_3\|^2+\left\|\boldsymbol{w}_3^{\aleph}\right\|^2\delta_3)-\boldsymbol{w}_1\boldsymbol{w}_3\boldsymbol{w}_2\boldsymbol{w}_3}{|\boldsymbol{w}_1\boldsymbol{w}_3|^2-\|\boldsymbol{w}_1\|^2(\|\boldsymbol{w}_3\|^2+\left\|\boldsymbol{w}_3^{\aleph}\right\|^2\delta_3)},\\
&\xi_{23}=\tfrac{\|\boldsymbol{w}_1\|^2\boldsymbol{w}_2\boldsymbol{w}_3-\boldsymbol{w}_1\boldsymbol{w}_2\boldsymbol{w}_1\boldsymbol{w}_3}{|\boldsymbol{w}_1\boldsymbol{w}_3|^2-\|\boldsymbol{w}_1\|^2(\|\boldsymbol{w}_3\|^2+\left\|\boldsymbol{w}_3^{\aleph}\right\|^2\delta_3)}, \xi_{12}=\tfrac{\boldsymbol{w}_1\boldsymbol{w}_2(\|\boldsymbol{w}_3\|^2+\mu)-\boldsymbol{w}_1\boldsymbol{w}_3\boldsymbol{w}_2\boldsymbol{w}_3}{|\boldsymbol{w}_2\boldsymbol{w}_3|^2-(\|\boldsymbol{w}_2\|^2+\alpha)(\|\boldsymbol{w}_3\|^2+\mu)},\\
&\xi_{13}=\tfrac{\boldsymbol{w}_1\boldsymbol{w}_3(\|\boldsymbol{w}_2\|^2+\alpha)-\boldsymbol{w}_1\boldsymbol{w}_2\boldsymbol{w}_2\boldsymbol{w}_3}{|\boldsymbol{w}_2\boldsymbol{w}_3|^2-(\|\boldsymbol{w}_2\|^2+\alpha)(\|\boldsymbol{w}_3\|^2+\mu)}, \alpha=\left\|\boldsymbol{w}_2^{\aleph}\right\|^2\delta_2+\xi_{23}^2\left\|\boldsymbol{w}_3^{\aleph}\right\|^2\delta_2\delta_3, \mu=\left\|\boldsymbol{w}_3^{\aleph}\right\|^2\delta_3, \qquad (6.15)\\
&\boldsymbol{w}_3^{\aleph}=\xi_{31}\boldsymbol{w}_1+\xi_{32}\boldsymbol{w}_2+\boldsymbol{w}_3, \boldsymbol{w}_2^{\aleph}=\xi_{21}\boldsymbol{w}_1+\boldsymbol{w}_2+\xi_{23}\boldsymbol{w}_3, \boldsymbol{w}_1^{\aleph}=\boldsymbol{w}_1+\xi_{12}\boldsymbol{w}_2+\xi_{13}\boldsymbol{w}_3,\\
&\triangle P_{\mathcal{G}_{c_2}}=\delta_3 In_3(|\xi_{31}||\boldsymbol{w}_1\boldsymbol{w}_3|+|\xi_{32}||\boldsymbol{w}_2\boldsymbol{w}_3|)+\delta_2 In_2(|\xi_{21}||\boldsymbol{w}_1\boldsymbol{w}_2|+|\xi_{23}||\boldsymbol{w}_2\boldsymbol{w}_3|)+\\
&\delta_1 In_1(|\xi_{12}||\boldsymbol{w}_1\boldsymbol{w}_2|+|\xi_{13}||\boldsymbol{w}_1\boldsymbol{w}_3|).
\end{aligned}$$

The MU's decoding order and successful SIC decoding conditions are discussed in Appendixes C.3 and C.4, respectively.

6.4 UAV Deployment

We consider a joint approach to calculate UAV-NOMA beamformings. Then, the calculated beamforming will be used in UAV deployment.

6.4.1 UAV-NOMA

Let MUs from 1 to m be served by the BS with UAV l associated, and the first n MUs form a n-MU NOMA cluster (i.e., $\mathcal{G}_{c_1}=\{1,...,n\}$). Obviously, beamforming coefficients for MUs from $n+1$ to m can be derived by (6.11). For MU $i\in\mathcal{G}_{c_1}$, its beamforming vector is calculated by $\boldsymbol{w}_i^{\aleph}=\lambda_{i1}\boldsymbol{w}_1+...+\lambda_{im}\boldsymbol{w}_m$ (similar to (6.14) and (6.15)) and should

satisfy

$$\left[\boldsymbol{h}_i^T, h_{li}^{'}\right]\begin{bmatrix}\lambda_{i1}\boldsymbol{w}_1+...+\lambda_{im}\boldsymbol{w}_m\\ w_{li}^{'}\end{bmatrix}=1,$$

$$\left[\boldsymbol{h}_j^T, h_{lj}^{'}\right]\begin{bmatrix}\lambda_{i1}\boldsymbol{w}_1+...+\lambda_{im}\boldsymbol{w}_m\\ w_{li}^{'}\end{bmatrix}=\begin{cases}\xi_{ij}, & \text{if } j\neq i \text{ and } j\in\{1,..,n\},\\ 0, & \text{if } j\neq i \text{ and } j\in\{n+1,..,m\},\end{cases}$$

where ξ_{ij} is MIMO-NOMA power coefficient. Therefore, we can obtain

$$\lambda_{i1}=\xi_{i1}-h_{l1}^{'}w_{li}^{'},...,\lambda_{ii}=1-h_{li}^{'}w_{li}^{'},...,\lambda_{in+1}=-h_{ln+1}^{'}w_{li}^{'}.... \tag{6.16}$$

The superposed signal for $\mathcal{G}_{c_1}$ can be written as

$$\boldsymbol{s}_{c_1}=\hat{\boldsymbol{w}}_1^{\aleph}\sqrt{p_1}x_1+...+\hat{\boldsymbol{w}}_n^{\aleph}\sqrt{p_n}x_n. \tag{6.17}$$

After decoding the superposed message, the received signal at MU i can be represented as

$$y_i=\hat{\boldsymbol{h}}_i^H\boldsymbol{s}_k+I_i+\nu_i=\begin{cases}\hat{\boldsymbol{h}}_i^H\hat{\boldsymbol{w}}_i^{\aleph}\sqrt{p_i}x_i+I_i+\nu_i, & \text{if } i=1,\\ \hat{\boldsymbol{h}}_i^H\hat{\boldsymbol{w}}_i^{\aleph}\sqrt{p_i}x_i+\sum_{j=1}^{i-1}\hat{\boldsymbol{h}}_i^H\hat{\boldsymbol{w}}_j^{\aleph}\sqrt{p_j}x_j+I_i+\nu_i, & \text{otherwise.}\end{cases} \tag{6.18}$$

To satisfy the SINR requirement, the power consumption for MU i can be derived by

$$P_i=\left\|\boldsymbol{w}_i^{\aleph}\right\|^2p_i=\begin{cases}\left\|\boldsymbol{w}_i^{\aleph}\right\|^2(I_i+\sigma^2)\delta_i, & \text{if } i=1,\\ \left\|\boldsymbol{w}_i^{\aleph}\right\|^2(\sum_{j=1}^{i-1}\left|\hat{\boldsymbol{h}}_i^H\hat{\boldsymbol{w}}_j^{\aleph}\right|^2p_j+I_i+\sigma^2)\delta_i, & \text{otherwise.}\end{cases} \tag{6.19}$$

Our objective is to minimize the cluster power consumption through optimizing ξ_{ij} and $w_{li}^{'}$, $i,j\in\{1,2,...n\}$, i.e.,

$$\min_{\{\xi_{11},...,\xi_{nn}\}\{w_{l1}^{'},...,w_{ln}^{'}\}}P_1+...+P_n=f(\xi_{11},...,\xi_{nn},w_{l1}^{'},...,w_{ln}^{'}). \tag{6.20}$$

Note that since this problem can be decoupled by the order from MU n to MU 1, we employ a recursive approach to solve it. Specifically, the first subproblem for MU n is

$$\min f(\xi_{n1},...,\xi_{nn-1},w_{ln}^{'})=\left\|\boldsymbol{w}_n^{\aleph}\right\|^2=\left\|(\xi_{n1}\boldsymbol{w}_1+...+\boldsymbol{w}_n)-w_{ln}^{'}\boldsymbol{B}_l\right\|^2, \tag{6.21}$$

where $\boldsymbol{B}_l = h_{l1}^{'}\boldsymbol{w}_1 + ... + h_{lm}^{'}\boldsymbol{w}_m$. Since $w_{ln}^{'}$ may be a complex value, we let $w_{ln}^{'} = a+bi$, and (6.21) can be further rewritten as

$$\begin{aligned}&\xi_{n1}^2\|\boldsymbol{w}_1\|^2+...+\|\boldsymbol{w}_n\|^2+(a^2+b^2)\|\boldsymbol{B}_l\|^2+2\xi_{n1}\xi_{n2}\boldsymbol{w}_1\boldsymbol{w}_2+...+2\xi_{n1}\boldsymbol{w}_1\boldsymbol{w}_n\\&-2a(\xi_{n1}\boldsymbol{w}_1\boldsymbol{B}_l+...+\xi_{nn}\boldsymbol{w}_n\boldsymbol{B}_l)+2b(\xi_{n1}\boldsymbol{w}_1\check{\boldsymbol{B}}_l+...+\xi_{nn}\boldsymbol{w}_n\check{\boldsymbol{B}}_l).\end{aligned} \tag{6.22}$$

By letting the 1st-order derivative of $f(.)$ be zero, we can obtain

$$\begin{aligned}&[\xi_{n1},\xi_{n2},...,\xi_{nn-1}]=\boldsymbol{E}\boldsymbol{A}^{-1}, w_{ln}^{'}=\tfrac{(\boldsymbol{C}[\xi_{n1},\xi_{n2},...,\xi_{nn-1}]^H+\boldsymbol{w}_n\boldsymbol{B}_l)-(\boldsymbol{D}[\xi_{n1},\xi_{n2},...,\xi_{nn-1}]^H+\boldsymbol{w}_n\check{\boldsymbol{B}}_l)i}{\|\boldsymbol{B}_l\|^2},\\&\boldsymbol{E}=-[\boldsymbol{w}_1\boldsymbol{w}_n,\boldsymbol{w}_2\boldsymbol{w}_n,...,\boldsymbol{w}_{n-1}\boldsymbol{w}_n]+\tfrac{(\boldsymbol{w}_n\boldsymbol{B}_l)\boldsymbol{C}+(\boldsymbol{w}_n\check{\boldsymbol{B}}_l)\boldsymbol{D}}{\|\boldsymbol{B}_l\|^2}, \boldsymbol{C}=[\boldsymbol{w}_1\boldsymbol{B}_l,...,\boldsymbol{w}_{n-1}\boldsymbol{B}_l],\\&\boldsymbol{D}=[\boldsymbol{w}_1\check{\boldsymbol{B}}_l,...,\boldsymbol{w}_{n-1}\check{\boldsymbol{B}}_l],\\&\boldsymbol{A}=\begin{bmatrix}\|\boldsymbol{w}_1\|^2 & \boldsymbol{w}_1\boldsymbol{w}_2 & ... & \boldsymbol{w}_1\boldsymbol{w}_{n-1}\\ \vdots & \vdots & & \vdots\\ \boldsymbol{w}_{n-1}\boldsymbol{w}_1 & \boldsymbol{w}_{n-1}\boldsymbol{w}_2 & ... & \|\boldsymbol{w}_{n-1}\|^2\end{bmatrix}-\tfrac{\boldsymbol{C}^T\boldsymbol{C}+\boldsymbol{D}^T\boldsymbol{D}}{\|\boldsymbol{B}_l\|^2}.\end{aligned} \tag{6.23}$$

Substituting (6.23) into (6.20), we can formulate the second subproblem for MU $n-1$ based on the fact that $p_{ln-1} > 0$ as

$$\begin{aligned}&\min f(\xi_{n-11},...,\xi_{n-1n-1},w_{ln-1}^{'}) = \left\|\boldsymbol{w}_{n-1}^{\aleph}\right\|^2+\left\|\boldsymbol{w}_n^{\aleph}\right\|^2\xi_{n-1n}^2\delta_n\\&=\left\|(\xi_{n-11}\boldsymbol{w}_1+...+\boldsymbol{w}_{n-1}+\xi_{n-1n}\boldsymbol{w}_n)-w_{ln-1}^{'}\boldsymbol{B}_l\right\|^2+\left\|\boldsymbol{w}_n^{\aleph}\right\|^2\xi_{n-1n}^2\delta_n.\end{aligned}$$

We can follow this procedure until all ξ_{ij} and $w_{li}^{'}$, $i,j\in\{1,2,...n\}$ are obtained.

For $\mathcal{G}_{c_1}=\{1,2\}$, we have

$$\begin{aligned}&A=\|\boldsymbol{w}_1\|^2-\tfrac{(\boldsymbol{w}_1\boldsymbol{B}_l)^2+(\boldsymbol{w}_1\check{\boldsymbol{B}}_l)^2}{\|\boldsymbol{B}_l\|^2}, E=-\boldsymbol{w}_1\boldsymbol{w}_2+\tfrac{(\boldsymbol{w}_1\boldsymbol{B}_l)(\boldsymbol{w}_2\boldsymbol{B}_l)+(\boldsymbol{w}_1\check{\boldsymbol{B}}_l)(\boldsymbol{w}_2\check{\boldsymbol{B}}_l)}{\|\boldsymbol{B}_l\|^2},\\&F=(\|\boldsymbol{w}_2\|^2+\left\|\boldsymbol{w}_2^{\aleph}\right\|^2\delta_2)-\tfrac{(\boldsymbol{w}_2\boldsymbol{B}_l)^2+(\boldsymbol{w}_2\check{\boldsymbol{B}}_l)^2}{\|\boldsymbol{B}_l\|^2}, \xi_{21}=EA^{-1},\\&w_{l2}^{'}=\tfrac{(\boldsymbol{w}_1\boldsymbol{B}_l\xi_{21}+\boldsymbol{w}_2\boldsymbol{B}_l)-(\boldsymbol{w}_1\check{\boldsymbol{B}}_l\xi_{21}+\boldsymbol{w}_2\check{\boldsymbol{B}}_l)i}{\|\boldsymbol{w}_1\|^2}, \xi_{12}=EF^{-1}, w_{l1}^{'}=\tfrac{(\boldsymbol{w}_2\boldsymbol{B}_l\xi_{12}+\boldsymbol{w}_1\boldsymbol{B}_l)-(\boldsymbol{w}_2\check{\boldsymbol{B}}_l\xi_{12}+\boldsymbol{w}_1\check{\boldsymbol{B}}_l)i}{\|\boldsymbol{w}_1\|^2}.\end{aligned}$$

The power reduction of this cluster is

$$\triangle P_{\mathcal{G}_{c_1}} = (\delta_1 In_1|\xi_{12}|+\delta_2 In_2|\xi_{21}|)\left|\boldsymbol{w}_1\boldsymbol{w}_2-\tfrac{(\boldsymbol{w}_1\boldsymbol{B}_l)(\boldsymbol{w}_2\boldsymbol{B}_l)+(\boldsymbol{w}_1\check{\boldsymbol{B}}_l)(\boldsymbol{w}_2\check{\boldsymbol{B}}_l)}{\|\boldsymbol{B}_l\|^2}\right|. \tag{6.24}$$

For $\mathcal{G}_{c_1} = \{1, 2, 3\}$, the derived closed-form solutions are

$$
\begin{aligned}
&[\xi_{31}, \xi_{32}] = \boldsymbol{E}\boldsymbol{A}^{-1}, w_{l3}^{'} = \tfrac{(\boldsymbol{w}_1\boldsymbol{B}_l\xi_{31}+\boldsymbol{w}_2\boldsymbol{B}_l\xi_{32}+\boldsymbol{w}_3\boldsymbol{B}_l)-(\boldsymbol{w}_1\check{\boldsymbol{B}}_l\xi_{31}+\boldsymbol{w}_2\check{\boldsymbol{B}}_l\xi_{32}+\boldsymbol{w}_3\check{\boldsymbol{B}}_l)i}{\|\boldsymbol{w}_1\|^2}, \\
&\text{where } \boldsymbol{E} = -[\boldsymbol{w}_1\boldsymbol{w}_3 - \tfrac{(\boldsymbol{w}_1\boldsymbol{B}_l)(\boldsymbol{w}_3\boldsymbol{B}_l)+(\boldsymbol{w}_1\check{\boldsymbol{B}}_l)(\boldsymbol{w}_3\check{\boldsymbol{B}}_l)}{\|\boldsymbol{B}_l\|^2}, \boldsymbol{w}_2\boldsymbol{w}_3 - \tfrac{(\boldsymbol{w}_2\boldsymbol{B}_l)(\boldsymbol{w}_3\boldsymbol{B}_l)+(\boldsymbol{w}_2\check{\boldsymbol{B}}_l)(\boldsymbol{w}_3\check{\boldsymbol{B}}_l)}{\|\boldsymbol{B}_l\|^2}], \\
&\boldsymbol{C} = [\boldsymbol{w}_1\boldsymbol{B}_l, \boldsymbol{w}_2\boldsymbol{B}_l], \boldsymbol{D} = [\boldsymbol{w}_1\check{\boldsymbol{B}}_l, \boldsymbol{w}_2\check{\boldsymbol{B}}_l], \\
&\boldsymbol{A} = \begin{bmatrix} \|\boldsymbol{w}_1\|^2 - \tfrac{(\boldsymbol{w}_1\boldsymbol{B}_l)^2+(\boldsymbol{w}_1\check{\boldsymbol{B}}_l)^2}{\|\boldsymbol{B}_l\|^2} & \boldsymbol{w}_1\boldsymbol{w}_2 - \tfrac{(\boldsymbol{w}_1\boldsymbol{B}_l)(\boldsymbol{w}_2\boldsymbol{B}_l)+(\boldsymbol{w}_1\check{\boldsymbol{B}}_l)(\boldsymbol{w}_2\check{\boldsymbol{B}}_l)}{\|\boldsymbol{B}_l\|^2} \\ \boldsymbol{w}_1\boldsymbol{w}_2 - \tfrac{(\boldsymbol{w}_1\boldsymbol{B}_l)(\boldsymbol{w}_2\boldsymbol{B}_l)+(\boldsymbol{w}_1\check{\boldsymbol{B}}_l)(\boldsymbol{w}_2\check{\boldsymbol{B}}_l)}{\|\boldsymbol{B}_l\|^2} & \|\boldsymbol{w}_2\|^2 - \tfrac{(\boldsymbol{w}_2\boldsymbol{B}_l)^2+(\boldsymbol{w}_2\check{\boldsymbol{B}}_l)^2}{\|\boldsymbol{B}_l\|^2} \end{bmatrix}.
\end{aligned} \tag{6.25}
$$

$$
\begin{aligned}
&[\xi_{21}, \xi_{23}] = \boldsymbol{E}\boldsymbol{A}^{-1}, w_{l2}^{'} = \tfrac{(\boldsymbol{w}_1\boldsymbol{B}_l\xi_{21}+\boldsymbol{w}_3\boldsymbol{B}_l\xi_{23}+\boldsymbol{w}_2\boldsymbol{B}_l)-(\boldsymbol{w}_1\check{\boldsymbol{B}}_l\xi_{21}+\boldsymbol{w}_3\check{\boldsymbol{B}}_l\xi_{23}+\boldsymbol{w}_2\check{\boldsymbol{B}}_l)i}{\|\boldsymbol{w}_1\|^2}, \\
&\text{where } \boldsymbol{E} = -[\boldsymbol{w}_1\boldsymbol{w}_2 - \tfrac{(\boldsymbol{w}_1\boldsymbol{B}_l)(\boldsymbol{w}_2\boldsymbol{B}_l)+(\boldsymbol{w}_1\check{\boldsymbol{B}}_l)(\boldsymbol{w}_2\check{\boldsymbol{B}}_l)}{\|\boldsymbol{B}_l\|^2}, \boldsymbol{w}_2\boldsymbol{w}_3 - \tfrac{(\boldsymbol{w}_2\boldsymbol{B}_l)(\boldsymbol{w}_3\boldsymbol{B}_l)+(\boldsymbol{w}_2\check{\boldsymbol{B}}_l)(\boldsymbol{w}_3\check{\boldsymbol{B}}_l)}{\|\boldsymbol{B}_l\|^2}], \\
&\boldsymbol{C} = [\boldsymbol{w}_1\boldsymbol{B}_l, \boldsymbol{w}_3\boldsymbol{B}_l], \boldsymbol{D} = [\boldsymbol{w}_1\check{\boldsymbol{B}}_l, \boldsymbol{w}_3\check{\boldsymbol{B}}_l], \\
&\boldsymbol{A} = \begin{bmatrix} \|\boldsymbol{w}_1\|^2 - \tfrac{(\boldsymbol{w}_1\boldsymbol{B}_l)^2+(\boldsymbol{w}_1\check{\boldsymbol{B}}_l)^2}{\|\boldsymbol{B}_l\|^2} & \boldsymbol{w}_1\boldsymbol{w}_3 - \tfrac{(\boldsymbol{w}_1\boldsymbol{B}_l)(\boldsymbol{w}_3\boldsymbol{B}_l)+(\boldsymbol{w}_1\check{\boldsymbol{B}}_l)(\boldsymbol{w}_3\check{\boldsymbol{B}}_l)}{\|\boldsymbol{B}_l\|^2} \\ \boldsymbol{w}_1\boldsymbol{w}_3 - \tfrac{(\boldsymbol{w}_1\boldsymbol{B}_l)(\boldsymbol{w}_3\boldsymbol{B}_l)+(\boldsymbol{w}_1\check{\boldsymbol{B}}_l)(\boldsymbol{w}_3\check{\boldsymbol{B}}_l)}{\|\boldsymbol{B}_l\|^2} & \|\boldsymbol{w}_3\|^2 + \left\|\boldsymbol{w}_3^{\aleph}\right\|^2\delta_3 - \tfrac{(\boldsymbol{w}_3\boldsymbol{B}_l)^2+(\boldsymbol{w}_3\check{\boldsymbol{B}}_l)^2}{\|\boldsymbol{B}_l\|^2} \end{bmatrix}.
\end{aligned} \tag{6.26}
$$

$$
\begin{aligned}
&[\xi_{12}, \xi_{13}] = \boldsymbol{E}\boldsymbol{A}^{-1}, w_{l1}^{'} = \tfrac{(\boldsymbol{w}_2\boldsymbol{B}_l\xi_{12}+\boldsymbol{w}_3\boldsymbol{B}_l\xi_{13}+\boldsymbol{w}_1\boldsymbol{B}_l)-(\boldsymbol{w}_2\check{\boldsymbol{B}}_l\xi_{12}+\boldsymbol{w}_3\check{\boldsymbol{B}}_l\xi_{13}+\boldsymbol{w}_1\check{\boldsymbol{B}}_l)i}{\|\boldsymbol{w}_1\|^2}, \\
&\text{where } \boldsymbol{E} = -[\boldsymbol{w}_1\boldsymbol{w}_2 - \tfrac{(\boldsymbol{w}_1\boldsymbol{B}_l)(\boldsymbol{w}_2\boldsymbol{B}_l)+(\boldsymbol{w}_1\check{\boldsymbol{B}}_l)(\boldsymbol{w}_2\check{\boldsymbol{B}}_l)}{\|\boldsymbol{B}_l\|^2}, \boldsymbol{w}_1\boldsymbol{w}_3 - \tfrac{(\boldsymbol{w}_1\boldsymbol{B}_l)(\boldsymbol{w}_3\boldsymbol{B}_l)+(\boldsymbol{w}_1\check{\boldsymbol{B}}_l)(\boldsymbol{w}_3\check{\boldsymbol{B}}_l)}{\|\boldsymbol{B}_l\|^2}], \\
&\boldsymbol{C} = [\boldsymbol{w}_2\boldsymbol{B}_l, \boldsymbol{w}_3\boldsymbol{B}_l], \boldsymbol{D} = [\boldsymbol{w}_2\check{\boldsymbol{B}}_l, \boldsymbol{w}_3\check{\boldsymbol{B}}_l], \\
&\boldsymbol{A}= \\
&\begin{bmatrix} \|\boldsymbol{w}_2\|^2+\left\|\boldsymbol{w}_2^{\aleph}\right\|^2\delta_2+\xi_{32}^2\left\|\boldsymbol{w}_3^{\aleph}\right\|^2\delta_3\delta_2-\tfrac{(\boldsymbol{w}_2\boldsymbol{B}_l)^2+(\boldsymbol{w}_2\check{\boldsymbol{B}}_l)^2}{\|\boldsymbol{B}_l\|^2} & \boldsymbol{w}_2\boldsymbol{w}_3-\tfrac{(\boldsymbol{w}_2\boldsymbol{B}_l)(\boldsymbol{w}_3\boldsymbol{B}_l)+(\boldsymbol{w}_2\check{\boldsymbol{B}}_l)(\boldsymbol{w}_3\check{\boldsymbol{B}}_l)}{\|\boldsymbol{B}_l\|^2} \\ \boldsymbol{w}_2\boldsymbol{w}_3-\tfrac{(\boldsymbol{w}_2\boldsymbol{B}_l)(\boldsymbol{w}_3\boldsymbol{B}_l)+(\boldsymbol{w}_2\check{\boldsymbol{B}}_l)(\boldsymbol{w}_3\check{\boldsymbol{B}}_l)}{\|\boldsymbol{B}_l\|^2} & \|\boldsymbol{w}_3\|^2+\left\|\boldsymbol{w}_3^{\aleph}\right\|^2\delta_3-\tfrac{(\boldsymbol{w}_3\boldsymbol{B}_l)^2+(\boldsymbol{w}_3\check{\boldsymbol{B}}_l)^2}{\|\boldsymbol{B}_l\|^2} \end{bmatrix}.
\end{aligned} \tag{6.27}
$$

Then, the power reduction of this cluster can be calculated as

$$
\triangle P_{\mathcal{G}_{c_2}} = \sum_{i=1}^{3}\sum_{j=2,j\neq i}^{3}(\delta_i In_i|\xi_{ij}| + \delta_j In_j|\xi_{ji}|)\left|\boldsymbol{w}_i\boldsymbol{w}_j - \tfrac{(\boldsymbol{w}_i\boldsymbol{B}_l)(\boldsymbol{w}_j\boldsymbol{B}_l)+(\boldsymbol{w}_i\check{\boldsymbol{B}}_l)(\boldsymbol{w}_j\check{\boldsymbol{B}}_l)}{\|\boldsymbol{B}_l\|^2}\right|. \tag{6.28}
$$

6.4.2 UAV placement and UAV channel gain estimation

From (6.9) and (6.12), we can find that UAV power consumption for data transmission is determined by channel conditions, i.e., $h_{l1}^{'}, ..., h_{lm}^{'}$, which are closely related to the location

and the height of UAV. Without loss of generality, we denote MU i's ground location by $\boldsymbol{u}_i(t)=[x_i(t), y_i(t)]$, $i \in g_l$. UAV l is assumed to fly at an altitude $H_l(t)$ ($H_l(t) \in [\underline{H}, \overline{H}]$) with horizontal location $\boldsymbol{q}_l(t)=[x^{[l]}(t), y^{[l]}(t)]$. Here, $\underline{H}$ and $\overline{H}$ are the hight limitations in order to ensure the flight safety. Then, the distance from UAV l to MU i can be denoted as

$$d_{li}(t) = \sqrt{H_l^2(t) + \|\boldsymbol{q}_l(t) - \boldsymbol{u}_i(t)\|^2}. \tag{6.29}$$

Following the common assumption as in the literature [33, 39], we let the links between the UAV and MUs be line-of-sight (LoS) (which is named as the air-to-ground (A2G) channel), so that the channel quality is determined by the distance between them. The path loss and fast fading effects are separately denoted as,

$$h'_{li}(t) = \frac{\tilde{h}_{li}(t)}{\sqrt{PL}}, \tilde{h}_{li}(t) = \sqrt{\frac{K}{K+1}} e^{i\phi_{li}} \tilde{h}^{LoS} + \sqrt{\frac{1}{K+1}} \tilde{h}^{NLoS},$$

where $\tilde{h}_{li}(t)$ is the normalized gain of the channel, ϕ_{li} is the phase shift of the signal from UAV l to MU i, PL is the average A2G free space path loss, $\tilde{h}^{LoS}$ and $\tilde{h}^{NLoS}$ are constant terms corresponding to the LoS and the NLoS fading components, respectively. Besides, K is the Rician factor. Since the LoS links between the flying UAV and the ground nodes are assumed to be available with a certain probability, i.e., p^{LoS}, PL can be calculated as

$$PL = p^{LoS} PL^{LoS} + (1 - p^{LoS}) PL^{NLoS}, p^{LoS} = \frac{1}{1+\psi_1 \exp(-\psi_2[\frac{180}{\pi}\theta_{li} - \psi_1])},$$

where θ_{li} is the elevation angle between UAV l to MU i in degree, and ψ_1 and ψ_2 are constant values related to the environment. PL^{LoS} and PL^{NLoS} (in dB) denote the LoS and NLoS free space path losses, and can be represented, respectively, as

$$PL^{LoS} = 10vlog10(\frac{4\pi f d_{li}(t)}{C}) + L_{LoS}, PL^{NLoS} = 10vlog10(\frac{4\pi f d_{li}(t)}{C}) + L_{NLoS},$$

where v is the path loss exponent, f denotes the carrier frequency, C represents the speed of light, and L_{LoS} and L_{NLoS} are the average additional losses to the free-space propagation losses for the LoS and NLoS links, respectively.

We assume that UAV hovering has a constant power consumption [122] as it depends on air density, drag coefficient, wing area etc. The UAV's objective function to minimize the power consumption of UAV can be formulated as

$$\begin{aligned}&\min w_{l1}^{'2}p_1+w_{l2}^{'2}p_2+...+w_{lm}^{'2}p_m\\&=\sum^{i\in g_l}\frac{(\boldsymbol{w}_i\boldsymbol{B}_l)^2+(\boldsymbol{w}_i\check{\boldsymbol{B}}_l)^2}{\|\boldsymbol{B}_l\|^4}p_i\leq\sum^{i\in g_l}\frac{\|\boldsymbol{w}_i\|^2\|\boldsymbol{B}_l\|^2}{\|\boldsymbol{B}_l\|^4}p_i=\frac{\sum_{i=1}^{m}\|\boldsymbol{w}_i\|^2p_i}{\|\boldsymbol{B}_l\|^2}.\end{aligned}$$

Thus, the original objective function can be simplified as

$$\max\|\boldsymbol{B}_l\|^2=\sum_{i=1}^{m}h_{li}^{'2}\|\boldsymbol{w}_i\|^2+2\sum_{i=1}^{m}\sum_{j=i}^{m}(h_{li}^{'}\boldsymbol{w}_i)(h_{lj}^{'}\boldsymbol{w}_j). \tag{6.30}$$

From (6.30), we can observe that the UAV should be close to a MU with the maximum value of $\|\boldsymbol{w}_i\|^2$. In this work, we consider to place UAV at the top of a certain MU to estimate UAV channel condition without CSI. However, UAV placement depends on not only $\|\boldsymbol{w}_i\|^2$, but also its grouped MUs. Moreover, their SINR requirements are different, which makes the MU with the maximum power consumption may not have maximum $\|\boldsymbol{w}_i\|^2$. Therefore, we design an approach in Tables 4.2 and 4.4 to solve this problem.

If the CSI is unavailable (e.g., long-term contract), we use channel correlation coefficient to estimate UAV channel gains, which is inspired from [83]. For MU $i\in g_l$,

$$h_{li}=\begin{cases}\kappa\frac{\boldsymbol{w}_i\boldsymbol{w}_1}{\|\boldsymbol{w}_i\|\|\boldsymbol{w}_1\|}, \text{ if } \frac{\boldsymbol{w}_i\boldsymbol{w}_1}{\|\boldsymbol{w}_i\|\|\boldsymbol{w}_1\|}>0,\\0, \qquad\qquad\qquad \text{otherwise},\end{cases} \tag{6.31}$$

where κ is a predefined value, which is an average value and can be obtained from simulations.

Moreover, if UAVs are close to each other, interactions between UAVs will be increased. Also, the MU with a large beamforming vector is usually located nearby the cell edge. Thus, we consider the cell edge as the trajectory of UAV, and the movement of it is judged by: i) UAV should close to target MU; ii) the distance between UAVs should be large enough.

6.5 Problem Formulation

We assume that system has L=$\{1, ...l_1, l_2, ...L\}$ UAVs in total, in which UAVs $\{1, ...l_1\}$ are rented by the BS, and UAVs $\{l_2, ...L\}$ are available for renting. The purpose of renting UAV [4] is to increase the benefit of BS through reducing the total BS power consumption. However, since UAV CSI may not be available ahead, the BS signs only one contract at a single time slot. Therefore, this problem can be regarded as finding the UAV $l \in \{l_2, ...L\}$ which can maximize the benefit of BS in an unit time slot $g_2^{[l]}/T$, i.e.,

$$l = \begin{cases} \underset{\boldsymbol{W},\boldsymbol{P},\boldsymbol{X},\boldsymbol{C}}{\arg\max} g_2^{[l]}/T & \text{If } g_2^{[l]} > 0, \\ \emptyset & \text{Otherwise.} \end{cases} \tag{6.32}$$

Here, $\boldsymbol{W}$, $\boldsymbol{P}$, $\boldsymbol{X}$, $\boldsymbol{C}$ denote the strategy set of beamforming [5], power allocation, UAV association and NOAM cluster mapping (for MIMO-NOMA and UAV-NOMA), respectively. The time durations are S or T for different contracts. If $g_2^{[l]} \leq 0$ and $l = \emptyset$, the BS will not rent any UAV at this time slot. Otherwise, the BS will rent UAV l. The benefit of BS is judged by the difference between the price of power reduction and the renting cost, i.e.,

$$g_2^{[l]} = P^{[b]} \sum_{t=1}^{S} (g_0(\boldsymbol{W},\boldsymbol{P},\boldsymbol{X},\boldsymbol{C})^t_{\mathscr{L}=\{1,..l\}} - g_0(\boldsymbol{W'},\boldsymbol{P'},\boldsymbol{X'},\boldsymbol{C'})^t_{\mathscr{L}'=\{1,..l-1\}}) - P^{[s]}. \tag{6.33}$$

Here, $P^{[b]}$ denotes the unit price of power consumption, and $g_0(\boldsymbol{W}, \boldsymbol{P}, \boldsymbol{X}, \boldsymbol{C})^t_{\mathscr{L}=\{1,..l\}}$ indicates the minimal power consumption after resource allocation at time slot t when the BS rents $\mathscr{L}$ UAVs. In order to keep the expression consistency with later proposed approach, we use $g_1(\boldsymbol{W}, \boldsymbol{P}, \boldsymbol{X}, \boldsymbol{C})^t_{\mathscr{L}}$ to replace $g_0(\boldsymbol{W}, \boldsymbol{P}, \boldsymbol{X}, \boldsymbol{C})^t_{\mathscr{L}}$, which indicates the maximum power reduction after resource allocation. The power reduction is evaluated by the difference of power consumptions before and after UAV association. Therefore, the

[4] UAV renting indicates whether the BS rents a UAV or not. UAV association denotes whether a specific MU is served by a specific UAV which is a strategy of the BS on rented UAVs.

[5] For a simplified expression, we employ $\boldsymbol{W}$ to denote a set beamforming vectors for all MUs, under any of 4 transmission modes, so as to $\boldsymbol{P}$, $\boldsymbol{X}$ and $\boldsymbol{C}$.

power consumptions before UAV association for both $g_1(.)^t_{\mathscr{L}}$ and $g_1(.)^t_{\mathscr{L}'}$ are same, so that $g_2^{[l]}$ will not change.

Then, we formulate a power reduction maximization problem to obtain $g_2^{[l]}$ through optimizing system resource allocation in (6.15), which includes MIMO-NOMA clustering, beamforming, power allocation, UAV association and UAV-NOMA clustering. Since $g_1(.)^t$ is formulated for a single time slot, we remove the time variables in the following to keep a simplified expression. $g_1(.)^t$ can be expressed as:

$$\max g_1(\boldsymbol{W},\boldsymbol{P},\boldsymbol{X},\boldsymbol{C})_{\mathscr{L}}=\sum_{i\notin g_{\mathscr{L}},i\in\mathcal{G}}^{N}(\|\boldsymbol{w}_i\|^2-\left\|\boldsymbol{w}_i^{\aleph}\right\|^2(1-x_{li}))p_i+\sum_{l=1}^{\mathscr{L}}\sum_{i\in g_l}(\|\boldsymbol{w}_i\|^2-\|\boldsymbol{w}_i^*\|^2x_{li})p_i, \tag{6.34a}$$

$$\text{s.t.}\sum_{i\in g_l}P_i\leq P_{max} \tag{6.34b}$$

$$x_{li}=1 \text{ or } 0, \text{for all } \ i\in N, l\in L. \tag{6.34c}$$

$$\boldsymbol{h}_i\boldsymbol{w}_j\begin{cases}\neq 0 & \text{If MUs } i \text{ and } j \text{ in the same MIMO-NOMA cluster,}\\ =0 & \text{Otherwise,}\end{cases} \tag{6.34d}$$

$$\hat{\boldsymbol{h}}_i\hat{\boldsymbol{w}}_j\begin{cases}\neq 0 & \text{If MUs } i \text{ and } j \text{ in the same UAV-NOMA cluster,}\\ =0 & \text{Otherwise,}\end{cases} \tag{6.34e}$$

$$\text{SIC decoding condition,} \tag{6.34f}$$

$$c_{i,j}+c_{j,i}\leq 1 \text{ for any MUs } i,j\in N, \tag{6.34g}$$

$$\sum^{i\in\mathcal{G}_l}\frac{(\boldsymbol{w}_i\boldsymbol{B}_l)^2+(\boldsymbol{w}_i\check{\boldsymbol{B}}_l)^2}{\|\boldsymbol{B}_l\|^4}x_{li}\delta_i\sigma^2\leq\overline{P}. \tag{6.34h}$$

Here, $\boldsymbol{w}_i$, $\boldsymbol{w}_i^{\aleph}$, $\boldsymbol{w}_i^*$ and $\hat{\boldsymbol{w}}_j$ indicate beamforming vectors of MU i in MIMO-OMA, MIMO-NOMA, UAV-MIMO/UAV-NOMA from the BS and UAV-MIMO, respectively. P_i is the power consumption of BS for MU i, which is determined by its beamforming vector ($\boldsymbol{w}_i$ or $\boldsymbol{w}_i^*$) and the required transmit power p_i. $\boldsymbol{h}_i$ and $\hat{\boldsymbol{h}}_i$ denote MU i channel gain vectors of MIMO-OMA and UAV-MIMO from the BS respectively. Moreover, $i\in g_l$ means MU i is in UAV group l, $i\in\mathcal{G}_{\cdot}$ indicates MU i is in any NOMA cluster $\mathcal{G}_{\cdot}\in\boldsymbol{C}$, and $i\notin g_{\mathscr{L}}$ denotes MU i is not in any UAV groups. We define a binary decision variable $x_{li}=0$

or 1 to indicate that MU i is served by UAV l or not. Constrain (6.34b) is the power limit of UAV transmissions. Constrain (6.34c) indicates the UAV association. Constrains (6.34d) and (6.34e) are the orthogonal and non-orthogonal conditions of MIMO-NOMA and UAV-NOMA, respectively. In (6.34f), if MUs $i, j \in \{1, 2, ...i, j..., n\}$ in a NOMA cluster $\mathcal{G}_{c_1} = \{1, ..., n\}$, the SIC decoding condition can be expressed by the SINR of MUs satisfying $\gamma_i^j > \gamma_i^{j-1}, ..., > \gamma_i$ (Appendix C.4). Since each MU can form NOMA cluster with any MU or multiple MUs, for simple notations, we name each cluster by the MU in the first of decoding order. For example, if MUs 2, 3, 5 form a NOMA cluster with the decoding order $\{3, 5, 2\}$, this cluster is denoted as $\boldsymbol{c}_3$, and the coefficients in mapping $\boldsymbol{C}$ can be set as $c_{3,3}, c_{3,5}, c_{3,2} = 1$, and $c_{5,3}, c_{2,3} = 0$. If MU 1 is not grouped in any NOMA cluster, we set $c_{1,1:N} = 0$ and $c_{1:N,1} = 0$. Therefore, constrain (6.34g) is to ensure that any MU can not join more than 1 cluster simultaneously.

In summary, UAV selection in (6.32) is based on the solution in (6.33), which is a solution for a long-term duration. Since UAVs are moving randomly, the CSI of the BS and UAVs can not be estimated for future time slots. Thus, we employ the learning approach for the BS benefit estimation in (6.33), and use the solution of (6.34), i.e., the optimal solution in current time slot, as an input.

6.6 System Optimization

The system optimization will start from problem (6.34). We notice that: i) MIMO-NOMA clustering and UAV-NOMA clustering can be solved by coalition games, while UAV grouping should be formulated as a matching game; ii) the closed-form optimal solution of each kind of clustering or association has already been obtained in (6.10) and (6.23)-(6.28). However, UAV-NOMA clustering should be conduct after UAV association association, because NOMA clustering requires CSI to meet SIC decoding conditions. Thus, we decouple this problem into two subproblem and solve them in sequence. In the

first subproblem, we deal with MIMO-NOMA clustering and UAV grouping. We notice that MIMO-NOMA clustering can be integrated with UAV grouping, as CSI from the BS is available. Since MIMO-NOMA is more effective on power reduction than UAV grouping, proceeding MIMO-NOMA clustering before UAV grouping is more advisable, which can shrink the computational complexity. After that, the result from coalition game will be used to design the utility functions of the matching game. Since the UAV association conducts between two type of players, we formulate a two side framework: the MU side and the UAV side, in which both sides can have its' own utility functions, and the strategy of each side is trigged by its utility improvement. In the second subproblem, we conduct the coalition game approach to find the optimal combination of UAV-NOMA clustering.

The steps to solve this problem are listed as follows: In the initial stage, we optimize MIMO-NOMA clustering by exploiting the coalition game approach as proposed in our previous work of Chapter 3. [6] After that, UAVs are added for further reducing total power consumption by our proposed matching game. Note that if any MU in a MIMO-NOMA cluster is selected to be served by UAVs, the formed MIMO-NOMA cluster is automatically split, and this process is irreversible. After MUs join UAV groups, MUs are served by UAV-MIMO, so that we reuse the coalition game to handle the UAV-NOMA clustering.

We propose different matching games for different situations, i.e., single or multiple UAVs, and short-term or long-term contracts. After (6.34) is solved, a learning approach is proposed for (6.33) to estimate the benefit of BS.

6.6.1 Matching approaches for a single UAV

To transform problem (6.34) to be a two side matching game, we defined the utility of MU side to be the power reduction of each player, while the utility of the UAV side to be

[6]For more details of the coalition game approach, please refer to our previous work in Chapter 3, which stability and optimality has been proved. This work focus on our proposed matching game.

the total power reduction of the BS, i.e., the objective in (6.34a). Thus, when the utility of UAV is maximized, the power reduction in (6.34a) is also maximized.

Since MIMO-NOMA is calculated before UAV-MIMO, the player in the MU side (i.e., the MU player) should be either a single MU or a MIMO-NOMA cluster $\mathcal{G}_{c_2}$. If system has only one UAV l is available for renting, the utility of MU player i is denoted as

$$U_{li}^{I} = \begin{cases} \triangle P_{li}, & \text{if select UAV } l, \\ 0, & \text{otherwise}, \end{cases} \tag{6.35}$$

where

$$\triangle P_{li} = \sum^{j \in \mathcal{G}_{c_2}} \frac{(\boldsymbol{w}_j \boldsymbol{B}_l)^2 + (\boldsymbol{w}_j \check{\boldsymbol{B}}_l)^2}{\|\boldsymbol{B}_l\|^2} (I_j + \sigma^2)\delta_j - \triangle P_{\mathcal{G}_{c_2}}.$$

If MU player i is in a MIMO-NOMA cluster $\mathcal{G}_{c_2}$, $\triangle P_{\mathcal{G}_{c_2}} = \sum^{j \in \mathcal{G}_{c_2}} (\|\boldsymbol{w}_j\|^2 - \|\boldsymbol{w}_j^{\aleph}\|^2) p_j$. Otherwise, $j = i$ and $\triangle P_{\mathcal{G}_{c_2}} = 0$. Then, the utility of UAV l can be formulated as

$$U_l^I = \sum^{i \in g_l} \triangle P_{li} + \sum^{c_2 \in \boldsymbol{C}} \triangle P_{\mathcal{G}_{c_2}}. \tag{6.36}$$

In case of the short-term contract with UAV CSI, according to above discussions, UAV placement will not be included into system optimization, and problem (6.34) can be regarded as a many-to-one matching game. Since $\boldsymbol{B}_l$ will be changed as different MUs in g_l, in each iteration of the matching approach, UAV can select one MU or a group of MUs in a MIMO-NOMA cluster. After that, system will update $\boldsymbol{B}_l$, and the rest of MU players will recalculate their utilities. The solution of this game is shown in Table 6.1. The stability and optimality of it will be discussed later.

In case of the long-term contract without UAV's CSI, each MU' location is regarded as a hypothetic UAV position selection. Therefore, we assume in the UAV side, there are N hypothetic UAV position selections which channel gain coefficients can be estimated through (6.31). Since those hypothetic UAV selections are only used to decide the UAV location while not for real UAVs' placement, there is no interactions among them, and the

Table 6.1: Many-to-one matching with UAV's CSI

Initialization:	Calculate power consumption of MIMO-NOMA system and corresponding beamforming vectors (i.e., $\boldsymbol{w}_i^{\aleph}$). Find the MU (such as MU i) with the maximum value of UAV channel gain, and let $\boldsymbol{B}_l = h_{li}\boldsymbol{w}_i$.
Step 1:	Calculate $\triangle P_{li}$ for unselected MUs by (6.35). If $\triangle P_{li} > 0$, it will select this UAV.
Step 2:	UAV select one or a group MUs which can maximize its utility by (6.36). If no one selects, go to **Step 3**. Otherwise, go to **Step 1**.
Step 3:	Conduct UAV-NOMA clustering and get the final solution.

MU players can select many UAVs simultaneously. Therefore, for each MU player i, it will have a UAV set $\boldsymbol{K_i}$ to indicate the selected UAVs, and the utility of it is denoted as

$$U_i^{III} = \sum^{l \in \boldsymbol{K_i}} U_{li}^{I}.$$

The utility of UAV l is still the total power reduction, which is same as in (6.36). We propose a many-to-may matching game (as shown in Table 6.2) to solve this problem.

6.6.2 Matching approaches for multiple UAVs

If the BS has multiple UAV associations, we should consider the interactions among UAVs. In this case, the matching approach in Table 6.1 are not applicable since the utilities between two sides are all effected by those interactions (it will be explained by an example after defining utility functions). Thus, we propose a two-layer matching approach to decouple the interaction between different UAVs, which is inspired by the structure of a Stackelberg game. The short-term contract and the long-term contract have the same utilities at the both sides.

In the MU side, there are L=$\{1, ...l_1, l_2, ...L\}$ UAVs in total, in which UAVs $\{1, ...l_1\}$ are rented by the BS, and UAVs $\{l_2, ...L\}$ are available for renting. In a single time slot, the BS will only rent one UAV from $\{l_2, ...L\}$. For example, if consider l_1, there will exist $2^{|l_1|+1}$ possible combinations for UAV association. For stability, the power reduction of

Table 6.2: Many-to-many matching without UAV's CSI

Initialization:	Calculate power consumption of MIMO-NOMA system and corresponding beamforming vectors (i.e., $\boldsymbol{w}_i^{\aleph}$). In the UAV side, let $i \in N$ hypothetic UAV selection has group $G_i = \{i\}$ with power reduction $\triangle P_i = 0$, and estimate UAV channel gain coefficients by (6.35). Let $\boldsymbol{B}_i = \kappa \boldsymbol{w}_i$.
Step 1:	In the MU side, such as MU j, if $\|\boldsymbol{w}_j\|^2 < \|\boldsymbol{w}_i\|^2$ and $i \neq j$, calculate the power reduction of this selection, i.e., $\triangle P_{ij}$. If $\triangle P_{ij} > 0$, MU j selects the UAV player i.
Step 2:	In the UAV side, each UAV player will select one or a group MUs which can maximize its utility U_i^I by (6.36). If no one selects, go to **Step 3**. Otherwise, update $\boldsymbol{B}_i$ and G_i, and go to **Step 1**.
Step 3:	Conduct UAV-NOMA clustering and select the group with a maximum U_i. If $U_i^I = 0$, the long-term contract is not considered. Otherwise, outcome the UAV selection for this contract.

Table 6.3: Two-layer matching with UAV's CSI

Initialization:	Calculate power consumption of MIMO-NOMA system and corresponding beamforming vectors (i.e., $\boldsymbol{w}_i^{\aleph}$). In the UAV side, for all UAVs, find the MU (such as MU i) with the maximum value of UAV channel gain, and let $\boldsymbol{B}_l = h_{li}\boldsymbol{w}_i$, $G_l = \{k\}$. The iteration is start from $l = l_1$.
Step 1:	If $l = l_1$, the UAV players in the UAV side are $\{1, ..., l_1\}$. Otherwise, the UAV players are $\{1, ..., l_1, l\}$, where l indicates the BS renting UAV l.
Step 2:	Calculate $U_{\boldsymbol{K_i}}^{II} = \triangle P_i^{[1]}$ for each MU player by (6.37). If $U_{\boldsymbol{K_i}}^{II}$ is increased, MU i will select the corresponding UAVs. If $length(\boldsymbol{K_i}) > 1$, it will generate a UAV leader in the up layer. The leader is responsible for the utility adjustment to ensure an increasing tendency of the utilities on each selected UAV. If no one will change its selections, go to **Step 5**.
Step 3:	In the UAV side, the UAV player will select one or a group MUs which can maximize its utility.
Step 4:	Check the utilities of the leaders in the upper layer. If utilities in both sides are changed, adjust their utilities. After that, update $\boldsymbol{B}_i$ and G_i, and go to **Step 2**. If no MU player is selected by any UAV, go to **Step 5**.
Step 5:	Conduct UAV-NOMA clustering and get the power reduction of iteration l. If $l \neq L$, $l = l + 1$ and go to **Step 1**.
Outcome	The final solution will be the one with a maximum power reduction, and the BS will sign a short-term contract with the corresponding UAV in this iteration. If $l = l_1$, no contract will be signed.

Table 6.4: Two-layer matching without UAV CSI

Initialization:	Calculate power consumption of MIMO-NOMA system and corresponding beamforming vectors (i.e., $\boldsymbol{w}_i^{\aleph}$). In the UAV side, find the MU (such as MU k) with the maximum value of UAV channel gain, and let $\boldsymbol{B}_l = h_{lk}\boldsymbol{w}_k$ and $G_l = \{k\}$. Let the rest of MU $i \notin G_l$ to be a hypothetic UAV selection, which is ranged by an order of $\{l_1$+1,l_1+2,...,$N\}$. For each selection, it has G_i=$\{i\}$ with power reduction $\triangle P_i = 0$, and the estimated UAV channel gain coefficients are derived by (6.35). Let $\boldsymbol{B_i}$=$\kappa\boldsymbol{w}_i$, and the iteration is start from $l = l_1$.
Step 1-5:	The same as corresponding steps in Table 6.3.
Outcome	The final solution will be the one with a maximum power reduction in $\{l_1$,l_1+1,l_1+2,...,$N\}$. If $l \neq l_1$, the BS will sign a long-term contract with UAV l, and place it at the location of this UAV. Otherwise, no contract will be signed.

associated UAV should be larger than $\triangle P_{\mathcal{G}_{c_2}}$. The MU player i will select a UAV set $\boldsymbol{K_i}$ which can maximize its power reduction, i.e.,

$$\triangle P_i^{[1]} = max\{p_1, p_2, ..., p_{2^{l_1}}\}, \text{and } \boldsymbol{K_i} = \arg\max_{l}\{p_1, p_2, ..., p_{2^{l_1}}\},$$
$$p_1 = \sum_{j\in\mathcal{G}_{c_2}}^{j\in\mathcal{G}_{c_2}} \frac{(\boldsymbol{w}_j\boldsymbol{B}_l)^2+(\boldsymbol{w}_j\check{\boldsymbol{B}}_l)^2}{\|\boldsymbol{B}_l\|^2}(I_j+\sigma^2)\delta_j, \text{if served by UAV } l \in \{1, ...l_1, L\},$$
$$p_{2^{l_1}} = \sum_{j\in\mathcal{G}_{c_2}}^{} (\|\boldsymbol{w}_j\|^2 - \left\|\boldsymbol{w}_j - w_{l_1 j}^{'}\boldsymbol{B}_l - ... - w_{l_n j}^{'}\boldsymbol{B}_n\right\|^2)p_j, \text{if served by all UAVs.}$$

Then, the utility of MU player i can be calculated as

$$U_{\boldsymbol{K_i}}^{II} = \begin{cases} \triangle P_i^{[1]} - \triangle P_{\mathcal{G}_{c_2}}, & \text{if select UAV set } \boldsymbol{K_i}, \\ 0, & \text{otherwise.} \end{cases} \tag{6.37}$$

If the MU player i is in a MIMO-NOMA cluster $\mathcal{G}_{c_2}$, $\triangle P_{\mathcal{G}_{c_2}} = \sum^{j\in\mathcal{G}_{c_2}} (\|\boldsymbol{w}_j\|^2 - \left\|\boldsymbol{w}_j^{\aleph}\right\|^2)p_j$. Otherwise, $j = i$ and $\triangle P_{\mathcal{G}_{c_2}} = 0$. Similarly, (6.37) is also available for any $l_2 \in L$.

In the UAV side, each UAV aims to maximize its group utility, and the total utility of them should be equal to the total power reduction of UAV-MIMO MUs in (6.34). For UAV $l \in \boldsymbol{K_i}$, the utility of it can be calculated as

$$U_l^{II} = \sum_{i\in\mathcal{G}_l} \triangle P_{li}^{[2]}, \tag{6.38}$$

where

$$\triangle P_{li}^{[2]}=\begin{cases}\sum\limits^{j\in\mathcal{G}_{c_2}}(\frac{(\boldsymbol{w}_j\boldsymbol{B}_l)^2+(\boldsymbol{w}_j\check{\boldsymbol{B}}_l)^2}{\|\boldsymbol{B}_l\|^2}(I_j+\sigma^2)\delta_j-(\boldsymbol{w}_j\boldsymbol{B}_l)\sum\limits_{k\in\boldsymbol{K}_i}(\boldsymbol{w}_j\boldsymbol{B}_k)), & \text{if } length(\boldsymbol{K}_i)>1,\\ \sum\limits^{j\in\mathcal{G}_{c_2}}\frac{(\boldsymbol{w}_j\boldsymbol{B}_l)^2+(\boldsymbol{w}_j\check{\boldsymbol{B}}_l)^2}{\|\boldsymbol{B}_l\|^2}(I_j+\sigma^2)\delta_j, & \text{otherwise.}\end{cases}$$

The number of UAVs in $\boldsymbol{K}_i$ is denoted by $length(\boldsymbol{K}_i)$. Since MU i may also select other UAVs in $\boldsymbol{K}_i$, the power reduction should delete the overlapped term, i.e., $(\boldsymbol{w}_j\boldsymbol{B}_l)\sum\limits_{k\in\boldsymbol{K}_j}(\boldsymbol{w}_j\boldsymbol{B}_k))$.

We notice that i) a MU in the MU side (e.g., MU i) selects different UAVs will have different utilities; and ii) the utility of a MU i is equal to the sum utility of its maximum group utility. Thus, if all UAVs make decision independently, some UAVs may select MU i, while others may not. It will result in utilities in both sides are changed. Besides, each UAV maximizing its utility independently dose not indicate that the total power reduction of system is maximized. To overcome this issue, a two-layer matching approach (shown in Tables 4.3 and 4.4) is proposed to solve MU grouping problem, which is inspired by the structure of a Stackelberg game. In the top layer, for each MU player which selects multiple UAVs, it will have a UAV leader to manage a cooperation between selected UAVs and divides they shared utilities (i.e., utility sharing approach).

For example, consider a system that has only two UAVs, demoted by l_1 and l_2, and three MUs, demoted by j and k. If a MU player i (i.e., MU i) selects UAVs l_1 and l_2, the corresponding utilities of both sides can denoted by $U_i^I=\triangle P_{l_1i}^{[2]}+\triangle P_{l_2i}^{[2]}$, $U_{l_1i}^{II}=\triangle P_{l_1i}^{[2]}>0$ and $U_{l_2i}^{II}=\triangle P_{l_2i}^{[2]}>0$ without a UAV leader. Besides, if a MU player j (i.e., MU j) selects UAV l_2, the utilities of both sides are denoted by $U_j^I=U_{l_2j}^{II}=\triangle P_{l_2j}^{[2]}$, and of the MU player k (i.e., MU k) selects UAV l_1, the utilities of both sides are $U_k^I=U_{l_1k}^{II}=\triangle P_{l_1k}^{[2]}$. Then, if UAV l_2 finds $\triangle P_{l_2j}^{[2]}>\triangle P_{l_2i}^{[2]}$, it will select MU j while refuse MU i. Similarly, UAV l_1 will select MU i due to $U_{l_1i}^{II}>U_{l_1k}^{II}>0$. However, since MU i is refused by l_2, its utility is changed to be $\triangle P_{l_1i}^{\prime[2]}$, and satisfies $\triangle P_{l_1i}^{\prime[2]}<\triangle P_{l_1i}^{[2]}$ as the interference is increased. Therefore, the utilities of both sides on a same MU become different, and the total power

reduction is $\triangle P'^{[2]}_{l_1 i} + \triangle P^{[2]}_{l_2 j}$ in this case. However, it may not be an optimal solution as MU i find that selecting both UAVs will obtain a larger utility, i.e., $\triangle P^{[2]}_{l_1 i} + \triangle P'^{[2]}_{l_1 j} > \triangle P'^{[2]}_{l_1 i}$. In the second iteration, MU i may select UAV j again. It may exist two possible results. If $\triangle P'^{[2]}_{l_2 i} + \triangle P'^{[2]}_{l_2 j} < \triangle P^{[2]}_{l_2 j}$, UAV l_2 will refuse MU i, and the total power reduction is unchanged. Otherwise, it will accept MU i, and the total power reduction is increased to be $\triangle P^{[2]}_{l_1 i} + \triangle P'^{[2]}_{l_2 i} + \triangle P'^{[2]}_{l_2 j}$. We can observe that maximizing UAVs' utilities dose not mean to minimize the system power consumption.

If a UAV leader exists, it will adjust the utility of MU i before and after UAV selection. The leader is the UAV with the maximum utility share, such as UAV l_1, which share is larger than UAV l_2, i.e., $\triangle P^{[2]}_{l_1 i} > \triangle P^{[2]}_{l_2 i}$. Before UAV selection, the leader will check whether to share utility among MUs. If the utilities of all selected UAVs are increased, an utility share is unnecessary, for example, in the first term with $\triangle P^{[2]}_{l_1 i} > 0$ and $\triangle P^{[2]}_{l_2 i} > 0$. Otherwise, it will check whether its group utility is increased. In the second term, if $A = (\triangle P^{[2]}_{l_1 i} + \triangle P'^{[2]}_{l_2 i} + \triangle P'^{[2]}_{l_2 j}) - (\triangle P'^{[2]}_{l_1 i} + \triangle P^{[2]}_{l_2 j}) > 0$ and $A > \triangle P'^{[2]}_{l_1 k}$, the utility will be shared between UAVs l_1 and l_2 equally. Before sharing, the utilities of selected UAVs can be divided into two categories: the utility increased, i.e., UAV l_1; and the utility decreased, i.e., UAV l_2. The purpose of utility sharing is to ensure that when system power reduction is increased, the utilities of all selected UAVs are also increased. Thus, after sharing, the utilities of two UAV selections become $U^{II}_{l_1 i} = \triangle P'^{[2]}_{l_1 i} + A/2$ and $U^{II}_{l_2 i} = \triangle P^{[2]}_{l_2 j} + A/2$. As a result, MU i will resent a request to UAV l_2. It can be accepted by UAV l_2 even when $\triangle P'^{[2]}_{l_2 i} + \triangle P'^{[2]}_{l_2 j} < \triangle P^{[2]}_{l_2 j}$. If $A > 0$ while $A < \triangle P'^{[2]}_{l_1 k}$, the utility will not be shared because of the stability considerations, which will be explained later. After UAV selection, the leader will recheck the utility of both sides and adjust them to be uniformed. For example, when MU i is rejected by UAV l_2 while accepted by UAV l_1, the leader will let $U^{II}_{l_1 i} = \triangle P'^{[2]}_{l_1 i}$, instead of $\triangle P^{[2]}_{l_1 i} + \triangle P^{[2]}_{l_2 i}$. In summery, the UAV leader is responsible for utility adjusting when conducts utility sharing.

In case of the short-term contract with UAV CSI, we propose a two-layer many-to-many matching approach (as shown in Table 6.3) to solve this problem. Since UAVs in

$\{l_2, ...L\}$ are independent, we use an iteration approach to calculate the maximum total power reduction as the BS for each independent UAV selection. It means that only one UAV in $\{l_2, ...L\}$ (e.g., l_2) will be considered as a UAV player in each iteration, and the many-to-many matching is recurrently employed by $L - l_2$ times. For example, for UAV l_2, in the bottom layer, the UAV players in the UAV side are UAVs $\{1, ...l_1, l_2\}$, which have interactions with each other. In the MU side, players can select multiple UAVs simultaneously, and find the optimal set of UAVs, i.e., $\boldsymbol{K}_i$. For each MU player which selects multiple UAVs, it will have a leader in the up layer for utility adjustment. After obtaining $\boldsymbol{K}_i$, the UAV players will accept the MU player with maximum utility. After conducting many-to-many matching game in the bottom layer, the leader will normalize utilities of both sides, and prepare for the next round selection. When the many-to-many matching game is over, UAV-NOMA clustering is conducted. The total power reduction is denoted by l_2 for the comparison after calculating the power reduction of all unrented UAVs. At the end of iteration, the final solution will be the one with a maximum power reduction, and the BS will sign a short-term contract with the denoted UAV. There exists a case that no UAV will be signed, if the maximum power reduction is obtained when the UAV players in the UAV side are UAVs $\{1, ...l_1\}$.

If UAV's CSI is unavailable, different from before, in the UAV side, the UAV players include UAVs in $\{1, ...l_1\}$ and N hypothetic UAV selections. Those N hypothetic UAV selections will have interactions with UAVs in $\{1, ...l_1\}$ while independent with each other. Since only one UAV will be placed at each time slot, each MU player can only select one hypothetic UAV selection. Through (6.31), the channel gain coefficients can be estimated. Then, the rest of procedures are listed in Table 6.4, which are similar to the approach in Table 6.3.

The requirement for matching becoming stable is that our constructed processes can lead to a Pareto optimum [123]. Different from coalition game, the UAV strategy is based on the MU player's selection, so that the Pareto optimum in the UAV side of a final state

requires: i) UAV will not change its strategy (accept or refuse MUs) to improve its utility; and ii) no MU player can break the stable matching through changing its strategy, e.g., an accepted MU player withdraw a UAV group in a final state.

In case of many-to-one matching approach in Table 6.1. If we consider MUs i and j, and $\triangle P_{li} > \triangle P_{lj}$, MU player i will be selected and join G_l first. After that, $\triangle P_{lj}$ is changed to be $\triangle P'_{lj}$ and $\triangle P'_{lj} < \triangle P_{lj}$ (proved in Appendix C.2). If $\triangle P_{li} < (\triangle P'_{li} + \triangle P'_{lj})$, the MU player j will be selected by the UAV player l, i.e., $G_l = \{i, j\}$, and $\triangle P_{li}$ is changed to be $\triangle P'_{li}$ ($\triangle P'_{li} < \triangle P_{li}$). Since $\triangle P'_{lj} < \triangle P_{lj} < \triangle P_{li}$, we will have $\triangle P'_{li} > 0$. Thus, if each UAV selects MU players based on the order of utilities, the utilities of selected MUs will still keep positive after other MU players join this UAV group, so that the requirement ii) is always satisfied. If UAV l moves MU i out of its group, the utility of UAV l will be decreased as $\triangle P_{lj}$, so that this UAV player will not move any selected MU player out of its group, and the requirement i) is satisfied. If more than 2 MUs are considered, due to $\triangle P_{li} \approx \|\boldsymbol{w}_i\|^2 p_i$ and $\triangle P_{li} > \triangle P_{lj} > ...$, algorithm will not move any selected MU player out of its group, and i) is always satisfied. If the player i is a MIMO-NOMA cluster with utility $\triangle P_{li} \approx \|\boldsymbol{w}_i\|^2 p_i - \triangle P_{\mathcal{G}_{c_2}}$, since $\triangle P_{\mathcal{G}_{c_2}}$ can be regarded as a constant, the analysis is similar. In summary, the proposed many-to-one matching approach can obtain a stable and Parato optimal solution.

In case of many-to-many matching approach in Table 6.2, due to no interactions between UAV players, we can treat this approach as a combination of several many-to-one matching approaches, so that the optimality is obvious. Therefore, it also can obtain a stable and Parato optimal solution.

In case of two-layer matching approach in Table 6.3, UAV associations are not independent. Since the utilities of cooperated UAVs are interacted with each other, the matching approach may become unstable, and i) may be violated. Moreover, the utilities of MU players on a common UAV player may not follow an order of $\|\boldsymbol{w}_i\|^2 p_i$, so that the utility sharing approach may make ii) to be unsatisfied. For example, $U^{II}_{l_1 i} = \triangle P'^{[2]}_{l_1 i} + A/2$

and $U_{l_2 i}^{II} = \triangle P_{l_2 j}^{[2]} + A/2$ while not $\triangle P_{l_1 i}^{[2]}$ and $\triangle P_{l_2 j}^{\prime[2]}$. The proposed two-layer matching approach can leverage the relationship between UAVs, and analyze these two situations in sequence.

In the given example, the MU player i is accepted by UAV l_2 when UAV leader finds $A > U_{l_1,k}^{\prime II} > 0$ and resents a request to UAV l_2. The utility of MU k is changed from $U_{l_1,k}^{II} = \triangle P_{l_1 k}^{[2]}$ to $U_{l_1,k}^{\prime II} = \triangle P_{l_1 k}^{\prime[2]}$. The condition of UAV l_1 to accept MU player k is that its utility can be improved. More specifically, the utility of MU i will be reduced, while $\triangle P_{l_1 i}^{[2]} - \triangle P_{l_1 i}{*}^{[2]} < U_{l_1,k}^{\prime II}$. We use $\triangle P_{l_1 i}{*}^{[2]}$ and $\triangle P_{l_1 i}{*}^{\prime[2]}$ to denote renewed utilities (corresponding to $\triangle P_{l_1 i}^{[2]}$ and $\triangle P_{l_1 i}^{\prime[2]}$) when the UAV player l_1 accepts the MU player k, which will satisfy $\triangle P_{l_1 i}^{[2]} > \triangle P_{l_1 i}{*}^{[2]} > \triangle P_{l_1 i}{*}^{\prime[2]}$ and $(\triangle P_{l_1 i}^{[2]} - \triangle P_{l_1 i}^{\prime[2]}) > (\triangle P_{l_1 i}{*}^{[2]} - \triangle P_{l_1 i}{*}^{\prime[2]})$ as $\boldsymbol{B}_{l_1}$ changes. Therefore, if $C = \triangle P_{l_2 i}^{\prime[2]} + \triangle P_{l_2 j}^{\prime[2]} - \triangle P_{l_2 j}^{[2]} < 0$, we have $A = (\triangle P_{l_1 i}^{[2]} - \triangle P_{l_1 i}^{\prime[2]}) + C$ and $A' = (\triangle P_{l_1 i}{*}^{[2]} - \triangle P_{l_1 i}{*}^{\prime[2]}) + C$. Since $\triangle P_{l_1 i}^{[2]} - \triangle P_{l_1 i}{*}^{[2]} < U_{l_1,k}^{\prime II} < A < \triangle P_{l_1 i}^{[2]} - \triangle P_{l_1 i}^{\prime[2]}$ and $A > 0$, we can derive $A' > 0$. It means that the accepted MU i will not be rejected by both UAVs, and the interactions will not affect the stability of the matching approach. Thus, i) can be satisfied. Moreover, since $A' > 0$, the leader will not withdraw any UAV groups, and ii) can be satisfied.

The difference between the two-layer matching approaches in Table 6.4 and Table 6.3 is that we add a step of channel gain coefficients estimation. Thus, the stability and optimality are similar as above, which are also obviously confirmed.

6.6.3 Learning approach

We consider a long-time process, and employ a learning approach to build up the relationship between system state and UAV benefits. The state of BS is denoted by $s_t(N, n, \triangle P)$, where n is the number of MUs in a UAV group, and $\triangle P$ denotes the BS power reduction. To decrease the dimension of state at time t, $s_t(N, n, \triangle P)$ is simplified to be $s_t(n, Le)$ as N is fixed, and Le represents the level of power reduction $Le = \lfloor \triangle P / de \rfloor$

(or $\lfloor \triangle P/de^n \rfloor$) with a parameter de. The action of UAV group is either to select (i.e., $a_t = 1$) or not (i.e., $a_t = 0$). In the training progress, exploitation action is a ϵ-greedy action with the maximum Q-value and a probability 0.9. The reword of action a_t=0 is $r_{t+1}(s_t, 0)$=0. If $a_t = 1$, the reword is evaluated by the sum benefits during T, which is a delayed reward. The BS explores all state-action pairs (s_t, a_t) and updates their respective Q-values $Q_t^{II}(s_t, a_t)$ using Q-function as follows:

$$Q_{t+1}^{II}(s_t, a_t) \leftarrow (1-\alpha) Q_t^{II}(s_t, a_t) + \alpha\{r_{t+1}(s_t, a_t)) + \gamma \max_a Q_{t+1}^{II}(s_{t+1}, a_{t+1})\}, \quad (6.39)$$

where parameters α and γ can be obtained from simulations.

6.7 Numerical Results

In this section, the channel model and parameter settings are introduced first. Then, we compare the proposed UAV-NOMA with counterparts (i.e., MIMO-OMA, MIMO-NOMA, and UAV-MIMO) at a single time slot. Last, we compare and analyze the performances of short-term and long-term contracts, and observe the situation of hybrid contract.

6.7.1 Channel model and parameter settings

From the well-established narrowband transmission model [114, 124, 125], the downlink channel vector of LoS path between BS and MU i can be expressed as

$$\boldsymbol{h}_i = \sum_{k=1}^{Pa} \beta_{ik} \frac{\boldsymbol{A}(\theta_{ik})}{\sqrt{Pa}}, \quad (6.40)$$

where β_{ik} is the downlink channel gain of 3GPP long-term evolution (LTE) path, and $Pa = 6$ is the total number of paths. $\boldsymbol{A}(\theta_{ik})$ denotes the steering matrix, which can be expressed

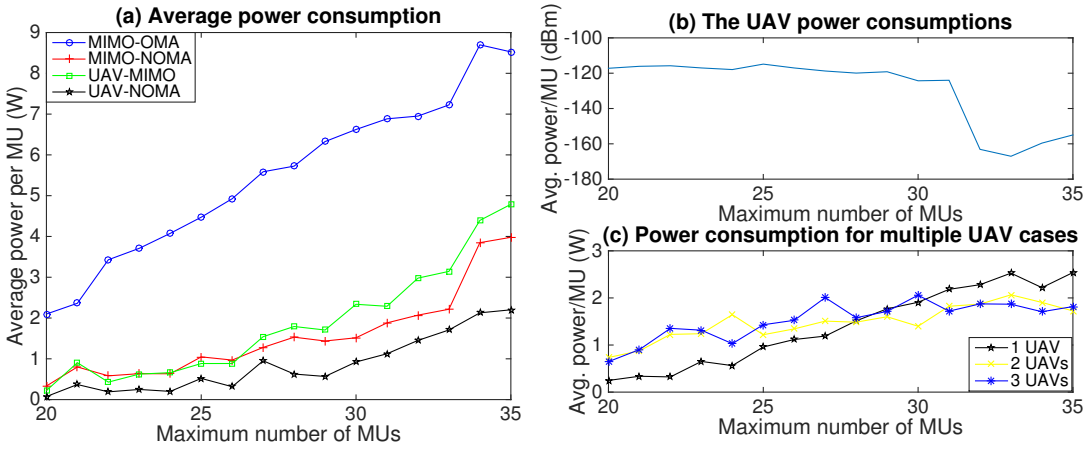

Figure 6.2: System performance on different numbers of MUs.

as

$$\boldsymbol{A}(\theta_{ik}) = \left[\ 1, e^{-j2\pi\frac{D}{\lambda}\cos(\theta_{ik})}, \ldots, e^{-j2\pi(M-1)\frac{D}{\lambda}\cos(\theta_{ik})}\ \right]^T,$$

in which $D \leq \frac{\lambda}{2}$ is the BS antenna spacing, λ is the wavelength of the carrier frequency, and $\theta_{ik} \in [-\frac{\triangle}{2} + \theta_i, \frac{\triangle}{2} + \theta_i]$ is the angle of arrival for $1 \leq k \leq Pa$, and $\triangle = 1^\circ$ is the users' angular spread. The LTE path loss parameters are given by $PL(dB) = 148.1 + 37.6log10(d_i)$, the Rayleigh fading with zero mean and unit variance $(\Gamma_i^{(n)} \sim CN(0,1))$, a log-normal shadowing $\gamma_i \sim N(0dB, 8dB)$, and the transmit antenna power gain $G = 9dB$ [114].

We consider a single cell network with a radius of 400m and a centrally located BS. The number of antennas at the BS is $M = 20$. The variance of Gaussian noise is $\sigma_u^2 = -135dBm$. The SINR requirement is $\delta = 4dB$. We assume that $\tilde{h}^{LoS} = 1$, and $\tilde{h}^{NLoS}$ is a Rayleigh fading. Other parameters setting are given as: $L_{LoS} = 1dB$, $L_{NLoS} = 10dB$, $\psi_1 = 9.6$, $\psi_2 = 0.28$, $v = 2$, and $B = 200kHz$. $f = 2GHz$. $\phi_{li} = \pi/4$. Rician factor K is selected such that $p^{LoS} = \frac{K}{K+1}$.

6.7.2 Approaches comparison

To compare UAV-NOMA with MIMO-OMA, MIMO-NOMA, and UAV-MIMO, we randomly generate 100 data for each number of MUs at a single time slot, and assume that UAV CSI is available. UAVs will be placed at the location of MUs with the descending order of power consumption. As the number of MUs is increased and close to the number of antennas, the transmit power will also be increased incredibly to increase the spatial multiplexing. However, the power limitation of the BS is assumed to be 200w which will limit the number of MUs can be served in the same spectrum.

In Fig. 6.2 (a), only MIMO-OMA and MIMO-NOMA are the approaches without UAV association, while UAV-MIMO is only consider UAV grouping without NOMA clustering. From this figure, we notice that, as the number of MUs is increased, the power consumption per MU of UAV-NOMA is significantly lower than other approaches, and MIMO-NOMA is better than UAV-MIMO when the number of MUs is over 26. It indicates that i) UAV-NOMA association can achieve the highest power reduction, because it benefits from both UAV grouping and NOMA clustering; and ii) when system has many MUs, NOMA clustering is more effective on power reduction than UAV grouping. Thus, we can conclude that MIMO-NOMA clustering should be proceed before UAV grouping. Moreover, the power consumption on UAV for data transmission is very small, which can be also observed in Fig. 6.2 (b).

In Fig. 6.2 (c), we observe the performance when the BS rents multiple UAVs. We let each UAV serves for at least one MU in this simulation. From this figure, if the number of MUs is small, renting 1 UAV is better than others as renting multiple UAVs will increase the interference towards those unconnected MUs, so that their power consumptions are increased. However, if MU increases, the power consumption will be greatly increased as the required spatial multiplexing increased. Therefore, renting more UAVs can reduce the power consumption of MIMO system as the orthogonal requirements are relaxed (as

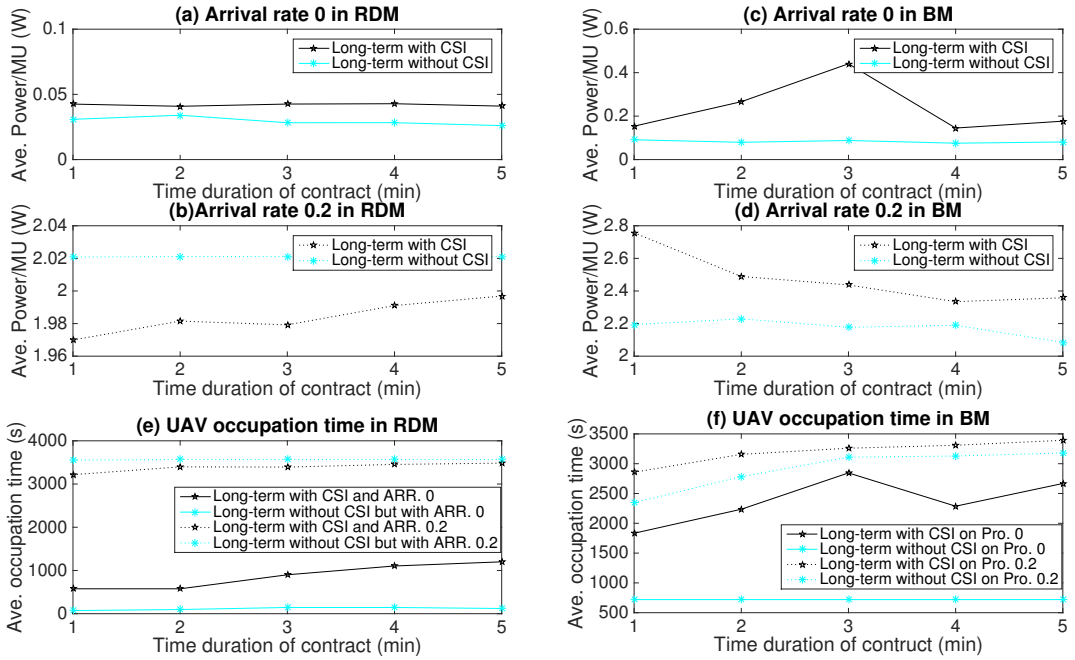

Figure 6.3: Performance comparison: with CSI vs without CSI in different time durations

shown in (6.7)), and the spatial multiplexing is changed through adding an extra antenna. Nonetheless, if we consider a balanced solution between increased interferences and reduced spatial multiplexing, renting 2 UAVs are the best choice in our simulation settings.

6.7.3 Long-term results

Motivated by [126], we consider two different mobility models:

- ***Random direction model (RDM)***: In this model, each MU moves (with probability p_0) from one location in a randomly generated direction (uniformly between 0 and 2π) during an exponentially distributed amount of time (mean $E(\tau)$) with speed v.
- ***Brownian motion (BM)***: The stochastic differential equation is given by $dX(t) = \mu X(t)dt + \sigma X(t)dW(t)$, where $W(t)$ is a Wiener process, and μ and σ are the drift and volatility of the process, respectively.

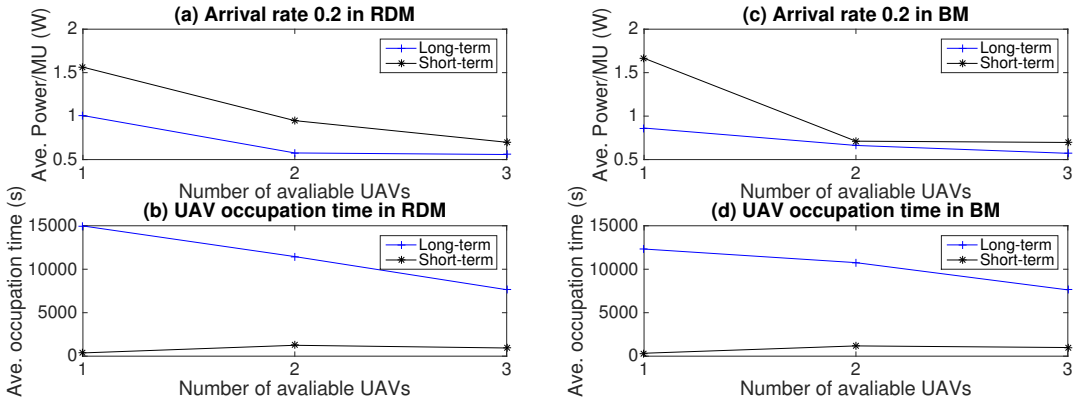

Figure 6.4: System performance within 1 hour

We assume that the system has 25 randomly distributed MUs at the beginning of each simulation, and the arrival rate (denoted by ARR. in Fig. 6.3) is selected within [0,0.2] per minute. In Fig. 6.3, we compare the performances of two situations: CSI is available and CSI is unavailable (i.e., denoted by with and without CSI in Fig. 6.3). From Figs. 6.3(a) and (c), we notice that if CSI is unavailable (Long-term without CSI), the performance is slightly better than that when it is available. Since the CSI estimation is based on channel correlation coefficient, the accuracy will decrease with the increase of the number of MUs. When the arrival rate is 0, the number of MUs will be decreased as time passed, so that the number of MUs under the coverage of a UAV is small, and nearby MUs with high channel correlation coefficients will have high values of estimated channel state, while others are close to zero. Then, the power reduction based on estimated channel state will slightly lower than that with CSI, which will result in shorter the UAV renting time (as shown in Figs. 6.3(e)-(f)). However, when the number of MUs increases and the arrival rate is 0.2 (i.e., ARR. 0.2), the estimation error will be decreased. It is because that, when system has a large quantity of MUs, the high demands from MUs under the coverage of a UAV will tend to stable as the time duration of contract increased. However, if the number of MUs is decreasing and the arrival rate is 0 (i.e., ARR. 0), since the average power consumption is low, the accuracy is still low. From this observation, we can conclude that our proposed estimation approach is effective, and can achieve high accuracy when time duration is 5

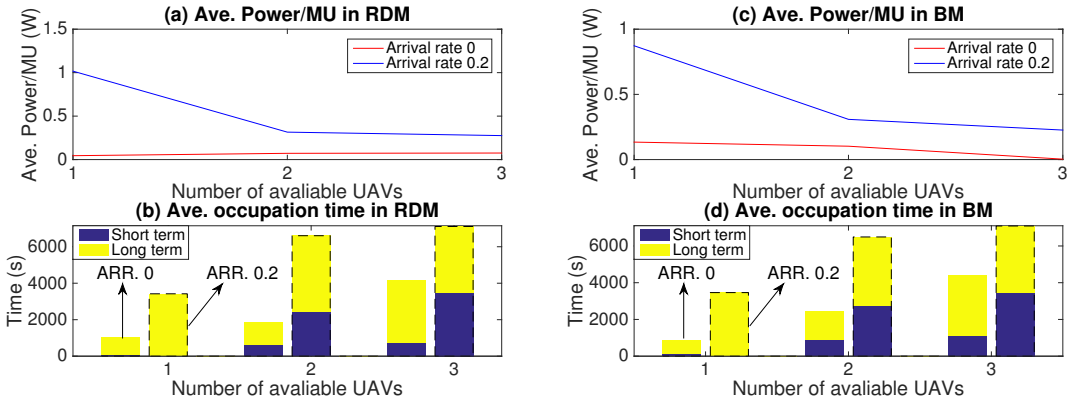

Figure 6.5: UAV renting MIMO-NOMA system in hybrid contract situation

min.

From Figs. 6.4(a)-(d), we observe that when the system has few MUs, the long-term contract is better than short-term one, as UAV can be placed at the appointed location and has a lower payment than the short-term contract. However, when the number of UAVs increases, the difference between the benefits from long-term contract and short-term contract is decreased. It is because that i) the short-term contract decision is based on UAV CSI, ii) the BS can make a more flexible choice when multiple MUs are available for renting. However, the long-term contract is more profitable due to low cost, especially when a BS serves for many MUs.

Fig. 6.5 shows power consumption when the BS can sign a short-term (1 min) or long-term contract (5 min), namely, hybrid contract situation. By comparing Figs. 6.4 and 6.5, we can notice that the hybrid contract situation is obviously better than the situation with only one kind of contract. In our environment settings, when the system has a large number of MUs, increasing the number of available UAVs will result in a better performance, while renting one UAV is good enough when the system has fewer MUs. From Figs. 6.5(c)-(d), we notice that in both cases, the long-term contract is more preferred than the short-term one. When the arrival rate is 0, the total renting time is increased when 2 more UAVs are available as the BS can have more flexible choices, while the performance of average power

consumption per MU almost keeps the same. It is because the interference from multiple UAVs almost offsets the benefits from renting them. However, when the arrival rate is 0.2, and 3 UAVs are available, the total renting time is slightly increased, and the proportion of short-term contract is increased. It results from the fact that the BS prefer more short-term contract than the long-term when the system has many MUs and more flexible UAV choices. However, we still can conclude that in our environment settings, the system can obtain a high performance when there are 2 UAVs available for renting services.

Chapter 7

Conclusions and Future Works

7.1 Conclusions

This thesis mainly investigated the MIMO-NOMA resource allocation problem in wireless networks, which is regarded as one promising technology in future 5G networks. The following three aspects are presented in this thesis: i) the basic principles of MIMO-NOMA and required SIC conditions; ii) the basic concepts of two game theory (coalition game and matching game) and corresponding stable conditions. iii) the combinations of MIMO-NOMA with other 5G technologies, such as CoMP, UAV. More details and insights are summarized as follows.

In Chapter 3, we formulate a joint optimization problem for MU clustering in the MIMO communication system to minimize the total power consumption for the BS and propose a cluster beamforming strategy to calculate the beamforming vector and power allocation coefficients for MIMO-NOMA clusters. Based on the proposed approach and the derived decoding order, a closed-form expression for cluster beamforming vector is obtained. Furthermore, we show that our proposed approach can avoid the peer effect when MUs are grouped in different clusters. Then, we carefully design an improved coalition

game for MU clustering, by which the size of a NOMA cluster can be flexible and the performance of the optimal results is close to that of the global optimal solution in terms of power consumption minimization. Moreover, we compare two different MIMO-NOMA scenarios for MU clustering and find that MIMO-NOMA1 (allocated a power coefficient set for each MU) is superior than MIMO-NOMA2 (allocated a single power coefficient for each MU) in power reduction. In the simulation part, we analyze the three factors that may affect the performance of MIMO-NOMA clustering to theoretically explain that our proposed clustering approach is a high-efficient algorithm compared with other existing approaches. Furthermore, we conduct two comparisons to demonstrate that the proposed cluster beamforming strategy and the improved coalition game approach are effective in significantly improving energy efficiency for the MIMO system with a large quantity of MUs.

In Chapter 4, we consider a joint BS selection and MIMO-NOMA clustering problem, and propose several approaches for different objectives. Especially, a new objective function (i.e., the relative fairness) and a two-side coalitional matching game approach are introduced for a win-win solution. Moreover, we derive the closed form solution for MIMO-NOMA clustering and discuss computational complexity and stabilities. Last, we employ the Pauta criterion algorithm to re-evaluate the system performance by excluding MUs with extreme high data rates (as an outliers). In simulations, we compare different objectives and approaches to conclude that by involving MU preference, BSs' decisions can satisfy the purposes of improving sum data rate while also maintaining a relative high MU fairness. Moreover, the relative fairness can ensure that system performance will not be dominated by the outliers and effectively balance the data rate among difference MUs. Furthermore, we show that in our environment settings, the best cluster size is 3.

In Chapter 5, we formulate a hybrid resource allocation problem to reduce the system total power consumption in a large-scale MIMO network. RRH cooperation by CoMP and MU cooperation by NOMA clustering are both involved into system optimization for

improving both power and spectral efficiencies. Moreover, we consider a hybrid CoMP-NOMA approach which includes both JT and CT to make RRH cooperation to be flexible in different environmental settings. Simulation results show that the proposed Co-NOMA approach can efficiently improve the system performance through forming cooperation within and outside of RRHs.

In Chapter 6, we discuss a resource allocation problem for UAV renting MIMO-NOMA wireless networks, which includes BS resource management and UAV renting. In this work, we propose a new UAV-MIMO transmission approach, and UAV-NOMA for power reduction. Our designed contract theoretic framework included the short-term and long-term contracts. Moreover, we employ improved matching approaches to solve the joint optimization of MU grouping and resource allocation for the case of single UAV or multiple UAVs. The stability and optimality of the proposed game approaches are proved. Furthermore, simulation results show that our proposed approaches can efficiently reduce power consumptions for UAV renting MIMO-NOMA wireless networks. Also, in our environment settings, the system performance is good enough when there are 2 UAVs available for renting services.

7.2 Future Works

Based on the research presented in this thesis, our study on MIMO-NOMA is still in an academic stage. There are two main directions for our future study: i) the proposed MIMO-NOMA approach can be employed in many more MIMO scenarios in 5G networks; and ii) we can use data from real applications to verify and improve our proposed approaches. The first direction is due to the advantages of MIMO-NOMA approach. More specifically, since it is a comparative approach among MUs, it can be combined with many advanced technologies in 5G networks with the intention of formulating cooperative resource allocation problems. Moreover, the game theory is excellent on solving such kind

of problem, and the computational complexity is low by designing a distributed approach. The second direction is based on the fact that the real applications of MIMO-NOMA are still in the stage of theory assumption. As a result, the public data base for MIMO-NOMA applications is not available currently. Therefore, it is significant to verify the academic model with real applications to make a further improvement on our proposed approaches.

In current stage, we consider to conduct the following potential researches:

i) An extension work on CoMP-NOMA. Our proposed approach in this thesis is a two-stage approach, which makes RRH cooperation and MU cooperation are independent. In our future work, we will improve our approach to achieve a joint optimized solution.

ii) An extension work on D2D transmission. In existing researches, NOMA has been employed in D2D transmission scenario. However, few of them are consider a D2D assisted MIMO-NOMA transmission approach. It can overcome the SIC condition constrain, and makes the signals of any grouped MUs be successfully decoded.

iii) An extension work on imperfect CSI MIMO networks. We current work is based on an assumption that the CSI information is perfect. However, this assumption is difficult to be realized as pilot contamination will result in the accuracy of channel estimation reducing, and improving this accuracy is time cost. Therefore, in the case of imperfect CSI, we need to estimate the packet loss rate of our proposed MIMO-NOMA approach. Then, we should propose an MU clustering approach which aims at reducing the packet loss rate.

iv) An extension work on massive MIMO networks. It has been envisioned that massive MIMO will be widely deployed in future cellular networks. Interference management will be a key issue of transmission. Thus, MIMO-NOMA combined antenna selection can be an available choice to reduce the pilot contamination.

Reference

[1] Z. Ding, Z. Yang, P. Fan, and H. V. Poor, "On the performance of non-orthogonal multiple access in 5g systems with randomly deployed users," *IEEE Signal Process. Lett.*, vol. 21, no. 12, pp. 1501–1505, 2014.

[2] X. Chen, A. Benjebboui, Y. Lan, A. Li, and H. Jiang, "Evaluations of downlink non-orthogonal multiple access (noma) combined with su-mimo," in *Proc. 2014 IEEE 25th Annual Inter. Symposium Personal, Indoor, and Mobile Radio Commun. (PIMRC)*, 2014, pp. 1887–1891.

[3] H. Bolcskei, "Mimo-ofdm wireless systems: basics, perspectives, and challenges," *IEEE Trans. Wireless Commun.*, vol. 13, no. 4, pp. 31–37, 2006.

[4] D. Gesbert, M. Shafi, D. shan Shiu, P. J. Smith, and A. Naguib, "From theory to practice: an overview of mimo space-time coded wireless systems," *IEEE J. Sel. Areas Commun.*, vol. 21, no. 3, pp. 281–302, 2003.

[5] L. Lv, Q. Ni, Z. Ding, and J. Chen, "Application of non-orthogonal multiple access in cooperative spectrum-sharing networks over nakagami- m fading channels," *IEEE Trans. Veh. Technol.*, vol. 66, no. 6, pp. 5506–5511, 2017.

[6] S. M. R. Islam, M. Zeng, O. A. Dobre, and K. Kwak, "Resource allocation for downlink noma systems: Key techniques and open issues," *IEEE Trans. Wireless Commun.*, vol. 25, no. 2, pp. 40–47, 2018.

[7] T. Yoo and A. Goldsmith, "Optimality of zero-forcing beamforming with multiuser diversity," in *Proc. IEEE Inter. Conf. Commun.*, vol. 1, 2005, pp. 542–546.

[8] Z. Rosberg, A. Cantoni, and R. P. Liu, "Resource allocation for qos multiuser mimo with zero forcing and mmse beamforming," in *Proc. 2010 IEEE 18th Inter. Workshop Quality of Service (IWQoS)*, 2010, pp. 1–6.

[9] A. Maaref and S. Aissa, "Closed-form expressions for the outage and ergodic shannon capacity of mimo mrc systems," *IEEE Trans. Commun.*, vol. 53, no. 7, pp. 1092–1095, 2005.

[10] R. Rai, H. Zhu, and J. Wang, "Resource scheduling in non-orthogonal multiple access (noma) based cloud-ran systems," in *Proc. 2017 IEEE 8th Annual Ubiquitous Comput., Electronics and Mobile Commun. Confer. (UEMCON)*, 2017, pp. 418–422.

[11] H. Wang, S. Leung, and R. Song, "Precoding design for two-cell mimo-noma uplink with comp reception," *IEEE Commun. Lett.*, vol. 22, no. 12, pp. 2607–2610, 2018.

[12] Xi Zhang and Fan Yang, "Spectrum utility driven wifi offloading over noma-based cellular network edges," in *Proc. 2017 51st Annual Confer. Inf. Sciences Systems (CISS)*, 2017, pp. 1–6.

[13] Y. Dai, M. Sheng, J. Liu, N. Cheng, X. Shen, and Q. Yang, "Joint mode selection and resource allocation for d2d-enabled noma cellular networks," *IEEE Trans. Veh. Technol.*, vol. 68, no. 7, pp. 6721–6733, 2019.

[14] L. Dai, B. Wang, M. Peng, and S. Chen, "Hybrid precoding-based millimeter-wave massive mimo-noma with simultaneous wireless information and power transfer," *IEEE J. Sel. Areas Commun.*, vol. 37, no. 1, pp. 131–141, 2019.

[15] L. Song, Y. Li, Z. Ding, and H. V. Poor, "Resource management in non-orthogonal multiple access networks for 5g and beyond," *IEEE Netw.*, vol. 31, no. 4, pp. 8–14, 2017.

[16] C. B. Chae, D. Mazzarese, and R. W. Heath, "Coordinated beamforming for multiuser mimo systems with limited feedforward," in *Proc. 40th Asilomar Conf. Signals, Syst. Comput.*, 2006, pp. 1511–1515.

[17] J. Choi, "Minimum power multicast beamforming with superposition coding for multiresolution broadcast and application to noma systems," *IEEE Trans. Commun.*, vol. 63, no. 3, pp. 791–800, 2015.

[18] T. Obara, S. Suyama, and Y. Okumura, "Channel estimation for super high bit rate massive mimo systems using joint processing of analog fixed beamforming and csi-based precoding," in *Proc. IEEE Conf. Standards Commun. Netw. (CSCN)*, 2015, pp. 300–304.

[19] Y. Cheng, M. Pesavento, and A. Philipp, "Joint network optimization and downlink beamforming for comp transmissions using mixed integer conic programming," *IEEE Trans. Signal Process.*, vol. 61, no. 16, pp. 3972–3987, 2013.

[20] B. Kimy, S. Lim, H. Kim, S. Suh, J. Kwun, S. Choi, C. Lee, S. Lee, and D. Hong, "Non-orthogonal multiple access in a downlink multiuser beamforming system," in *Proc. IEEE Military Commun. Conf.*, 2013, pp. 1278–1283.

[21] Y. F. Liu, Y. H. Dai, and Z. Q. Luo, "Coordinated beamforming for miso interference channel: Complexity analysis and efficient algorithms," *IEEE Trans. Signal Process.*, vol. 59, no. 3, pp. 1142–1157, 2011.

[22] T. Yoo and A. Goldsmith, "On the optimality of multiantenna broadcast scheduling using zero-forcing beamforming," *IEEE J. Sel. Areas Commun.*, vol. 24, no. 3, pp. 528–541, 2006.

[23] S. M. R. Islam, N. Avazov, O. A. Dobre, and K. S. Kwak, "Power-domain non-orthogonal multiple access (noma) in 5g systems: Potentials and challenges," *Commun. Surveys Tuts.*, vol. 66, no. 99, pp. 1–1, 2016.

[24] Z. Ding, R. Schober, and H. V. Poor, "A general mimo framework for noma downlink and uplink transmission based on signal alignment," *IEEE Trans. Wireless Commun.*, vol. 15, no. 6, pp. 4438–4454, 2016.

[25] S. Ali, E. Hossain, and D. I. Kim, "Non-orthogonal multiple access (noma) for downlink multiuser mimo systems: User clustering, beamforming, and power allocation," *IEEE Access*, vol. 5, pp. 565–577, 2017.

[26] Y. Liu, G. Pan, H. Zhang, and M. Song, "On the capacity comparison between mimo-noma and mimo-oma," *IEEE Access*, vol. 4, pp. 2123–2129, 2016.

[27] Z. Chen and X. Dai, "Med precoding for multi-user mimo-noma downlink transmission," *IEEE Trans. Veh. Technol.*, vol. 66, no. 99, pp. 1–1, 2016.

[28] Z. Ding, F. Adachi, and H. V. Poor, "The application of mimo to non-orthogonal multiple access," *IEEE Trans. Wireless Commun.*, vol. 15, no. 1, pp. 537–552, 2016.

[29] R. Wang, H. Hu, and X. Yang, "Potentials and challenges of c-ran supporting multi-rats toward 5g mobile networks," *IEEE Access*, vol. 2, pp. 1187–1195, 2014.

[30] C. Pan, H. Zhu, N. J. Gomes, and J. Wang, "Joint precoding and rrh selection for user-centric green mimo c-ran," *IEEE Trans. Wireless Commun.*, vol. 16, no. 5, pp. 2891–2906, 2017.

[31] W. Zhao and S. Wang, "Traffic density-based rrh selection for power saving in c-ran," *IEEE J. Sel. Areas Commun.*, vol. 34, no. 12, pp. 3157–3167, 2016.

[32] J. Wu, Z. Zhang, Y. Hong, and Y. Wen, "Cloud radio access network (c-ran): a primer," *IEEE Netw.*, vol. 29, no. 1, pp. 35–41, 2015.

[33] L. Sboui, H. Ghazzai, Z. Rezki, and M. Alouini, "On the throughput of cognitive radio mimo systems assisted with uav relays," in *Proc. 2017 13th Inter. Wireless Commun. Mobile Computing Confer. (IWCMC)*, 2017, pp. 939–944.

[34] Y. Zeng, R. Zhang, and T. J. Lim, "Throughput maximization for uav-enabled mobile relaying systems," *IEEE Trans. Commun.*, vol. 64, no. 12, pp. 4983–4996, 2016.

[35] X. Jiang, Z. Wu, Z. Yin, and Z. Yang, "Power and trajectory optimization for uav-enabled amplify-and-forward relay networks," *IEEE Access*, vol. 6, pp. 48 688–48 696, 2018.

[36] X. Zhang and L. Duan, "Fast deployment of uav networks for optimal wireless coverage," *IEEE Trans. Mobile Computing*, vol. 18, no. 3, pp. 588–601, 2019.

[37] E. Turgut and M. C. Gursoy, "Downlink analysis in unmanned aerial vehicle (uav) assisted cellular networks with clustered users," *IEEE Access*, vol. 6, pp. 36 313–36 324, 2018.

[38] M. Gruber, "Role of altitude when exploring optimal placement of uav access points," in *Proc. 2016 IEEE Wireless Commun. Netw. Confer.*, 2016, pp. 1–5.

[39] Q. Wu, Y. Zeng, and R. Zhang, "Joint trajectory and communication design for multi-uav enabled wireless networks," *IEEE Trans. Wireless Commun.*, vol. 17, no. 3, pp. 2109–2121, 2018.

[40] M. Gharibi, R. Boutaba, and S. L. Waslander, "Internet of drones," *IEEE Access*, vol. 4, pp. 1148–1162, 2016.

[41] R. Jia, Y. Li, X. Cheng, and B. Ai, "3d geometry-based uav-mimo channel modeling and simulation," *China Commun.*, vol. 15, no. 12, pp. 64–74, 2018.

[42] Y. Li and X. Cheng, "New deterministic and statistical simulation models for non-isotropic uav-mimo channels," in *Proc. 2017 9th Inter. Confer. Wireless Commun. Signal Process. (WCSP)*, 2017, pp. 1–6.

[43] L. Sboui, H. Ghazzai, Z. Rezki, and M. Alouini, "Achievable rates of uav-relayed cooperative cognitive radio mimo systems," *IEEE Access*, vol. 5, pp. 5190–5204, 2017.

[44] Q. Sun, S. Han, Z. Xu, S. Wang, I. Chih-Lin, and Z. Pan, "Sum rate optimization for mimo non-orthogonal multiple access systems," in *Proc. IEEE WCNC*, 2015, pp. 747–752.

[45] Y. Liu, M. Elkashlan, Z. Ding, and G. K. Karagiannidis, "Fairness of user clustering in mimo non-orthogonal multiple access systems," *IEEE Commun. Lett.*, vol. 20, no. 7, pp. 1465–1468, 2016.

[46] R. B. Myerson, *Game theory*. Harvard university press, 2013.

[47] Z. Han, *Game theory in wireless and communication networks: theory, models, and applications*. Cambridge University Press, 2012.

[48] L. Shi, L. Zhao, G. Zheng, Z. Han, and Y. Ye, "Incentive design for cache-enabled d2d underlaid cellular networks using stackelberg game," *IEEE Trans. Veh. Technol.*, vol. 68, no. 1, pp. 765–779, 2019.

[49] R. Yin, C. Zhong, G. Yu, Z. Zhang, K. K. Wong, and X. Chen, "Joint spectrum and power allocation for d2d communications underlaying cellular networks," *IEEE Trans. Veh. Technol.*, vol. 65, no. 4, pp. 2182–2195, 2016.

[50] H. Shah-Mansouri and V. W. S. Wong, "Hierarchical fog-cloud computing for iot systems: A computation offloading game," *IEEE Internet of Things Journal*, vol. 5, no. 4, pp. 3246–3257, 2018.

[51] Z. Xiong, S. Feng, W. Wang, D. Niyato, P. Wang, and Z. Han, "Cloud/fog computing resource management and pricing for blockchain networks," *IEEE Internet of Things Journal*, vol. 6, no. 3, pp. 4585–4600, 2019.

[52] Y. Wang, X. Dai, J. M. Wang, and B. Bensaou, "A reinforcement learning approach to energy efficiency and qos in 5g wireless networks," *IEEE J. Sel. Areas Commun.*, vol. 37, no. 6, pp. 1413–1423, 2019.

[53] S. Guruacharya, D. Niyato, M. Bennis, and D. I. Kim, "Dynamic coalition formation for network mimo in small cell networks," *IEEE Trans. Wireless Commun.*, vol. 12, no. 10, pp. 5360–5372, 2013.

[54] W. Saad, Z. Han, M. Debbah, and A. Hjorungnes, "A distributed coalition formation framework for fair user cooperation in wireless networks," *IEEE Trans. Wireless Commun.*, vol. 8, no. 9, pp. 4580–4593, 2009.

[55] A. E. Roth and M. Sotomayor, "Two-sided matching," *Handbook of game theory with economic applications*, vol. 1, pp. 485–541, 1992.

[56] A. M. El-Hajj, Z. Dawy, and W. Saad, "A stable matching game for joint uplink/downlink resource allocation in ofdma wireless networks," in *Proc. IEEE Inter. Conf. Commun. (ICC)*, 2012, pp. 5354–5359.

[57] T. Sanguanpuak, S. Guruacharya, N. Rajatheva, M. Bennis, and M. Latva-Aho, "Multi-operator spectrum sharing for small cell networks: A matching game perspective," *IEEE Trans. Wireless Commun.*, vol. 16, no. 6, pp. 3761–3774, 2017.

[58] S. Banerjee, H. Konishi, and T. Sönmez, "Core in a simple coalition formation game," *Social Choice and Welfare*, vol. 18, no. 1, pp. 135–153, Jan 2001.

[59] D. Gale *et al.*, *Strategic foundations of general equilibrium: dynamic matching and bargaining games*. Cambridge University Press, 2000.

[60] D. Gale and M. Sotomayor, "Ms. machiavelli and the stable matching problem," *The American Mathematical Monthly*, vol. 92, no. 4, pp. 261–268, 1985.

[61] Z. Jiao and G. Tian, "The stability of many-to-many matching with max–min preferences," *Economics Lett.*, vol. 129, pp. 52–56, 2015.

[62] Y. Saito, Y. Kishiyama, A. Benjebbour, T. Nakamura, A. Li, and K. Higuchi, "Non-orthogonal multiple access (noma) for cellular future radio access," in *Proc. 2013 IEEE 77th Veh. Technol. Confer. (VTC Spring)*, 2013.

[63] M. Zeng, A. Yadav, O. A. Dobre, G. I. Tsiropoulos, and H. V. Poor, "Capacity comparison between mimo-noma and mimo-oma with multiple users in a cluster," *IEEE J. Sel. Areas Commun.*, vol. 35, no. 10, pp. 2413–2424, 2017.

[64] B. Wang, L. Dai, Z. Wang, N. Ge, and S. Zhou, "Spectrum and energy-efficient beamspace mimo-noma for millimeter-wave communications using lens antenna array," *IEEE J. Sel. Areas Commun.*, vol. 35, no. 10, pp. 2370–2382, 2017.

[65] K. Yang, X. Yan, K. Qin, and Q. Wang, "A uniform beam selection algorithm for beamspace mimo-noma in millimeter-wave communication system," in *Proc. 2018 15th Inter. Comput. Confer. Wavelet Active Media Technol. Inf. Process. (ICCWAMTIP)*, 2018, pp. 166–169.

[66] J. Kaur and M. L. Singh, "User assisted cooperative relaying in beamspace massive mimo noma based systems for millimeter wave communications," *China Commun.*, vol. 16, no. 6, pp. 103–113, 2019.

[67] Y. Chen, L. Wang, Y. Ai, B. Jiao, and L. Hanzo, "Performance analysis of noma-sm in vehicle-to-vehicle massive mimo channels," *IEEE J. Sel. Areas Commun.*, vol. 35, no. 12, pp. 2653–2666, 2017.

[68] X. Liu, Y. Liu, X. Wang, and H. Lin, "Highly efficient 3d resource allocation techniques in 5g for noma enabled massive mimo and relaying systems," *IEEE J. Sel. Areas Commun.*, vol. PP, no. 99, pp. 1–1, 2017.

[69] D. Zhang, Y. Liu, Z. Ding, Z. Zhou, A. Nallanathan, and T. Sato, "Performance analysis of non-regenerative massive-mimo-noma relay systems for 5g," *IEEE Trans. Commun.*, vol. 65, no. 11, pp. 4777–4790, 2017.

[70] J. Ma, C. Liang, C. Xu, and L. Ping, "On orthogonal and superimposed pilot schemes in massive mimo noma systems," *IEEE J. Sel. Areas Commun.*, vol. 35, no. 12, pp. 2696–2707, 2017.

[71] H. V. Cheng, E. Bjrnson, and E. G. Larsson, "Performance analysis of noma in training-based multiuser mimo systems," *IEEE Trans. Wireless Commun.*, vol. 17, no. 1, pp. 372–385, 2018.

[72] D. Kudathanthirige and G. Amarasuriya, "Massive mimo noma downlink," in *Proc. 2018 IEEE Global Telecommun. Conf. (GLOBECOM)*, 2018, pp. 1–7.

[73] D. Kudathanthirige and G. A. A. Baduge, "Noma-aided multicell downlink massive mimo," *IEEE J. Sel. Topics Signal Process.*, vol. 13, no. 3, pp. 612–627, 2019.

[74] S. Chinnadurai and D. Yoon, "Energy efficient mimo-noma hcn with iot for wireless communication systems," in *Proc. 2018 Inter. Confer. Inf. Commun. Technol. Convergence (ICTC)*, 2018, pp. 856–859.

[75] A. Nasser, O. Muta, M. Elsabrouty, and H. Gacanin, "Interference mitigation and power allocation scheme for downlink mimo-noma hetnet," *IEEE Trans. Veh. Technol.*, vol. 68, no. 7, pp. 6805–6816, 2019.

[76] C. Chen, W. Zhong, H. Yang, and P. Du, "On the performance of mimo-noma-based visible light communication systems," *IEEE Photonics Technol. Lett.*, vol. 30, no. 4, pp. 307–310, 2018.

[77] V. D. Nguyen, H. D. Tuan, T. Q. Duong, H. V. Poor, and O. S. Shin, "Precoder design for signal superposition in mimo-noma multicell networks," *IEEE J. Sel. Areas Commun.*, vol. 35, no. 12, pp. 2681–2695, 2017.

[78] Z. Q. Al-Abbasi, D. K. C. So, and J. Tang, "Resource allocation for mu-mimo non-orthogonal multiple access (noma) system with interference alignment," in *Proc. 2017 IEEE Inter. Confer. Commun. (ICC)*, 2017, pp. 1–6.

[79] A. Farzamnia, N. W. Hlaing, M. Mariappan, and L. C. Fan, "Network coding schemes with mimo-noma for two-way relay networks," in *Proc. 2018 IEEE Inter. Confer. Artificial Intelligence Engineering and Technol. (IICAIET)*, 2018, pp. 1–5.

[80] Y. Chi, L. Liu, G. Song, C. Yuen, Y. L. Guan, and Y. Li, "Practical mimo-noma: Low complexity and capacity-approaching solution," *IEEE Trans. Wireless Commun.*, vol. 17, no. 9, pp. 6251–6264, 2018.

[81] J. Cui, Z. Ding, and P. Fan, "Outage probability constrained mimo-noma designs under imperfect csi," *IEEE Trans. Wireless Commun.*, vol. 17, no. 12, pp. 8239–8255, 2018.

[82] W. A. Al-Hussaibi and F. H. Ali, "Efficient user clustering, receive antenna selection, and power allocation algorithms for massive mimo-noma systems," *IEEE Access*, vol. 7, pp. 31 865–31 882, 2019.

[83] J. Kim, J. Koh, J. Kang, K. Lee, and J. Kang, "Design of user clustering and precoding for downlink non-orthogonal multiple access (noma)," in *Proc. IEEE Military Commun. Conf.*, 2015, pp. 1170–1175.

[84] X. Liu and X. Wang, "Efficient antenna selection and user scheduling in 5g massive mimo-noma system," in *Proc. 2016 IEEE 83rd Veh. Technol. Confer. (VTC Spring)*, 2016, pp. 1–5.

[85] Y. I. Choi, J. W. Lee, M. Rim, and C. G. Kang, "On the performance of beam division nonorthogonal multiple access for fdd-based large-scale multi-user mimo systems," *IEEE Trans. Wireless Commun.*, vol. 16, no. 8, pp. 5077–5089, 2017.

[86] S. Park, A. Q. Truong, and T. H. Nguyen, "Power control for sum spectral efficiency optimization in mimo-noma systems with linear beamforming," *IEEE Access*, vol. 7, pp. 10 593–10 605, 2019.

[87] C. Chen, W. Cai, X. Cheng, L. Yang, and Y. Jin, "Low complexity beamforming and user selection schemes for 5g mimo-noma systems," *IEEE J. Sel. Areas Commun.*, vol. 35, no. 12, pp. 2708–2722, 2017.

[88] D. Tong, Y. Ding, Y. Liu, and Y. Wang, "A mimo-noma framework with complex-valued power coefficients," *IEEE Trans. Veh. Technol.*, vol. 68, no. 3, pp. 2244–2259, 2019.

[89] C. Xiao, J. Zeng, W. Ni, X. Su, R. P. Liu, T. Lv, and J. Wang, "Downlink mimo-noma for ultra-reliable low-latency communications," *IEEE J. Sel. Areas Commun.*, vol. 37, no. 4, pp. 780–794, 2019.

[90] X. Zhang, X. Zhu, and H. Zhu, "Joint user clustering and multi-dimensional resource allocation in downlink mimo-noma networks," *IEEE Access*, vol. 7, pp. 81 783–81 793, 2019.

[91] M. Zeng, A. Yadav, O. A. Dobre, G. I. Tsiropoulos, and H. V. Poor, "On the sum rate of mimo-noma and mimo-oma systems," *IEEE Wireless Commun. Lett.*, vol. 6, no. 4, pp. 534–537, 2017.

[92] B. Di, L. Song, and Y. Li, "Sub-channel assignment, power allocation, and user scheduling for non-orthogonal multiple access networks," *IEEE Trans. Wireless Commun.*, vol. 15, no. 11, pp. 7686–7698, 2016.

[93] A. M. Ahmadian, W. Zirwas, R. S. Ganesan, and B. Panzner, "Low complexity moore-penrose inverse for large comp areas with sparse massive mimo channel matrices," in *Proc. 2016 IEEE 27th Annual Inter. Symposium on Personal, Indoor, and Mobile Radio Commun. (PIMRC)*, 2016, pp. 1–7.

[94] D. Choi, D. Lee, and J. H. Lee, "Resource allocation for comp with multiuser mimo-ofdma," *IEEE Trans. Veh. Technol.*, vol. 60, no. 9, pp. 4626–4632, 2011.

[95] Y. Mao and V. O. K. Li, "Cluster-based resource allocation with adaptive comp in multi-cell mu-mimo ofdma system," in *Proc. 2016 IEEE Inter. Confer. on Signal Process., Commun. Comput. (ICSPCC)*, 2016, pp. 1–6.

[96] J. Pastor-Prez, F. Riera-Palou, and G. Femenias, "Evolutionary algorithms for multiobjective optimization of frequency reuse schemes in comp-based mimo-ofdma networks," in *Proc. Inter. Symposium Wireless Commun. Syst. (ISWCS)*, 2016, pp. 235–241.

[97] J. Liu, X. Li, H. Ji, and Y. Tang, "Traffic-pairing scheme based on particle swarm optimization in downlink comp-mu-mimo system," in *Proc. IEEE Wireless Commun. Netw. Conf. (WCNC)*, 2014, pp. 1779–1784.

[98] P. Rost, C. J. Bernardos, A. D. Domenico, M. D. Girolamo, M. Lalam, A. Maeder, D. Sabella, and D. Wbben, "Cloud technologies for flexible 5g radio access networks," *IEEE Commun. Mag.*, vol. 52, no. 5, pp. 68–76, 2014.

[99] S. A. R. Zaidi, A. Imran, D. C. McLernon, and M. Ghogho, "Characterizing coverage and downlink throughput of cloud empowered hetnets," *IEEE Commun. Lett.*, vol. 19, no. 6, pp. 1013–1016, 2015.

[100] Y. Cai, F. R. Yu, and S. Bu, "Cloud computing meets mobile wireless communications in next generation cellular networks," *IEEE Netw.*, vol. 28, no. 6, pp. 54–59, 2014.

[101] C. L. I, C. Rowell, S. Han, Z. Xu, G. Li, and Z. Pan, "Toward green and soft: a 5g perspective," *IEEE Commun. Mag.*, vol. 52, no. 2, pp. 66–73, 2014.

[102] M. Peng, S. Yan, and H. V. Poor, "Ergodic capacity analysis of remote radio head associations in cloud radio access networks," *IEEE Wireless Commun. Lett.*, vol. 3, no. 4, pp. 365–368, 2014.

[103] D. Liu, S. Han, C. Yang, and Q. Zhang, "Semi-dynamic user-specific clustering for downlink cloud radio access network," *IEEE Trans. Veh. Technol.*, vol. PP, no. 99, pp. 1–1, 2015.

[104] A. Davydov, G. Morozov, I. Bolotin, and A. Papathanassiou, "Evaluation of joint transmission comp in c-ran based lte-a hetnets with large coordination areas," in *Proc. IEEE GLOBECOM Workshop*, 2013, pp. 801–806.

[105] M. U. Aminu, J. Kaleva, and A. Tolli, "Dynamic clustering for max-min fairness with joint processing comp," in *Proc. Int. Symp. Personal Indoor Mobile Radio Commun.*, 2016, pp. 1–5.

[106] Y. Shi, J. Zhang, and K. B. Letaief, "Statistical group sparse beamforming for green cloud-ran via large system analysis," in *IEEE Int. Symposium Inf. Theory*, 2016, pp. 870–874.

[107] B. Farhang-Boroujeny, Q. Spencer, and L. Swindlehurst, "Layering techniques for space-time communication in multi-user networks," in *Proc. IEEE Veh. Technol. Conf.*, vol. 2, 2003, pp. 1339–1343 Vol.2.

[108] J. Ding and J. Cai, "Efficient mimo-noma clustering integrating joint beamforming and power allocation," in *Proc. IEEEGLOBECOM Conf.*, 2017.

[109] Y. Zhou, V. W. S. Wong, and R. Schober, "Dynamic decode-and-forward based cooperative noma with spatially random users," *IEEE Trans. Wireless Commun.*, vol. 17, no. 5, pp. 3340–3356, 2018.

[110] M. Fabbri, M. Chiani, and A. Giorgetti, "Introducing erasures in mimo with successive interference cancellation to reduce error propagation," in *Proc. 2009 IEEE Inter. Confer. Ultra-Wideband*, 2009, pp. 312–315.

[111] J. Kennedy, "Particle swarm optimization," in *Encyclopedia of Mach. Learning*. Springer, 2011, pp. 760–766.

[112] S. Mathur, L. Sankar, and N. B. Mandayam, "Coalitions in cooperative wireless networks," *IEEE J. Sel. Areas Commun.*, vol. 26, no. 7, pp. 1104–1115, 2008.

[113] A. Papadogiannis and G. C. Alexandropoulos, "The value of dynamic clustering of base stations for future wireless networks," in *Proc. IEEE World Congr. Comput. Intell.*, 2010, pp. 1–6.

[114] A. Papadogiannis, H. J. Bang, D. Gesbert, and E. Hardouin, "Efficient selective feedback design for multicell cooperative networks," *IEEE Trans. Veh. Technol.*, vol. 60, no. 1, pp. 196–205, 2011.

[115] C. Guo, B. Liao, L. Huang, X. Lin, and J. Zhang, "On convexity of fairness-aware energy-efficient power allocation in spectrum-sharing networks," *IEEE Commun. Lett.*, vol. 20, no. 3, pp. 534–537, 2016.

[116] A. C. Cirik, M. J. Rahman, and L. Lampe, "Robust fairness transceiver design for a full-duplex mimo multi-cell system," *IEEE Trans. Commun.*, vol. 66, no. 3, pp. 1027–1041, 2018.

[117] D. Dimitrov and E. Lazarova, "Two-sided coalitional matchings," *Mathematical Social Sciences*, vol. 62, no. 1, pp. 46–54, 2011.

[118] A. Basit, G. A. S. Sidhu, A. Mahmood, and F. Gao, "Efficient and autonomous energy management techniques for the future smart homes," *IEEE Trans. Smart Grid*, vol. 8, no. 2, pp. 917–926, 2017.

[119] M. S. Ali, E. Hossain, and D. I. Kim, "Coordinated multi-point (comp) transmission in downlink multi-cell noma systems: Models and spectral efficiency performance," *arXiv preprint arXiv:1703.09255*, 2017.

[120] H. R. Ahmed, E. Sourour, and H. M. Elkamchouchi, "Analysis for noma-comp-jt global precoding matrix and irc receiver for lte-a," in *Proc. IEEE 13th Inter. Confer. Netw. Sensing Control (ICNSC)*, 2016, pp. 1–6.

[121] J. Ding, J. Cai, and C. Yi, "An improved coalition game approach for mimo-noma clustering integrating beamforming and power allocation," *IEEE Trans. Veh. Technol.*, vol. 68, no. 2, pp. 1672–1687, 2019.

[122] Y. Zeng and R. Zhang, "Energy-efficient uav communication with trajectory optimization," *IEEE Trans. Wireless Commun.*, vol. 16, no. 6, pp. 3747–3760, 2017.

[123] K. Cechlárová, P. Eirinakis, T. Fleiner, D. Magos, I. Mourtos, and E. Potpinková, "Pareto optimality in many-to-many matching problems," *Discrete Optimization*, vol. 14, pp. 160–169, 2014.

[124] D. Fan, F. Gao, G. Wang, Z. Zhong, and A. Nallanathan, "Angle domain signal processing-aided channel estimation for indoor 60-ghz tdd/fdd massive mimo systems," *IEEE J. Sel. Areas Commun.*, vol. 35, no. 9, pp. 1948–1961, 2017.

[125] H. Lin, F. Gao, S. Jin, and G. Y. Li, "A new view of multi-user hybrid massive mimo: Non-orthogonal angle division multiple access," *IEEE J. Sel. Areas Commun.*, vol. 35, no. 10, pp. 2268–2280, 2017.

[126] A. Orsino, D. Moltchanov, M. Gapeyenko, A. Samuylov, S. Andreev, L. Militano, G. Araniti, and Y. Koucheryavy, "Direct connection on the move: Characterization of user mobility in cellular-assisted d2d systems," *IEEE Veh. Technol. Mag.*, vol. 11, no. 3, pp. 38–48, 2016.

Publication List

[1] J. Ding and J. Cai, "Efficient mimo-noma clustering integrating joint beamforming and power allocation," in *Proc. IEEE GLOBECOME Conf.*, 2017.

[2] J. Ding, J. Cai and C. Yi, "An Improved Coalition Game Approach for MIMO-NOMA Clustering Integrating Beamforming and Power Allocation," *IEEE Trans. Veh. Technol.*, vol. 68, no. 2, pp. 1672-1687, 2019.

[3] J. Ding, and J. Cai, "Two-side Coalitional Matching Approach for Joint MIMO-NOMA Clustering and BS Selection in Multi-cell MIMO-NOMA Systems," *IEEE Trans. Wireless Commun.*, vol. 19, no. 3, pp. 2006-2021, 2020.

[4] J. Ding, and J. Cai, " UAV renting MIMO-NOMA Wireless Networks: A Contract Theoretic Approach," *submitted to IEEE Trans. Wireless Commun.*, (under review).

Appendix A

Proof in Chapter 3

A.1 MUs' Decoding Order

The decoding order is based on the principle that the power consumption should be minimized.

In MIMO-NOMA1, if signals are first decoded on MU_j, the optimal function is shown in (3.13). If signals are first decoded on MU_i, the optimal function can be rewritten as

$$f^{'}(\boldsymbol{w}_i^*, \boldsymbol{w}_j^*) = \left\|\boldsymbol{w}_j^*\right\|^2 + \|\boldsymbol{w}_i^*\|^2(\left|\boldsymbol{h}_i^H \boldsymbol{w}_j^*\right|^2\delta + 1). \tag{A.1}$$

By the same way, the optimal solution of (48) is $\lambda^{'} = \frac{-\left\|\boldsymbol{w}_j'\right\|^2 \boldsymbol{w}_i'\boldsymbol{w}_j'}{\left\|\boldsymbol{w}_i'\right\|^2\left\|\boldsymbol{w}_j'\right\|^2(1+\delta)-\delta\left|\boldsymbol{w}_i'\boldsymbol{w}_j'\right|^2}$ and $\beta' = -\frac{\boldsymbol{w}_j'\boldsymbol{w}_i'}{\left\|\boldsymbol{w}_j'\right\|^2}$. If $f(\boldsymbol{w}_i, \boldsymbol{w}_j) < f^{'}(\boldsymbol{w}_i^*, \boldsymbol{w}_j^*)$, we will adopt the decoding order in (3.13). To compare (3.13) and (A.1), we substitute the optimal solutions into each functions and let

$$\begin{aligned} &f(\boldsymbol{w}_i, \boldsymbol{w}_j) - f^{'}(\boldsymbol{w}_i^*, \boldsymbol{w}_j^*) \\ &= \frac{\delta\left|\boldsymbol{w}_i'\boldsymbol{w}_j'\right|^6}{(\left\|\boldsymbol{w}_i'\right\|^2\left\|\boldsymbol{w}_j'\right\|^2(1+\delta)-\delta\left|\boldsymbol{w}_i'\boldsymbol{w}_j'\right|^2)^2}(\left\|\boldsymbol{w}_i'\right\|^2 - \left\|\boldsymbol{w}_j'\right\|^2)(\delta\rho^2 - (1+\delta))(\rho^2 - 1), \end{aligned} \tag{A.2}$$

where $\rho = \frac{\left|\boldsymbol{w}_i'\boldsymbol{w}_j'\right|}{\left\|\boldsymbol{w}_i'\right\|\left\|\boldsymbol{w}_j'\right\|}$. Since coefficient $\rho < 1$, $\|\boldsymbol{w}_i'\|^2 < \left\|\boldsymbol{w}_j'\right\|^2$ is the necessary condition for $f(\boldsymbol{w}_i, \boldsymbol{w}_j) - f^{'}(\boldsymbol{w}_i^*, \boldsymbol{w}_j^*) < 0$.

For MIMO-NOMA2, we can employ the same way to prove that the decoding order of MU_i and MU_j cannot be changed. If signals are first decoded on MU_j, we take the optimal solution $\chi = -\frac{\boldsymbol{w}_i^{'}\boldsymbol{w}_j^{'}}{\left\|\boldsymbol{w}_i^{'}\right\|^2}$ into (3.35) and get

$$g(\chi) = (\left\|\boldsymbol{w}_i^{'}\right\|^2\chi^2 + 2\chi\boldsymbol{w}_i^{'}\boldsymbol{w}_j^{'} + \left\|\boldsymbol{w}_j^{'}\right\|^2) = \left\|\boldsymbol{w}_j^{'}\right\|^2 - \frac{\left|\boldsymbol{w}_i^{'}\boldsymbol{w}_j^{'}\right|^2}{\left\|\boldsymbol{w}_i^{'}\right\|^2}. \tag{A.3}$$

If signals are first decoded on MU_i, the optimal function will be

$$\min g^{'}(\beta^*, \lambda^*) = (\left\|\boldsymbol{w}_i^{'}\right\|^2\chi^{*2} + 2\chi^*\boldsymbol{w}_i^{'}\boldsymbol{w}_j^{'} + \left\|\boldsymbol{w}_j^{'}\right\|^2)((\delta+1) + \tfrac{1}{\chi^{*2}}).$$

As the same way, we obtain $\chi^* = -\frac{\boldsymbol{w}_i^{'}\boldsymbol{w}_j^{'}}{\left\|\boldsymbol{w}_i^{'}\right\|^2}$. The minimal power consumption is

$$g^{'}(\chi^*) = (1+\delta)(\left\|\boldsymbol{w}_j^{'}\right\|^2 - \frac{\left|\boldsymbol{w}_i^{'}\boldsymbol{w}_j^{'}\right|^2}{\left\|\boldsymbol{w}_i^{'}\right\|^2}). \tag{A.4}$$

Thus, NOMA decoding should be always started from the MU with a maximum $\left\|\boldsymbol{w}_j^{'}\right\|^2$. For a cluster with the size larger than 2, the decoding order still need to satisfy this condition.

A.2 Proof for the Nonexistence of $\frac{\delta+1}{\chi^2} \geq 1$

If $\frac{\delta+1}{\chi^2} \geq 1$, the approximated problem of (3.34) becomes

$$\begin{aligned} \min g(\chi) &= (\left\|\boldsymbol{w}_i^{'}\right\|^2\chi^2 + 2\chi\boldsymbol{w}_i^{'}\boldsymbol{w}_j^{'} + \left\|\boldsymbol{w}_j^{'}\right\|^2)\tfrac{\delta+1}{\chi^2} \\ &= (\delta+1)(\left\|\boldsymbol{w}_j^{'}\right\|^2 y^2 + 2\boldsymbol{w}_i^{'}\boldsymbol{w}_j^{'}y + \left\|\boldsymbol{w}_i^{'}\right\|^2). \end{aligned} \tag{A.5}$$

Since $\frac{\partial^2 g(y)}{\partial y^2} = 2\left\|\boldsymbol{w}_j^{'}\right\|^2 > 0$, the result can be obtained from $\frac{\partial g(y)}{\partial y} = 0$. Thus, $\chi^* = 1/y = -\frac{\left\|\boldsymbol{w}_j^{'}\right\|^2}{\boldsymbol{w}_i^{'}\boldsymbol{w}_j^{'}}$ is the approximate solution. Comparing χ^{*2} with χ^2 in (3.34), we get

$$\begin{aligned} \chi^2 &= \frac{(\boldsymbol{w}_i^{'}\boldsymbol{w}_j^{'})^2}{\left\|\boldsymbol{w}_i^{'}\right\|^4} = \frac{\left\|\boldsymbol{w}_j^{'}\right\|^2}{\left\|\boldsymbol{w}_i^{'}\right\|^2}\frac{(\boldsymbol{w}_i^{'}\boldsymbol{w}_j^{'})^2}{\left\|\boldsymbol{w}_i^{'}\right\|^2\left\|\boldsymbol{w}_j^{'}\right\|^2}, \\ \chi^{*2} &= \frac{\left\|\boldsymbol{w}_j^{'}\right\|^4}{(\boldsymbol{w}_i^{'}\boldsymbol{w}_j^{'})^2} = \frac{\left\|\boldsymbol{w}_j^{'}\right\|^2}{\left\|\boldsymbol{w}_i^{'}\right\|^2}\frac{\left\|\boldsymbol{w}_i^{'}\right\|^2\left\|\boldsymbol{w}_j^{'}\right\|^2}{(\boldsymbol{w}_i^{'}\boldsymbol{w}_j^{'})^2}. \end{aligned} \tag{A.6}$$

Since χ^2 is based on the assumption of $\frac{\delta+1}{\chi^2} \ll 1$, χ^2 must be larger than χ^{*2}. However, this conclusion is a contrast to the fact that $\frac{(\boldsymbol{w}_i^{'}\boldsymbol{w}_j^{'})^2}{\left\|\boldsymbol{w}_i^{'}\right\|^2\left\|\boldsymbol{w}_j^{'}\right\|^2} \leq 1$. Therefore, the solution for the case of $\frac{\delta+1}{\chi^2} \geq 1$ does not exist.

A.3 Explanation for the Correlation Coefficient Results

Fig. 3.5 shows that the power reduction is mainly positive associated with the absolute value of the real part of correlation coefficient while weakly associated with the imaginary part. This is caused by the ZF-beamforming and the proposed cluster beamforming strategy. Let

$$\rho_R = \frac{\boldsymbol{w}_i^{'}\boldsymbol{w}_j^{'}}{\left\|\boldsymbol{w}_i^{'}\right\|\left\|\boldsymbol{w}_j^{'}\right\|} = \frac{(\Re(\boldsymbol{w}_i^{'})\Re(\boldsymbol{w}_j^{'})+\Im(\boldsymbol{w}_i^{'})\Im(\boldsymbol{w}_j^{'}))}{\left\|\boldsymbol{w}_i^{'}\right\|\left\|\boldsymbol{w}_j^{'}\right\|}. \tag{A.7}$$

From (A.11) and (A.12), we notice that ΔP_k is positive related with ρ_R. Then, we need to prove ρ_R is mainly related with the real part of correlation coefficient R as shown in (A.10). According to (3.1), we have

$$\begin{aligned}\boldsymbol{W}^{'*}\boldsymbol{W}^{'} &= \begin{bmatrix} \left\|\boldsymbol{w}_1^{'}\right\|^2 & \boldsymbol{w}_1^{'*}\boldsymbol{w}_2^{'} & \dots & \boldsymbol{w}_1^{'*}\boldsymbol{w}_n^{'} \\ \vdots & \vdots & & \vdots \\ \boldsymbol{w}_n^{'*}\boldsymbol{w}_1^{'} & \boldsymbol{w}_n^{'*}\boldsymbol{w}_2^{'} & \dots & \left\|\boldsymbol{w}_n^{'}\right\|^2 \end{bmatrix} = Q^T(\boldsymbol{H}\boldsymbol{H}^{*})Q \\ &= \begin{bmatrix} \left\|\boldsymbol{h}_1^{'}\right\|^2 & \boldsymbol{h}_1^{'*}\boldsymbol{h}_2^{'} & \dots & \boldsymbol{h}_1^{'*}\boldsymbol{h}_n^{'} \\ \vdots & \vdots & & \vdots \\ \boldsymbol{h}_n^{'*}\boldsymbol{h}_1^{'} & \boldsymbol{h}_n^{'*}\boldsymbol{h}_2^{'} & \dots & \left\|\boldsymbol{h}_n^{'}\right\|^2 \end{bmatrix} Q^TQ, Q = (\boldsymbol{H}\boldsymbol{H}^{*})^{-1},\end{aligned}$$

where, $\boldsymbol{H}\boldsymbol{H}^{*}$ and Q are both symmetric matrixes, in which diagonal elements is real. Thus, Q^TQ is a real symmetric matrix. We notice that only off-diagonal elements in Q are related with the imaginary part of correlation coefficient, and which is smaller than the value of diagonal elements. Due to $\boldsymbol{w}_i^{'}\boldsymbol{w}_j^{'}$ is the real part of $\boldsymbol{w}_i^{'*}\boldsymbol{w}_j^{'}$, which is corresponding to the real part of $[\boldsymbol{h}_i^{'*}\boldsymbol{h}_1^{'}, ..., \boldsymbol{h}_i^{'*}\boldsymbol{h}_n^{'}]$, ρ_R is mainly related with the real part of correlation coefficient.

Here, we give a two-antenna and two-MU example as a special case for discussion. We assume that two MUs (i and j) form a MIMO-NOMA1 cluster with channel gains $[a+Bi, D+ei]$ and $[a+bi, d+ei]$, respectively. Based on (3.1), the beamforming vectors $\boldsymbol{w}_i^{'}$ and $\boldsymbol{w}_j^{'}$ in the OM state can be obtained by

$$\begin{cases} w_{i1}^{'} = (d-D)(ad+be)/[F^2+G^2], \\ w_{i2}^{'} = (eF-dG)/[F^2+G^2], \\ w_{i3}^{'} = (aF+bG)/[F^2+G^2], \\ w_{i4}^{'} = (b-B)(ad+be)/[F^2+G^2], \end{cases} \begin{cases} w_{j1}^{'} = (D-d)(aD+Be)/[F^2+G^2], \\ w_{j2}^{'} = (-eF+DG)/[F^2+G^2], \\ w_{j3}^{'} = (-aF-bG)/[F^2+G^2], \\ w_{j4}^{'} = (B-b)(aD+Be)/[F^2+G^2], \end{cases} \tag{A.8}$$

where $F = a(d-D)+e(b-B)$ and $G = dB-bD$. The channel gain correlation coefficient between MU_1 and MU_2 (denoted by ρ), $\|\boldsymbol{w}_i'\|^2$, $\left\|\boldsymbol{w}_j'\right\|^2$ and $\left|\boldsymbol{w}_i'\boldsymbol{w}_j'\right|^2$ are calculated as

$$\begin{aligned} &\rho = \tfrac{(a^2+e^2+Bb+Dd)+(a(b-B)-e(d-D))i}{\sqrt{a^2+e^2+b^2+d^2}\sqrt{a^2+e^2+B^2+D^2}} = R + \tfrac{(a(b-B)-e(d-D))i}{\sqrt{a^2+e^2+b^2+d^2}\sqrt{a^2+e^2+B^2+D^2}}, \\ &\left\|\boldsymbol{w}_i^{'}\right\|^2 = \tfrac{(a^2+e^2+B^2+D^2)(a^2(d-D)^2+e^2(b-B)^2+(Bd-Db)^2)}{((a(d-D)+e(b-B))^2+(Bd-Db)^2)^2} = \tfrac{\|\boldsymbol{h}_j\|^2\gamma}{((a(d-D)+e(b-B))^2+(Bd-Db)^2)}, \\ &\left\|\boldsymbol{w}_j^{'}\right\|^2 = \tfrac{(a^2+e^2+b^2+d^2)(a^2(d-D)^2+e^2(b-B)^2+(Bd-Db)^2)}{((a(d-D)+e(b-B))^2+(Bd-Db)^2)^2} = \tfrac{\|\boldsymbol{h}_i\|^2\gamma}{((a(d-D)+e(b-B))^2+(Bd-Db)^2)}, \\ &\tfrac{\left|\boldsymbol{w}_i^{'}\boldsymbol{w}_j^{'}\right|^2}{\left\|\boldsymbol{w}_i^{'}\right\|^2\left\|\boldsymbol{w}_j^{'}\right\|^2} = \tfrac{R^2}{\gamma^2}, \end{aligned} \tag{A.9}$$

where $R = \frac{(a^2+e^2+Bb+Dd)}{\sqrt{a^2+e^2+b^2+d^2}\sqrt{a^2+e^2+B^2+D^2}}$ and $\gamma = \frac{(a^2(d-D)^2+e^2(b-B)^2+(Bd-Db)^2)}{((a(d-D)+e(b-B))^2+(Bd-Db)^2)} < 1$. Note that R is the real part of correlation coefficient, γ is a variable which is related to $e(b-B)$ and $a(d-D)$. If they are equal to zero, $\|\boldsymbol{w}_i'\|^2$ and $\left\|\boldsymbol{w}_j'\right\|^2$ are both infinite. However, in the simulation of Fig. 3.4, radius of two MUs are unchanged, and channel gains in 40 antennas are generated by random valuables following $CN(0,1)$. It indicates that $\|\boldsymbol{h}_i\|^2$ and $\|\boldsymbol{h}_j\|^2$ can only be changed in a small range. Since MU j is first decoded, we have $(D^2+B^2) > (d^2+b^2)$ by condition $\|\boldsymbol{w}_i{'}\|^2 < \|\boldsymbol{w}_j{'}\|^2$. Then, we take results of λ and β into (3.12) as

$$\begin{aligned} &\Delta P_k = \rho_R^2\left\|\boldsymbol{w}_j^{'}\right\|^2 + \tfrac{\left\|\boldsymbol{w}_i^{'}\right\|^2}{\frac{1}{\rho_R^2}(1+\delta)-\delta} = R^2(\|\boldsymbol{h}_i\|^2+\|\boldsymbol{h}_j\|^2\theta)\tfrac{1}{(a^2(d-D)^2+e^2(b-B)^2+(Bd-Db)^2)}, \\ &x = \tfrac{\left|\boldsymbol{w}_i^{'}\boldsymbol{w}_j^{'}\right|^2}{\left\|\boldsymbol{w}_i^{'}\right\|^2\left\|\boldsymbol{w}_j^{'}\right\|^2}, \theta = \tfrac{x(\delta-2)+(\delta+1)}{(1+\delta-x)^2} < 1. \end{aligned} \tag{A.10}$$

From (A.11), we notice that ΔP_k is directly related to the real part of correlation coefficient R^2 while weakly related to the imaginary part of correlation coefficient through

$(a^2(d-D)^2+e^2(b-B)^2+(Bd-Db)^2)$. Based on this structure, we can explain that, first of all, MIMO-NOMA1 is always better than MIMO-OMA as $\Delta P_k > 0$. However, not all beneficial MIMO-NOMA1 cluster has $\Delta P_k > 0.01w$. Therefore, the gap in Fig. 3.4(c) is larger than that in Fig. 3.4(a) if we reduce R_2 and make $\|\boldsymbol{h}_j\|^2$ small. Second, ΔP_k increases if we increase R_1 or R_2, which can be observed from comparing the value of color bar between Figs. 3.4(a) and (c). Last, the influence of the imaginary part increases with R^2.

We conduct the same example for MIMO-NOMA2. In this case, the channel gain correlation coefficient between MU_1 and MU_2 (denoted as ρ), $\|\boldsymbol{w}_i'\|^2$ and $\left\|\boldsymbol{w}_j'\right\|^2$ are the same as in (A.9). Then, if we assume $\lambda = 1$ and $\beta = -\frac{\boldsymbol{w}_i'\boldsymbol{w}_j'}{\|\boldsymbol{w}_i'\|^2}$, the cluster beamforming vector $\|\boldsymbol{v}_k\|^2$ and power reduction can be calculated as

$$\begin{aligned}
\|\boldsymbol{v}_k\|^2 &= \left\|\boldsymbol{w}_j'\right\|^2 - \frac{\left|\boldsymbol{w}_i'\boldsymbol{w}_j'\right|^2}{\left\|\boldsymbol{w}_i'\right\|^2}, \\
\Delta P_k &= \left\|\boldsymbol{w}_j'\right\|^2 \rho_R^2 + \left\|\boldsymbol{w}_i'\right\|^2 (\delta + 2 - \tfrac{\delta+1}{\rho_R^2}) \\
&= \tfrac{\sigma^2\delta}{(a^2(d-D)^2+e^2(b-B)^2+(Bd-Db)^2)} (\tfrac{R^2}{\gamma}\|\boldsymbol{h}_i\|^2 + ((2+\delta)\gamma - (1+\delta)\gamma\tfrac{\gamma^2}{R^2})\|\boldsymbol{h}_j\|^2).
\end{aligned} \tag{A.11}$$

Note that if $((2+\delta)\gamma - (1+\delta)\gamma\frac{\gamma^2}{R^2}) > 0$, we have $\frac{\gamma^2}{R^2} < 2$ which makes $\rho > 1/\sqrt{2}$. In Fig. 3.4(b), since $\rho < 0.6$, we have $\frac{\gamma^2}{R^2} > 2$ and $((2+\delta)\gamma - (1+\delta)\gamma\frac{\gamma^2}{R^2}) < -\delta\gamma$. Moreover, since $\frac{R^2}{\gamma} < \gamma < 1$ and $\delta > 1$, $\|\boldsymbol{h}_i\|^2$ should be larger than $\|\boldsymbol{h}_j\|^2$ to make $\Delta P_k > 0$, which indicates that a beneficial MIMO-NOMA2 cluster should include both a cell-center MU and a cell-edge MU. Furthermore, if we increase $|R|$, ΔP_k will be increased more efficiently than that when we decrease γ. For the case of a cluster with the size larger than 2, according to (3.26), we will have

$$\left\|\boldsymbol{w}_l'\right\|^2 - \|\boldsymbol{w}_l\|^2 = \left\|\boldsymbol{w}_l'\right\|^2 \frac{1+\rho_R^2}{1-\rho_R^2}(\rho_{R2}^2 + \rho_{R3}^2 - 2\rho_R\rho_{R2}\rho_{R3}). \tag{A.12}$$

where, ρ_{R2} (ρ_{R3}) is calculated as the same formula in (A.7) between i and l (j and l).

A.4 SIC Decoding Conditions

The achievable rate (or SINR) should be larger than a predefined threshold $\zeta\delta$ in order to ensure successful SIC decoding [109]. We transform (3.8d) into a constraint which can be judged by power coefficients.

For MIMO-NOMA1, the condition to make x_j successfully decode on MU i is that $\gamma_i^j > \zeta\delta = \zeta\gamma_i$. Through taking the beamforming results into this inequality, we will have $\lambda^2 > (1+\delta)\zeta$ in a 2-MU cluster. Similarly, for an n-MU cluster, if $i, j \in \{1, 2, ..., n\}$ and $i < j$, the signal from MU $j-1$ (and j) will be decoded at MU i, and the SINR after SIC operation can be denoted as

$$\gamma_i^{j-1} = \frac{\left|\boldsymbol{h}_i^H \boldsymbol{w}_{j-1}\sqrt{p_{j-1}}\right|^2}{(\sum_{\epsilon=1}^{j-2}\left|\boldsymbol{h}_i^H \boldsymbol{w}_\epsilon\sqrt{p_\epsilon}\right|^2+\sigma^2)},$$
$$\gamma_i^j = \frac{\left|\boldsymbol{h}_i^H \boldsymbol{w}_j\sqrt{p_j}\right|^2}{(\sum_{\epsilon=1}^{j-1}\left|\boldsymbol{h}_i^H \boldsymbol{w}_\epsilon\sqrt{p_\epsilon}\right|^2+\sigma^2)} = \frac{\left|\boldsymbol{h}_i^H \boldsymbol{w}_j\sqrt{p_j}\right|^2}{(\frac{1}{\gamma_i^{j-1}}+1)\left|\boldsymbol{h}_i^H \boldsymbol{w}_{j-1}\sqrt{p_{j-1}}\right|^2} > \frac{\left|\boldsymbol{h}_i^H \boldsymbol{w}_j\right|^2}{\left|\boldsymbol{h}_i^H \boldsymbol{w}_{j-1}\right|^2}\frac{\gamma_i^{j-1}}{1+\gamma_i^{j-1}}.$$

Therefore, if $\gamma_i^j > \gamma_i^{j-1}$, we have $\left|\boldsymbol{h}_i^H \boldsymbol{w}_j\right|^2 > (1+\gamma_i^{j-1})\left|\boldsymbol{h}_i^H \boldsymbol{w}_{j-1}\right|^2$ for any $i+2 < j < n$. If $\gamma_i^j > \zeta\delta$, we have $\left|\boldsymbol{h}_i^H \boldsymbol{w}_j\right|^2 > \zeta\delta(1+\frac{1}{\gamma_i^{j-1}})\left|\boldsymbol{h}_i^H \boldsymbol{w}_{j-1}\right|^2$. Then, we observe that

$$\gamma_i = \frac{p_i}{(\sum_{\epsilon=1}^{i-1}\left|\boldsymbol{h}_j^H \boldsymbol{w}_\epsilon\sqrt{p_\epsilon}\right|^2+\sigma^2)} = \delta,$$
$$\gamma_i^{i+1} = \frac{\left|\boldsymbol{h}_i^H \boldsymbol{w}_{i+1}\sqrt{p_{i+1}}\right|^2}{(p_i+\sum_{\epsilon=1}^{i-1}\left|\boldsymbol{h}_j^H \boldsymbol{w}_\epsilon\sqrt{p_\epsilon}\right|^2+\sigma^2)}, = \frac{\left|\boldsymbol{h}_i^H \boldsymbol{w}_{i+1}\sqrt{p_{i+1}}\right|^2}{p_i(1+\frac{1}{\delta})} > \frac{\left|\boldsymbol{h}_i^H \boldsymbol{w}_{i+1}\right|^2}{(1+\frac{1}{\delta})} > \zeta\delta.$$

Therefore, we have $\left|\boldsymbol{h}_i^H \boldsymbol{w}_{i+1}\right|^2 > (1+\delta)\zeta$. Taking a 3-MU cluster for example, the condition for successful decoding is that $(1+\delta)\zeta < \lambda_4^2, \lambda_1^2$ and $\lambda_1^2(1+\frac{1}{\gamma_i^j})\zeta\delta < \lambda_2^2$.

For MIMO-NOMA2, the condition for successful decoding is that $\frac{\mu_{\epsilon+1}}{\mu_\epsilon} > \min\{\zeta\delta(1+\frac{1}{\gamma_1^\epsilon}),$ $..., \zeta\delta(1+\frac{1}{\gamma_{\epsilon-1}^\epsilon}), \zeta(1+\delta)\}$.

Appendix B

Proof in Chapter 4

B.1 MUs' Decoding Order

The decoding order is based on the principle that the power consumption should be minimized.

For a 2-MU cluster, such as $g_{l_d} = \{1, 2\}$, by taking (4.17) and (4.18) back to (4.16), we obtain the power reduction of this cluster. Similarly, we can obtain the power reduction of $g^{'}_{l_d} = \{2, 1\}$. Then, the difference between them can be denoted as

$$f(g_{l_d}) - f(g^{'}_{l_d}) = \frac{\delta\left|\boldsymbol{w}^{'}_{l1}\boldsymbol{w}^{'}_{l2}\right|^6}{(\left\|\boldsymbol{w}^{'}_{l1}\right\|^2\left\|\boldsymbol{w}^{'}_{l2}\right\|^2(1+\delta)-\delta\left|\boldsymbol{w}^{'}_{l1}\boldsymbol{w}^{'}_{l2}\right|^2)^2}(\left\|\boldsymbol{w}^{'}_{l1}\right\|^2-\left\|\boldsymbol{w}^{'}_{l2}\right\|^2)(\delta\rho^2-(1+\delta))(\rho^2-1), \tag{B.1}$$

where $\rho=\frac{\left|\boldsymbol{w}^{'}_{l1}\boldsymbol{w}^{'}_{l2}\right|}{\left\|\boldsymbol{w}^{'}_{l1}\right\|\left\|\boldsymbol{w}^{'}_{l2}\right\|}$. Since $\rho<1$, $\left\|\boldsymbol{w}^{'}_{l1}\right\|^2<\left\|\boldsymbol{w}^{'}_{l2}\right\|^2$ is the necessary condition for $f(g_{l_d})-f^{'}(g^{'}_{l_d})<0$.

For a n-MU cluster, we focus on $\|\boldsymbol{w}_{li}\|^2$ and $\|\boldsymbol{w}_{lj}\|^2$ with $\left\|\boldsymbol{w}^{'}_{lj}\right\|^2>\left\|\boldsymbol{w}^{'}_{li}\right\|^2$, $i,j \in 1, 2, ...n$.

If $j=n$, according to (14), we have

$$\|\boldsymbol{w}_{lj}\|^2 = \left\|\boldsymbol{w}'_{lj}\right\|^2 - BA^{-1}B^H$$
$$= \left\|\boldsymbol{w}'_{lj}\right\|^2(1 - [\boldsymbol{w}'_{l1}, \boldsymbol{w}'_{l2}, ..., \boldsymbol{w}'_{ln-1}]A^{-1}[\boldsymbol{w}'_{l1}, \boldsymbol{w}'_{l2}, ..., \boldsymbol{w}'_{ln-1}]^H),$$
$$\|\boldsymbol{w}_{li}\|^2 = \left\|\boldsymbol{w}'_{li}\right\|^2(1 - [\boldsymbol{w}'_{l1}, ..., \boldsymbol{w}'_{li-1}, \boldsymbol{w}'_{li-1}, ..., \boldsymbol{w}'_{ln}]A'^{-1}[\boldsymbol{w}'_{l1}, ..., \boldsymbol{w}'_{li-1}, \boldsymbol{w}'_{li-1}, ..., \boldsymbol{w}'_{ln}]^H).$$

If the order of MUs i and j are changed, $|A|$ will be increased while $|A'|$ will be decreased (refer to (4.22) and (4.23)). Therefore, $\|\boldsymbol{w}_{li}\|^2 + \|\boldsymbol{w}_{lj}\|^2$ will be increased, so that the power consumption will be increased. Thus, the decoding order should be depend on a descending order of the ℓ_2-norm square value of beamforming vectors.

B.2 Beamforming Properties

Since the beamforming vectors are obtained from (4.1), the ℓ_2-norm square value of MU 1's beamforming vector on BS l can be denoted by $G(\boldsymbol{w}_{l1}) = \|\boldsymbol{w}_{l1}\|^2$, which is the first term of $\boldsymbol{W}_l^*\boldsymbol{W}_l$. Let the total number of MUs on BS l be n_l. Through derivation, we will obtain

$$G(\boldsymbol{w}_{l1}) = \begin{vmatrix} |\boldsymbol{h}_{l2}|^2 & ... & \boldsymbol{h}_{l2}^H\boldsymbol{h}_{ln_l} \\ \vdots & & \vdots \\ \boldsymbol{h}_{l2}^H\boldsymbol{h}_{ln_l} & ... & |\boldsymbol{h}_{ln_l}|^2 \end{vmatrix} / |\theta|,$$
$$\text{where} \quad \theta = \begin{bmatrix} |\boldsymbol{h}_{l1}|^2 & \boldsymbol{h}_{l1}^H\boldsymbol{h}_{l2} & ... & \boldsymbol{h}_{l1}^H\boldsymbol{h}_{ln_l} \\ \vdots & \vdots & & \vdots \\ \boldsymbol{h}_{l1}^H\boldsymbol{h}_{ln_l} & \boldsymbol{h}_{l2}^H\boldsymbol{h}_{ln_l} & ... & |\boldsymbol{h}_{ln_l}|^2 \end{bmatrix}. \tag{B.2}$$

Therefore, $G(\boldsymbol{w}_{l1})$ increases with more MUs are selected by this BS.

B.3 Max-min Fairness

The objective is to maximize the minimum achievable data rate. In our case, the BS with the minimum data rate has high priority to let MU join or leave it's group to improve the data rate. Then, the optimization problem can be formulated as

$$\boldsymbol{O}_3 : \max_{\boldsymbol{W},\boldsymbol{p}} \min_{l \in L} \sum_{i=1}^{n_l} R_{li}(\boldsymbol{w}_{li}, p_{li}), \tag{B.3a}$$

$$\text{s.t} \ \ \text{(4.7b)-(4.7e)}. \tag{B.3b}$$

B.4 Two-stage Approach

The BS selection and MIMO-NOMA clustering are separated into two sub-optimization problems and independently optimized in two stages. In the first stage, each MU will select a BS to maximize it's data rate in the OMA state. We defined a BS selection of a certain MU is beneficial if the sum data rate can be improved through accessing this MU to the selected BS. The solution procedure is described as follows.

1) Initialization Each MU selects the nearest BS as an initial accessed BS.

2) Iteration

- **Step 1:** Update the states of all BSs and MUs (i.e., BS selections and MU channel state information), and calculate the achievable data rate for each MU in the OMA state. Find all beneficial selections for each BS and arrange these selections into a set $R = \{r_1, r_2, ..., r_m\}$ with the decreasing order of the sum data rate.
- **Step 2:** If set R is empty, stop the iteration. Otherwise, select the first component in R, i.e., r_1, and go back to step 1.

In the second stage, each BS further improves the data rate through forming NOMA

clusters independently. The initial strategies of all MUs are in the outside of any NOMA cluster.

- **Step 1:** Through employing coalition game approach on each BS, MUs will decide to join or leave a MIMO-NOMA cluster for utility improvement (i.e., change its strategy). After system convergence, each BS ($i \in L$) will obtain a MIMO-NOMA clustering solution which satisfies Pareto optimum.
- **Step 2:** If no MU changes it's strategy in step 1, stop the iteration. Otherwise, update the states of all BSs and MUs, and go back to step 1.

B.5 Max-min Approach

This approach is proposed for the problem with the objective of max-min fairness. The coalition game approach is employed to conduct MIMO-NOMA clustering and calculate the BS data rate. We consider a strategy of MU i (such as, MU i may leave from BS l_1 and join BS l_2) is beneficial, if it satisfies: i) the data rate of MU i is increased; and ii) the data rate of BS l_1 is increased. Let $R_{l_1 i}$ and $R_{l_2 i}$ denote the data rates of BSs l_1 and l_2 when MU i is served by BS l_1, and $R'_{l_1 i}$ and $R'_{l_2 i}$ denote the corresponding data rates when MU i is served by BS l_2. The conditions of a beneficial strategy include $R_{l_1 i} < R'_{l_2 i}$ and $R_{l_1 i} < R'_{l_1 i}$.

1) Initialization

Each MU selects the nearest BS as the initial accessed BS. Employ the coalition game approach and the approach in Table 4.1 to evaluate the data rate of each BS.

2) Iteration

- **Step 1:** Update the states of all BSs and MUs. Arrange all BSs into a set $B = \{l_1, l_2, ..., l_L\}$ with the increasing order of the sum data rate, and define $f = 1$.
- **Step 2:** Find all beneficial strategies for MUs served by BS l_f. Arrange those strategies into a set $R_{l_f} = \{r_1, r_2, ..., r_{m_l}\}$ by the decreasing order of $R'_{l_f i}$. If

$R'_{l_f i} = R'_{l_f j}$ for MU i and MU j, the order of them follows $R'_{l_2 i}$ and $R'_{l_3 j}$(l_2, $l_3 \in B - l_f$).

- **Step 3:** If R_{l_f} is not empty, adopt r_1, and go back to step 1. Otherwise, $f = f + 1$. If $f = L$ and R_{l_f} is empty, stop the iteration.

B.6 Greedy Approach

The greedy approach is employed as the opposite of BS cooperation strategies, and each BS will only accept the decision which can improve it's sum data rate. Thus, to make MU i leave BS l_1 and joint BS l_2, the necessary condition is that the utilities of two BSs are increased, i.e., $U_{l_1 i}>0$ and $U_{l_2 i}>0$, which is different from other approaches. The approach is described as follows.

1) Initialization

All MUs will select the nearest BS as the initial accessed BS. Update the states of all BSs and MUs, and calculate the utility of each MU.

2) Iteration

- **Step 1:** For each MU ($l_2 \in L$), find all beneficial MU strategies. Then, select the strategy with the largest utility $U_{l_2 i}$, and send the request to it's preferred BS, such as, BS l_1. If no beneficial MU strategy is found in all BSs, stop the iteration.

- **Step 2:** For each BS ($l_1 \in L$), find the request with the highest utility, such as $U_{l_1 i}$ and accept it. If no request is received by any BS, stop the iteration. Otherwise, go back to step 1.

B.7 SIC Decoding Conditions

The achievable rate (or SINR) should be larger than a predefined threshold ζ in order to ensure successful SIC decoding [109]. For an n-MU cluster served by BS l, if $i, j \in \{1, ..., n\}$ and $i < j$, the signal from MU $j-1$ (and j) will be decoded at MU i, and the SINR after SIC operation can be denoted as

$$\gamma_{li}^{j-1} = \frac{\left|\boldsymbol{h}_{li}^H \boldsymbol{w}_{lj-1}\sqrt{p_{j-1}}\right|^2}{(\sum_{\epsilon=1}^{j-2}\left|\boldsymbol{h}_{li}^H \boldsymbol{w}_{l\epsilon}\sqrt{p_\epsilon}\right|^2 + \sum\limits_{u\neq i}\left|\sum\limits_{j\in B-l}\boldsymbol{h}_{ji}^H \boldsymbol{w}_{ju}\sqrt{p_{ju}}x_u\right|^2 + \sigma^2)},$$

$$\gamma_{li}^{j} = \frac{\left|\boldsymbol{h}_{li}^H \boldsymbol{w}_{lj}\sqrt{p_j}\right|^2}{(\sum_{\epsilon=1}^{j-1}\left|\boldsymbol{h}_{li}^H \boldsymbol{w}_{l\epsilon}\sqrt{p_{l\epsilon}}\right|^2 + \sum\limits_{u\neq i}\left|\sum\limits_{j\in B-l}\boldsymbol{h}_{ji}^H \boldsymbol{w}_{ju}\sqrt{p_{ju}}x_u\right|^2 + \sigma^2)}$$

$$= \frac{\left|\boldsymbol{h}_{li}^H \boldsymbol{w}_{lj}\sqrt{p_j}\right|^2}{(\frac{1}{\gamma_i^{j-1}}+1)\left|\boldsymbol{h}_{li}^H \boldsymbol{w}_{lj-1}\sqrt{p_{j-1}}\right|^2} > \frac{\left|\boldsymbol{h}_{li}^H \boldsymbol{w}_{lj}\right|^2}{\left|\boldsymbol{h}_{li}^H \boldsymbol{w}_{lj-1}\right|^2}\frac{\gamma_i^{j-1}}{1+\gamma_i^{j-1}}.$$

Therefore, if $\gamma_{li}^{j} > \gamma_{li}^{j-1}$, we have $\left|\boldsymbol{h}_{li}^H \boldsymbol{w}_{lj}\right|^2 > (1+\gamma_{li}^{j-1})\left|\boldsymbol{h}_{li}^H \boldsymbol{w}_{lj-1}\right|^2$ for any $i+2 < j < n$. Similarly,

$$\gamma_{li}^{i+1} = \frac{\left|\boldsymbol{h}_{li}^H \boldsymbol{w}_{li+1}\sqrt{p_{i+1}}\right|^2}{p_i(1+\frac{1}{\delta})} > \frac{\left|\boldsymbol{h}_{li}^H \boldsymbol{w}_{li+1}\right|^2}{(1+\frac{1}{\delta})} > \delta.$$

Therefore, the decoding conditions are $\lambda_{ii+1}^2 > (1+\delta)$ and $\lambda_{ij}^2 > (1+\gamma_{li}^{j-1})\lambda_{ij-1}^2$. Taking a 3-MU cluster for example, the condition for successful decoding is that $(1+\delta) < \lambda_4^2$, λ_1^2 and $\lambda_1^2(1+\gamma_{li}^{j}) < \lambda_2^2$.

Appendix C

Proof in Chapter 6

C.1 Derivation of Formula (6.10)

Here, we show the progress of deriving equation (6.10). For an easy understanding, we firstly give three basic equation transformations as follows, which includes a complex number $\omega = a + bi$, and two complex vectors $\boldsymbol{A} = [c_1 + d_1 i, c_2 + d_2 i]^T$, $\boldsymbol{B} = [e_1 + f_1 i, e_2 + f_2 i]^T$.

$$\|\omega \boldsymbol{A}\|^2 = \left\| \begin{array}{c} (a+bi) * (c_1 + d_1 i) \\ (a+bi) * (c_2 + d_2 i) \end{array} \right\|^2 = (a^2+b^2)(c_1^2 + d_1^2 + c_2^2 + d_2^2) = \|\omega\|^2 \|\boldsymbol{A}\|^2,$$

$$(\omega \boldsymbol{A})\boldsymbol{B} = \left[\begin{array}{c} (a+bi) * (c_1 + d_1 i) \\ (a+bi) * (c_2 + d_2 i) \end{array} \right] \left[\begin{array}{c} e_1 + f_1 i \\ e_2 + f_2 i \end{array} \right] = a\boldsymbol{A}\boldsymbol{B} + b\boldsymbol{A}\check{\boldsymbol{B}} = a\boldsymbol{A}\boldsymbol{B} - b\check{\boldsymbol{A}}\boldsymbol{B},$$

$$(\omega \boldsymbol{A})(\omega \boldsymbol{B}) = a\boldsymbol{A}(\omega \boldsymbol{B}) + b\boldsymbol{A}(\omega \check{\boldsymbol{B}}) = a^2 \boldsymbol{B}\boldsymbol{A} + ab\boldsymbol{B}\check{\boldsymbol{A}} - ab\boldsymbol{B}\check{\boldsymbol{A}} + b^2 \boldsymbol{B}\boldsymbol{A} = (a^2+b^2)\boldsymbol{B}\boldsymbol{A}.$$

According to these transformations, we can derive formula (6.10). Take $\|\boldsymbol{w}_1^*\|^2$ for example,

$$\begin{aligned} &\|\boldsymbol{w}_1^*\|^2 = \left\|\boldsymbol{w}_1 - h_{l1}^{'} w_{l1}^{'} \boldsymbol{w}_1 - ... h_{lm}^{'} w_{lm}^{'} \boldsymbol{w}_m\right\|^2 = \|\boldsymbol{w}_1\|^2 + \left\|h_{l1}^{'} w_{l1}^{'} \boldsymbol{w}_1\right\|^2 + ... \left\|h_{lm}^{'} w_{lm}^{'} \boldsymbol{w}_m\right\|^2 \\ &-2(h_{l1}^{'} w_{l1}^{'} \boldsymbol{w}_1)\boldsymbol{w}_1 - ... 2(h_{lm}^{'} w_{l1}^{'} \boldsymbol{w}_m)\boldsymbol{w}_1 + ... 2(h_{lm-1}^{'} w_{l1}^{'} \boldsymbol{w}_{m-1})(h_{lm}^{'} w_{l1}^{'} \boldsymbol{w}_m) \qquad \text{(C.1)} \\ &= \|\boldsymbol{w}_1\|^2 + (a_{l1}^2 + b_{l1}^2)\|\boldsymbol{B}_l\|^2 - 2(a_{l1}\boldsymbol{w}_1 \boldsymbol{B}_l - b_{l1}\boldsymbol{w}_1 \check{\boldsymbol{B}}_l). \end{aligned}$$

C.2 Proof of $\triangle P_{li} > \triangle P_{li}{}'$

In case of many-to-one matching game, we assume MU i has been selected and has $\triangle P_{li} = \frac{(\boldsymbol{w}_i\boldsymbol{B}_l)^2+(\boldsymbol{w}_i\check{\boldsymbol{B}}_l)^2}{\|\boldsymbol{B}_l\|^2}(I_i+\sigma^2)\delta_i$. If MU j is also being selected after MU i, $\boldsymbol{B}_l$ is changed to be $\boldsymbol{B}'_l = \boldsymbol{B}_l + h'_{lj}\boldsymbol{w}_j$, and $\triangle P_{li}$ will be changed to be $\triangle P'_{li}$ as

$$\begin{aligned}\triangle P'_{li} = \frac{(\boldsymbol{w}_i\boldsymbol{B}'_l)^2+(\boldsymbol{w}_i\check{\boldsymbol{B}}'_l)^2}{\|\boldsymbol{B}'_l\|^2}(I_i+\sigma^2)\delta_i = \big((\boldsymbol{w}_i\boldsymbol{B}_l)^2+(\boldsymbol{w}_i\check{\boldsymbol{B}}_l)^2+(a^2+b^2)((\boldsymbol{w}_i\boldsymbol{w}_j)^2+(\check{\boldsymbol{w}}_i\boldsymbol{w}_j)^2)+\\ 2(a((\boldsymbol{w}_i\boldsymbol{B}_l)(\boldsymbol{w}_i\boldsymbol{w}_j)+(\check{\boldsymbol{w}}_i\boldsymbol{B}_l)(\check{\boldsymbol{w}}_i\boldsymbol{w}_j))+b((\boldsymbol{w}_i\boldsymbol{B}_l)(\check{\boldsymbol{w}}_i\boldsymbol{w}_j)+(\boldsymbol{w}_i\check{\boldsymbol{B}}_l)(\boldsymbol{w}_i\boldsymbol{w}_j)))\big)\\ (I_i+\sigma^2)\delta_i/\left(\|\boldsymbol{B}_l\|^2+(a^2+b^2)\|\boldsymbol{w}_j\|^2+2(a\boldsymbol{w}_j\boldsymbol{B}_l+b\boldsymbol{w}_j\check{\boldsymbol{B}}_l)\right).\end{aligned} \tag{C.2}$$

Since

$$\begin{aligned}&(a^2+b^2)((\boldsymbol{w}_i\boldsymbol{w}_j)^2+(\check{\boldsymbol{w}}_i\boldsymbol{w}_j)^2) < (a^2+b^2)\|\boldsymbol{w}_j\|^2\|\boldsymbol{w}_i\|^2,\\ &2a((\boldsymbol{w}_i\boldsymbol{B}_l)(\boldsymbol{w}_i\boldsymbol{w}_j)+(\check{\boldsymbol{w}}_i\boldsymbol{B}_l)(\check{\boldsymbol{w}}_i\boldsymbol{w}_j)) < 2a\boldsymbol{w}_j\boldsymbol{B}_l\|\boldsymbol{w}_i\|^2 \; and\\ &2b((\boldsymbol{w}_i\boldsymbol{B}_l)(\check{\boldsymbol{w}}_i\boldsymbol{w}_j)+(\boldsymbol{w}_i\check{\boldsymbol{B}}_l)(\boldsymbol{w}_i\boldsymbol{w}_j)) < 2b\boldsymbol{w}_j\check{\boldsymbol{B}}_l\|\boldsymbol{w}_i\|^2,\end{aligned}$$

we have $\triangle P'_{li} < \triangle P_{li}$. Thus, we can conclude that $\triangle P_{li}$ will be decreased with more MUs joining this UAV group.

C.3 MU Decoding Order

The decoding order of a MU cluster aims to maximize the power reduction. For a 2-MU NOMA cluster $\mathcal{G}_{c_1}=\{1,2\}$ and $\mathcal{G}'_{c_1}=\{2,1\}$, the power reduction can be respectively transformed to be

$$\begin{aligned}\triangle P_{\mathcal{G}_{c_1}} &= \left(\frac{\delta_1 In_1}{\|\boldsymbol{w}_2\|^2+\frac{\delta_2}{\|\boldsymbol{w}_1\|^2}(\|\boldsymbol{w}_1\|^2\|\boldsymbol{w}_2\|^2-|\boldsymbol{w}_1\boldsymbol{w}_2|^2)}+\frac{\delta_2 In_2}{\|\boldsymbol{w}_1\|^2}\right)|\boldsymbol{w}_1\boldsymbol{w}_2|^2,\\ \triangle P_{\mathcal{G}'_{c_1}} &= \left(\frac{\delta_2 In_2}{\|\boldsymbol{w}_1\|^2+\frac{\delta_1}{\|\boldsymbol{w}_2\|^2}(\|\boldsymbol{w}_1\|^2\|\boldsymbol{w}_2\|^2-|\boldsymbol{w}_1\boldsymbol{w}_2|^2)}+\frac{\delta_1 In_1}{\|\boldsymbol{w}_2\|^2}\right)|\boldsymbol{w}_1\boldsymbol{w}_2|^2.\end{aligned}$$

To ensure $\triangle P_{\mathcal{G}_{c_1}} > \triangle P_{\mathcal{G}'_{c_1}}$, we have $In_2\|\boldsymbol{w}_2\|^2(1+\delta_2(1-\frac{|\boldsymbol{w}_1\boldsymbol{w}_2|^2}{\|\boldsymbol{w}_1\|^2\|\boldsymbol{w}_2\|^2})) > In_1\|\boldsymbol{w}_1\|^2(1+\delta_1(1-\frac{|\boldsymbol{w}_1\boldsymbol{w}_2|^2}{\|\boldsymbol{w}_1\|^2\|\boldsymbol{w}_2\|^2}))$. Since its interference comes from UAV transmission, it can be regarded as a constant. Therefore, if this condition is satisfied, the decoding order from MU 2 to MU 1 is more profitable.

In case of a 3-MU NOMA cluster, we compare $\mathcal{G}_{c_2} = \{1, 2, 3\}$ and $\mathcal{G}'_{c_2} = \{1, 3, 2\}$,

$$\triangle P_{\mathcal{G}_{c_2}} - \triangle P_{\mathcal{G}'_{c_2}} = (\|\boldsymbol{w}_1\|^2 \boldsymbol{w}_2\boldsymbol{w}_3 - \boldsymbol{w}_1\boldsymbol{w}_3\boldsymbol{w}_1\boldsymbol{w}_2)^2(\frac{\delta_3 In_3 \left\|\boldsymbol{w}_2^N\right\|^2\delta_2}{\|\boldsymbol{w}_1\|^2(\|\boldsymbol{w}_2\|^2+\left\|\boldsymbol{w}_2^N\right\|^2\delta_2)-|\boldsymbol{w}_1\boldsymbol{w}_2|^2} - \frac{\delta_2 In_2 \left\|\boldsymbol{w}_3^N\right\|^2\delta_3}{\|\boldsymbol{w}_1\|^2(\|\boldsymbol{w}_3\|^2+\left\|\boldsymbol{w}_3^N\right\|^2\delta_3)-|\boldsymbol{w}_1\boldsymbol{w}_3|^2}) + \delta_1 In_1(\frac{(\boldsymbol{w}_1\boldsymbol{w}_3)^2(\|\boldsymbol{w}_3\|^2+\mu)+(\boldsymbol{w}_1\boldsymbol{w}_2)^2(\|\boldsymbol{w}_2\|^2+a)-2\boldsymbol{w}_1\boldsymbol{w}_3\boldsymbol{w}_1\boldsymbol{w}_2\boldsymbol{w}_2\boldsymbol{w}_3}{(\|\boldsymbol{w}_3\|^2+\mu)(\left\|\boldsymbol{w}_2^N\right\|^2+a)-(\boldsymbol{w}_2\boldsymbol{w}_3)^2} - \frac{(\boldsymbol{w}_1\boldsymbol{w}_3)^2(\|\boldsymbol{w}_3\|^2+\mu')+(\boldsymbol{w}_1\boldsymbol{w}_2)^2(\|\boldsymbol{w}_2\|^2+a')-2\boldsymbol{w}_1\boldsymbol{w}_3\boldsymbol{w}_1\boldsymbol{w}_2\boldsymbol{w}_2\boldsymbol{w}_3}{(\|\boldsymbol{w}_3\|^2+\mu')(\|\boldsymbol{w}_2\|^2+a')-(\boldsymbol{w}_2\boldsymbol{w}_3)^2})$$

After transformation, we have $\left\|\boldsymbol{w}_3^N\right\|^2(\|\boldsymbol{w}_1\|^2\|\boldsymbol{w}_2\|^2-|\boldsymbol{w}_1\boldsymbol{w}_2|^2) = \left\|\boldsymbol{w}_2^N\right\|^2(\|\boldsymbol{w}_1\|^2\|\boldsymbol{w}_3\|^2-|\boldsymbol{w}_1\boldsymbol{w}_3|^2)$. Thus, the conditions to fulfill $\triangle P_{\mathcal{G}_{c_2}} > \triangle P_{\mathcal{G}'_{c_2}}$ include $\delta_2 < \delta_3$ and $\|\boldsymbol{w}_2\|^2 < \|\boldsymbol{w}_3\|^2$. Then, we compare $\mathcal{G}_{c_3} = \{1, 2, 3\}$ and $\mathcal{G}'_{c_3} = \{2, 1, 3\}$, and observe that

$$\triangle P_{\mathcal{G}_{c_3}} - \triangle P_{\mathcal{G}'_{c_3}} =$$
$$((\|\boldsymbol{w}_3\|^2+\mu)\boldsymbol{w}_1\boldsymbol{w}_2 - \boldsymbol{w}_1\boldsymbol{w}_3\boldsymbol{w}_2\boldsymbol{w}_3)^2(\frac{\alpha'}{k_1(k_1+\alpha'(\|\boldsymbol{w}_3\|^2+\mu))} - \frac{\alpha}{k_2(k_2+\alpha(\|\boldsymbol{w}_3\|^2+\mu))}),$$
$$\alpha = \left\|\boldsymbol{w}_2^{\aleph}\right\|^2\delta_2 + \xi_{32}^2\left\|\boldsymbol{w}_3^{\aleph}\right\|^2\delta_2\delta_3, \mu = \left\|\boldsymbol{w}_3^{\aleph}\right\|^2\delta_3, \alpha' = \left\|\boldsymbol{w}_1^{\aleph}\right\|^2\delta_1 + \xi_{31}^2\left\|\boldsymbol{w}_3^{\aleph}\right\|^2\delta_1\delta_3,$$
$$k_1 = \|\boldsymbol{w}_1\|^2(\|\boldsymbol{w}_3\|^2 + \mu) - |\boldsymbol{w}_1\boldsymbol{w}_3|^2, k_2 = \|\boldsymbol{w}_2\|^2(\|\boldsymbol{w}_3\|^2 + \mu) - |\boldsymbol{w}_2\boldsymbol{w}_3|^2.$$

Therefore, if $(\frac{\alpha'}{k_1(k_1+\alpha'(\|\boldsymbol{w}_3\|^2+\mu))} - \frac{\alpha}{k_2(k_2+\alpha(\|\boldsymbol{w}_3\|^2+\mu))}) > 0$, we have $\triangle P_{\mathcal{G}_{c_3}} > \triangle P_{\mathcal{G}'_{c_3}}$. For the simplicity of NOMA clustering, we only consider the case that $\delta_1 < \delta_2 < \delta_3$ and $\|\boldsymbol{w}_1\|^2 < \|\boldsymbol{w}_2\|^2 < \|\boldsymbol{w}_3\|^2$ in our simulations, which ordering is from MU 3 to MU 1.

C.4 SIC Decoding Conditions

The SIC decoding conditions require that for a n-MU cluster, if $i, j \in \{1, 2, ...i, j..., n\}$, the SINR should satisfy $\gamma_i^j > \gamma_i^{j-1}, ..., > \gamma_i$. In case of a 2 MU cluster, we will have $\gamma_2 = \delta_2$, $\gamma_1 = \delta_1$, and the SIC decoding condition requires $\gamma_1^2 > \gamma_1$. According to (6.14), we can obtain $\xi_{21}^2 > \frac{\sigma^2\delta_1(1+\delta_1)}{p_2} = \frac{\delta_1(1+\delta_1)}{\delta_2(1+\delta_1\xi_{12}^2)}$. In case of a 3 MU cluster, the conditions of SIC are $\gamma_1^3 > \gamma_1^2 > \gamma_1$ and $\gamma_2^3 > \gamma_2$. After transformation, we can obtain $\xi_{21}^2 > \frac{\sigma^2\delta_1(1+\delta_1)}{p_2}$, $\xi_{31}^2 > \frac{\sigma^2\gamma_1^2(1+\delta_1)(1+\gamma_1^2)}{p_3}$ and $\xi_{32}^2 > \frac{p_2(1+\delta_2)}{p_3}$.